Tomas Bata University in Zlín
Faculty of Technology

Doctoral Thesis

Magnetorheological Systems with Optimized Performance

Magnetoreologické systémy s optimalizovaným výkonem

Author:	**Ing. Martin Cvek**
Degree programme:	P2808 Chemistry and Materials Technology
Degree course:	2808V006 Technology of Macromolecular Compounds
Supervisor:	doc. Ing. Michal Sedlačík, Ph.D.
Consultant:	Ing. Miroslav Mrlík, Ph.D.
External examiners:	Ing. Igor Lacík, DrSc. prof. Dr. Robert Luxenhofer prof. Dr. Bernhard Möginger doc. Ing. Petr Filip, CSc.
Internal examiners:	prof. Ing. Martin Zatloukal, Ph.D. DSc. prof. Ing. Petr Slobodian, Ph.D. doc. Ing. et Ing. Ivo Kuřitka, Ph.D. et Ph.D. doc. Ing. Jarmila Vilčáková, Ph.D.

Zlín, September 2018

Published by **Tomas Bata University in Zlín** in the Edition **Doctoral Thesis.**
The publication was issued in the year 2018.

Key words in Czech: *magnetoreologie, suspenze, elastomer, magnetická částice, radikálová polymerace s přenosem atomu, stabilita suspenze, částicové systémy, termo-oxidační stabilita, chemická stabilita, viskoelasticita*

Key words: *magnetorheology, suspension, elastomer, magnetic particle, atom transfer radical polymerization, suspension stability, particulate systems, thermo-oxidation stability, chemical stability, viscoelasticity*

Full text of the scientific publication is available in the Library of TBU in Zlín.

ISBN 978-80-……

ABSTRACT

The field-responsive materials belong among necessary attributes of today´s modern society as they offer a sophisticated solution for many technical needs. From this perspective, the immense potential is assigned to the magnetorheological (MR) systems, which are composed of micron-sized soft ferromagnetic particles dispersed either in non-magnetic dispersing medium or an elastomeric matrix. The feature of these systems known as the MR effect is the ability to rapidly, reversibly and in a controlled manner change their rheological/viscoelastic properties upon the exposure of an external magnetic field.

The presented doctoral thesis is devoted to the development of novel MR systems with controlled performance and enhanced stability properties through the advanced particle-grafting technology. The emphasis is given to the design and synthesis of ferromagnetic core-shell structured particles via atom transfer radical polymerization (ATRP). Using different reaction conditions, this technique allows achieving desired polymer shells with defined structure, molecular weight and thickness. As known, the quality of polymer shell plays a major role in particle stability and also significantly influences the performance of both, the MR suspensions and the MR elastomers. Herein, synthesized particles exhibit remarkably enhanced thermo-oxidation and chemical stability without unsuitably affected magnetization. To this date, this combination of characteristics was challenging to achieve via conventional modification techniques and majority of attempts was not successful. The inventions in Thesis provide significantly enhanced sedimentation stability with negligibly lower MR effect of the MR suspensions. Further, the embedding the ATRP polymer–grafted particles into suitable polymer matrix improves interfacial compatibility and even intensifies the relative MR effect when used in the MR elastomer systems. Moreover, the obtained MR elastomer is characterized by improved magnetostriction and damping capabilities.

As presented in this doctoral thesis, the specially-designed core-shell structures prepared via surface-initiated ATRP may contribute to the development of the next-generation of the MR systems with well-balanced properties tailored towards a specific application, which was not possible to achieve by foregoing conventional methods.

In a view of potential applications, the prospects are expected in the areas ranging from automotive to civil engineering, especially in the development of emission-free MR brakes or semi-active MR bridge bearings preventing the bridge degradation.

ABSTRAKT

Materiály reagující na vnější fyzikální pole nepochybně patří mezi atributy moderní společnosti, jelikož nabízejí sofistikovaná řešení pro mnoho technických potřeb. V tomto ohledu je velký potenciál přisuzován magnetoreologickým (MR) systémům, které jsou složeny z feromagnetických mikročástic dispergovaných v nemagnetické nosné kapalině nebo elastomerní matrici. Hlavním charakteristickým rysem těchto systémů je tzv. MR efekt, což je jejich schopnost rychle, vratně a řízeným způsobem měnit své reologické/viskoelastické vlastnosti v přítomnosti vnějšího magnetického pole.

Předkládaná doktorská práce je věnována vývoji nových MR systémů s regulovatelným výkonem a zvýšenou stabilitou, čehož je dosaženo pomocí pokročilé technologie využívající roubování polymeru na povrch částic. Důraz je kladen na návrh a syntézu feromagnetických částic typu jádro-obal pomocí kontrolované radikálové polymerace s přenosem atomu (ATRP). Použitím různých reakčních podmínek tato technika umožňuje připravit žádaný polymerní obal s definovanou strukturou, molekulovou hmotností a tloušťkou. Jak známo, kvalita polymerního obalu hraje hlavní roli zajišťující stabilitu částic, ale také významně ovlivňuje výkon jak MR suspenzí, tak i MR elastomerů. Částice syntetizované v rámci této doktorské práce vykazují značně zvýšenou termo-oxidační a chemickou stabilitu bez nežádoucího ovlivnění jejich magnetizace. Tuto kombinaci vlastností je v současné době velmi obtížné dosáhnout pomocí konvenčních technik modifikace. Vylepšení prezentovaná v této tezi umožňují významně zvýšit sedimentační stabilitu MR suspenzí s nepatrným snížením MR efektu MR suspenzí. Inkorporace polymerem roubovaných částic připravených pomocí ATRP do vhodně zvolené elastomerní matrice může zlepšit mezifázovou kompatibilitu a dokonce zintenzivnit relativní MR efekt u výsledných MR elastomerních systémů. Získané MR elastomery jsou navíc charakteristické zlepšenou magnetostrikcí a tlumícími schopnostmi.

Jak je prezentováno v této doktorské práci, speciálně navržené struktury typu jádro-obal připravené z povrchu iniciovanou ATRP se mohou uplatnit ve vývoji následující generace MR systémů s vhodně uzpůsobenými vlastnostmi přímo pro konkrétní aplikaci, čehož nebylo možné dosáhnout pomocí konvenčních metod.

S ohledem na potenciální aplikace je očekáváno uplatnění výsledků v řadě odvětví včetně automobilového a stavebního průmyslu, obzvláště při vývoji bezemisních MR brzd nebo semiaktivních MR uložení mostů potlačujících jejich degradaci.

CONTENTS

ACKNOWLEDGEMENTS

Here is my chance to express the immense gratitude to those who made this work possible.

Firstly, I would like to thank my supervisors Assoc. prof. Vladimír Pavlínek (from 06/2014 to 07/2017) and Assoc. prof. Michal Sedlačík (from 08/2017) for providing me the tremendous opportunity to join their research group, their guidance, support and encouragement during the entire period of my Ph.D. study.

I would like to express the immense gratitude and personal respect to my consultant and mentor Dr. Miroslav Mrlík who gave me an extraordinary support, guidance and valuable advice, which had remarkable impact on my research.

I am highly grateful to prof. Petr Sáha for ensuring the excellent research environment at the Centre of Polymer Systems, which offers the top equipment necessary for polymer and material science.

My special gratitude is directed to Dr. Jaroslav Mosnáček for the possibility to carry out the part of my research at Slovak Academy of Sciences and his remarks regarding the atom transfer radical polymerizations.

Furthermore, I would like to acknowledge the co-authors of my publications, particularly Dr. Markéta Ilčíková, Dr. Robert Moučka and Dr. Tomáš Plachý for their advice, cooperation and technical help during the experiments.

I cannot finish without acknowledging my great family for supporting me during my studies.

LIST OF SYMBOLS AND ABBREVIATIONS

Latin Abbreviations and Acronyms

2-B*i*BB	2-bromoisobutyryl bromide
3-APTES	(3-aminopropyl)triethoxysilane
ATRP	atom transfer radical polymerization
CI	carbonyl iron
CI-*g*-PGMA	CI particles grafted with PGMA
CI-*g*-PHEMATMS	CI particles grafted with PHEMATMS
CSR	controlled shear rate
CSS	controlled shear stress
EB*i*B	ethyl 2-bromoisobutyrate
EDS	energy-dispersive spectroscopy
EMF	external magnetic field
ER	electrorheological
ERS	ER suspension
FTIR	Fourier-transform infrared spectroscopy
GPC	gel permeation chromatography
H–B	Herschel–Bulkley
J–A	Jiles–Atherton
LVR	linear viscoelasticity region
M–B	Mizrahi–Berk
MR	magnetorheological
MRE	MR elastomer
MRS	MR suspension

NLVR	non-linear viscoelasticity region
NMR	nuclear magnetic resonance
PCL	polycaprolactone
PDMS	poly(dimethylsiloxane)
PGMA	poly(glycidyl methacrylate)
PHEMATMS	poly(trimethylsilyloxyethyl methacrylate)
PMDETA	*N,N,N',N'',N''*-pentamethyldiethylenetriamine
RP	radical polymerization
R–S	Robertson–Stiff
TEA	triethyleneamine
TEM	transmission electron microscopy
TGA	thermogravimetric analysis
VSM	vibrating-sample magnetometry

Latin Symbols

A	(–)	parameter describing hysteresis-free VSM curve
G^*	(Pa)	complex shear modulus
G'	(Pa)	real part of G^*
G''	(Pa)	imaginary part of G^*
G'_0	(Pa)	off–state storage modulus
G'_H	(Pa)	on–state storage modulus
H	($\mathrm{A \cdot m^{-1}}$)	magnetic field strength
H_C	($\mathrm{A \cdot m^{-1}}$)	critical H

H_e	($A \cdot m^{-1}$)	effective H
K	($Pa \cdot s^n$)	consistency index
M	($emu \cdot g^{-1}$)	magnetization (mass)
M_S	($emu \cdot g^{-1}$)	saturation M
$\bar{M}_n$	($g \cdot mol^{-1}$)	number–average molecular weight
$\bar{M}_w$	($g \cdot mol^{-1}$)	weight–average molecular weight
n	($Pa \cdot s^n$)	power-law exponent
T_C	(°C)	Curie temperature

Greek Symbols

α	(–)	coefficient describing domain coupling
γ	(–)	strain
$\dot{\gamma}$	(s^{-1})	shear rate
η	(Pa·s)	shear viscosity
η_0	(Pa·s)	off–state η
η_H	(Pa·s)	on–state η
η_{pl}	(Pa·s)	plastic viscosity
τ_0	(Pa)	yield stress

Special Symbols

$Đ$	(–)	dispersity index

LIST OF FRAMING PAPERS

PAPER I

CVEK, M.; MRLIK, M.; ILCIKOVA, M.; PLACHY, T.; SEDLACIK, M.; MOSNACEK, J.; PAVLINEK, V. A facile controllable coating of carbonyl iron particles with poly(glycidyl methacrylate): A tool for adjusting MR response and stability properties. *J. Mater. Chem. C.* **2015**; vol. 3(18), pp. 4646–56, IF 2015 = 5.066.

PAPER II

CVEK, M.; MRLIK, M.; ILCIKOVA, M.; MOSNACEK, J.; BABAYAN, V.; KUCEKOVA, Z.; HUMPOLICEK, P.; PAVLINEK, V. The chemical stability and cytotoxicity of carbonyl iron particles grafted with poly(glycidyl methacrylate) and magnetorheological activity of their suspensions. *RSC Adv.* **2015**; vol. 5(89), pp. 72816–24, IF 2015 = 3.289.

PAPER III

CVEK, M.; MRLIK, M.; ILCIKOVA, M.; MOSNACEK, M.; MUSNTER, L.; PAVLINEK, V. The synthesis of silicone elastomers containing silyl-based polymer-grafted carbonyl iron particles: An efficient way to improve magnetorheological, damping and sensing performances. *Macromolecules*. **2017**; vol. 50(5), pp. 2189–200, IF 2017 = 5.914.

PAPER IV

CVEK, M.; MRLIK, M.; ILCIKOVA, M.; SEDLACIK, M.; MOSNACEK, J. Tailoring performance, damping and stability properties of magnetorheological elastomers via particle-grafting technology. *Submitted manuscript*.

PAPER V

CVEK, M.; MRLIK, M.; MOUCKA, R.; SEDLACIK, M. A systematical study of the overall influence of carbon allotrope additives on performance, stability and redispersibility of magnetorheological fluids. *Colloids Surf., A,* **2018**; vol. 543, pp. 83–92, IF 2017 = 2.829.

1. THEORETICAL BACKGROUND

1.1 Introduction to Magnetorheology

The special-type materials belong among progressively developing areas of materials science and engineering. Particularly, the external stimulus-responsive materials are of interest for many scientists and researchers, due to their ability to rapidly and reversibly change their physical properties upon the application of an external stimulus, which can involve magnetic or electric fields, mechanical stress, UV light, pH change etc.

A concept of the field-responsive materials was introduced in 1947 when Winslow patented a method for translating electrical impulses into mechanical force [1]. He found that certain substances added into non-conducting liquid are able to develop highly-organized internal structures upon the exposure of an external electric field. As the system reacted on the electrical stimulus by changing its rheological behavior, the system was named as the electrorheological suspension (ERS). This finding inspired Rabinow, who experimented with analogous systems consisting of fine magnetic particles dispersed in a liquid and exposing them to magnetic fields [2]. The electromagnetically-controlled behavior – today termed as magnetorheological (MR) effect – was further used in a device that could serve either as a clutch or as a brake.

In the following years, most research activities were devoted to ERSs rather than to MR suspensions (MRSs) probably due to easier technical aspects of creating homogeneous electrical fields. Nevertheless, the ERSs have several drawbacks including relatively low yield stress, high sensitivity to contaminants (e.g. water), demands on high voltage or relatively narrow operating temperature range [3]. On the contrary, the MRSs are capable to develop superior yield stress, they are insensitive to contaminants and have relatively broad operating temperature range. Since the early 1990s the MRSs started commercially dominate over the ERSs and were introduced to many engineering fields including automotive [4-8], civil engineering [5, 8-10], robotics and haptic devices [11-14], exercise equipment [3], or polishing technology [3, 5, 15, 16].

As will be discussed further in text (Chapter 1.5), the sedimentation stability of the MRSs is a limiting factor due to high density of magnetic particles. To restrict the sedimentation problem, a subclass of the MR materials known as MR elastomers (MREs) has been under development since 1983. First report dealing with the MREs is attributed to Rigbi et al. who embedded magnetic particles into an elastomeric matrix [17]. The MREs are stable against sedimentation and they eliminate sealing issues, possible leakage or environmental contamination which may accompany the application of the MRSs [18]. Being the stable solid analogues to MRSs, the particle displacements are controlled by matrix elasticity and the MR effects are generally less pronounced [19]. Despite that, their

properties are suitable for various applications such as fast-response dampers, seismic protection of buildings [9, 20, 21], artificial muscles [22], piezoresistive sensors [23] or even electromagnetic shielding materials [24, 25] and flexible micro-channels for biological fluid transport [26] etc.

1.2 Physical Mechanisms Behind the MR Effect

Before describing physical phenomena occurring in the MR systems after the application of an external magnetic field (EMF), the basic mathematical definition of the MR effect as an important evaluation tool is presented (Eq. 1):

$$MR\ effect = \frac{\eta_{\mathrm{H}} - \eta_0}{\eta_0} \equiv \frac{G_{\mathrm{H}} - G_0}{G_0} \tag{1}$$

Here, the symbols η_{H} and η_0 denote the viscosity of the MRS in the presence (on–state) and in the absence (off–state) of the EMF, respectively. The relation is analogous for the MRE for which the on–state and off–state quantities are expressed using storage moduli, G'_{H}, G'_0, formalism. The MR effect is usually presented as a relative quantity and its typical values for the MRSs are laying in the range from hundreds to thousands of percent [27]. For the MREs, the relative MR effects are much lower most commonly in tens of percent [28, 29], which is caused mainly due to high initial stiffness of the matrix. Nevertheless, the existence of the MREs with a giant response to the EMF was also reported [30], but the G_0 of such MRE was notably diminished due to high plasticizer content.

The fundamental principle behind the MR effect is based on the microstructure change as a reaction on the EMF. The EMF however affects the microstructure of the MRSs and MREs differently due to their different compositions. While the MRSs contain freely-movable particles dispersed in a Newtonian liquid, in the MREs they are locked in their positions upon the completion of the matrix polymerization process [31]. Due to this difference, the MR effect is driven by various mechanisms in both systems.

The conventional MRSs are consisted of micron-sized, soft, ferromagnetic particles dispersed in a Newtonian liquid, which is the most-commonly silicone or mineral oils [5, 27, 32]. In the absence of the EMF, the particles are randomly dispersed and the MRS behaves almost according to the Newton's law or slightly in pseudoplastic manner [33]. When a certain EMF is imposed, the particles become magnetized and build-up the internal chain-like structures aligned in the field direction (Figure 1a) due to mutual field-induced dipolar magnetic interactions [5]. On the micro-level, the structure development process is a complex phenomenon involving the initial aggregation of the particles into single-width chain-like structures that later laterally aggregate to form column-like structures. Besides the inherent properties of the system, the structure formation

is also affected by the rate of field increase [27]. The MRS transition from liquid-like to solid-like state is accompanied by significant (several orders of magnitude) increase of the rheological parameters (viscosity, viscoelastic moduli) [34].

As indicated above, the MREs are fabricated by incorporating the magnetic particles into an elastomeric matrix and locking their position upon final curing. However, depending on the matrix elasticity the applied EMF can shift the magnetic particles from their original positions resulting in highly-anisotropic composite properties including the modulus increase. The MR effect of the MREs is generally characterized by Jolly's dipole-interaction model [34] similarly as for MRSs, however, this model assumes straight particle chains, which have in reality rather wavy character in the MREs and the original model was therefore modified. Moreover, the additional mechanism related to the matrix elasticity is involved as the non-affine matrix deformation and also plays a certain role in the MREs stiffening (Figure 1b) [35].

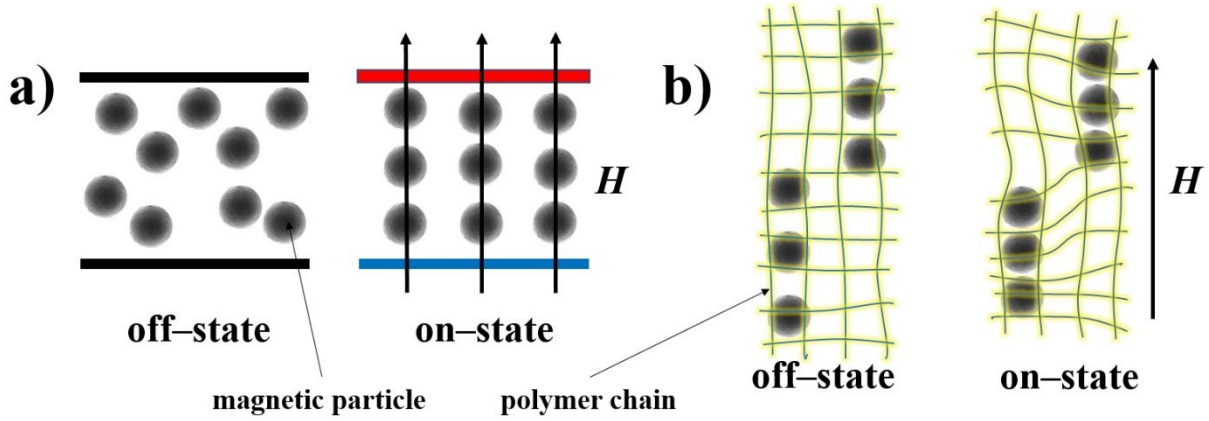

Figure 1. Schematics of the MR effect mechanism in the MRS (a), and non-affine deformation of the polymer matrix as one of the possible mechanisms responsible for the field-stiffening of the MREs (b). Redrawn from [35].

1.3 Rheological Aspects

Due to their unusual composition the MR systems exhibit complicated flow characteristics, which are necessary to be determined in order to assess their suitability in practical applications. Their rheological properties are typically investigated under both situations, the off–state as well as the on–state, while the experimental conditions are preferably chosen with a connection to the potential application. While the rheological behavior of the MRSs can be studied either in (magneto-)shear mode or in (magneto-)oscillatory regime, the MREs can be subjected only to the latter conditions.

1.3.1 Steady-Shear Behavior

In the most devices incorporating the MRSs the operating fluid is subjected to a shear flow (e.g. clutch, brake). In the off–state, the shear stress of the MRSs is almost proportional to the shear rate, which corresponds to nearly Newtonian-like (or slightly pseudoplastic) behavior, which can be approximated by the Newton's model (Eq. 2):

$$\tau = \eta\dot{\gamma} \tag{2}$$

where τ denotes the shear stress, η represents the shear viscosity, and $\dot{\gamma}$ is the shear rate. In the on–state, the field-induced structures represent a resistance against shearing resulting in the τ increase by several orders of magnitude (Figure 2). The on–state τ values are strongly dependent on the applied magnetic field strength, *H* [5, 27, 32].

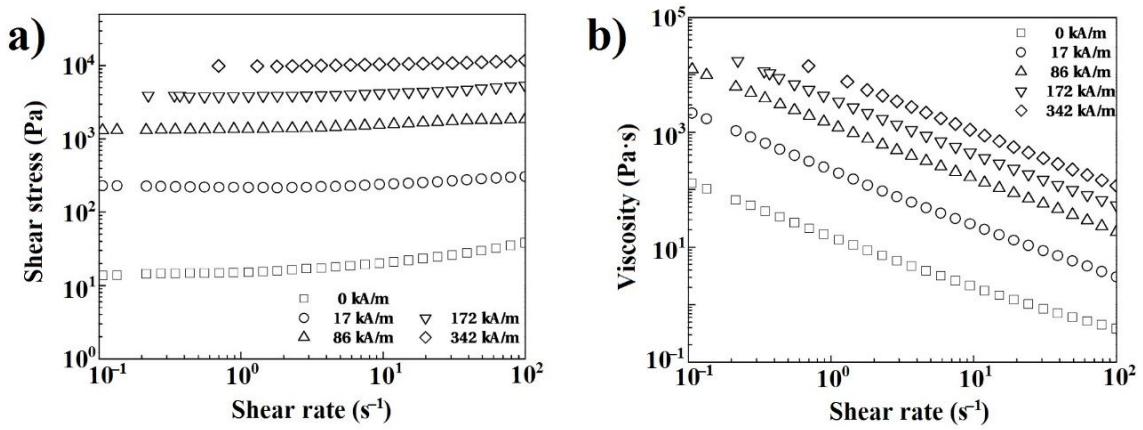

Figure 2. Typical rheological behavior of the MRSs. Shear stress (a) and shear viscosity (b) as a function of shear rate under different magnetic fields strengths. The MRS contained 30 vol.% of the carbonyl iron (CI) particles dispersed in mineral oil at 20 °C. Adopted from Cho et al. [36].

The studies dealing with steady shear magnetorheology tend to classify the MRSs (on–state) as non-Newtonian that behave according to the Bingham plastic (Eq. 3) or the Herschel–Bulkley (H–B) models (Eq. 4) [32, 37-40]. The former is represented by the original viscoplastic equation as follows:

$$\tau = \tau_0 + \eta_{\mathrm{pl}}\dot{\gamma} \tag{3}$$

where τ_0 is the yield stress controlled by *H*, and the constant of η_{pl} denotes the plastic viscosity of the system. The parameters τ_0 and η_{pl} can be obtained applying the Bingham plastic model to macroscale experimental measurements [41]. The Bingham plastic model has gained popularity mainly because of its simplicity [42]. However, its accuracy is questionable due to its

linear character once τ_0 is exceeded. Recently, it was concluded [33] that the H–B model is more appropriate for the MRSs especially in high $\dot{\gamma}$ region. Replacing constant η_{pl} with the $\dot{\gamma}$-dependent power-law relation the H–B model can be expressed as:

$$\tau = \tau_0 + K\dot{\gamma}^n \tag{4}$$

where *K* and *n* are the consistency index and power-law exponent, respectively. The *K* and *n* are material parameters related to materials' flow behaviors. Other viscoplastic equation was originally proposed by Casson to describe rheology of printing inks. Later, this empirical model was shown to have the applicability in hemorheology and food technology [42]. Due to its ability to fit behavior of wide variety of viscoplastic materials the Casson model was later used in magnetorheology [16, 27] showing high accuracy for the MR fluids containing the nano-sized iron particles [43].

The Robertson–Stiff (R–S) model (also known as the Vocadlo model) was proposed to describe the rheological behavior with non-linear characteristics of bentonite suspensions, cement slurries, or polymer solutions and gels [42, 44]. Due to the similar flow behavior of these materials with the MRSs, Cvek et al. [33] have employed the R–S model in magnetorheology for the first time. The R–S model was applied in the form [45] (Eq. 5) in order to obtain parameters with a physical meaning applicable for the MRSs:

$$\tau = \left[K^{\frac{1}{n}}|\dot{\gamma}|^{\frac{n-1}{n}} + \left(\frac{\tau_0}{|\dot{\gamma}|}\right)^{\frac{1}{n}}\right]^n \dot{\gamma} \tag{5}$$

with all variables defined similarly as in models above. The application of the R–S model resulted in even better agreement with the experimental data than in the case of the H–B model. Moreover, the Mizrahi–Berk (M–B) model (Eq. 6), which is commonly used in food engineering [46] was recently used in magnetorheology, however, its fitting capability to predict behavior of the MRSs in low $\dot{\gamma}$ steady shear regime was found to be insufficient [33].

$$\tau^{\frac{1}{2}} = \tau_0^{\frac{1}{2}} + K\dot{\gamma}^n \tag{6}$$

Figure 3 compares the fitting/predictive capabilities of 3-parameter viscoplastic models used in magnetorheology. As seen, the H–B and the M–B models tend to under-/overestimate τ values at a lower/higher $\dot{\gamma}$ range, while the best fit was provided with the R–S model.

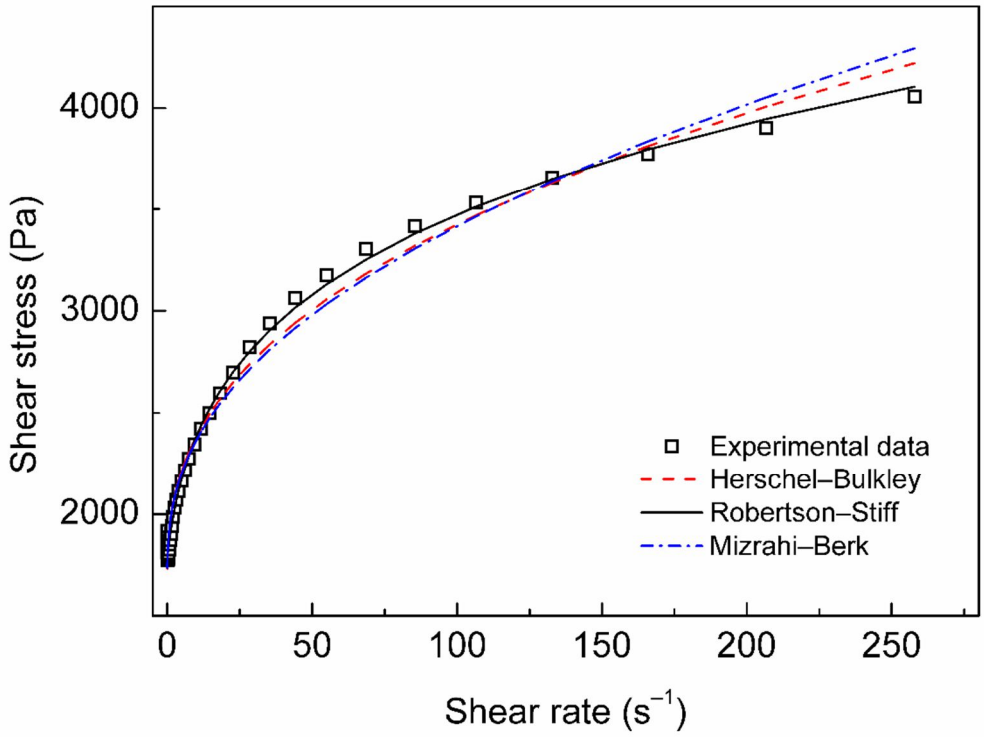

Figure 3. Shear stress vs. shear rate experimental data for the MRS containing 15 vol.% of the CI particles at 216 kA·m^{-1} with the H–B (dashed line), the R–S (solid line), and the M–B (dash/dot line) models applied. Reprinted from Cvek et al. [33].

For the equations above (Eqs. 3–6), the following condition (Eq. 7) can be applied:

$$\dot{\gamma} = 0\,, |\tau| < \tau_0 \tag{7}$$

The expression shows that τ_0 must be overcome to initiate deformation or flow of the material [27]. However, there is still some debate [47] whether a true τ_0 exists or not. Despite the controversy, the engineering reality of τ_0 is a desirable and useful concept in a whole range of applications, once τ_0 is properly defined. There is no standard procedure to measure τ_0 value therefore the common technique is an indirect determination involving appropriate rheological models [48, 49].

1.3.2 Yield Stress

Yield stress is one of the most relevant rheological properties of the MRSs [27]. Basically, there are two approaches that can be utilized to determine τ_0 value. The first approach is based on the measurements in the controlled shear stress (CSS) mode, which can provide information about the static (or frictional) τ_0 (Figure 4a). However, this type of τ_0 is frequently associated with the slipping of

the aggregates on the wall of the geometry used rather than with the structure collapse under an applied shear. Another procedure involves the indirect determination based on the applying appropriate viscoplastic constitutive models (Eqs. 3–6) for the data obtained in the controlled shear rate (CSR) mode. The τ_0 obtained from the CSR mode is referred as dynamic and it is associated with the continuous breaking the aggregates during the magneto-shear. According to the literature [27, 50], the CSR mode is undoubtedly the most widely used τ_0 estimator. The dependence of dynamic τ_0 developed in the MRSs on applied H is basically underlying three regimes (Figure 4b) [51]. At low magnetic fields, τ_0 is quadratically proportional to H owing to the magnetic polarization mechanism. When H overcomes a certain critical value, H_C, the local saturation of the particles becomes more prevailing and the τ_0 further increases sub-quadratically with H. At high magnetic fields, the particles saturate and τ_0 eventually becomes field-independent [27, 33, 51, 52]. From the engineering perspective, it is important to mention that dynamic τ_0 can be also roughly estimated based on the elemental mathematical expressions as reported elsewhere [53]. As it relies from the paragraph above, τ_0 is quantity relevant mainly for MRSs, thus it is not mentioned in connection to MREs.

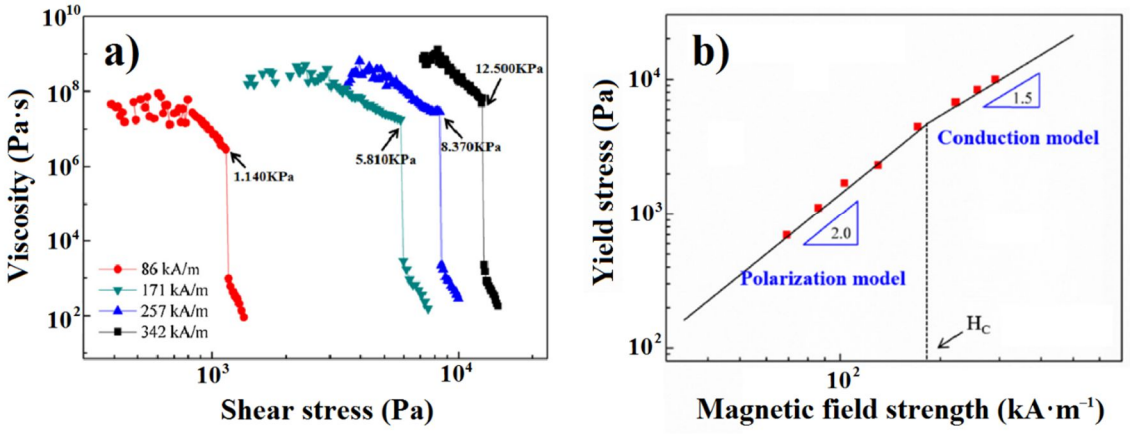

Figure 4. Shear viscosity as a function of applied shear stress obtained from the CSS mode (a) and dynamic yield stress as a function of magnetic field strength obtained from the CSR mode (b) for the MRS containing 20 vol.% of the CI particles coated with polyaniline. Adopted from Moon et al. [52].

1.3.3 Dynamic Behavior

The certain devices incorporating the MR systems such as dampers of seismic vibrations or shock attenuators are designed to operate under dynamic loading conditions [3, 9, 10, 54]. As mentioned above, the steady shear mode is accompanied by breaking and reforming the induced particle structures [55], while the dynamic loading represented as oscillatory shear has rather deformation character. Oscillatory tests at sufficiently low strains, γ, do not destroy the particles internal structures [54], therefore they are established to be a suitable

tool to investigate the viscoelastic properties of the MR systems using the complex shear modulus, G^*, formalism. The both, the real part – storage modulus, G', as well as the imaginary one – loss modulus, G'', of the G^* possess a physical meaning only when the internal structures are not broken [56], thus the investigation of linear viscoelasticity region (LVR) is a basic prerequisite that should be accomplished. The LVR is obtained from γ-sweeps under various H (Figure 5a) as its position is typically shifting to lower γ with increasing H [57]. Then, the linear response of the material is evaluated using the frequency-sweeps. As seen from Figure 5b, in the off–state the G'' dominates over the G' reflecting the liquid-like behavior, however, in the on–state the transition to solid-like behavior occurs and the G' starts to prevail. This situation is typical for the MRSs as the MREs mostly demonstrate dominating G' even in the off–state due to inherent elasticity of the matrix [28].

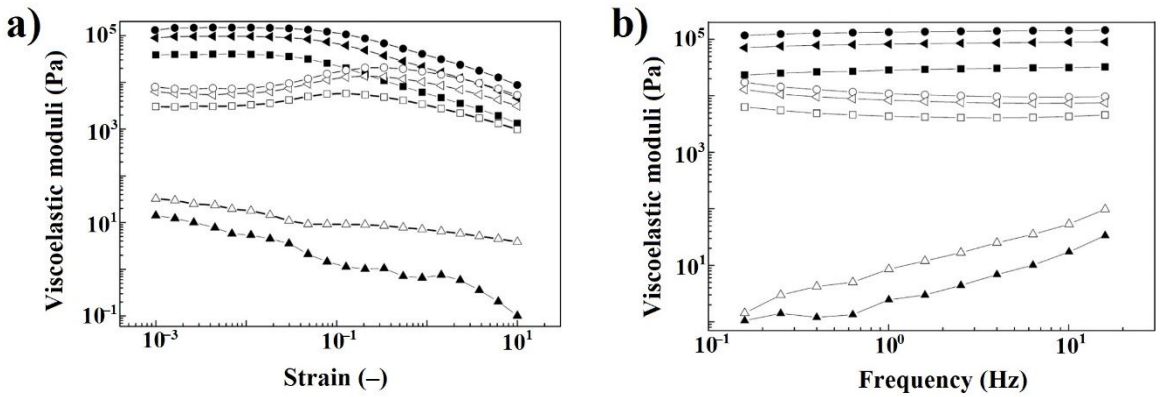

Figure 5. Dependences of the storage (solid symbols) and the loss (open symbols) moduli on applied strain (a) and on applied frequency (b) for the MRS containing 40 wt.% of cholesteryl-coated CI particles in silicone oil at temperature of 25 °C. The measurements were performed in the absence (triangles) as well as in the presence of the EMF with magnetic flux densities of 87 (squares), 178 (left-pointing triangles), and 267 mT (circles). Adopted from Mrlik et al. [58].

The linear response of the MR systems is widely-studied while their behavior in non-linear viscoelastic regime (NLVR) is often ignored although it can be a great source of information related to particles' interactions [27]. The NLVR investigations are better known from rubber industry as the filler-containing rubbers exhibit so-called Payne effect, i.e., rapid *G'* decrease with increasing γ amplitude due to breakdown of the filler structure [19]. In the case of the MR systems this phenomenon was recently termed as "magnetic Payne effect" by Arief et al. [59] who investigated dynamic breakdown and rearrangement of the particle network in the MRSs under the application of the EMF. Nevertheless, the concept of the Payne effect is more relevant for the MREs due to their inherent elasticity. Sorokin et al. [19] found that the Payne effect is larger in the MREs with softer matrix which is closely connected to the mobility of the particles

within a matrix and consequently to achievable MR effects. Despite the comprehensive research of his group [19, 60], some phenomena remain poorly understood and require further investigations, in particular the effect of polymer-modified particles having enhanced compatibility with the matrix on the Payne effect appearance.

1.4 Composition of MRSs and MREs

In presented MR systems, magnetic particles are dispersed either in a liquid medium or elastomeric matrix. There are several aspects, that should both types of surroundings fulfill to provide stable systems with high performance and durability. Sufficient chemical and thermo-oxidation stability was mentioned in a connection with magnetic particles but these requirements are relevant also for their surroundings. In addition, they should not interact with the particles in any negative way to achieve sufficient stability. The mostly used dispersing medium in the MRSs is silicone oil as it fulfills all the mentioned criteria. Moreover, silicone oils are manufactured with various viscosities, so one can choose the most appropriate type regarding the needs of final application. However, the experiments with mineral oil [61], paraffinic oil [62], kerosene [63], octanol [64], glycol [65] or water-based [66] MRSs have been reported. On the contrary, the majority of the MREs is based on rubber matrices, such as natural rubber [67, 68], or synthetic ones as silicone [24, 28, 69, 70], *cis*-polybutadiene [71, 72], or nitrile rubbers [73]. Also epoxidized-natural rubber [74], waste tire rubbers [75], or even thermosetting polymers e.g. polyurethanes [76, 77] have been recently investigated for this purpose. Important point regarding this topic is connected to the employment of rubber or thermoset matrices, which makes the recycling process very difficult. Due to rising number of devices based on the MREs, the recycling of these components may become a crucial aspect in the next decades. Despite that, the number of papers devoted to development of the MREs based on easily-recyclable elastomeric materials, such as thermo-plastic elastomers matrices is rather limited [25, 78-80].

The materials used as a dispersed phase in the MR systems are limited to ferro- or ferri-magnetic particles. An overwhelming majority of these systems contains the carbonyl iron (CI) particles (references e.g. [25, 81-83]) as a filler due to their suitable size (Figure 6a) and excellent magnetic properties such as high permeability, low remanent magnetization, and high saturation magnetization (Figure 6b). Also cobalt-ferrite ($CoFe_2O_4$) [57], magnetite (Fe_3O_4) [84], maghemite (γ-Fe_2O_3) [85] or neodymium-iron-boron alloy (NdFeB) [61] particles have been recently used as a magnetic filler, however, their magnetization is considerably lower in comparison with the CI particles which reduces the MR effect.

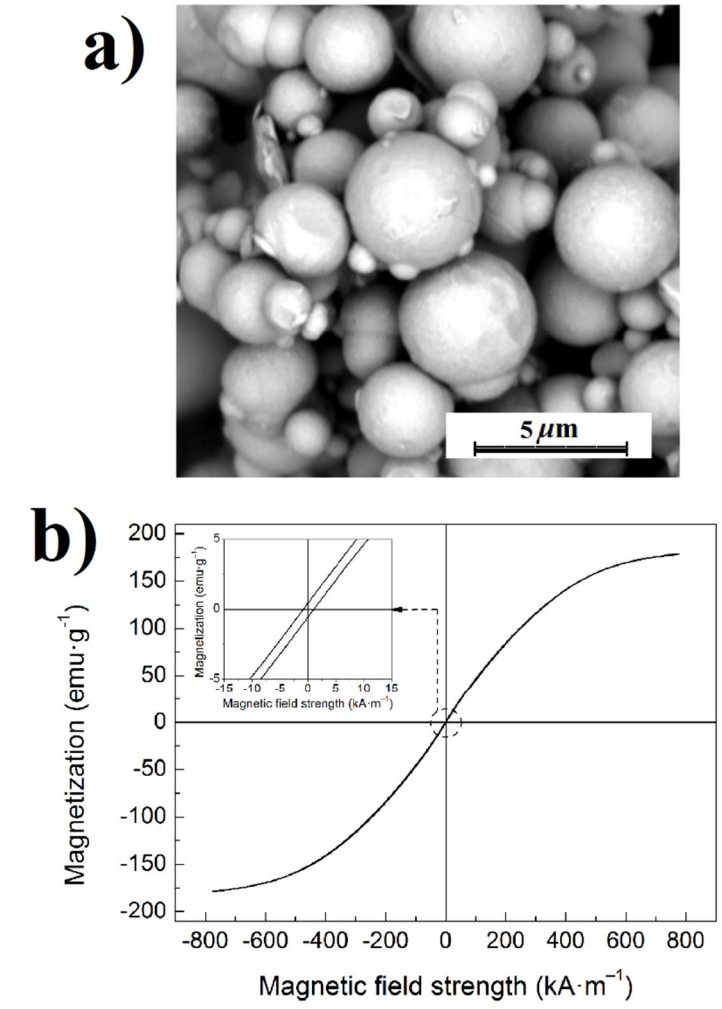

Figure 6. Scanning electron microscopy micrograph of the CI particles (a), together with their magnetization curve (b). The inset figure displays particles' magnetic hysteresis. Adopted from Cvek et al. [33].

To numerically-assess the suitability of the particles to meet the requirements of the MR systems, the Jiles–Atherton (J–A) model can be used. This mathematical formula sufficiently describes the non-linear magnetization curves typical for ferromagnetic particles. Despite that, the J–A magnetic model is still being improved to eliminate, or at least, minimize its drawbacks, which mainly include insufficient reproducibility of data fitting near the saturation state [86]. In the J–A model, the hysteresis-free curve is generally described by the modified Langevin equation (Eq. 8) having the following form:

$$M(H) = M_S \left[\coth\left(\frac{H_e}{A}\right) - \left(\frac{A}{H_e}\right) \right] \tag{8}$$

Here, M denotes the magnetization of material, M_S is the saturation magnetization and H is the magnetic field strength. The magnetization curve shape without hysteresis is given by the parameter A, whereas the effective magnetic field strength is denoted with H_e, which is calculated according to the expression (Eq. 9):

$$H_e = H + \alpha M \tag{9}$$

where α represents the coefficient describing coupling between domains [87]. Recently, this model was successfully used by Cvek et al. [88] in magnetorheology to correlate the thickness of polymer coating with the reduction of magnetic properties of modified CI particles.

1.5 Common Drawbacks of the MR Systems

Despite their singularity, the MRSs suffer from several drawbacks which hinder their potential. Previously addressed issue of the MRSs is their poor sedimentation stability, which occurs due to the density mismatch between the magnetic particles and the dispersing medium. Once the particles settle down, severe redispersibility problems may arise due to their inter-particle aggregation [27]. Such situation can cause performance decrease and malfunctioning of the MR device.

The main advantage of the MREs over MRSs is that the particle sedimentation is eliminated [28]. However, the interface between the particles and the matrix plays a key role in performance and durability of the MREs. As the magnetic particles are mostly hydrophilic and the elastomeric matrix hydrophobic, the particle/matrix compatibility and matrix properties must be taken into consideration when designing the effective MREs.

The mutual issues of the MRSs and the MREs are connected to their poor thermo-oxidation and insufficient chemical stability [27, 58, 88-93]. The MR devices can be exposed to demanding operating conditions, e.g. they can operate during subterranean gas and oil exploration works, where the temperature is relatively high (~150 °C) due to geothermal gradient [94]. Moreover, they can be exposed to the presence of reactive species such as acid rains, sea humidity etc. [25]. High chemical resistance of magnetic particles is essential in final polishing of high precision optics, because this technology requires a decrease in pH to improve the MR finishing of certain polycrystalline materials [95].

1.6 State-of-the-Art

In order to reduce the above-mentioned drawbacks of the MR systems, several methods and approaches have been developed over the years and these will be further discussed in more details. As indicated in the title of the treatise, this work was devoted to MR fundamentals along with the performance enhancements of the MR systems through particle's modifications. Admittedly, a great portion of MR research has been performed via the employment of additives therefore a brief insight into the topic of additives is included in the first part of this chapter. In the second part, a special emphasis is devoted to the preparation of the core-shell structures as a mutual denominator connecting the areas of the MRSs and the MREs.

1.6.1 Additives

Facile but effective approach to enhance poor sedimentation stability and difficult redispersibility of the MRSs is the addition of stabilizing agents such as nanofillers. Using this method, no special or toxic chemicals are needed thus it is preferable way from the environmental point of view. The incorporated additives are mostly submicron-sized low-density gap fillers that occupy the interspaces between the magnetic particles (Figure 7) reducing their sedimentation rate while increasing the dispersion stability and enhancing rigidity of the internal structures in the on–state [96]. The diverse materials including fumed silica [97], organoclays [98], γ-Fe_2O_3 nanoparticles [99], graphene oxide [96] *etc*. were utilized in the MRSs for the mentioned purpose. The preparation of dimorphic [100] or bidispersed [101, 102] MRSs was also found to be beneficial. Recent study [103] compares the effect of non-magnetic rod-like ferrous oxalate dihydrate particles and their magnetic iron oxide rod-like analogues on the MR effect and stability properties. Both variants effectively enhanced magneto-induced shear stress and sedimentation stability of the MRSs; moreover the addition of magnetic rods was superior at low shear rates due to their contribution to magneto-static forces. Since the above-mentioned additives were of different sizes, shapes (spherical, rod-like/fibrous, plate-like), and were tested under various conditions (particle/additive ratio, dispersion medium, applied EMF) the overall efficiency is still unclear. Due to high interest in comparative studies and precise evaluation techniques, Cvek et al. [104] recently presented a systematical study evaluating the role of different carbon nano-additives on complex behavior of the MRSs. Based on their findings, the optimization of the MRSs for commercial applications could be based on combining the additives varying in the mechanism of their action to ensure both, rigidity of the internal structures as well as the sufficient sedimentation stability and redispersibility.

The additives are relevant due to their enhancing effects to be used mainly in the MRSs, however it should be mentioned that some work regarding this topic

was also applied on the MREs. Recently, Wang et al. [105] found that the addition of carbon black into ethylene propylene diene rubber-based MREs during the processing lead to in-situ formation of complex particle structures, which ultimately resulted in increased tensile strength, and damping of as-designed composite. Although the addition of nano-fillers is efficient regarding the sedimentation and redispersibility phenomena in the MRSs, it is ineffective for enhancements of thermo-oxidation or chemical stability of the particles. Therefore, more advanced approaches such as synthesis of the core-shell structures have been thoroughly investigated.

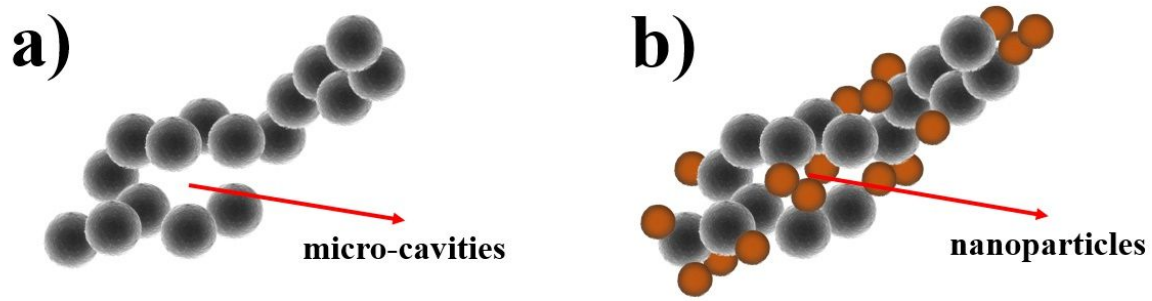

Figure 7. Magnetically-induced particle chain-like structure formation in conventional MRS with observable micro-cavities (a) and after stabilization with magnetic nanoparticles filling the micro-cavities (b). Redrawn from Ashtiani et al. [106].

1.6.2 Core-Shell Structures

The fabrication of complex particles such as core-shell-type structures has gained significant attention in the last two decades. In the early work, Shchukin et al. [107] have designed a novel photocatalytic systems based on magnetic cores coated with silica and titania shells and studied their rheological properties. Nevertheless, the first core-shell particles directly intended to enhance properties of the MRSs were prepared few years later [36]. Since that time many different types of the core-shell particles with either organic or inorganic shells have been fabricated. Prior reviewing the recent developments in the area, the basic functions of the shell material are outlined.

As concluded in numerous studies (references e.g. [5, 27, 89, 93]), the shell material generally has a lower density in comparison with metallic magnetic cores and therefore its presence contributes to lower bulk density of the core-shell structure reducing the sedimentation rate of the MRSs. High temperature or the presence of reactive species result in a degradation of magnetic particles and a formation of less magnetic products, which leads to lower response to EMFs. Therefore, the shell basically serves as a protection layer of magnetic particles prolonging the durability of the MR systems [25, 93]. In the MREs, the particles incorporated in the matrix are not directly exposed to air, but the moisture and

oxygen can diffuse through the matrix. This process is further accelerated at higher temperatures and finally results in a reduction of particle/matrix strength and lower the MR performance [81]. In the case of MRSs, the abrasiveness of the magnetic particles must be taken into consideration as well. Depending on the final application the abrasiveness can be favored or not. Jacobs [95] has shown that inorganic shell such as zirconia applied on magnetic particles enhances aqueous corrosion stability and efficiency in polishing a variety of optical glasses or crystalline ceramics due to high abrasiveness. On the other hand, organic shell generally reduces the abrasion of device surfaces extending the service life of the MR device itself [108], which is important for the majority of applications. Therefore, the attention in Thesis will be paid mainly to organics shells while omitting their inorganic analogues.

Organic shells represent the largest group of materials used in magnetorheology, which include low-molecular weight substances or different polymer coatings. Among the most investigated organic layers applied on the magnetic particles belong silane-based coupling agents [25, 78, 106, 109-112]. These substances bear hydrolysable groups (methoxy, ethoxy, acetoxy) at one end on the molecule, which enable covalent bonding to the inorganic surface, i.e., particles. The other end the molecule can contain organofunctional group (amino, vinyl, sulphide) allowing the reaction with the elastomeric matrix in the case of the MREs. Thus, silica coupling agents are used mainly to improve interfacial adhesion as they can act as a bridge between inorganic and organic materials [112]. Particle treatment with these substances is relatively straightforward, and economical, however, the modifications performed via more advanced techniques bring other advantages into the MR systems as will be explained further.

Besides low-molecular compounds such as silanes, also large spectrum of polymers has been applied as a shell material. Poly(methyl methacrylate) [36, 113, 114], poly(vinylbutyral) [108], polyaniline [115], polypyrrole [116], polydopamine [117], etc. represent only a small fraction of polymer shells examined in magnetorheology. The conventional encapsulation techniques included an in-situ dispersion polymerization [36, 115], suspension polymerization [118], or solvent evaporation [119], but these do not allow precise control of shell thickness, which results in significantly reduced particle magnetization. Moreover, such polymer shells are frequently attached via non-covalent interaction therefore the durability of prepared systems is rather questionable.

All the prepared material combinations enhanced utility properties of the MR systems to a certain degree, however, for further enhancements the researchers experimented with several other innovative methods to suitably modify the surface of magnetic particles. Fang et al. [120] employed dual-step functionality

coatings by applying the polyaniline layer and subsequent multi-walled carbon nanotube layer. This combination of materials was cautiously chosen due to their properties and intended contribution to the overall performance. For more details please see the original paper [120]. Other material combinations of sequential coatings were also investigated [120-122]. The remarkable approach introduced by Sedlacik et al. [123] involved vacuum plasma deposition of fluorinated substances onto the magnetic particle surface. With this method, it was possible to tune the particle properties to a certain degree by changing the modification times. Recently, Chuah et al. [124] showed a conceptually interesting method in which the applied polystyrene layer on the CI particles was further foamed using a supercritical carbon dioxide, which resulted in significantly enhanced sedimentation stability of the MRS.

To the author's knowledge, the literature dealing with special type coatings applied on the magnetic particles embedded in the MREs is rather limited. One example noted is the preparation of the flower-like CI particles by an in-situ reduction method [125]. Such structures were successfully used to prepare polyurethane-based MREs with significantly enhanced microwave-absorbing performance due to improved electric impedance-matching characteristics.

In general, the fabrication of core-shell particles is recognized as an effective approach to enhance performance and stability properties of the MRSs. However, there is a strong correlation among the properties which are affected by the particle modification. It is therefore a necessity to employ a strategy that allows precise tuning of modifying layers (on a molecular level) and consequently the overall behavior of the MR systems. To this date, no comprehensive research focused on this topic has been performed. Therefore, the main objective of work in Thesis will be addressed to this need. As a suitable synthesis tool the atom transfer radical polymerization (ATRP) has been chosen.

1.7 Atom Transfer Radical Polymerization

Conventional radical polymerization (RP) has a great significance in preparation of large amount of various polymers. The architectural control of resulting polymers is however limited due to very fast termination rate of the radicals. This obstacle can be avoided by applying an advanced concept known as controlled or "living" RP. A major difference between conventional RP and controlled RP is the lifetime of propagating radicals during the reaction. In the former, radical generated by decomposition of the initiator undergoes propagation and termination within a second, while in the controlled RP the lifetime of the living radical can be extended to several hours [126]. With this concept, it is possible to tailor the polymers with precisely controlled molecular weight, relatively low polydispersity, diverse composition or functionality [127, 128].

There are several types of controlled RPs among which metal-catalyzed ATRP plays the important role. This ATRP-type can be further modified to be initiated directly from the substrate which is called a surface-initiated ATRP. Assuming the suitable treatment of the substrate, this technique allows covalent grafting of the polymer chains from an inorganic surface leading to the creation of polymer brushes, which in a connection to the MR systems can positively affect the interactions with the surrounding medium or the matrix [28, 83, 89, 126]. To this date, the surface-initiated ATRP is considered as one of the most suitable fabrication techniques to gently modify the magnetic substrates and to prepare core-shell structures intended to magnetorheology.

1.8 Further Factors Influencing the MR Effect

Although the conventional MR systems are only two-phase entities, there is large variability of the individual components, what makes the understanding of these systems relatively complex. In the following part, the major factors influencing the MR effect are presented, and some of them were considered when designing novel MR systems in the experimental part of this Thesis. The next goal of this chapter is to point out some aspects which can be considered as important for further practical applications and are not covered in the current literature.

1.8.1 Particle-Related Factors

As the particles are the only magnetically-active component in the conventional MR systems, their properties such as size, shape, porosity etc. are of high importance. But the first basic assumption is related to the inherent magnetic properties of the particles as described in Chapter 1.4. Additionally, it is important to mention that the vast majority of the MR systems contains magnetically-soft materials, which allow fast demagnetization process [129] necessary for practical applications. From obvious reasons, magnetically-hard materials are not used for the preparation of the MRSs, but they were already applied in the MREs [130]. According to the authors [130], such hybrid material cannot be demagnetized by the application of reverse field, which indicates a potential to be used as active and simultaneously passive damping element.

Regarding the particle concentration; there exists a minimal threshold concentration below which no obvious field-induced response of the MR system is observed. In practice, the effective particle volume fraction for the MRSs ranges from 20 to 40 vol.%, which corresponds with a typical iron content in weight between 75 and 85 wt.% [131] as documented by the composition of commercially-available MRSs. However, the maximum yield stress (~210 kPa) can be obtained by using 50 vol.% of the particles as estimated via finite element analysis by Ginder et al. [53]. The situation is different in the MREs as in their

case the certain mechanical properties are expected even in the off–state. Thus, to ensure both, the maximal MR effect and retained mechanical properties the optimum particle fraction should not exceed 30 vol% [73].

As known, the dimensions of the particles correlate with their magnetic properties. Generally, magnetic microparticles exhibit higher M_S values when compared with nano-sized ones [132] leading to higher MR effect in such systems. Nevertheless, the sedimentation stability of the MRS should be still taken into the consideration because according to the Stokes' law, the sedimentation rate increases with the squared spherical particle radius (assuming fulfilled Stokes' law conditions). In this sense, the design of the MRS is always a compromise between high MR performance and sufficient sedimentation stability, which is usually ensured by applying the particles with the average diameter around 1–10 μm [27]. On the contrary, the MREs are stable against sedimentation which allows the incorporation of much larger particles [133], typically with the average diameter around 10–100 μm [110]. However, in some fabrication techniques of the MREs such as casting the particle sedimentation may play also a major role. To investigate the number of factors affecting the behavior of the MREs, Khimi et al. [110] designed the Taguchi method (a statistical method identifying the performance trends among multiple factors and determining their combination that yields the optimum results). This approach seems to be an effective tool in optimization of the MR systems for practical applications.

Undoubtedly, the shape of magnetic particles can severely affect the behavior of the MR systems. In principle, the particles having their major axis aligned with the direction of the EMF, i.e. rod-like particles, will have a higher induced moment and thus, the stiffer internal particles structures are formed when compared with their spherical analogues [134]. However, this aspect was found to be negligible at large particle contents and/or high magnetic field strengths [37]. The MRSs containing the rod-like particles moreover exhibited better sedimentation stability and structuration at lower magnetic fields [135], but their maximum volume fraction was less than desired 20–40 vol.% [134]. Eventually, the majority of the MRSs' research was performed on spherical particles (references e.g. [51, 53, 64, 104, 124]) probably due to their better availability from the commercial sources. In the MREs, the particles are locked in their positions in the matrix, thus their field-induced reorientation is practically impossible, although in soft matrices a certain particle rotation has been observed [136]. Therefore, the application of rod-like particles will not significantly increase magnetic permeability of the MREs when compared to their spherical analogues. To maximize magnetic permeability, the development of so called anisotropic MREs was proposed [32]. Such kind of the MREs is fabricated by particle alignment using the EMF during the curing process [69]. The anisotropic structures were found to increase the MR efficiency [137], electric conductivity [23], electromagnetic shielding capability and heat transport

properties [24] in the direction of the particle structures. These recent findings may significantly influence the development of the MREs in the near future as this approach basically allows achieving the desired utility property at lower particle volume fraction, which decreases weight of the MR devices.

Finally, it was found that also particle porosity can affect flow behavior of the MRSs. In the research performed by Vereda et al. [138] the porous iron suspensions exhibited atypical thickening behavior, which was not observed in their solid counterparts even if the particle size and magnetization were similar. The effect of particle porosity on the behavior of the MREs has not been studied yet, probably due to problematic embedding the particles into usually high-viscosity polymer matrices.

1.8.2 Dispersing Phase-Related Factors

The behavior of both MR systems is undoubtedly affected by the type of liquid medium or elastomeric matrix, respectively. Various surroundings utilized to design the MRSs or the MREs were briefly mentioned in Chapter 1.4. Here, more in-depth insights into the technology of the MR systems are given. Dealing with the MRSs, one must pay attention to the viscosity of carrier liquid with respect to the final application. Whereas the utilization of low viscosity liquid can lead to serious sedimentation instability, high viscosity inevitably increases the off–state MRS viscosity and eventually reduces the MR effect (Eq. 1) [106]. In the commercial MRSs it is also necessary to incorporate the thixotropic agents (e.g. metallic soaps as lithium and/or sodium stearate), dispersants (e.g. iron napthanate or iron oleate), anti-friction and anti-abrasion compounds. These additives are necessary to control not only the viscosity of the MRSs, but also sedimentation of the particles, the inter-particle friction, and they prevent fluid-thickening after several cycles of use [139].

As indicated further in Chapter 1.4, there is more variability in the continuous phase, when designing the MREs. Considering the wide range of elastomers and the possibility of their mutual miscibility [140] the number of possible matrices is impressively high. However, as recently published by eminent prof. Choi [141] the burdensome issue of the current MREs is their relatively high initial stiffness, thus the progress in the matrix-softening methods is expected.

Currently, there are several ways to control the matrix stiffness in the technology of MREs. The first approach is based on a reduction of the matrix cross-link density, which can be achieved by reducing the amounts of the cross-link agents [28, 29], or by tuning the ratio between the vulcanizing agent and the plasticizer such as sulfur and naphthenic oil, respectively [71]. Also, the incorporation of the particles treated with various surfactants such as fatty acids or calcium and aluminum soaps was shown to be an effective approach [70].

However, the use of low-molecular weight substances can cause durability problems as they have a tendency to migrate through the polymer matrix [142]. Other approach in controlling the MREs properties introduced by Gong et al. [72] involves the addition of polycaprolactone (PCL) as a temperature-controlled component. The PCL can transform from a semi-crystalline solid to a liquidated soft material once the temperature is increased above the PCL melting point. Thus, the MREs' stiffness properties can be controlled by varying the PCL content and temperature. Further, the matrix properties can be affected by the exposure to γ radiation [143], which is relevant mainly in aerospace and nuclear power station applications. As observed recently, the natural rubber-based MREs increased/decreased their off–state modulus depending on γ radiation dose, which was explained as a competition between cross-linking and degradation processes in the matrix. Although these approaches are effective in tuning the MREs properties, they rather omit the protection of the incorporated particles against high temperatures or acidic environment, which is essential in some practical applications [94]. Thus, there is a need to address the demands related to both, the performance and stability properties of the MREs, ideally in a single-step way. This topic was very recently solved by Cvek et al. [144], who applied the ATRP polymer-grafted particles into the MREs. Their particles were thermally and chemically resistant and at the same time, they ensured the appropriate matrix stiffness by modulating the matrix cross-link density in the vicinity of the particles.

1.8.3 Temperature

Temperature is considered as an important factor affecting the physical and mechanical properties of all the materials, which is in the case of the MR systems manifested in their MR efficiency changes. As presented above, some industrial or military applications require operations at elevated temperatures as a result of surrounding conditions or intense viscous heating [94]. This topic is unfortunately rather omitted and only sparse literature sources can be found. Aggravating fact is that the experiments in these studies were performed solely in the temperature range conditions close to ambient temperature [145]. However, these experimental studies unambiguously describe the "significant" reduction of the on-state τ in the MRSs with increasing temperature. The results of temperature sensitivity change slightly depending on the MRS used during the experiments, but generally an average normalized sensitivity of the MR dynamic yield stress is in order of –units × 10^{-3} °C^{-1} [145, 146]. This parameter describes the ratio between the change in the measured yield stress and the yield stress value at the reference temperature. The explanation of this phenomenon is not straightforward and one has to consider different functional relations that evolve with increasing temperature, such as decreasing particle magnetization (ferromagnetic material), intensified Brownian motion, decreased fluid viscosity, changes in expansion

coefficients of the particles and the fluid etc. These changes were mathematically described and correlated by Ocalan et al. [94]. In the practice, the reduction of the τ at high temperatures can be compensated by increasing the applied H. Interestingly, in less concentrated MRSs the opposite trend was observed, and the toughness of the induced internal structures generated in the MRSs increased with the temperature [147]. In any case, the design of the MRSs that withstand such demanding conditions has to be considered. The water-based MRSs are essentially excluded [66], while theoretically having more freedom in the choice of magnetic particles as they are generally characterized by the Curie temperature, T_C, well-above the tested temperatures (e.g. for iron, T_C = 770 °C) [94].

In the case of the MREs, the effect of temperature on their properties is probably even more relevant. The fact stems predominantly from their polymer basis, which is in some cases prone to thermo-oxidation. The undesirable aging and durability phenomena of the MREs were recently investigated through both theoretical and experimental approaches by Zhang et al. [140]. As known, the MR effect of the MREs tends to increase in a normal temperature range (20–90 °C) when the samples are exposed to the desired temperatures for only a limited period of time [148]. However, in the aging tests the MR effect of the *cis*-polybutadiene rubber-based MREs notably decreased after their several-hour aging at the temperature of 70 °C. The results showed that decrease of the MR effect was dependent on the type of rubber matrix, and aging conditions such as time and temperature [140].

In theory, the MR systems can be used in the middle latitudes or polar region, where the surrounding temperature can drop below water freezing-point due to seasonal changes. To the authors' knowledge, the literature dealing with the behavior of the MR systems in low temperatures is less than scarce, and the studies dealing with this topic would probably deserve more attention.

2. MOTIVATION AND AIMS OF THE DOCTORAL STUDY

2.1 Motivation

The MR systems belong among advanced materials that can change their physical properties upon the external magnetic stimulus. These materials play an important role in many disciplines ranging from automotive to civil or even biomedical engineering. In the first-mentioned field, they belong among safety systems (e.g. brakes, clutches, fast-response dampers) that can improve the comfort of passengers and contribute to lower risk of vehicle crash and consequently minimize the number of casualties and injuries. Further, the consequences of wind gusts and seismic vibrations in high-rise buildings can be efficiently reduced with the use of the vibration absorption components based on the MR systems. Their employment in medicine is in a stage of testing as drug delivery systems, or local embolization agents. The special-type particle modification may serve as a versatile tool to reduce specific as well as general drawbacks of presented MR systems across the utilization fields.

Despite the significant improvements and broad industrial applications, there are still certain physical phenomena that need to be clarified to understand and precisely predict the behavior of MR systems. Nowadays, the tailoring of the properties is of particular interest, which helps to design a material towards a specific application. The MR systems are among rapidly developing areas of materials science due to their unique properties allowing their versatile use. Figure 8 presents the number of articles published during the past 25 years devoted to the MR systems. The growth in the number of publications reflects the increasing interest in this field.

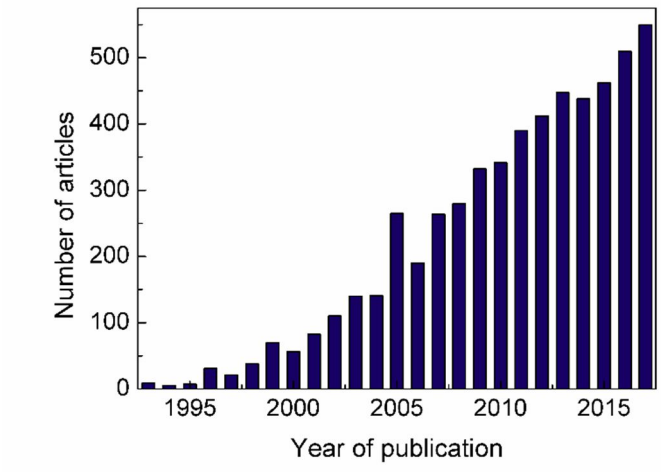

Figure 8. Number of articles published on "Web of Science" database during past 25 years (using the term magnetorheol as a topic item).*

2.2 Aims of the Doctoral Study

The main aim of the doctoral study was to eliminate common drawbacks of the conventional MR systems. The experimental work stems from the previously-published scientific papers describing the fundamental phenomena occurring in the MR systems, however the large portion of the results was not predicable and could not be obtained by any kind of simulation prior the laboratory experiments. Thus, the data was analyzed by comparing the performance and stability properties of the MR systems containing bare magnetic particles and their specifically-designed ATRP-grafted analogues. The key tasks were defined as follows:

a) Complex study of physical and chemical aspects affecting the performance of the conventional as well as recent MR systems.

b) Design and preparation of novel magnetic core-shell particles with tailored properties via surface-initiated ATRP, which could be successfully used as a dispersed phase in the MR systems in order to enhance their performance and stability properties.

c) Analysis of the shell thickness and graft molecular weight influences on magnetic properties, thermo-oxidation and chemical stability of as-designed particles.

d) Fabrication of the MR systems (suspensions or elastomers) containing the ATRP-modified particles and the study of their interactions with the dispersing medium and the elastomeric matrix, respectively.

e) The incorporation of submicron-sized additives into the MRSs and the investigation of their influence on complex behavior of such systems with the help of mathematical modeling and complementary experimental techniques.

f) Analysis of the effects of the particle modifications and additive incorporation on the MR performance, and other relevant utility properties (cytotoxicity, magnetostriction, redispersibility etc.) of as-designed MR systems. Evaluation of the systems' efficiency by comparing their properties with a reference based on bare magnetic particles.

3. OBJECTIVES OF THE WORK AND FINDINGS SYNOPSIS

The Thesis predominantly deals with the synthesis of precisely-defined core-shell particles and their possible use in the MR systems in order to reduce the outlined drawbacks of their conventional analogues. As the most of the framing papers is topically inter-connected via ATRP technique, the summary of performed syntheses and particles' general characterization are firstly given. Further, the most significant results of the individual papers are specified with respect to their primary emphasis.

3.1 Syntheses of Core-Shell Particles via ATRP

The advantages of core-shell structures in the MR systems are indisputable (Chapter 1.6.2), and shell characteristics play an important role in the overall performance and achieving high MR response. In this work, precisely-defined core-shell particles were prepared using the surface-initiated ATRP as a versatile synthesis tool. The CI particles were used as a substrate due to their suitable magnetic properties (Chapter 1.4). Under normal conditions the surface of the CI particles is covered with a thin oxide layer, therefore they were treated in acidic solution in order to increase their reactivity according to the procedure presented elsewhere [149]. Then, the activated CI particles were functionalized with (3-aminopropyl) triethoxysilane (3-APTES) and subsequently modified via amidation reaction with 2-bromoisobutyryl bromide (2-B*i*BB). The modified material was thoroughly washed and dried [89]. Finally, the surface-initiated ATRP of the desired monomer from the 2-B*i*BB-treated particles was performed and the core-shell structures grafted with either poly(glycidyl methacrylate) (PGMA) or poly(trimethylsilyloxyethyl methacrylate) (PHEMATMS) as different shells materials were synthesized (Figure 9).

The former shell variant was chosen due to suitable polymerization kinetics of its monomer during the ATRP and the presence of the oxyrane groups preserving the possibility to bond other substances [150]. The CI particles grafted with PGMA (CI-*g*-PGMA) were utilized to prepare novel MRSs (Papers I, II). The PHEMATMS was used as a shell material modifying the CI particles resulting in CI-*g*-PHEMATMS intended for use as the filler in the MREs (Papers III, IV). The PHEMATMS is hydrophobic, thus it was assumed that this silyl-based polymer will enhance the interaction of the CI particles with poly(dimethylsiloxane) (PDMS) representing the matrix material in newly-designed MREs. The shell thicknesses expressed as molar mass of PGMA and PHEMATMS were controlled by tailoring the monomer : initiator ratio, reaction time and temperature.

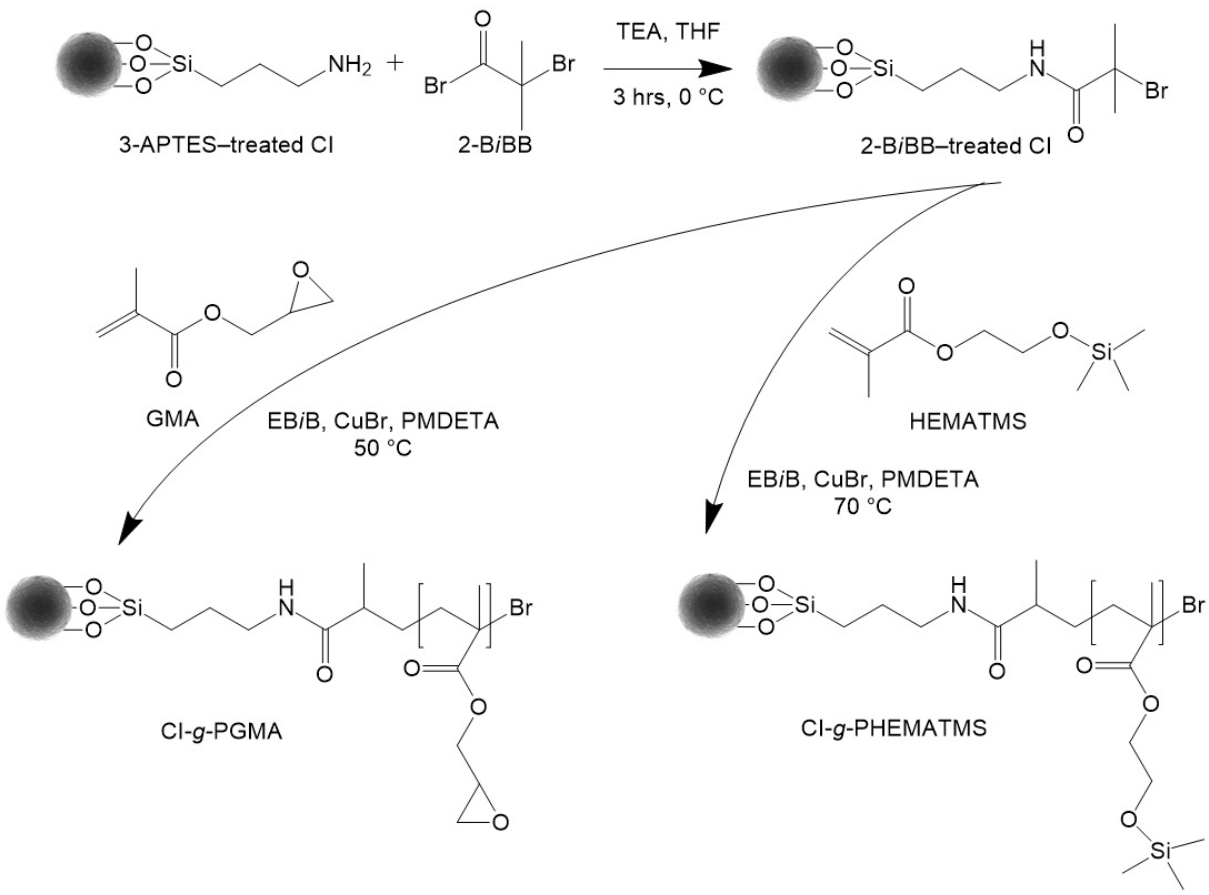

Figure 9. Immobilization of 2-BiBB initiator on functionalized CI particles with their subsequent grafting with PGMA and PHEMATMS via surface-initiated ATRP. The names of the chemicals are explained below[*].*

For each reaction, the feed ratio between the monomer and the initiator was tailored in order to obtain the desired shell thickness, and its maximal value was theoretically determined before the experiment. Thus, two different molecular weights of each polymer shell (sample code 1 and 2), consisting of either PGMA or PHEMATMS, respectively, were prepared and characterized. The determination of their molecular weight was possible due to the presence of a sacrificial initiator, namely ethyl 2-bromoisobutyrate (EB*i*B) in the reaction system. Molecular weight of grafted polymers and monomer conversions were obtained via gel permeation chromatography (GPC) and nuclear magnetic resonance (NMR) spectroscopy, respectively. The GPC results were evaluated considering the assumption of Goncalves et al. [151] and together with NMR ones they are summarized in Table 1. A relatively low dispersity index (*Đ*) reflects a high polymerization control via ATRP and uniformity of grafted polymer layers.

[*] *TEA – Triethyleneamine, THF – Tetrahydrofuran, EBiB – Ethyl 2-bromoisobutyrate, CuBr – Copper bromide, PMDETA – N,N,N',N'',N''-Pentamethyldiethylenetriamine*

Table 1. Conversion and molecular characteristics of prepared core-shell particles.

sample code	conversion[a] (%)	$\bar{M}_W$ (g·mol^{-1})	$\bar{M}_n$ (g·mol^{-1})	$Đ$ (–)
CI-*g*-PGMA-1	87.0	6 600	5 000	1.32
CI-*g*-PGMA-2	88.5	12 500	9 700	1.29
CI-*g*-PHEMATMS-1	90.0	11 800	9 200	1.28
CI-*g*-PHEMATMS-2	75.0	23 500	17 900	1.31

[a]Based on ^{1}H NMR spectra

3.2 Characterization of Prepared Particles

To limit the size of this Thesis summary, only some results are presented. For more data, the reader will be referred to the corresponding articles. The transmission electron microscopy (TEM) images were acquired to observe the thicknesses and uniformity of grafted layers. Figures 10b and 10c show the presence of a lower contrast polymer shell grafted onto the darker CI core. As can be seen, the grafted layers were generally uniform in both cases with the thicknesses of around ~15 nm and ~35 nm. The increasing molar mass of the grafted polymer thus led to increasing layer thickness.

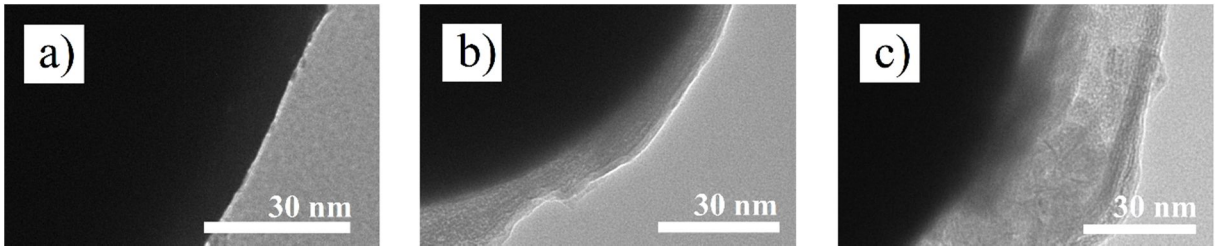

Figure 10. TEM images of bare CI (a), CI-g-PHEMATMS-1 (b), and CI-g-PHEMATMS-2 (c) showing a part of the corresponding single particle.

The energy-dispersive spectroscopy (EDS) and Fourier-transform infrared (FTIR) spectroscopy were used in order to verify the presence of polymer brushes grafted onto the CI substrate. Besides strong peaks representing iron, the EDS spectra generally confirmed the presence of expected elements coming from APTES and 2-B*i*BB residues, and the presence of elements constituting the

PGMA or PHEMATMS polymer grafts. The core-shell particles with higher molecular weight contained slightly higher percentage of carbon when compared to their thinner-shell analogues. Additionally, the peaks occurring in FTIR spectra confirmed the presence of expected functional groups in all samples, thus the ATRPs performed on the CI particles were proved to be successful. More detailed data descriptions are shown in already published papers by Cvek et al. [28, 89].

The magnetic properties of bare CI particles as well as their polymer-grafted analogues were investigated using a vibrating-sample magnetometry (VSM). The magnetization of the CI particles decreased due to the presence of both non-magnetic coatings – PGMA (please see full paper by Cvek et al. [89]) and PHEMATMS (Figure 11) – however, the decrease was negligible as the shell thicknesses were controlled via ATRP means to be in nanometer scale. Admittedly, the presence of thicker shells further reduced particle magnetization, but this difference can be interpreted as rather marginal. At the maximum employed field (780 kA·m^{-1}), the PHEMATMS coatings decreased magnetization by less than ~10 % when compared to the magnetization of bare CI (Figure 11, inset). The reported magnetization decrease of core-shell particles prepared via conventional methods was more than ~50 % [152]. Furthermore, at the examined temperature the particles preserved their almost hysteresis-free character, small coercivities, and remanent magnetizations suggesting fast demagnetization processes important for the implementation to the MR applications.

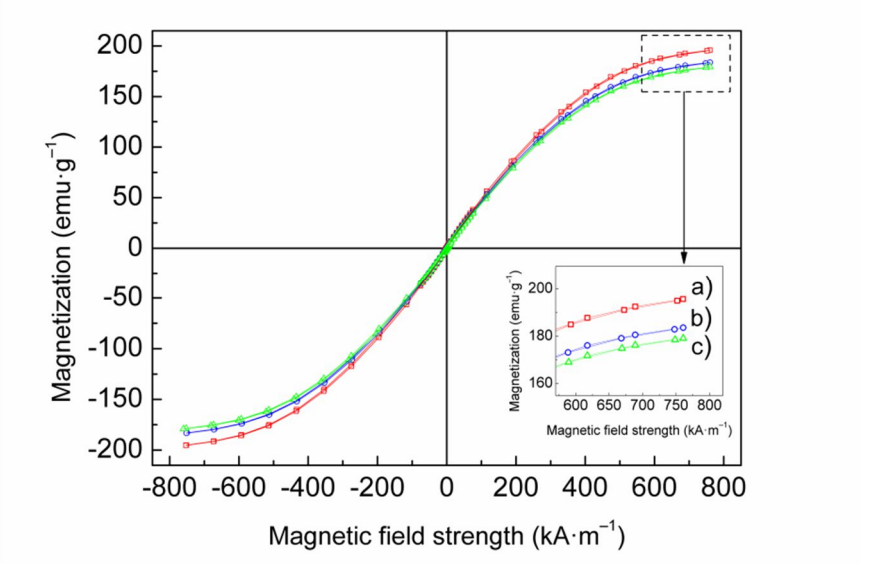

Figure 11. Magnetization curves of bare CI (a), CI-g-PHEMATMS-1 (b), and CI-g-PHEMATMS-2 (c) particles obtained using VSM. The inset figure shows the data differences near the saturation magnetization.

In service life, the MR systems can be exposed to demanding operating conditions such as high temperatures or acidic reactive species (e.g. acid rains, sea humidity, operating fluid leakage), which are key factors affecting their long-

term stability and durability [69]. Therefore, the effects of grafted polymer layers and their thicknesses on thermo-oxidation and chemical stability of the particles were also thoroughly investigated. The thermo-oxidative stability of the particles was analyzed using a thermogravimetric analysis (TGA). Figure 12a summarizes the results obtained by Cvek et al. [89] showing the TGA curves of all the studied particles. Comparing the thermo-oxidation process of bare CI particles and their PGMA- as well as PHEMATMS-grafted analogues a significant difference is notable. The presence of polymeric layers generally shifted the beginning of the particle thermo-degradation to higher temperatures, as these layers effectively shielded the iron core, which is susceptible to oxidize.

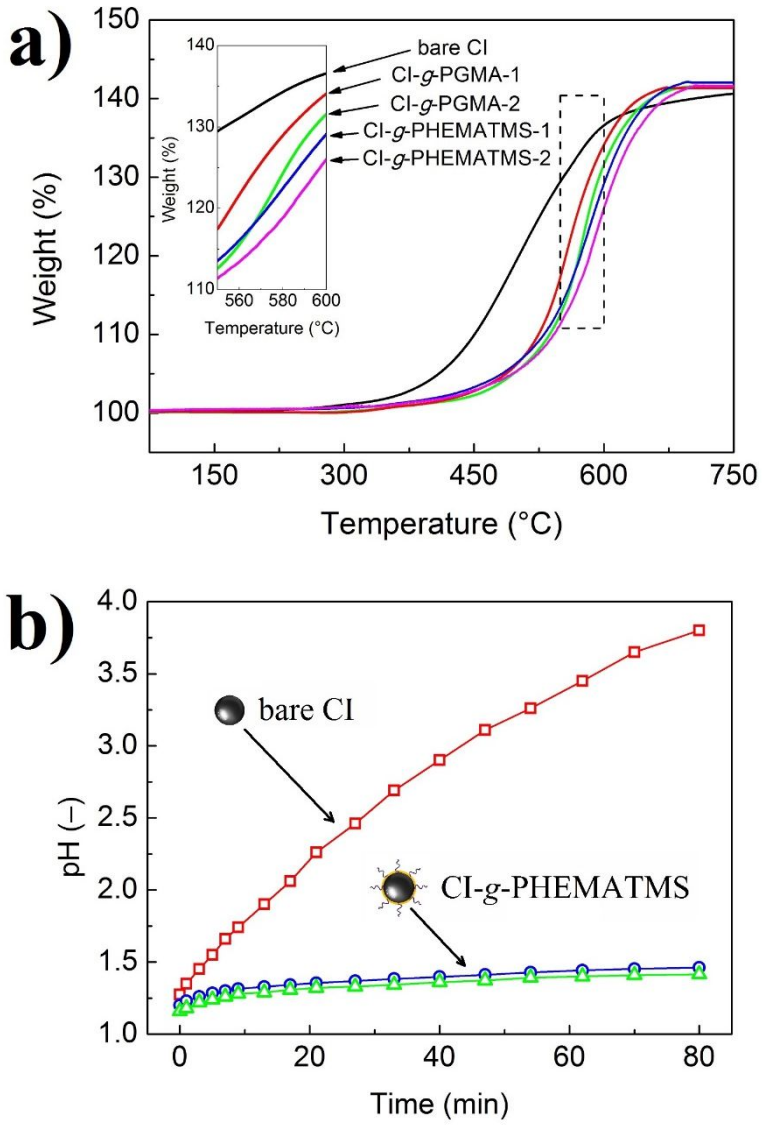

Figure 12. TGA curves of bare CI particles and their PGMA- or PHEMATMS-grafted analogues (a), and the comparison between the chemical stability of bare CI particles and their PHEMATMS-grafted analogues (b).

The chemical stability of the particles was examined by a facile corrosion test [25, 88, 93]. Here, the particles were dispersed in acidic solution (0.1 M HCl), while pH value was recorded as a function of time. As seen in Figure 12b, bare CI particles were relatively unstable in acidic environment, which caused the decrease of their magnetic properties [25, 88]. Both variants of CI-*g*-PHEMATMS particles were however extremely stable indicating that the grafted layers were compact without any defects and the CI core was efficiently protected. The similar results were obtained also for the particles' variant with PGMA shell [88]. To conclude, the presence of polymer shell is necessary to enhance stability of the CI particles (assuming compact shell without defects) but its thickness plays rather a minor role for further stability enhancement.

3.3 Enhancements of the MRSs

Having thermally- and chemically-stable magnetic particles allowed their further implementation into the MR systems. First, the appropriate amounts of either bare CI particles or their PGMA-grafted analogues were dispersed in silicone oil to prepare novel stable MRSs. The effects of the PGMA layers and their thicknesses on the MR performance and sedimentation stability were investigated and the results were introduced in ***Paper I – A facile controllable coating of carbonyl iron particles with poly(glycidyl methacrylate): A tool for adjusting MR response and stability properties***. The MR behavior of the representative MRSs was obtained using a rotational rheometer equipped with a magneto-cell device and a parallel plate geometry. Uniformity of the EMF, suspension sedimentation and the wall slip phenomenon as major possible issues related to magnetorheometry were considered [153]. The repeatability and accuracy of the data was ensured by following the protocol [33]. Figure 13 illustrates the rheological data obtained from the CSR mode for the examined MRSs. Generally, the obtained flow curves exhibited typical characteristics for the MRSs. In the off–state, almost Newtonian-like behavior corresponding to the linear increase of the τ with $\dot{\gamma}$ was observed, while in the on–state the yield stress appeared and the τ values of all MRSs dramatically increased and the flow became pseudoplastic [5, 27, 32]. Admittedly, the presence of PGMA grafts slightly increased off–state τ (and consequently η), while decreasing the on–state τ values resulting in a weaker response to the EMF. Nevertheless, these changes were much smaller than those in the conventional core-shell systems [112]. From obvious reasons, the MR behavior was more affected when CI-*g*-PGMA-2 particles were used as a dispersed. In order to exclude possible data distortion, the off–state flow curves are not shown within the whole $\dot{\gamma}$ range due to the inappropriateness of measuring MR geometry for low $\dot{\gamma}$ as was also presented by authors [154]. The results suggest that the MRSs containing PGMA-grafted

particles synthesized via ATRP are able to develop considerable τ sufficient for practical applications.

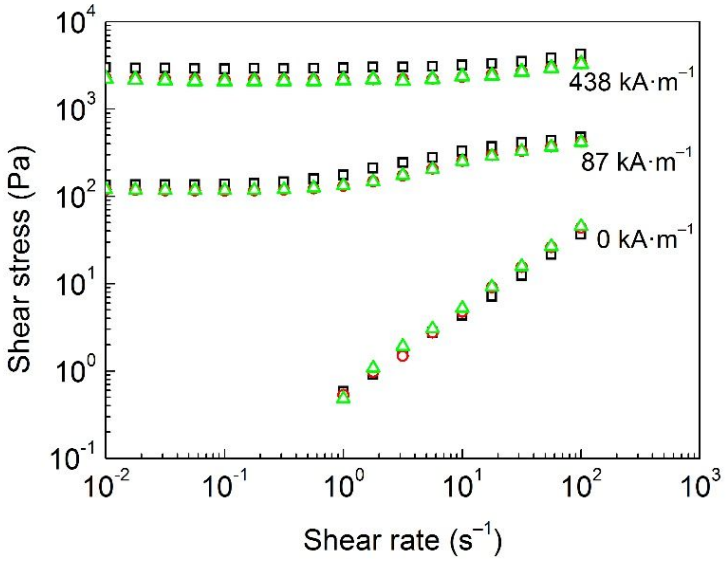

Figure 13. The dependences of the shear stress on the shear rate for the MRSs containing 40 wt.% of bare CI particles (open squares), CI-g-PGMA-1 particles (open circles), or CI-g-PGMA-2 particles (open triangles) under various magnetic field strengths.

Further, the sedimentation stability of tested MRSs was determined via tensiometric method which was recently proposed by Sedlacik et al. [93]. In this method, the funnel-shaped probe hanging up on scales is immersed into the tested suspension, and the weight of settling particles is measured as a function of time (Figure 14). In order to avoid the overfilling of the probe during the experiment, the particle concentration of the MRSs was set to 10 wt.%. Based on the results, it is evident, that the use of CI-*g*-PGMA particles as dispersed phase considerably enhanced sedimentation stability of the MRSs when compared to their analogue containing the same amount of bare CI particles. Improved sedimentation stability is explained as a consequence of PGMA grafts which contributed to reduced bulk density of composite particles and better compatibility with silicone oil [5, 27]. The MRSs containing both variants of PGMA-grafted CI particles exhibited similar sedimentation stability, but the molecular weight of PGMA did not play that important role as expected.

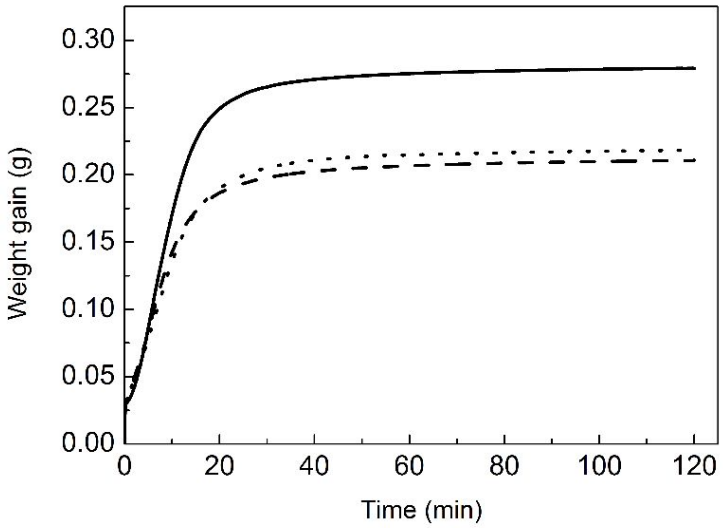

Figure 14. Time dependences of the weight gain representing settled particles of the MRSs containing 10 wt.% of bare CI particles (solid line), CI-g-PGMA-1 particles (dotted line), or CI-g-PGMA-2 particles (dashed line).

Apart from the industrial applications, the magnetic particles have also found promising applicability in biomedical field, e.g. in cancer therapy through embolization of blood veins [155], local drug delivery [156], or cell therapy [157]. According to Silva et al. [156] the use of magnetic microparticles (0.5–5 μm) is necessary in order to target organs that lie deeply in the body cavity (8–12 cm from the body surface). Besides that, the PGMA contains the oxyrane group preserving the possibility to bond other substances [150] and recently this polymer has gained interest in drug and biomolecule binding. Therefore, the special combination of materials such as CI-*g*-PGMA particles was investigated as a versatile platform for possible biomedical applications in ***Paper II – The chemical stability and cytotoxicity of carbonyl iron particles grafted with poly(glycidyl methacrylate) and the magnetorheological activity of their suspensions***. It was found, that CI-*g*-PGMA exhibited extremely enhanced anti-acid-corrosion stability enabling their potential application in medicine. Further, their cytotoxicity was tested according to the international standard EN ISO 10993-5 using NIH/3T3 mouse embryonic fibroblast cell line (ATCC, CRL-1658). Subsequently, the particle extracts were prepared according to ISO 10993-12 and diluted to desired concentrations. The cytotoxicity was evaluated using MTT assay, which was analyzed using microscopic observations. Figure 15a–c shows the effect of extracts on the cell morphologies. Based on the results it was stated that bare CI particles as well as their PGMA-grafted analogues belong to the category with the absence of cytotoxicity within the whole tested concentration range (please see full paper [88]). The absence of cytotoxicity,

gained functionality, and preserved magnetization make the CI-*g*-PGMA particles very interesting from a further research point of view. Moreover, the rheological data of the investigated MRSs was analyzed using the H–B model (Eq. 4) in order to predict possible τ_0 decrease caused by the polymer grafts. Due to controllable coating via ATRP the decreases in magnetization were considered to be insignificant, which was also reflected in slightly decreased MR efficiency (Figure 15). Assuming these findings CI-*g*-PGMA particles prepared via ATRP were found to be a versatile material for miscellaneous applications.

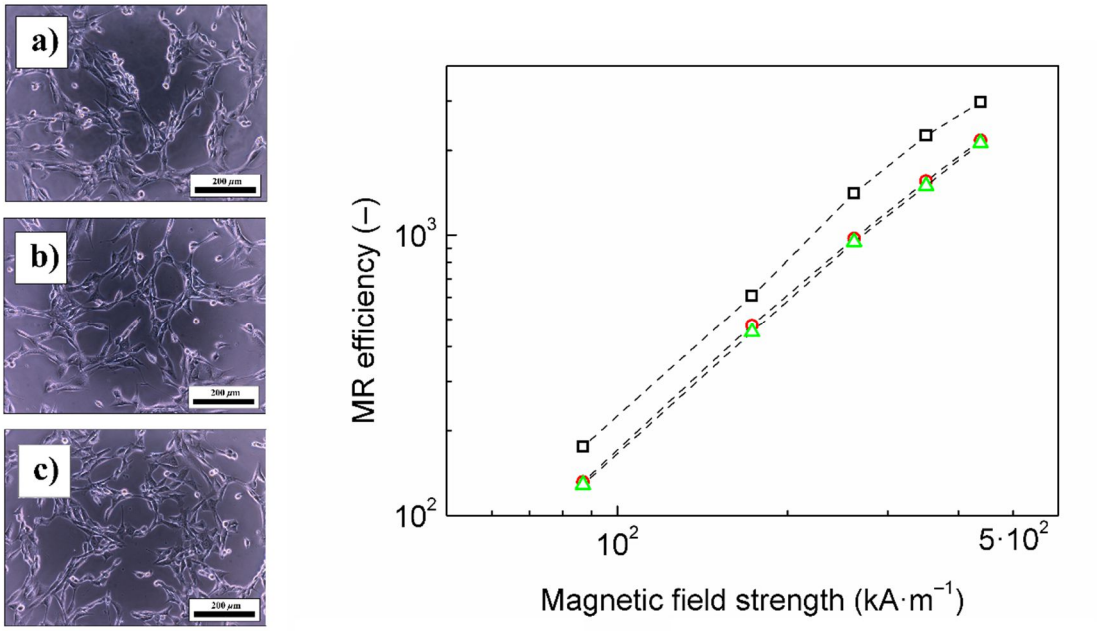

Figure 15. Micrographs of the NIH/3T3 mouse embryonic fibroblast cell line treated with 50% CI extract (a), 50% CI-g-PGMA extract (b), and the reference (c). On the right-hand side the dependences of the MR efficiency on the applied magnetic field strength for the MRSs containing 40 wt.% of bare CI particles (open squares), CI-g-PGMA-1 particles (open circles) or CI-g-PGMA-2 particles (open triangles) are presented.

3.4 Enhancements of the MREs

To fabricate the MREs with enhanced thermo-oxidation stability, chemical stability and improved particle/matrix compatibility the CI-*g*-PHEMATMS particles were used as a suitable filler. This topic was the main objective of ***Paper III – Synthesis of silicone elastomers containing silyl-based polymer-grafted carbonyl iron particles: An efficient way to improve magnetorheological, damping and sensing performances.*** In this research, the desired amounts of either bare CI particles or their PHEMATMS-grafted analogues were mixed with the silicone elastomer/curing agent components and

the homogeneous mixture was casted into the molds. The curing process was accelerated by elevated temperature (100 °C) to obtain the isotropic MREs (concentration of 60 wt.%). The representative samples were tested using a rotational rheometer under dynamic conditions and the applied EMF. Firstly, the γ-sweeps under various H were performed to ensure that all the data fall into the LVR. Besides the MR effect, the MREs were shown to exhibit magnetostriction and hysteresis behavior [60] when exposed to the ascending/descending EMFs. The shear viscoelastic moduli, and damping factor were recorded as a function of H (Figure 16), while the ascending/descending character of H was denoted by the arrows.

As clearly seen, the fabricated MREs exhibited characteristics typical for magnetically-active materials. Expectedly, the G' of neat matrix (as a reference) was independent on the applied H due to the absence of magnetic particles, however the G' distinctly increased by the addition of the CI particles, since rigid inorganic particles have a much higher stiffness than PDMS matrix [158]. The increase of G' with the H was explained by gradual particle magnetization and magnetic interactions resulting in particle network formation, which reinforced the MRE structure. For more details, please see the full article by Cvek et al. [28].

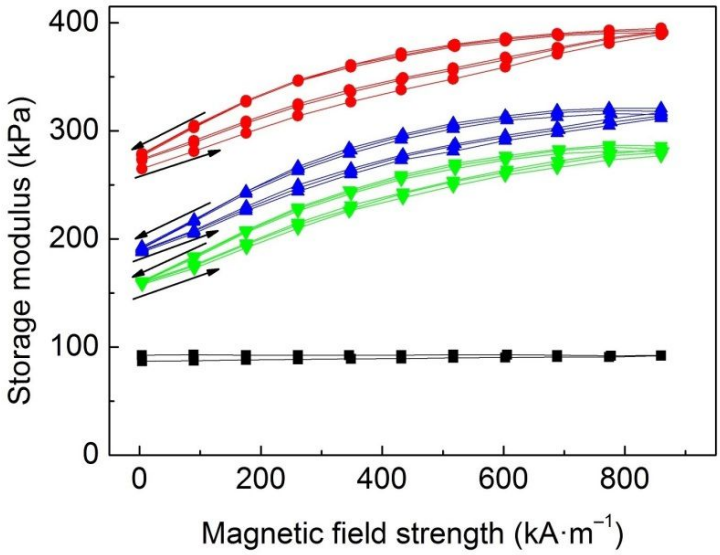

Figure 16. The storage modulus of neat matrix (black squares), and the MREs containing bare CI (red circles), CI-g-PHEMATMS-1 (blue up–triangles), and CI-g-PHEMATMS-2 (green down–triangles) particles as a function of applied magnetic field strength.

In particular, the effect of PHEMATMS coating on viscoelastic properties of the MREs was evaluated. Surprisingly, the highest *G'* possessed the MRE containing bare CI, which was explained as a consequence of possible particle/matrix chemical bonding as the hydroxyl groups on the surface of bare CI particles can form covalent bonds with the silane-groups of PDMS curing agent [70]. Nevertheless, it is believed that the bonding was limited due to poor adhesion between these two materials. As it was shown via microstructure analysis (Figure 17), bare CI particles were surrounded by the cavities as the result of particle/matrix incompatibility, which can consequently lead to decreased mechanical properties over time. However, the presence of PHEMATMS grafts increased the particle mobility within the matrix most likely due to loosen PDMS cross-link density in the vicinity of the particles. This phenomenon was more pronounced in the MRE containing CI-*g*-PHEMATMS-2 due to the presence of longer grafts, which enabled higher relative particle motions as a reaction on the applied EMF. As a result, the MREs containing the PHEMATMS-grafted particles ultimately exhibited increased relative MR effects (Eq. 1), which suggests their versatility and better practical applicability.

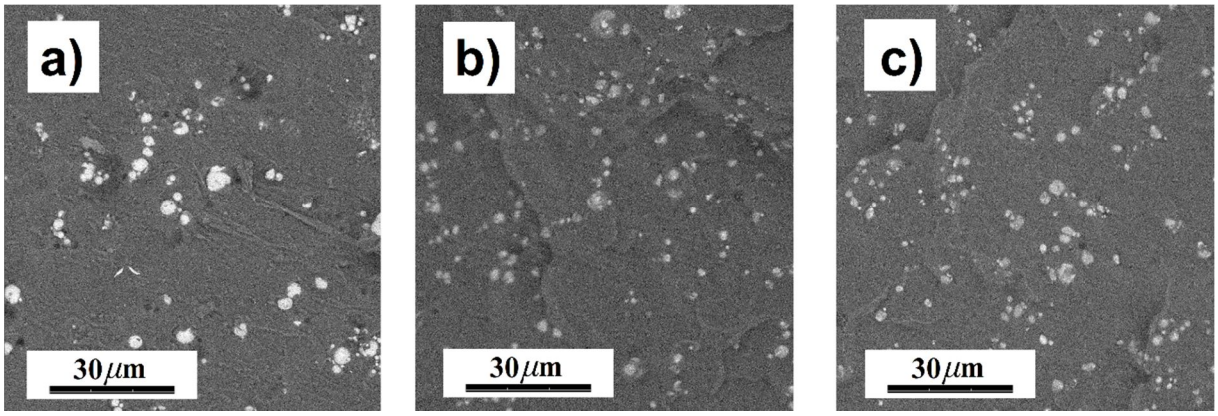

Figure 17. SEM images of the isotropic MREs containing bare CI (a), CI-g-PHEMATMS-1 (b) and CI-g-PHEMATMS-2 (c) particles.

The principal function of the MREs is their damping capability. As indicated above (Chapter 1.8.2), the damping control of the MREs can be executed via the incorporation of temperature-sensitive components [72] or by the addition of plasticizers [71]. These approaches may fail when the MREs are exposed to demanding operating conditions such as extreme temperatures or chemically-contaminated environment inducing the particle degradation and the loss of the MR performance. Therefore, the main idea of ***Paper IV – Tailoring performance, damping and stability properties of magnetorheological elastomers via particle-grafting technology*** was to develop a new concept, which allows enhancing the both, performance and stability properties of the MREs preferably in a single-step procedure. The stability properties of modified particles were assessed above (Figure 12). However, the PHEMATMS-grafted particles were found to be multi-

functional because due to the different molecular weight of PHEMATMS they modulated particle/matrix interface to a different degree. Therefore, the effect of the PHEMATMS molecular weight on the damping capability was investigated. As known [159], total damping capability of the MREs includes several damping mechanisms, namely damping by the viscous flow of the rubber matrix, interfacial damping and magnetism-induced damping. As demonstrated in Figure 18, the viscous flow mechanism appeared to be the main contribution for damping as the neat PDMS exhibited the average damping factor of ~0.155. The inclusion of particles generally enabled additional damping mechanisms. The incorporation of bare CI particles, however decreased the damping capability, which straighten the theory that bare CI particles rather acted as micro-cavities in the body of the matrix. The presence of CI-*g*-PHEMATMS particles increased particle mobility and energy dissipation (associated with interfacial slipping between particles and the matrix) and impressive enhancements of damping properties occurred. The MRE containing the CI-*g*-PHEMATMS-2 particles achieved the average damping factor of ~0.234, which was explained as a consequence of the additional interfacial friction as a result of higher molecular weight PHEMATMS grafts occurrence. Finally, herein fabricated MREs exhibited similar damping capability as the recently-reported ones [31], however at lower particle fractions, which offers not only high MR performance, but also light weight and enhanced stability properties.

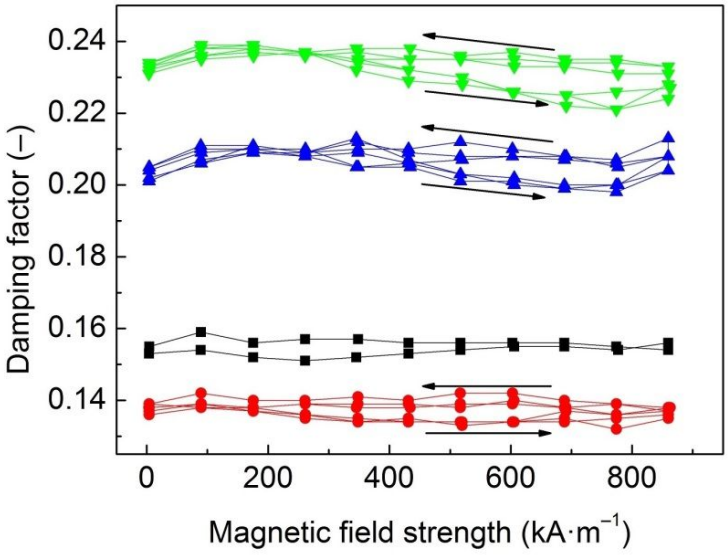

Figure 18. The damping factor of neat matrix (black squares), and the MREs containing bare CI (red circles), CI-g-PHEMATMS-1 (blue up–triangles), and CI-g-PHEMATMS-2 (green down–triangles) particles as a function of applied magnetic field strength.

3.5 Stabilization of MRSs using additives

The incorporation of submicron-sized additives into the MRSs is known as a facile approach to enhance their sedimentation stability [96-98], redispersibility [104] and in some cases also the MR performance [160]. Using the additives, no special or toxic chemicals are needed making this method feasible and preferable for large-scale applications. As reviewed above (Chapter 1.6.3), many different materials have been used as possible additives to stabilize the MRSs. It is important to mention that there is no standardized procedure to evaluate the effects of the individual additives, thus their unbiased efficiency is still unclear. Therefore, the motivation of ***Paper V – A systematical study of the overall influence of carbon allotrope additives on performance, stability and redispersibility of magnetorheological fluids*** was to introduce different shaped carbon additives (fullerene powder, carbon nanotubes, graphene nanoplatelets) into the MRSs and to methodically investigate their effects under defined conditions with the help of mathematical modelling and complementary experimental techniques. The MR performance of the MRSs was analyzed using the R–S model (Eq. 5) providing reliable data fits. It was found, that even 1 wt.% of the additives inevitably increased the off–state shear stress values of the MRSs. At the on–state, two different manifestations of the additives were distinguished. While the presence of fullerene powder anchored the field-induced CI particle structures possessing the "gap-filling" effect, the other employed additives rather disrupted the particle structures decreasing the obtained shear stress values. The differences were studied in the CSR mode, but they were also apparent under periodically changing magnetic field (Figure 19).

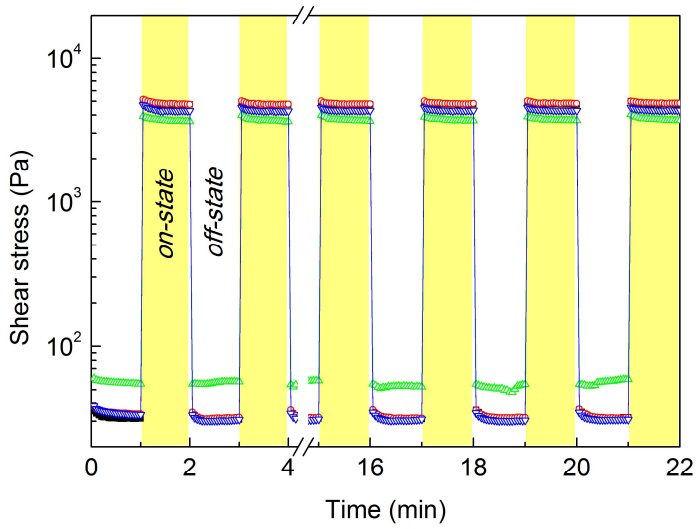

Figure 199. The shear stress vs. time dependences during periodically switching off/on magnetic field (~288 kA·m^{-1}) at a shear rate of 50 s^{-1} for the reference sample (black), and the MRSs containing 1 wt.% of fine fullerene powder (red), the carbon nanotubes (green), or the graphene nanoplateles (blue).

On the contrary, the carbon nanotubes and graphene nanoplateles as the additives decreasing the MR performance were able to enhance the sedimentation stability of the MRSs. The most significant stabilization effect was achieved using the carbon nanotubes, which were able to create a 3D network preventing the CI particle sedimentation. This result was complementarily proved by both, the conventional long-term direct observation and the advanced optical analyzer, i.e. Turbiscan. Finally, the recommendations to design the MRSs for practical applications were given. Based on the results, the optimization of the MRSs behavior could be based on combining the additives varying in the mechanism of their action (gap-filling, sedimentation enhancing effect) to ensure the both, rigidity of the internal structures as well as the sufficient sedimentation stability.

4. Contributions to the Science and Practice

The results obtained within this doctoral study will be beneficial to scientific community especially due to presented approach in particle's modifications using surface-initiated ATRP from the magnetic substrate leading to a design of particle's properties towards a specific application.

The achieved results were already presented at several international conferences and published in high-quality international peer-reviewed journals registered in *Scopus* and *Web of Science* databases. Some of the author's publications have already been numerously cited by foreign scientists demonstrating the interest in the subject and confirming its scientific relevance.

From the practical perspectives, the long-term stability enhancement of newly-designed MR systems can be pointed out, which is currently a very desirable aspect. The novel idea also covers the reliability and durability of the MR systems, which can prolong their service life and, thus, safe costs which were accompanied with their short-term replacements in the past.

The significance of the research outputs is expected to increase in following years due to increasing amount of the commercially available MR devices utilized in real-life applications.

5. CONCLUSIONS

Some of the common drawbacks of the conventional MRSs and MREs were successfully eliminated using a novel approach based on the fabrication of the precisely-defined core-shell structures via surface-initiated ATRP. The particle's modifications were performed in a controlled way, thus the potential of prepared materials exceeded the properties of the existing systems. The physical phenomena related to particle/matrix interaction were clarified, which may affect the development of the next-generation MREs. Although the approach involving ATRP is not straightforward, it offers a great possibility to enhance properties of the MR systems in a controlled way, which was not possible to achieve using the conventional methods. Besides the presented applications, the ATRP may found utilization in other research areas such as biology and medicine in which well-defined modification of magnetic substrate is necessary. Finally, the introduced methodological approach to evaluate the performance and stability of the MRSs may serve as a suitable tool to test the specific effect of the individual additives incorporated in the MRSs and to optimize these for practical applications.

6. REFERENCES

[1] WINSLOW, W.M. Method and means for translating electrical impulses into mechanical force. US Patent No. US2417850 A. Issued March, **1947**.

[2] RABINOW, J. Magnetic fluid torque and force transmitting device. US Patent No. US2575360 A. Issued November, **1951**.

[3] WANG, J.; MENG, G. Magnetorheological fluid devices: principles, characteristics and applications in mechanical engineering. *Proc. Inst. Mech. Eng., Part L*. **2001**; vol. 215, pp. 165–74.

[4] CHOI, S.B.; LI, W.H.; YU, M.; DU, H.P.; FU, J.; DO, P.X. State of the art of control schemes for smart systems featuring magneto-rheological materials. *Smart Mater. Struct*. **2016**; vol. 25, 043001.

[5] PARK, B.J.; FANG, F.F.; CHOI, H.J. Magnetorheology: materials and application. *Soft Matter*. **2010**; vol. 6, pp. 5246–53.

[6] STRECKER, Z.; MAZUREK, I.; ROUPEC, J.; KLAPKA, M. Influence of MR damper response time on semiactive suspension control efficiency. *Meccanica*. **2015**; vol. 50, pp. 1949–59.

[7] SUN, S.S.; YANG, J.; DENG, H.X.; DU, H.; LI, W.H.; ALICI, G.; et al. Horizontal vibration reduction of a seat suspension using negative changing stiffness magnetorheological elastomer isolators. *Int. J. Veh. Des.* **2015**; vol. 68, pp. 104-18.

[8] WANG, D.H.; LIAO, W.H. Magnetorheological fluid dampers: A review of parametric modelling. *Smart Mater. Struct.* **2011**; vol. 20, 023001.

[9] LI, Y.C.; LI, J.C.; LI, W.H.; SAMALI, B. Development and characterization of a magnetorheological elastomer based adaptive seismic isolator. *Smart Mater. Struct*. **2013**; vol. 22, 035005.

[10] LI, Y.C.; LI, J.C.; TIAN, T.F.; LI, W.H. A highly adjustable magnetorheological elastomer base isolator for applications of real-time adaptive control. *Smart Mater. Struct.* **2013**; vol. 22, 095020.

[11] CINQ-MARS, M.; GUROCAK, H. Pneumatic cylinder with magnetorheological brake using serpentine and helix flux guide as a linear hybrid actuator for haptics. *J. Intell. Mater. Syst. Struct.* **2017**; vol. 28, pp. 1303–21.

[12] GUO, J.; GUO, S.X.; SHAO, L.; WANG, P.; GAO, Q. Design and performance evaluation of a novel robotic catheter system for vascular interventional surgery. *Microsyst. Technol.* **2016**; vol. 22, pp. 2167–76.

[13] JIANG, N.; SUN, S.S.; OUYANG, Y.M.; XU, M.; LI, W.H.; ZHANG, S.W. A highly adaptive magnetorheological fluid robotic leg for efficient terrestrial locomotion. *Smart Mater. Struct.* **2016**; vol. 25, 095019.

[14] KOSTAMO, E.; FOCCHI, M.; GUGLIELMINO, E.; KOSTAMO, J.; SEMINI, C.; BUCHLI, J.; et al. Magnetorheologically damped compliant foot for legged robotic application. *J. Mech. Des.* **2014**; vol. 136, 021003.

[15] KORDONSKI, W.; SHOREY A. Magnetorheological (MR) jet finishing technology. *J. Intell. Mater. Syst. Struct*. **2007**; vol. 18, pp. 1127–30.

[16] SIDPARA, A.; DAS, M.; JAIN, V.K. Rheological characterization of magnetorheological finishing fluid. *Mater. Manuf. Processes.* **2009**; vol. 24, pp. 1467–78.

[17] RIGBI, Z.; JILKEN, L. The response of an elastomer filled with soft ferrite to mechanical and magnetic influences. *J. Magn. Magn. Mater.* **1983**; vol. 37, pp. 267–76.

[18] LI, Y.C.; LI, J.C.; LI, W.H.; DU, H.P. A state-of-the-art review on magnetorheological elastomer devices. *Smart Mater. Struct.* **2014**; vol. 23, 123001.

[19] SOROKIN, V.V.; ECKER, E.; STEPANOV, G.V.; SHAMONIN, M.; MONKMAN, G.J.; KRAMARENKO, E.Y.; et al. Experimental study of the magnetic field enhanced Payne effect in magnetorheological elastomers. *Soft Matter.* **2014**; vol. 10, pp. 8765–76.

[20] BOSE, H.; RABINDRANATH, R.; EHRLICH, J. Soft magnetorheological elastomers as new actuators for valves. *J. Intell. Mater. Syst. Struct.* **2012**; vol. 23, pp. 989–94.

[21] LAM, K.H.; CHEN, Z.H.; NI, Y.Q.; CHAN, H.L.W. A magnetorheological damper capable of force and displacement sensing. *Sens. Actuators, A* **2010**; vol. 158, pp. 51–9.

[22] ZRINYI, M.; SZABO, D. Muscular contraction mimiced by magnetic gels. *Int. J. Mod. Phys., B.* **2001**; vol. 15, pp. 557–63.

[23] MOUCKA, R.; SEDLACIK, M.; CVEK, M. Dielectric properties of magnetorheological elastomers with different microstructure. *Appl. Phys. Lett.* **2018**; vol. 112, 122901.

[24] CVEK, M.; MOUCKA, R.; SEDLACIK, M.; BABAYAN, V.; PAVLINEK, V. Enhancement of radio-absorbing properties and thermal conductivity of polysiloxane-based magnetorheological elastomers by the alignment of filler particles. *Smart Mater. Struct.* **2017**; vol. 26, 095005.

[25] SEDLACIK, M.; MRLIK, M.; BABAYAN, V.; PAVLINEK, V. Magnetorheological elastomers with efficient electromagnetic shielding. *Compos. Struct.* **2016**; vol. 135, pp. 199–204.

[26] BEHROOZ, M.; GORDANINEJAD, F. A flexible micro fluid transport system featuring magnetorheological elastomer. *Smart Mater. Struct.* **2016**; vol. 25, 025011.

[27] de VICENTE, J.; KLINGENBERG, D.J.; HIDALGO-ALVAREZ, R. Magnetorheological fluids: A review. *Soft Matter.* **2011**; vol. 7, pp. 3701–10.

[28] CVEK, M.; MRLIK, M.; ILCIKOVA, M.; MOSNACEK, J.; MUNSTER, L.; PAVLINEK, V. Synthesis of silicone elastomers containing silyl-based polymer grafted carbonyl iron particles: An efficient way to improve magnetorheological, damping, and sensing performances. *Macromolecules.* **2017**; vol. 50, pp. 2189–200.

[29] FAN, Y.C.; GONG, X.L.; JIANG, W.Q.; ZHANG, W.; WEI, B.; LI, W.H. Effect of maleic anhydride on the damping property of magnetorheological elastomers. *Smart Mater. Struct.* **2010**; vol. 19, 055015.

[30] CHERTOVICH, A.V.; STEPANOV, G.V.; KRAMARENKO, E.Y.; KHOKHLOV, A.R. New composite elastomers with giant magnetic response. *Macromol. Mater. Eng.* **2010**; vol. 295, pp. 336–41.

[31] SHUIB, R.K.; PICKERING, K.L.; MACE, B.R. Dynamic properties of magnetorheological elastomers based on iron sand and natural rubber. *J. Appl. Polym. Sci.* **2015**; vol. 132, 41506.

[32] CARLSON, J.D.; JOLLY, M.R. MR fluid, foam and elastomer devices. *Mechatronics*. **2000**; vol. 10, pp. 555–69.

[33] CVEK, M.; MRLIK, M.; PAVLINEK, V. A rheological evaluation of steady shear magnetorheological flow behavior using three-parameter viscoplastic models. *J. Rheol.* **2016**; vol. 60, pp. 687–94.

[34] JOLLY, M.R.; CARLSON, J.D.; MUNOZ, B.C. A model of the behaviour of magnetorheological materials. *Smart Mater. Struct.* **1996**; vol. 5, pp. 607–14.

[35] HAN, Y.; HONG, W.; FAIDLEY, L.A.E. Field-stiffening effect of magneto-rheological elastomers. *Int. J. Solids Struct.* **2013**; vol. 50, pp. 2281–8.

[36] CHO, M.S.; LIM, S.T.; JANG, I.B.; CHOI, H.J.; JHON, M.S. Encapsulation of spherical iron-particle with PMMA and its magnetorheological particles. *IEEE Trans. Magn.* **2004**; vol. 40, pp. 3036–8.

[37] de VICENTE, J.; VEREDA, F.; SEGOVIA-GUTIERREZ, J.P.; MORALES, M.D.; HIDALGO-ALVAREZ, R. Effect of particle shape in magnetorheology. *J. Rheol.* **2010**; vol. 54, pp. 1337–62.

[38] FARJOUD, A.; VAHDATI, N.; FAH, Y.F. Mathematical model of drum-type MR brakes using Herschel-Bulkley shear model. *J. Intell. Mater. Syst. Struct.* **2008**; vol. 19, pp. 565–72.

[39] GHAFFARI, A.; HASHEMABADI, S.H.; ASHTIANI M. A review on the simulation and modeling of magnetorheological fluids. *J. Intell. Mater. Syst. Struct.* **2015**; vol. 26, pp. 881–904.

[40] KITTIPOOMWONG, D.; KLINGENBERG, D.J.; ULICNY, J.C. Dynamic yield stress enhancement in bidisperse magnetorheological fluids. *J. Rheol.* **2005**; vol. 49, pp. 1521–38.

[41] AHMADKHANLOU, F.; MAHBOOB, M.; BECHTEL, S.; WASHINGTON G. An improved model for magnetorheological fluid-based actuators and sensors. *J. Intell. Mater. Syst. Struct.* **2010**; vol. 21, pp. 3–18.

[42] KELESSIDIS, V.C.; MAGLIONE, R. Modeling rheological behavior of bentonite suspensions as Casson and Robertson-Stiff fluids using Newtonian and true shear rates in Couette viscometry. *Powder Technol.* **2006**; vol. 168, pp. 134–47.

[43] CHOI, H.J.; KWON, T.M.; JHON, M.S. Effects of shear rate and particle concentration on rheological properties of magnetic particle suspensions. *J. Mater. Sci.* **2000**; vol. 35, pp. 889–94.

[44] SAYED-AHMED, M.E.; EL-YAZAL, A.S. Laminar fully developed flow and heat transfer of Robertson-Stiff fluids in a rectangular duct. *Can. J. Phys.* **2005**; vol. 83, pp. 165–82.

[45] FILIP, P.; DAVID, J. Axial Couette-Poiseuille flow of power-law viscoplastic fluids in concentric annuli. *J. Pet. Sci. Eng.* **2003**; vol. 40, pp. 111–9.

[46] PELEGRINE, D.H.; SILVA, F.C.; GASPARETTO, C.A. Rheological behavior of pineapple and mango pulps. *LWT - Food Sci. Technol.* **2002**; vol. 35, pp. 645–8.

[47] BARNES, H.A. The yield stress - a review or 'pi alpha nu tau alpha rho epsilon iota' - everything flows? *J. Non-Newtonian Fluid Mech.* **1999**; vol. 81, pp. 133–78.

[48] BALHOFF, M.T.; LAKE, L.W.; BOMMER, P.M.; LEWIS, R.E.; WEBER, M.J.; CALDERIN, J.M. Rheological and yield stress measurements of non-

Newtonian fluids using a Marsh Funnel. *J. Pet. Sci. Eng.* **2011**; vol. 77, pp. 393–402.

[49] SONG, K.W.; KIM, Y.S.; CHANG, G.S. Rheology of concentrated xanthan gum solutions: Steady shear flow behavior. *Fibers Polym.* **2006**; vol. 7, pp. 129–38.

[50] BONNECAZE, R.T.; BRADY, J.F. Yield stresses in electrorheological fluids. *J. Rheol.* **1992**; vol. 36, pp. 73–115.

[51] GINDER, J.M.; DAVIS, L.C. Shear stresses in magnetorheological fluids - Role of magnetic saturation. *Appl. Phys. Lett.* **1994**; vol. 65, pp. 3410–2.

[52] MOON, I.J.; KIM, M.W.; CHOI, H.J.; KIM, N.; YOU, C.Y. Fabrication of dopamine grafted polyaniline/carbonyl iron core-shell typed microspheres and their magnetorheology. *Colloids Surf., A,* **2016**; vol. 500, pp. 137–45.

[53] GINDER, J.M.; DAVIS, L.C.; ELIE, L.D. Rheology of magnetorheological fluids: models and measurements. *Int. J. Mod. Phys. B*. **1996**; vol. 10, pp. 3293–303.

[54] CLARACQ, J.; SARRAZIN, J.; MONTFORT, J.P. Viscoelastic properties of magnetorheological fluids. *Rheol. Acta.* **2004**; vol. 43, pp. 38–49.

[55] PIAO, S.H.; BHAUMIK, M.; MAITY, A.; CHOI, H.J. Polyaniline/Fe composite nanofiber added softmagnetic carbonyl iron microsphere suspension and its magnetorheology. *J. Mater. Chem. C.* **2015**; vol. 3, pp. 1861–8.

[56] RAMOS, J.; de VICENTE, J.; HIDALGO-ALVAREZ, R. Small-amplitude oscillatory shear magnetorheology of inverse ferrofluids. *Langmuir.* **2010**; vol. 26, pp. 9334–41.

[57] SEDLACIK, M.; PAVLINEK, V.; PEER, P.; FILIP, P. Tailoring the magnetic properties and magnetorheological behavior of spinel nanocrystalline cobalt ferrite by varying annealing temperature. *Dalton Trans.* **2014**; vol. 43, pp. 6919–24.

[58] MRLIK, M.; ILCIKOVA, M.; SEDLACIK, M.; MOSNACEK, J.; PEER, P.; FILIP, P. Cholesteryl-coated carbonyl iron particles with improved anti-corrosion stability and their viscoelastic behaviour under magnetic field. *Colloid Polym. Sci.* **2014**; vol. 292, pp. 2137–43.

[59] ARIEF, I.; MUKHOPADHYAY, P.K. Magnetorheological Payne effect in bidisperse MR fluids containing Fe nanorods and Fe3O4 nanospheres: A dynamic rheological study. *J. Alloys Compd.* **2017**; vol. 696, pp. 1053–8.

[60] SOROKIN, V.V.; STEPANOV, G.V.; SHAMONIN, M.; MONKMAN, G.J.; KHOKHLOV, A.R.; KRAMARENKO, E.Y. Hysteresis of the viscoelastic

properties and the normal force in magnetically and mechanically soft magnetoactive elastomers: Effects of filler composition, strain amplitude and magnetic field. *Polymer.* **2015**; vol. 76, pp. 191–202.

[61] YANG, J.J.; YAN, H.; DAI, J.; HU, Z.D.; ZHANG, H.S. The rheological response of carbonyl iron particles suspended in mineral oil solution of 12-hydroxy stearic acid. *J. Rheol.* **2017**; vol. 61, pp. 515–24.

[62] BALAN, C.; BROBOANA, D.; GHEORGHIU, E.; VELAS, L. Rheological characterization of complex fluids in electro-magnetic fields. *J. Non-Newtonian Fluid Mech.* **2008**; vol. 154, pp. 22–30.

[63] GHASEMIL, E.; MIRHABIBI, A.; EDRISSI, M.; AGHABABAZADEH, R.; BRYDSON, R.M. Study on the magnetorheological properties of maghemite-kerosene ferrofluid. *J. Nanosci. Nanotechnol.* **2009**; vol. 9, pp. 4273–8.

[64] MORILLAS, J.R.; BOMBARD, A.J.F; de VICENTE, J. Preparation and characterization of magnetorheological fluids by dispersion of carbonyl iron microparticles in PAO/1-octanol. *Smart Mater. Struct.* **2016**; vol. 25, 015023.

[65] BARBER, D.E.; CARLSON, J.D. Performance characteristics of prototype MR engine mounts containing glycol MR fluids. *J. Intell. Mater. Syst. Struct.* **2010**; vol. 21, pp. 1509-16.

[66] GALINDO-GONZALEZ, C.; LOPEZ-LOPEZ, M.T.; DURAN, J.D.G. Magnetorheological behavior of magnetite covered clay particles in aqueous suspensions. *J. Appl. Phys.* **2012**; vol. 112, 043917.

[67] LOKANDER, M.; REITBERGER, T.; STENBERG, B. Oxidation of natural rubber-based magnetorheological elastomers. *Polym. Degrad. Stab.* **2004**; vol. 86, pp. 467–71.

[68] WANG, Y.; GONG, X.L.; YANG, J.; XUAN, S.H. Improving the dynamic properties of mre under cyclic loading by incorporating silicon carbide nanoparticles. *Ind. Eng. Chem. Res.* **2014**; vol. 53, pp. 3065–72.

[69] CVEK, M.; MOUCKA, R.; SEDLACIK, M.; PAVLINEK, V. Electromagnetic, magnetorheological and stability properties of polysiloxane elastomers based on silane-modified carbonyl iron particles with enhanced wettability. *Smart Mater. Struct.* **2017**; vol. 26, 105003.

[70] RABINDRANATH, R.; BOSE, H. On the mobility of iron particles embedded in elastomeric silicone matrix. Editor: UNAL, H.I. *J. Phys. Conf. Ser.* **2013**; vol. 412, 012034.

[71] FAN, Y.C.; GONG, X.L.; XUAN, S.H.; QIN, L.J.; LI, X.F. Effect of cross-link density of the matrix on the damping properties of magnetorheological elastomers. *Ind. Eng. Chem. Res.* **2013**; vol. 52, pp. 771–8.

[72] GONG, X.L.; FAN, Y.C.; XUAN, S.H.; XU, Y.G.; PENG, C. Control of the damping properties of magnetorheological elastomers by using polycaprolactone as a temperature-controlling component. *Ind. Eng. Chem. Res.* **2012**; vol. 51, pp. 6395–403.

[73] LOKANDER, M.; STENBERG, B. Improving the magnetorheological effect in isotropic magnetorheological rubber materials. *Polym. Test.* **2003**; vol. 22, pp. 677–80.

[74] YUNUS, N.A.; MAZLAN, S.A.; UBAIDILLAH; CHOI, S.B.; IMADUDDIN, F.; AZIZ, S.A.A; et al. Rheological properties of isotropic magnetorheological elastomers featuring an epoxidized natural rubber. *Smart Mater. Struct.* **2016**; vol. 25, 107001.

[75] UBAIDILLAH; IMADUDDIN, F.; LI, Y.C.; MAZLAN, S.A.; SUTRISNO, J.; KOGA, T.; et al. A new class of magnetorheological elastomers based on waste tire rubber and the characterization of their properties. *Smart Mater. Struct.* **2016**; vol. 25, 115002.

[76] BOCZKOWSKA, A.; AWIETJAN, S.F.; WROBLEWSKI, R. Microstructure-property relationships of urethane magnetorheological elastomers. *Smart Mater. Struct.* **2007**; vol. 16, 1924.

[77] JU, B.X.; TANG, R.; ZHANG, D.Y.; YANG, B.L.; YU, M.; LIAO, C.R.; et al. Dynamic mechanical properties of magnetorheological elastomers based on polyurethane matrix. *Polym. Compos.* **2016**; vol. 37, pp. 1587–95.

[78] MALECKI, P.; KROLEWICZ, M.; KRZAK, J.; KALETA, J.; PIGLOWSKI, J. Dynamic mechanical analysis of magnetorheological composites containing silica-coated carbonyl iron powder. *J. Intell. Mater. Syst. Struct.* **2015**; vol. 26, pp. 1899–905.

[79] QIAO, X.Y.; LU, X.S.; GONG, X.L.; YANG, T.; SUN, K.; CHEN, X.D. Effect of carbonyl iron concentration and processing conditions on the structure and properties of the thermoplastic magnetorheological elastomer composites based on poly(styrene-b-ethylene-co-butylene-b-styrene) (SEBS). *Polym. Test.* **2015**; vol. 47, pp. 51–8.

[80] QIAO, X.Y.; LU, X.S.; LI, W.H.; CHEN, J.; GONG, X.L.; YANG, T.; et al. Microstructure and magnetorheological properties of the thermoplastic magnetorheological elastomer composites containing modified carbonyl iron particles and poly(styrene-b-ethylene-ethylenepropylene-b-styrene) matrix. *Smart Mater. Struct.* **2012**; vol. 21, 115028.

[81] BEHROOZ, M.; SUTRISNO, J.; ZHANG, L.Y.; FUCHS, A.; GORDANINEJAD, F. Behavior of magnetorheological elastomers with coated particles. *Smart Mater. Struct.* **2015**; vol. 24, 035026.

[82] FAN, Y.C.; GONG, X.L.; XUAN, S.H.; ZHANG, W.; ZHENG, J.A.; JIANG, W.Q. Interfacial friction damping properties in magnetorheological elastomers. *Smart Mater. Struct.* **2011**; vol. 20, 035007.

[83] FUCHS, A.; SUTRISNO, J.; GORDANINEJAD, F.; CAGLAR, M.B.; LIU, Y.M. Surface polymerization of iron particles for magnetorheological elastomers. *J. Appl. Polym. Sci.* **2010**; vol. 117, pp. 934–42.

[84] CHAE, H.S.; PIAO, S.H.; CHOI, H.J. Fabrication of spherical Fe3O4 particles with a solvothermal method and their magnetorheological characteristics. *J. Ind. Eng. Chem.* **2015**; vol. 29, pp. 129–33.

[85] SEO, Y.P.; KWAK, S.; CHOI, H.J.; SEO, Y. Static yield stress of a magnetorheological fluid containing Pickering emulsion polymerized Fe2O3/polystyrene composite particles. *J. Colloid Interface Sci.* **2016**; vol. 463, pp. 272–8.

[86] MALCZYK, R.; IZYDORCZYK, J. The frequency-dependent Jiles-Atherton hysteresis model. *Phys. B* **2015**; vol. 463, pp. 68–75.

[87] LIORZOU, F.; PHELPS, B.; ATHERTON, D.L. Macroscopic models of magnetization. *IEEE Trans. Magn.* **2000**; vol. 36, pp. 418–28.

[88] CVEK, M.; MRLIK, M.; ILCIKOVA, M.; MOSNACEK, J.; BABAYAN, V.; KUCEKOVA, Z.; et al. The chemical stability and cytotoxicity of carbonyl iron particles grafted with poly(glycidyl methacrylate) and the magnetorheological activity of their suspensions. *RSC Adv.* **2015**; vol. 5, pp. 72816–24.

[89] CVEK, M.; MRLIK, M.; ILCIKOVA, M.; PLACHY, T.; SEDLACIK, M.; MOSNACEK, J.; et al. A facile controllable coating of carbonyl iron particles with poly(glycidyl methacrylate): A tool for adjusting MR response and stability properties. *J. Mater. Chem. C.* **2015**; vol. 3, pp. 4646–56.

[90] MRLIK, M.; ILCIKOVA, M.; CVEK, M.; PAVLINEK, V.; ZAHORANOVA, A.; KRONEKOVA, Z.; et al. Carbonyl iron coated with a sulfobetaine moiety as a biocompatible system and the magnetorheological performance of its silicone oil suspensions. *RSC Adv.* **2016**; vol. 6, pp. 32823–30.

[91] MRLIK, M.; ILCIKOVA, M.; PAVLINEK, V.; MOSNACEK, J.; PEER, P.; FILIP, P. Improved thermooxidation and sedimentation stability of covalently-coated carbonyl iron particles with cholesteryl groups and their influence on magnetorheology. *J. Colloid Interface Sci.* **2013**; vol. 396, pp. 146–51.

[92] MRLIK, M.; PAVLINEK, V. Magnetorheological suspensions based on modified carbonyl iron particles with an extremely thin poly(n-butyl acrylate) layer and their enhanced stability properties. *Smart Mater. Struct.* **2016**; vol. 25, 085011.

[93] SEDLACIK, M.; PAVLINEK, V. A tensiometric study of magnetorheological suspensions' stability. *RSC Adv.* **2014**; vol. 4, pp. 58377–85.

[94] OCALAN, M.; MCKINLEY, G.H. High-flux magnetorheology at elevated temperatures. *Rheol. Acta.* **2013**; vol. 52, pp. 623–41.

[95] JACOBS, S.D. MRF with adjustable pH. Editors: DUPARRE, A.; GEYL, R. *Proc. SPIE 8169, Optical Fabrication, Testing, and Metrology* IV. **2011**; vol. 8169, 816902.

[96] ZHANG, W.L.; KIM S.D.; CHOI, H.J. Effect of graphene oxide on carbonyl-iron-based magnetorheological fluid. *IEEE Trans. Magn.* **2014**; vol. 50, 2500804.

[97] LIM, S.T.; CHO, M.S.; JANG, I.B.; CHOI, H.J. Magnetorheological characterization of carbonyl iron based suspension stabilized by fumed silica. *J. Magn. Magn. Mater.* **2004**; vol. 282, pp. 170–3.

[98] HATO, M.J.; CHOI, H.J.; SIM, H.H.; PARK, B.O.; RAY, S.S. Magnetic carbonyl iron suspension with organoclay additive and its magnetorheological properties. *Colloids Surf., A,* **2011**; vol. 377, pp. 103–9.

[99] JANG, D.S.; LIU, Y.D.; KIM, J.H.; CHOI, H.J. Enhanced magnetorheology of soft magnetic carbonyl iron suspension with hard magnetic gamma-Fe2O3 nanoparticle additive. *Colloid Polym. Sci.* **2015**; vol. 293, pp. 641–7.

[100] SEDLACIK, M.; PAVLINEK, V.; VYROUBAL, R.; PEER, P.; FILIP, P. A dimorphic magnetorheological fluid with improved oxidation and chemical stability under oscillatory shear. *Smart Mater. Struct.* **2013**; vol. 22, 035011.

[101] CHAND, M.; SHANKAR, A.; NOORJAHAN; JAIN, K.; PANT, R.P. Improved properties of bidispersed magnetorheological fluids. *RSC Adv.* **2014**; vol. 4, pp. 53960–6.

[102] IGLESIAS, G.R.; LOPEZ-LOPEZ, M.T.; DURAN, J.D.G; GONZALEZ-CABALLERO, F.; DELGADO, A.V. Dynamic characterization of extremely bidisperse magnetorheological fluids. *J. Colloid Interface Sci.* **2012**; vol. 377, pp. 153–9.

[103] PLACHY, T.; CVEK, M.; KOZAKOVA, Z.; SEDLACIK, M.; MOUCKA, R. The enhanced MR performance of dimorphic MR suspensions containing either magnetic rods or their non-magnetic analogs. *Smart Mater. Struct.* **2017**; vol. 26, 025026.

[104] CVEK, M.; MRLIK, M.; MOUCKA, R.; SEDLACIK, M. A systematical study of the overall influence of carbon allotrope additives on performance, stability and redispersibility of magnetorheological fluids. *Colloids Surf., A,* **2018**; vol. 543, pp. 83–92.

[105] WANG, Y.; ZHANG, X.; CHUNG, K.; LIU, C.; CHOI, S.B.; CHOI, H.J. Formation of core–shell structured complex microparticles during fabrication of magnetorheological elastomers and their magnetorheological behavior. *Smart Mater. Struct.* **2016**; vol. 25, 115028.

[106] ASHTIANI, M.; HASHEMABADI, S.H.; GHAFFARI, A. A review on the magnetorheological fluid preparation and stabilization. *J. Magn. Magn. Mater.* **2015**; vol. 374, pp. 716–30.

[107] SHCHUKIN, D.G.; SVIRIDOV, D.V.; KULAK, A.I. Magnetorheological photocatalytic systems. *Int. J. Photoenergy.* **1999**; vol. 1, pp. 65–67.

[108] JANG, I.B.; KIM, H.B.; LEE, J.Y.; YOU, J.L.; CHOI, H.J.; JHON, M.S. Role of organic coating on carbonyl iron suspended particles in magnetorheological fluids. *J. Appl. Phys.* **2005**; vol. 97, 10Q912.

[109] KHIMI, S.R.; PICKERING, K.L. Comparison of dynamic properties of magnetorheological elastomers with existing antivibration rubbers. *Composites, Part B*. **2015**; vol. 83, pp. 175–83.

[110] KHIMI, S.R.; PICKERING, K.L. The effect of silane coupling agent on the dynamic mechanical properties of iron sand/ natural rubber magnetorheological elastomers. *Composites, Part B*. **2016**; vol. 90, pp. 115–25.

[111] MALECKI, P.; KROLEWICZ, M.; HIPTMAIR, F.; KRZAK, J.; KALETA, J.; MAJOR, Z.; et al. Influence of carbonyl iron particle coating with silica on the properties of magnetorheological elastomers. *Smart Mater. Struct.* **2016**; vol. 25, 105030.

[112] PICKERING, K.L.; KHIMI, S.R.; ILANKO, S. The effect of silane coupling agent on iron sand for use in magnetorheological elastomers Part 1: Surface chemical modification and characterization. *Composites, Part A*. **2015**; vol. 68, pp. 377–86.

[113] JIANG, W.Q.; ZHU, H.; GUO, C.Y.; LI, J.F.; XUE, Q.; FENG, J.H.; et al. Poly(methyl methacrylate)-coated carbonyl iron particles and their magnetorheological characteristics. *Polym. Int.* **2010**; vol. 59, pp. 879–83.

[114] LI, J.F.; GONG, X.L.; ZHU, H.; JIANG, W.Q. Influence of particle coating on dynamic mechanical behaviors of magnetorheological elastomers. *Polym. Test.* **2009**; vol. 28, pp. 331–7.

[115] SEDLACIK, M.; PAVLINEK, V.; SAHA, P.; SVRCINOVA, P.; FILIP, P.; STEJSKAL, J. Rheological properties of magnetorheological suspensions based on core-shell structured polyaniline-coated carbonyl iron particles. *Smart Mater. Struct.* **2010**; vol. 19, 115008.

[116] MRLIK, M.; SEDLACIK, M.; PAVLINEK, V.; BAZANT, P.; SAHA, P.; PEER, P.; et al. Synthesis and magnetorheological characteristics of ribbon-like, polypyrrole-coated carbonyl iron suspensions under oscillatory shear. *J. Appl. Polym. Sci.* **2013**; vol. 128, pp. 2977–82.

[117] KIM, Y.H.; AHN, W.J.; CHOI, H.J.; SEO, Y. Fabrication and magnetic stimuli-response of polydopamine-coated core-shell structured carbonyl iron microspheres. *Colloid Polym. Sci.* **2016**; vol. 294, pp. 329–37.

[118] YOU, J.L.; PARK, B.J.; CHOI, H.J. Magnetorheological characteristics of carbonyl iron embedded suspension polymerized poly(methyl methacrylate) micro-bead. *IEEE Trans. Magn.* **2008**; vol. 44, pp. 3867–70.

[119] FANG, F.F.; LIU, Y.D.; CHOI, H.J. Fabrication of carbonyl iron embedded polycarbonate composite particles and magnetorheological characterization. *IEEE Trans. Magn.* **2009**; vol. 45, pp. 2507–10.

[120] FANG, F.F.; LIU, Y.D.; CHOI, H.J.; SEO, Y. Core-shell structured carbonyl iron microspheres prepared via dual-step functionality coatings and their magnetorheological response. *ACS Appl. Mater. Interfaces.* **2011**; vol. 3, pp. 3487–95.

[121] ANG, F.F.; CHOI, H.J.; SEO, Y. Sequential coating of magnetic carbonyliron particles with polystyrene and multiwalled carbon nanotubes and its effect on their magnetorheology. *ACS Appl. Mater. Interfaces.* **2010**; vol. 2, pp. 54–60.

[122] LIU, Y.D.; CHOI, H.J. Magnetorheology of core-shell typed dual-coated carbonyl iron particle fabricated by a sol-gel and self-assembly process. *Mater. Res. Bull.* **2015**; vol. 69, pp. 92–7.

[123] SEDLACIK, M.; PAVLINEK, V.; LEHOCKY, M.; MRACEK, A.; GRULICH, O.; SVRCINOVA, P.; et al. Plasma-treated carbonyl iron particles as a dispersed phase in magnetorheological fluids. *Colloids Surf., A,* **2011**; vol. 387, pp. 99–103.

[124] CHUAH, W.H.; ZHANG, W.L.; CHOI, H.J.; SEO, Y. Magnetorheology of core-shell structured carbonyl iron/polystyrene foam microparticles suspension with enhanced stability. *Macromolecules.* **2015**; vol. 48, pp. 7311–9.

[125] YU, M.; YANG, P.A.; FU, J.; LIU, S.Z.; QI, S. Study on the characteristics of magneto-sensitive electromagnetic wave-absorbing properties of magnetorheological elastomers. *Smart Mater. Struct.* **2016**; vol. 25, 085046.

[126] HU, B.; FUCHS, A.; HUSEYIN, S.; GORDANINEJAD, F.; EVRENSEL, C. Atom transfer radical polymerized MR fluids. *Polymer.* **2006**; vol. 47, pp. 7653–63.

[127] MATYJASZEWSKI, K. Atom Transfer Radical Polymerization (ATRP): Current status and future perspectives. *Macromolecules.* **2012**; vol. 45, pp. 4015–39.

[128] ZOPPE, J.O.; ATAMAN, N.C.; MOCNY, P.; WANG, J.; MORAES, J.; KLOK, H.A. Surface-initiated controlled radical polymerization: State-of-the-art, opportunities, and challenges in surface and interface engineering with polymer brushes. *Chem. Rev.* **2017**; vol. 117, pp. 1105–318.

[129] BROZ, J. Moderni problemy feromagnetismu. Edition: *Cesta k vedeni*, Praha; **1962**, pp. 192, ISBN: 1062-21-140-62.

[130] STEPANOV, G.V.; BORIN, D.Y.; BAKHTIIAROV, A.V.; STOROZHENKO, P.A. Magnetic properties of hybrid elastomers with magnetically hard fillers: rotation of particles. *Smart Mater. Struct.* **2017**; vol. 26, 035060.

[131] SPAGGIARI, A.; DRAGONI, E. Effect of pressure on the physical properties of magnetorheological fluids. *Fratt Integrita Strutturale* **2013**; vol. 23, pp. 75–86.

[132] BOMBARD, A.J.F.; ALCANTARA, M.R.; KNOBEL, M.; VOLPE, P.L.O. Experimental study of MR suspensions of carbonyl iron powders with different particle sizes. *Int. J. Mod. Phys. B* **2005**; vol. 19, pp. 1332–8.

[133] BORBATH, T.; GUNTHER, S.; BORIN, D.Y.; GUNDERMANN, T.; ODENBACH, S. XμCT analysis of magnetic field-induced phase transitions in magnetorheological elastomers. *Smart Mater. Struct.* **2012**; vol. 21, 105018.

[134] BELL, R.C.; KARLI, J.O.; VAVRECK, A.N.; ZIMMERMAN, D.T.; NGATU, G.T.; WERELEY, N.M. Magnetorheology of submicron diameter iron microwires dispersed in silicone oil. *Smart Mater. Struct.* **2008**; vol. 17, 015028.

[135] de VICENTE, J.; SEGOVIA-GUTIERREZ, J.P.; ANDABLO-REYES, E.; VEREDA, F.; HIDALGO-ALVAREZ, R. Dynamic rheology of sphere- and rod-based magnetorheological fluids. *J. Chem. Phys.* **2009**; vol. 131, 194902.

[136] STEPANOV, G.V.; BORIN, D.Y.; STOROZHENKO, P.A. Rotation of magnetic particles inside the polymer matrix of magnetoactive elastomers with a hard magnetic filler. *J. Magn. Magn. Mater.* **2017**; vol. 431, pp. 138–40.

[137] JUNG, H.S.; KWON, S.H.; CHOI, H.J.; JUNG, J.H.; KIM, Y.G. Magnetic carbonyl iron/natural rubber composite elastomer and its magnetorheology. *Compos. Struct.* **2016**; vol. 136, pp. 106–12.

[138] VEREDA, F.; de VICENTE, J.; SEGOVIA-GUTIERREZ, J.P.; HIDALGO-ALVAREZ, R. On the effect of particle porosity and roughness in magnetorheology. *J. Appl. Phys.* **2011**; vol. 110, 063520.

[139] OLABI, A.G.; GRUNWALD, A. Design and application of magneto-rheological fluid. *Mater. Des.* **2007**; vol. 28, pp. 2658–64.

[140] ZHANG, W.; GONG, X.L.; JIANG, W.Q.; FAN, Y.C. Investigation of the durability of anisotropic magnetorheological elastomers based on mixed rubber. *Smart Mater. Struct.* **2010**; vol. 19, 085008.

[141] CHOI, S.B. The grand challenges in smart materials research. *Front. Mater.* **2014**; vol. 1, pp. 1–3.

[142] YANG, D.L.; PACHECO, R.; HENDERSON, K.; HUBBARD, K.; DEVLIN, D. Diffusion and sorption of nitroplasticizers in vinyl copolymer elastomer and its composites. *J. Appl. Polym. Sci.* **2014**; vol. 131, 40729.

[143] LIAO, G.J.; XU, Y.G.; WANG, F.J.; WEI, F.Y.; WAN, Q. Influence of gamma radiation on the shear modulus of magnetorheological elastomer. *Mater. Lett.* **2016**; vol. 174, pp. 79–81.

[144] CVEK, M.; MRLIK, M.; ILCIKOVA, M.; SEDLACIK, M.; MOSNACEK, J. Tailoring performance, damping and stability properties of magnetorheological elastomers via particle-grafting technology. *Submitted manuscript.*

[145] LI, W.H.; CHEN, G.; YEO, S.H.; DU, H. Temperature dependence of MR fluids. *Int. J. Mod. Phys. B* **2002**; vol. 16, pp. 2725–31.

[146] ZSCHUNKE, F.; RIVAS, R.; BRUNN, P.O. Temperature behavior of magnetorheological fluids. *Appl. Rheol.* **2005**; vol. 15, pp. 116–21.

[147] SEDLACIK, M.; PAVLINEK, V.; SAHA, P.; SVRCINOVA, P.; FILIP, P. Core-shell structured polypyrrole-coated magnetic carbonyl iron microparticles and their magnetorheology. Editor: ZATLOUKAL, M. *Novel Trends in Rheology* **2011**; vol. 1375, pp. 284–91.

[148] JU, B.X.; TANG, R.; ZHANG, D.Y.; YANG, B.L.; YU, M.; LIAO, C.R. Temperature-dependent dynamic mechanical properties of magnetorheological

elastomers under magnetic field. *J. Magn. Magn. Mater.* **2016**; vol. 374, pp. 283–288.

[149] BELYAVSKII, S.G.; MINGALYOV, P.G.; GIULIERI, F.; COMBARRIEAU, R.; LISICHKIN, G.V. Chemical modification of the surface of a carbonyl iron powder. *Prot. Met.* **2006**; vol. 42, pp. 244–52.

[150] CANAMERO, P.F.; de la FUENTE, J.L.; MADRUGA, E.L.; FERNANDEZ-GARCIA, M. Atom transfer radical polymerization of glycidyl methacrylate: A functional monomer. *Macromol. Chem. Phys.* **2004**; vol. 205, pp. 2221–8.

[151] GONCALVES, G.; MARQUES, P.; BARROS-TIMMONS, A.; BDKIN, I.; SINGH, M.K.; EMAMI, N.; et al. Graphene oxide modified with PMMA via ATRP as a reinforcement filler. *J. Mater. Chem.* **2010**; vol. 20, pp. 9927–34.

[152] KIM, S.Y.; KWON, S.H.; LIU, Y.D.; LEE, J.S.; YOU, C.Y.; CHOI, H.J. Core-shell-structured cross-linked poly(glycidyl methacrylate)-coated carbonyl iron microspheres and their magnetorheology. *J. Mater. Sci.* **2014**; vol. 49, pp. 1345–52.

[153] SHOREY, A.B.; KORDONSKI, W.I.; GORODKIN, S.R.; JACOBS, S.D.; GANS, R.F.; KWONG, K.M.; et al. Design and testing of a new magnetorheometer. *Rev. Sci. Instrum.* **1999**; vol. 70, pp. 4200–6.

[154] CHO, M.S.; CHOI, H.J.; JHON, M.S. Shear stress analysis of a semiconducting polymer based electrorheological fluid system. *Polymer.* **2005**; vol. 46, pp. 11484–8.

[155] FLORES, G.A.; LIU, J. Embolization of blood vessels as a cancer therapy using magnetorheological fluids. *J. Intell. Mater. Syst. Struct.* **2002**; vol. 13, pp. 641–6.

[156] SILVA, A.K.A.; SILVA, E.L.; CARRICO, A.S.; EGITO, E.S.T. Magnetic carriers: A promising device for targeting drugs into the human body. *Curr. Pharm. Des.* **2007**; vol. 13, pp. 1179–85.

[157] ARIAS, J.L.; GALLARDO, V.; LINARES-MOLINERO, F.; DELGADO, A. Preparation and characterization of carbonyl iron/poly(butylcyanoacrylate) core/shell nanoparticles. *J. Colloid Interface Sci.* **2006**; vol. 299, pp. 599–607.

[158] FU, S.Y.; FENG, X.Q.; LAUKE, B.; MAI, Y.W. Effects of particle size, particle/matrix interface adhesion and particle loading on mechanical properties of particulate-polymer composites. *Composites, Part B.* **2008**; vol. 39, pp. 933–61.

[159] SHUIB, R.K.; PICKERING, K.L. Investigation and modelling of damping mechanisms of magnetorheological elastomers. *J. Appl. Polym. Sci.* **2016**; vol. 133, 43247.

[160] FANG, F.F.; CHOI, H.J.; JHON, M.S. Magnetorheology of soft magnetic carbonyl iron suspension with single-walled carbon nanotube additive and its yield stress scaling function. *Colloids Surf., A,* **2009**; vol. 351, 46–51.

7. LIST OF FIGURES

CURRICULUM VITAE

Personal Information

Surname / First Name	**Cvek Martin**
Address	Mistřice 404, 687 12 Bílovice, Czech Republic
Telephone	+420 732 122 529
E-mail	cvek@utb.cz
Nationality	Czech
Date of Birth	21/10/1989

Work Experience

Dates	01/2015–present
Occupation or Position Held	Junior Researcher
Name of Employer	Tomas Bata University (TBU) in Zlín, Centre of Polymer Systems
Dates	09/2014–12/2014
Occupation or Position Held	Technical Staff
Name of Employer	TBU in Zlín, University Institute

Education

Dates	2014–present
Title of Qualification Awarded	Doctoral Study – Expected defense in 09/2018
Principal Branch	Technology of Macromol. Compds. – P2808/2808V006
Organization Providing Education	TBU in Zlín, Faculty of Technology
Dates	2012–2014
Title of Qualification Awarded	Ing. (equivalent to M.Sc.)
Principal Branch	Materials Engineering – N2808/3911T011
Organization Providing Education	TBU in Zlín, Faculty of Technology
Dates	2009–2012
Title of Qualification Awarded	Bc.
Principal Branch	Chemistry and Materials Technology – B2808/2808R009
Organization Providing Education	TBU in Zlín, Faculty of Technology

Training Abroad

Dates	May–July 2018 (3 months) Scientific Mobility at University of Granada, Department of Applied Physics (Spain)
Field of Study	Advanced Phenomena Occurring in the MR Systems

Dates	March–April 2017 (2 months) Student Intership at Johannes Kepler University Linz, Institute of Polymer Science (Austria)
Field of Study	Processing of Polymer Materials
Dates	October–November 2015 (1 month) Research Period at Slovak Academy of Sciences, Polymer Institute (Slovakia)
Field of Study	Modification of Substrate via Controlled Radical Polymerization
Dates	June 2013 (2 weeks) Short-Term Study Stay at Clermont-Ferrand Superior National School of Chemistry (France)
Field of Study	Polymer Processing and Functionalization
Expertise	
Fields	Magnetorheology, Rheology, Particulate Systems, Polymer Processing, Mechanical Properties of Polymers
Other Languages	
	Level
English	C1
Russian	A2
Awards	
2017	Best Poster Award (co-author) – Miskolc (Hungary), Conference Paper "*Ferrous Oxalate Micro-Rods as a Promising Material for Electrorheology*"
2017	Aktion Österreich-Tschechien, AÖCZ-Semesterstipendien
2016	First-place Award at the Scientific conference held at the Faculty of Technology of TBU in Zlín
2014	Award by the Head of the Department of Physics and Materials Engineering for excellent Diploma thesis
2014	Best Poster Award – Granada (Spain), Conference paper "*Magnetorheology of Suspensions Based on Carbonyl Iron Particles Coated with Poly(Glycidyl Methacrylate)*"
2012	Award by the Dean of the Faculty of Technology of TBU in Zlín for excellent academic performance during the entire period of studies
Professional Service	Reviewer: *Journal of Industrial and Engineering Chemistry* *Journal of the Taiwan Institute of Chemical Engineers*

LIST OF PUBLICATIONS

Publications in the Journals with Impact Factor:

1. CVEK, M.; MRLIK, M.; ILCIKOVA, M.; SEDLACIK, M.; MOSNACEK, J. Tailoring performance, damping and stability properties of magnetorheological elastomers via particle-grafting technology. *Submitted manuscript*.
2. KUTALKOVA, E.; PLACHY, T.; OSICKA, J.; CVEK, M.; MRLIK, M.; SEDLACIK, M. Electrorheological behavior of fluids containing iron(II) oxalate micro-rods. *RSC Adv*. **2018**; vol. 8, pp. 24773–9, IF 2017 = 2.936.
3. MOUCKA, R.; SEDLACIK, M.; CVEK, M. Dielectric properties of magnetorheological elastomers with different microstructure. *Appl. Phys. Lett.* **2018**; vol. 112, 122901, IF 2017 = 3.495.
4. CVEK, M.; MRLIK, M.; MOUCKA, R.; SEDLACIK, M. A systematical study of the overall influence of carbon allotrope additives on performance, stability and redispersibility of magnetorheological fluids. *Colloids Surf., A*, **2018**; vol. 543, pp. 83–92, IF 2017 = 2.829.
5. MRLIK, M.; CVEK, M.; OSICKA, J.; MOUCKA, R.; SEDLACIK, M.; PAVLINEK, V. Surface-initiated atom transfer radical polymerization from graphene oxide: A way towards fine tuning of electrical conductivity and electro-responsive capabilities. *Mater. Lett.* **2018**; vol. 211, pp. 138–41, IF 2017 = 2.687.
6. CVEK, M.; MOUCKA, R.; SEDLACIK, M.; PAVLINEK, V. Electromagnetic, magnetorheological and stability properties of polysiloxane elastomers based on silane-modified carbonyl iron particles with enhanced wettability. *Smart Mater. Struct.* **2017**; vol. 26, 105003 (10pp), IF 2017 = 2.963.
7. CVEK, M.; MOUCKA, R.; SEDLACIK, M.; BABAYAN, V.; PAVLINEK, V. Enhancement of radio-absorbing properties and thermal conductivity of polysiloxane-based magnetorheological elastomers by the alignment of filler particles. *Smart Mater. Struct.* **2017**; vol. 26, 095005 (7pp), IF 2017 = 2.963.
8. CVEK, M.; MRLIK, M.; ILCIKOVA, M.; MOSNACEK, M.; MUNSTER, L.; PAVLINEK, V. The synthesis of silicone elastomers containing silyl-based polymer-grafted carbonyl iron particles: An efficient way to improve magnetorheological, damping and sensing performances. *Macromolecules.* **2017**; vol. 50(5), pp. 2189–200, IF 2017 = 5.914.
9. PLACHY, T.; CVEK, M.; KOZAKOVA, Z.; SEDLACIK, M.; MOUCKA, R. The enhanced MR performance of dimorphic MR suspensions containing either magnetic rods or their non-magnetic analogs. *Smart Mater. Struct.* **2017**; vol. 26, 025026 (8pp), IF 2017 = 2.963.
10. CVEK, M.; MRLIK, M.; PAVLINEK, V. A rheological evaluation of steady shear magnetorheological flow behavior using three-parameter viscoplastic models. *J. Rheol.* **2016**; vol. 60(4), pp. 687–94, IF 2016 = 3.136.
11. MRLIK, M.; ILCIKOVA, M.; CVEK, M.; PAVLINEK, V.; ZAHORANOVA, A.; KRONEKOVA, Z.; KASAK, P. Carbonyl iron coated with a sulfobetaine moiety as a biocompatible system and the magnetorheological performance of its silicone oil suspensions. *RSC Adv.* **2016**; vol. 6(39), pp. 32823–30, IF 2016 = 3.108.

12. CVEK, M.; MRLIK, M.; ILCIKOVA, M.; MOSNACEK, J.; BABAYAN, V.; KUCEKOVA, Z.; HUMPOLICEK, P.; PAVLINEK, V. The chemical stability and cytotoxicity of carbonyl iron particles grafted with poly(glycidyl methacrylate) and the magnetorheological activity of their suspensions. *RSC Adv.* **2015**; vol. 5(89), pp. 72816–24, IF 2015 = 3.289.
13. CVEK, M.; MRLIK, M.; ILCIKOVA, M.; PLACHY, T.; SEDLACIK, M.; MOSNACEK, J.; PAVLINEK, V. A facile controllable coating of carbonyl iron particles with poly(glycidyl methacrylate): A tool for adjusting MR response and stability properties. *J. Mater. Chem. C.* **2015**; vol. 3(18), pp. 4646–56, IF 2015 = 5.066.

Original Full Papers in Conference Proceedings (Indexed on Web of Science):

1. CVEK, M.; MRLIK, M.; ILCIKOVA, M.; MOSNACEK, J.; SEDLACIK, M. Electrorheological fluids containing graphene oxide sheets grafted with poly(methyl methacrylate). In Nanocon **2017** – Conference Proceedings – *9th International Conference on Nanomaterials – Research and Application*, p. 87, ISBN: 978-80-87294-78-9.
2. CVEK, M.; MRLIK, M.; ILCIKOVA, M.; MOSNACEK, J.; KRONEK, J.; SEDLACIK, M. Grafting of magnetic particles with poly(2-isopropenyl-2-oxazoline). In Nanocon **2017** – Conference Proceedings – *9th International Conference on Nanomaterials – Research and Application*, p. 123, ISBN: 978-80-87294-78-9.
3. OSICKA, J.; CVEK, M.; MRLIK, M.; ILCIKOVA, M.; PAVLINEK, V.; MOSNACEK, M. Light-induced and sensing capabilities of SI-ATRP modified graphene oxide particles in elastomeric matrix. In: *Proc. SPIE 10164, Active and Passive Smart Structures and Integrated Systems*, **2017**, 1016434.
4. CVEK, M.; MRLIK, M.; ILCIKOVA, M.; MOSNACEK, J.; PAVLINEK, V. Preparation and characterization of graphene oxide sheets controllably grafted with PMMA brushes via surface–initiated ATRP. In Nanocon **2016** – Conference Proceedings – *8th International Conference on Nanomaterials – Research and Application*, p. 116–21, ISBN: 978-808729471-0.
5. MRLIK, M.; ILCIKOVA, M.; CVEK, M.; URBANEK, P.; PAVLINEK, V.; MOSNACEK, J. Controllable reduction of graphene oxide/poly(butyl acrylate) hybrids under ATRP conditions. In Nanocon **2016** – Conference Proceedings – *8th International Conference on Nanomaterials – Research and Application*, p. 104–9, ISBN: 978-808729471-0.

Conference Contributions:

1. CVEK, M.; MRLIK, M.; ZAHORANOVA, A.; SRAMKOVA, P.; SEDLACIK, M.; KRONEK, J. The preparation of stable magnetorheological gels based on the poly(2-oxazoline) matrix (**2018**) – *16th International Conference on Electrorheological Fluids and Magnetorheological Suspensions*, Maryland, USA.
2. SEDLACIK, M.; CVEK, M.; KRACALIK, M.; MRLIK, M. The recyclable magnetorheological elastomers based on thermoplastic matrix (**2018**) – *16th International Conference on Electrorheological Fluids and Magnetorheological Suspensions*, Maryland, USA.

3. TORRES-MENDIETA, R.; URBANEK, M.; CVEK, M.; HAVELKA, O.; WACLAWEK, S.; PADIL, V.V.T.; JAKSIKOVA, D.; KOTEK, M.; CERNIK, M. Laser-mediated synthesis of Cu by photochemical reduction of metal salts in a continuous flow jet (**2018**) – *XII Reunion Nacional de Optica*, Castellon, Spain.
4. KUTALKOVA, E.; PLACHY, T.; OSICKA, J.; CVEK, M.; SEDLACIK, M. Iron(II) oxalate micro-rods as a promising material for electrorheology (**2018**) – *Polymers: Site of Advanced Horizons and Ambits*, Zlín, Czech Republic.
5. CVEK, M.; MRLIK, M.; SEDLACIK, M. Magnetorheological behavior of poly(2-isopropenyl-2-oxazoline)-grafted magnetic particles in physiological solution (**2018**) – *Polymers: Site of Advanced Horizons and Ambits*, Zlín, Czech Republic.
6. SEDLACIK, M.; CVEK, M.; MOUCKA, R.; SYKOROVA, L.; BILEK, O.; PAVLINEK, V.; SAHA, P. Electromagnetic shielding of elastomers containing particles with enhanced wettability (**2018**) – *Polymers: Site of Advanced Horizons and Ambits*, Zlín, Czech Republic.
7. CVEK, M.; PLACHY, T.; OSICKA, J.; KUTALKOVA, E.; MRLIK, M.; SEDLACIK, M. Ferrous oxalate micro-rods as a promising material for electrorheology (**2017**) – *3rd International Conference on Rheology and Modeling of Materials*, Miskolc-Lillafured, Hungary.
8. CVEK, M.; MRLIK, M.; SEDLACIK, M. Effect of carbon nano-additives on performance and stability properties of magnetorheological fluids (**2017**) – *3rd International Conference on Rheology and Modeling of Materials*, Miskolc-Lillafured, Hungary.
9. CVEK, M.; MRLIK, M.; ILCIKOVA, M.; SEDLACIK, M.; MOSNACEK, J.; PAVLINEK, V. Magnetorheological elastomers with tailored performance and stability properties based on multifunctional core-shell particles with various shell thickness (**2017**) – *3rd International Conference on Mechanics of Composites*, Bologna, Italy.
10. MOUCKA, R.; SEDLACIK, M.; CVEK, M.; PAVLINEK, V. Dielectric behavior of structured magnetorheological elastomers (**2017**) – *3rd International Conference on Mechanics of Composites*, Bologna, Italy.
11. CVEK, M.; MRLIK, M.; ILCIKOVA, M.; MOSNACEK, J.; PAVLINEK, V. Tunable damping of magnetorheological elastomers based on particles controllably grafted with polymer chains (**2016**) – *XXII. Bratislava International Conference on Macromolecules*, Bratislava, Slovakia.
12. CVEK, M.; MRLIK, M.; ILCIKOVA, M.; MOSNACEK, J.; PAVLINEK, V. Magnetorheological elastomers based on carbonyl iron particles grafted with trimethylsilyloxyethyl methacrylate (**2016**) – *15th International Conference on Electrorheological Fluids and Magnetorheological Suspensions*, Incheon, Korea.
13. CVEK, M.; MOUCKA, R.; SEDLACIK, M.; BABAYAN, V; PAVLINEK, V. Shielding and magnetorheological performance of elastomers containing silane–modified carbonyl iron particles (**2016**) – *15th International Conference on Electrorheological Fluids and Magnetorheological Suspensions*, Incheon, Korea.
14. CVEK, M.; MRLIK, M.; PAVLINEK, V. On the modelling of rheological behavior of MRFs as Robertson–Stiff fluids (**2015**) – *2nd International Conference on Rheology and Modeling of Materials*, Miskolc-Lillafured, Hungary.

15. CVEK, M.; MRLIK, M.; ILCIKOVA, M.; PLACHY, T.; SEDLACIK, M.; MOSNACEK, J.; PAVLINEK, V. Magnetorheology of suspensions based on carbonyl iron particles coated with poly(glycidyl methacrylate) (**2014**) – *14th International Conference on Electrorheological Fluids and Magnetorheological Suspensions*, Granada, Spain.

Work on Projects:

Project	Period	Position
EU Funds – OP Research, Development and Education in cooperation with Ministry of Education, Youth and Sports, *International Mobility of TBU in Zlín Researchers*, CZ.02.2.69/0.0/0.0/16_027/0008464	2018	Member of Research Team
Internal Grant Agency of TBU in Zlín, *Preparation and Characterization of Electrorheological Suspensions Based on Ferrous Oxalates and Clays*, IGA/CPS/2018/004	2018	Member of Research Team
Czech Science Foundation (GACR), *Novel Magnetorheological Elastomers Based on Modified Magnetic Fillers*, 17-24730S	2017–2019	Member of Research Team
Internal Grant Agency of TBU in Zlín, *Evaluation of Carbon-Based Nano-Additives' Influence on Magnetorheological Performance and Preparation of Electrorheological Suspension with Enhanced Sedimentation Stability*, IGA/CPS/2017/004	2017	Principal Investigator
Czech Science Foundation (GACR), *Smart systems based on modified graphene oxide particles*, GA0/GJ, GJ16-20361Y	2016–2018	Member of Research Team
Internal Grant Agency of TBU in Zlín, *Magnetorheological Elastomers Based on Modified Filler and Preparation of Advanced Suspensions of Magnetic Particles*, IGA/CPS/2016/008	2016	Principal Investigator
Ministry of Education Youth and Sports (MSMT), *Centre of Polymer Systems plus*, LO1504	2015–2020	Member of Research Team
Technology Agency of the Czech Republic (TACR), *Development of Polyurethane Matrixes for Composite Production*, PURKOMP, TH01011438	2015–2017	Member of Research Team
Ministry of Education Youth and Sports (MSMT), *Centre of Polymer Systems*, CZ.1.05/2.1.00/03.0111	2011–2015	Member of Research Team
Internal Grant Agency of TBU in Zlín, *Electrorheological Fluids with Enhanced Sedimentation Stability and Dimorphic Magnetorheological Suspensions*, IGA/CPS/2015/007	2015	Member of Research Team
Internal Grant Agency of TBU in Zlín, *Modification of Particles for Intelligent Systems with Higher Efficiency and Enhanced Stability*, IGA/FT/2014/017	2014	Member of Research Team

Martin Cvek

Magnetorheological Systems with Optimized Performance

Magnetoreologické systémy s optimalizovaným výkonem

Doctoral Thesis

Published by: Tomas Bata University in Zlín,

nám. T. G. Masaryka 5555, 760 01 Zlín.

Typesetting by: Martin Cvek

This publication has not undergone any proofreading or editorial review.

Publication year: 2018

ISBN 978-80-…….

PAPER I

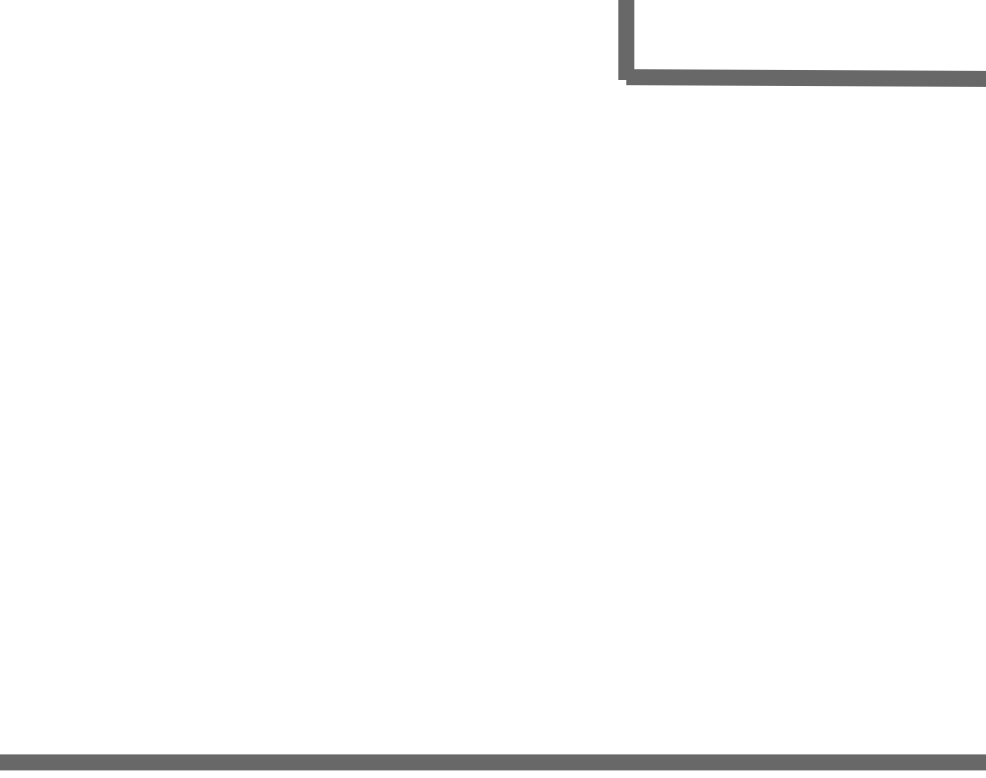

Royal Society of Chemistry

Journal of Materials Chemistry C

Accepted: 30th March 2015

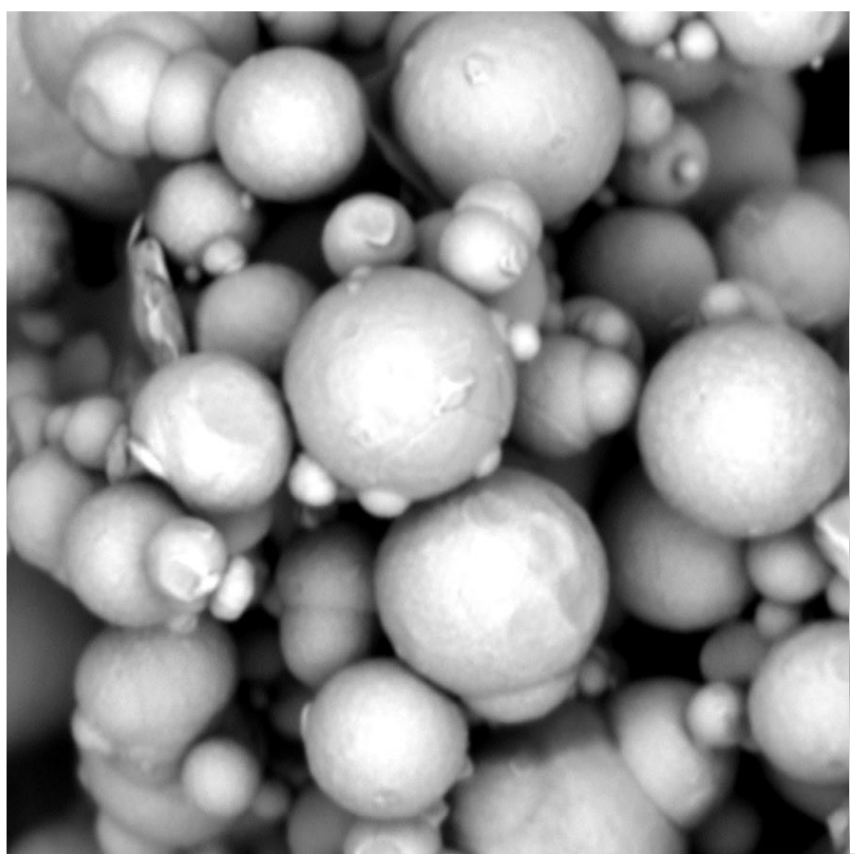

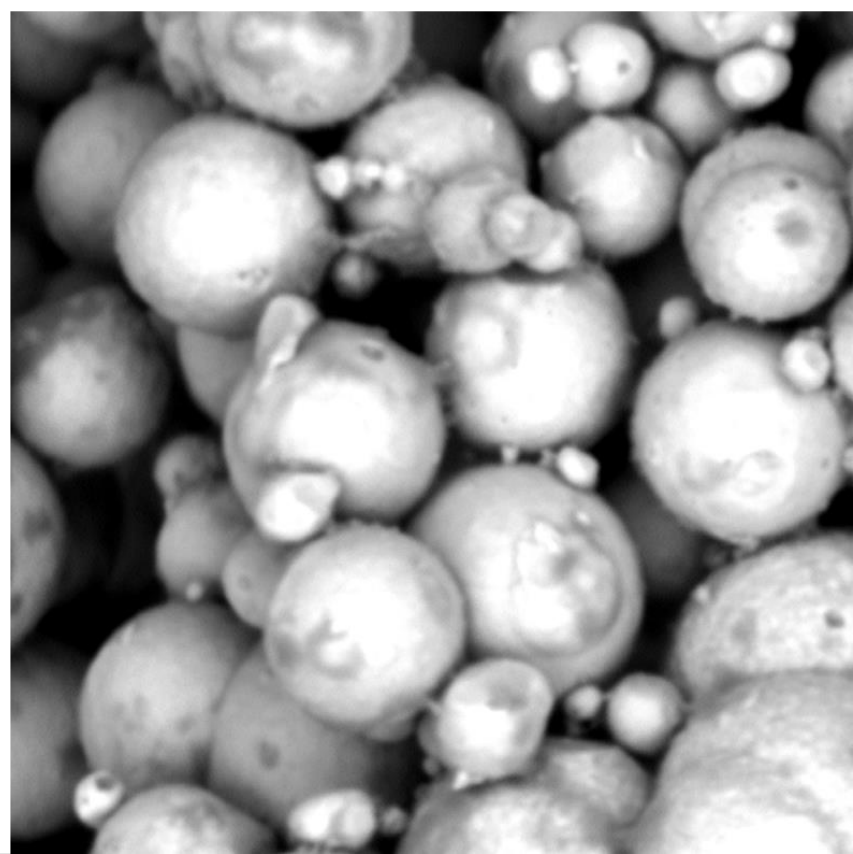

Journal of Materials Chemistry C

PAPER

Cite this: J. Mater. Chem. C, 2015, 3, 4646

A facile controllable coating of carbonyl iron particles with poly(glycidyl methacrylate): a tool for adjusting MR response and stability properties

Martin Cvek,[ab] Miroslav Mrlik,*[ac] Marketa Ilcikova,[cd] Tomas Plachy,[a] Michal Sedlacik,[a] Jaroslav Mosnacek[d] and Vladimir Pavlinek[a]

Received 31st January 2015,
Accepted 30th March 2015

DOI: 10.1039/c5tc00319a

www.rsc.org/MaterialsC

This study is focused on the controllable coating of the carbonyl iron (CI) particles widely applied in magnetorheology. These particles were grafted with poly(glycidyl methacrylate) (PGMA) with narrow polydispersity *via* surface-initiated atom transfer radical polymerization. Two types of core–shell particles differing in molecular weights of grafted polymer chains were synthesized. The effect of shell thickness on the thermo-oxidation stability of particles as well as the sedimentation stability of their silicone oil suspensions was evaluated. The successful coating process was confirmed by Fourier transform infrared spectroscopy and energy-dispersive spectrometry. The differences in the magnetic properties of bare and coated CI particles were clarified through vibrating sample magnetometry. Due to the controllable length of the PGMA grafts, the magnetic properties remain almost the same as those for bare CI. The magnetorheological (MR) behavior of silicone oil suspensions containing 60 wt% of bare CI particles as well as PGMA-coated analogues was investigated in the absence and in the presence of various magnetic field strengths, demonstrating the negligible impact of surface modification on final MR performance. Thus, the grafting of the particles with PGMA negligibly affected magnetic properties but considerably enhanced thermo-oxidation and sedimentation stabilities. Finally, a novel tensiometric method for sedimentation stability measurements of MR suspensions was successfully implemented.

1. Introduction

Magnetorheological (MR) suspensions are fluids that have their rheological behavior (yield stress, apparent viscosity, storage modulus) altered by the application of an external magnetic field.[1–3] Generally, MR suspensions consist of solid, usually micron-sized, magnetically-polarizable particles dispersed in a non-magnetic carrier liquid such as silicone or mineral oils. In the absence of an external magnetic field (off-state), particles are randomly dispersed in the carrier liquid. The MR suspension has low viscosity depending on the carrier liquid and behaves almost like a Newtonian fluid. After the application of an external field (on-state), the particles are polarized and in a fraction of a millisecond create highly-organized structures, which results in the predominance of magnetic forces over hydrodynamic ones. When the chain-like structures are formed, the viscosity and viscoelastic moduli increase by several orders of magnitude. The orientation of chain-like structures is along the magnetic field direction, and their toughness is a function of the applied magnetic field strength. This phenomenon is reversible and is called the MR effect.[1–6]

Nowadays, MR suspensions are well-known and referred to as ''intelligent'' or ''smart'' materials, which play an important role in many engineering applications due to their fine-tuning material behavior. Their unique properties preferably can be used for the active control of vibrations or the transmission of torque. Typical applications include dampers,[7–10] brakes,[11,12] clutches,[13,14] prosthetic devices[15] or ultrafine polishing devices.[16] Also, biomedical applications such as drug targeting[17] or hyperthermia in cancer therapy[18] have been recently studied with regard to these systems. The broad applicability of these suspensions therefore attracts both scientific and industrial interests.

Despite such broad applications, some drawbacks hinder their potential. Due to the large density difference between metal particles and carrier oils, poor sedimentation stability is a common problem.[19] Several methods can enhance sedimentation stability, including the addition of surfactant systems[20] or nano-sized particles such as fumed silica,[21] organic clays,[22] carbon nanotubes[23] or graphite micro-particles.[24] Although the

[a] Centre of Polymer Systems, University Institute, Tomas Bata University in Zlin, Nad Ovcirnou 3685, 760 01 Zlin, Czech Republic. E-mail: mrlik@ft.utb.cz
[b] Polymer Centre, Faculty of Technology, Tomas Bata University in Zlin, nam. T. G. Masaryka 275, 762 72 Zlin, Czech Republic
[c] Center for Advanced Materials, Qatar University, P. O. Box 2713, Doha, Qatar
[d] Polymer Institute, Slovak Academy of Sciences, Dubravska cesta 9, 845 41 Bratislava 45, Slovakia

addition of fillers can increase sedimentation stability, the off-state viscosity inevitably increases, which can be a problem in some applications. Therefore, the application of a polymer coating on the surface of the particles seems to be a wise strategy to counter this drawback.[2,25] Various processes for the preparation of core–shell particles have been used, including dispersion polymerization, suspension polymerization or solvent evaporation. Also many polymers have been used as shell materials, *e.g.*, poly(methyl methacrylate)[26] or polystyrene,[27] which were synthesized *via* both dispersion and suspension polymerizations. Coatings consisting of poly(vinyl butyral)[28] or polycarbonate[29] were prepared using solvent evaporation. Another approach is utilizing the vacuum plasma deposition of fluorinated substances.[30] Furthermore, electrically-conductive polymers such as polypyrrole[31] or polyaniline[3] were successfully used as non-covalently bonded shell materials for this reason. The thickness of the coating layer using suspension polymerization is 2–10 microns, while dispersion polymerization creates submicron coating layers. However, as is widely known, with the increasing thickness of polymer coating, the saturation magnetization (or magnetic susceptibility) decreases, which causes a lower yield stress generation in the on-state of MR suspensions.[2] Therefore, there is a need to precisely control the molecular weight of a grafted polymer and thus to be able to adjust the MR performance of prepared suspensions.

ATRP was introduced by Matyjaszewski *et al.*[32] in 1995 as one of the methods allowing for the preparation of polymers with precisely controlled molecular weight, narrow polydispersity, controlled chain composition and tailored functionalities. The ATRP system consists of alkyl halide as an initiator, metal halide as a catalyst and a ligand complexing the metal halide catalyst and thus improving its solubility in a polymerization mixture and fine tuning its catalytic efficiency. ATRP can be applied to a wide range of vinyl monomers under relatively mild conditions at elevated temperatures[33,34] or at room temperature under UV-VIS irradiation.[35] So far, only two polymers poly(butyl acrylate)[25] and poly(2-fluorostyrene)[34] with molecular weights above 15 000 g mol^{-1} were grafted using surface-initiated ATRP (SI-ATRP) in order to prepare core–shell CI-polymer particles for MR suspensions. However, magnetic properties were significantly suppressed in the mentioned studies due to the thick shells of the high molecular weight polymer chains.

Therefore, this study was aimed at using SI-ATRP for the preparation of CI particles grafted with poly(glycidyl methacrylate) (CI–PGMA) of short chain-lengths in order to investigate whether such short polymer chains can provide sufficient sedimentation and thermo-oxidation stability while not affecting their good magnetic properties, characteristics necessary for many industrial applications.

2. Experimental

2.1 Materials

The CI powder (SL grade) used throughout this work is a commercial product of BASF Corporation (Germany). The chemical composition of CI, as given by the manufacturer, is a minimum 99.5% pure iron. Glycidyl methacrylate (GMA, 97%) was purchased from Sigma Aldrich (USA), and before use it was purified by passing it through a basic alumina in order to remove a stabilizer. (3-Aminopropyl)triethoxysilane (APTES, ≥98%) was used as a coupling agent between the CI particles and the difunctional initiator α-bromoisobutyryl bromide (BiBB, 98%). Ethyl α-bromoisobutyrate (EBiB, 98%) was used as a sacrificial initiator. BiBB, APTES, EBiB and other chemicals such as triethylamine (Et_3N, ≥99%), *N*,*N*,*N*′,*N*″,*N*″-pentamethyldiethylenetriamine (PMDETA, ≥99%), copper bromide (CuBr, ≥99%), anisole (99%), and aluminum oxide (neural, Brockmann I) were produced by Sigma Aldrich (USA) and used as received. Silicone oil used for the preparation of MR suspensions was Lukosiol M200 (Chemical Works Kolín, Czech Republic; dynamic viscosity of 197 mPa s, density of 0.97 g cm^{-3}). Solvents and purification agents, namely tetrahydrofuran (THF, p.a.), acetone (p.a.), ethanol (absolute anhydrous, p.a.), toluene (p.a.), and hydrochloric acid (HCl, 35%, p.a.), were obtained from Penta Labs (Czech Republic).

2.2 Synthesis

Surface activation and functionalization of CI microparticles. The fundamental procedure of chemical activation and functionalization of CI was inspired by Belyavskii *et al.*[36] and was also successfully used by Mrlik *et al.*[37] The bulk of the CI powder (100 g) was placed into a beaker and treated with 250 mL of 0.5 M HCl for 10 minutes in order to attain reactive hydroxyl groups on the CI particle surface. Acid-treated CI powder was rinsed with distilled water (5 times, 300 mL each), ethanol (3 times, 150 mL each), and acetone (3 times, 100 mL each) using a decantation method with a magnet at the bottom of the beaker. Finally, the powder was dried for 3 hours at 60 °C under 200 mbar in order to remove residual acetone. Surface-activated dry CI powder (90 g) was weighted into a 500 mL three-neck flask and dispersed in 300 mL of a non-polar solvent, toluene. The flask was equipped with a mechanical stirrer, a reflux condenser and a thermometer. Then, 10 mL of APTES as a coupling agent was added, and the suspension formed was agitated under 250 rpm and refluxed for 6 hours at 110 °C. After the reaction, functionalized CI particles were thoroughly washed with toluene (3 times, 100 mL each), ethanol (3 times, 150 mL each), and acetone (3 times, 100 mL each), and dried for 24 hours under 200 mbar.

Immobilization of the initiator. The immobilization of the ATRP initiator BiBB was performed in the presence of dried THF (Scheme 1) as follows: 40 g of CI particles modified with an APTES silane agent (CI-NH_2) were added into a Schlenk flask (SF), and the space of the flask was evacuated for 30 minutes. Then, 50 mL of dried THF was distilled and moved to the SF under an argon atmosphere. After that, 16 mL of Et_3N were transferred into the SF. Finally, 8 mL of BiBB were added dropwise into the mixture, and the whole content of the SF was cooled down and kept in the ice bath for 3 hours. Subsequently, the mixture was stirred overnight. Then, the initiator-treated CI particles (CI–Br) were rinsed with acetone (3 times, 100 mL each) and dried for 24 hours at 60 °C under 200 mbar.

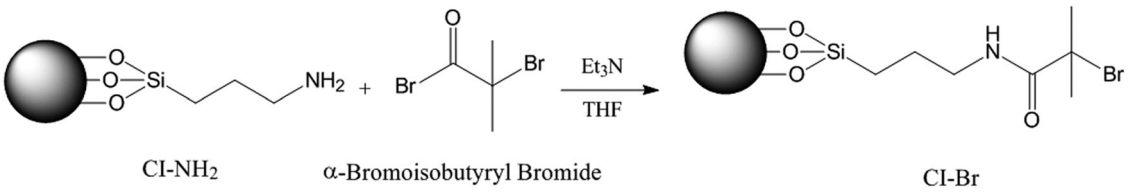

Scheme 1 Attachment of the initiator onto the surface of CI particles.

Surface-initiated polymerization from CI–Br particles. In this step, 10 g of CI–Br particles were placed into SF, evacuated several times and then backfilled with argon. Then, GMA (20 mL; 0.1466 mol), PMDETA (0.1530 mL; 0.733 mmol), EBiB (0.1076 mL; 0.733 mmol) and anisole (20 mL; 0.1840 mol), were injected into the SF. Several freeze–pump–thaw cycles with liquid nitrogen were performed to eliminate residual oxygen from the polymerization mixture, and finally the SF was filled with argon. The polymerization was initiated by the addition of a CuBr catalyst (0.1052 g; 0.733 mmol) into a polymerization mixture and placing the reaction flask into an oil bath pre-heated to 50 °C. The reaction mixture was stirred at 175 rpm for 2 hours, and then the reaction was stopped by opening the flask. The prepared particles were further denoted CI–PGMA-1. Scheme 2 illustrates the described SI-ATRP approach.

CI particles grafted with higher molecular weight PGMA polymer chain (CI–PGMA-2) were synthesized in the same manner but with a higher GMA:initiator molar ratio. The amounts of monomer and solvent in this case were as follows: GMA (30 mL; 0.2199 mol) and anisole (30 mL; 0.2760 mol). The PGMA-grafted core–shell structured particles were purified by washing with THF (3 times, 100 mL each) and acetone (3 times, 100 mL each) before being dried overnight at 60 °C.

2.3 General characterization

Monomer conversion was determined by ^{1}H NMR using a 400 MHz VNMRS Varian NMR spectrometer (Varian Inc. since 1999 part of Agilent, Japan) equipped with a 5 mm ^{1}H–^{19}F/^{15}N–^{31}P PFG AutoX DB NB probe at 25 °C. Deuterated chloroform ($CDCl_3$) was used as a solvent. For NMR measurements, a sample (green polymer solution) taken after 2 hours of polymerization was passed through aluminum oxide (neutral), absorbent cotton and a microfilter in order to remove the copper catalyst and CI–PGMA particles, and the colorless filtrate was supplemented by $CDCl_3$.

GPC PL–GPC220 (Agilent, Japan) was employed to determine the relative molecular weight of the polymer samples as well as the distribution of molecular weights during the polymerization. THF was used as an eluent (mobile phase) at a flow rate of 1.0 mL min^{-1}. The polystyrene was used as a standard to calibrate the GPC, and anisole was used as an internal standard to correct any fluctuations in the THF flow rate. The sample was mixed with THF, then purified in the same manner as for the ^{1}H NMR measurement and injected into a GPC column heated to 30 °C.

Morphologies of bare CI and the prepared CI–PGMA particles were examined using a scanning electron microscope (SEM; Tescan Vega II LMU, Czech Republic) employing 5–10 kV of accelerating voltage. A secondary electron (SE) detector was used due to its higher depth of field. A Tescan Vega II LMU is equipped with an energy-dispersive spectroscope (EDS), which is used for the surface elemental analysis of the studied particles.

Fourier transform infrared (FTIR) spectra were obtained from a Nicolet FTIR spectrometer (Nicolet 6700, USA) equipped with an ATR accessory in order to prove the success of the ATRP coating process. The measurement was performed at laboratory temperature using a Germanium crystal in the region of 4000–500 cm^{-1}.

The magnetic properties of the CI and CI–PGMA powders were characterized by vibrating sample magnetometry (VSM; 7407,

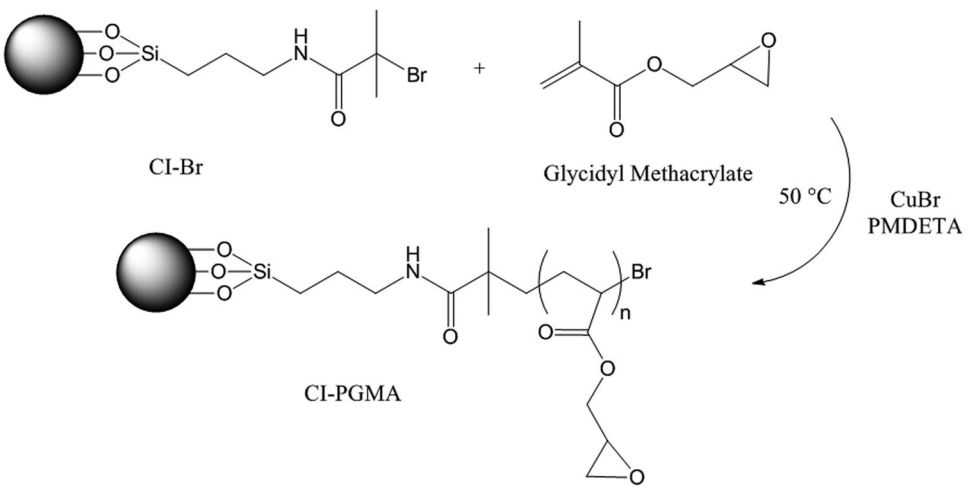

Scheme 2 Grafting of CI–Br particles with PGMA using the SI-ATRP.

Lakeshore, USA). Approximately 200–300 mg of the sample was subjected to a magnetic field in the range of ±780 kA m^{-1} at laboratory temperature.

Thermo-oxidative stability, an important characteristic of the MR particles, was investigated with the help of thermogravimetric analysis (TGA; TA Instruments Q500, USA) under an air atmosphere at a heating rate of 10 K min^{-1}. The weight gain of the samples was observed during all TGA measurements, indicating ongoing chemical reactions. The weight gain was further plotted as a function of temperature.

2.4 Suspension preparation and rheological measurements

Three variants of MR suspensions with a 60 wt% (approx. 16 vol%) particle concentration in silicone oil were prepared. The first suspension was based on bare CI particles, while the second and third suspensions contained CI–PGMA particles grafted with PGMA of different molecular weights.

The rheological properties of MR suspensions in the absence as well as in the presence of various magnetic field strengths were experimentally studied. Measurements were carried out using a Physica MCR502 (Anton Paar GmbH, Austria) rheometer equipped with a magnetic cell (Physica MRD 170 + H–PTD200) using a parallel plate (PP20/MRD/TI) geometry with a diameter of 20 mm. A gap of 0.5 mm was maintained between the plates, and a 0.2 mL sample of the MR suspension was placed between them. The steady shear measurements in the controlled shear mode were performed in the shear rate range (1–300 s^{-1}). The small-strain oscillatory tests were carried out through strain sweeps and frequency sweeps. The linear viscoelasticity region (LVR) was found through a storage modulus, G', measurement as a function of strain, γ. The used strain range was (10^{-3}–10^{1}%) at a fixed frequency of 1 Hz under different magnetic field strengths. Then, frequency sweeps were performed in a range of frequencies (0.1–10 Hz) at a constant amplitude strain (obtained from LVR investigation).

Prior to each on-state measurement, field-induced structures were agitated by continuous shearing (shear rate 50 s^{-1}) for one minute. Then, the new magnetic field strength was imposed (0–438 kA m^{-1}). The temperature was maintained at 25 °C using a closed-cycle cooling system (Julabo FS18, Germany). To avoid sedimentation, the tests were started as soon as the thoroughly-mixed suspension was injected into the measuring system. Finally, it has to be stated that the error bars were not included in the graphs, because these are not larger than the size of the data symbols.

2.5 Sedimentation stability measurements

The sedimentation stability of MR suspensions based on CI and both variants of CI–PGMA particles was determined using a Tensiometer Krüss K100 (MK2/SF/C, Hamburg, Germany) at laboratory temperature. An evaluation of sedimentation stability of MR suspensions *via* tensiometry was recently proposed by Sedlacik *et al.*[38] MR suspensions containing 10 wt% (approx. 1.5 vol%) of CI particles or their PGMA-coated analogues in silicone oil were prepared by thorough mixing followed by sonication using an ultrasound device (Sonopuls HD 2070, Bandelin electronic, Germany) for 2 minutes. This amount of particles in suspension was chosen in order to avoid the overfilling of the measuring probe during experiment. The funnel-shaped measuring probe was hung up on scales and then immersed in the test suspension. The total height of the tested suspension was 45 mm, while the measuring probe was placed 20 mm under the surface. The probe captured settling particles and evaluated their weight as a function of time. The sedimentation measurements were performed for 2 hours, *i.e.*, until a plateau in a mass increment was observed.

3. Results and discussion

3.1 CI–PGMA synthesis, ^{1}H NMR and GPC investigation

The molecular weight of a polymer coating can significantly affect the properties of MR particles. If the molecular weight is too low and thus the shell too thin, the polymer shell will not prevent CI particles from settling. In contrast, too high molecular weight of a polymer coating can cause an undesirably large increase in off-state viscosity.[25] Therefore, CI particles coated with PGMA of two different molecular weights were prepared. The syntheses of CI–PGMA particles were performed at 50 °C *via* SI-ATRP using EBiB as a macroinitiator, CuBr as a catalyst and PMDETA as a ligand in molar ratios [GMA]:[EBiB]:[CuBr]:[PMDETA] = [200]:[1]:[1]:[1] and [300]:[1]:[1]:[1]. The conversion value expresses the percentage of monomer units built into polymer chains and was determined by ^{1}H NMR. The weight-average molecular weight ($\bar{M}_w$) and number-average molecular weight ($\bar{M}_n$) of PGMA were determined by GPC analysis based on free PGMA chains grown from a free sacrificial initiator, under the assumption of the similar growth of polymers from free and bond initiators. The results are summarized in Table 1. A relatively narrow polydispersity in both polymerizations implies that the ATRP was well controlled and the thickness of the PGMA coating on the CI particles could be expected to be uniform.

3.2 Scanning electron microscopy

SEM micrographs of original CI particles and prepared CI–PGMA particles are displayed in Fig. 1. The SEM analysis confirmed that bare CI particles as well as CI–PGMA particles have a spherical shape. However, the presence of the rod-like particles in the sample of bare CI, probably as an incomplete product of CI synthesis, was also observed (Fig. 1a). Modification affected the particle morphology; the surface of bare CI particles is quite smooth, whereas the surface of coated CI particles is rougher,

Table 1 Results of SI-ATRP of PGMA performed at 50 °C

Sample code	GMA [mL]	Time [min]	Conversion[a] [%]	$\bar{M}_w$ [g mol^{-1}]	$\bar{M}_n$ [g mol^{-1}]	PDI [–]
CI–PGMA-1	20	120	87.0	6600	5000	1.32
CI–PGMA-2	30	120	88.5	12 500	9700	1.29

[a] Based on ^{1}H NMR spectra.

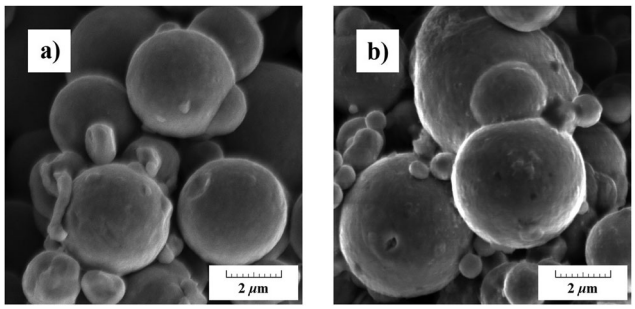

Fig. 1 SEM images of bare CI particles (a) and CI–PGMA-1 particles (b).

which indicates the presence of grafted PGMA polymer chains (Fig. 1b).

3.3 Energy dispersive spectroscopy

Fig. 2 shows a representative EDS spectrum of bare CI particles. As expected, the examined sample is almost pure iron with some carbon contained as a small impurity present in the CI after fabrication. The EDS spectrum of PGMA-coated CI particles is illustrated in Fig. 3. The most represented element is iron. The second most frequent element is carbon, which is partly from CI impurity and partly from the individual components (the coupling agent, residue of the initiator, and the PGMA chain) constituting the whole graft. An increased content of carbon in CI–PGMA-1 particles indicates the presence of the polymer layer on the CI surface. Similar data were presented by Kim *et al.*,[4] in their study, where an increase in carbon content from 15.7% to 40.5% due to the relatively thick polymer layer, was reported. In our measurements, an increase of carbon content from 17.9% to 27.8% was observed presuming a thinner polymer layer. Moreover, the EDS analysis also revealed silicon atoms, which originate from the APTES coupling agent. The presence of oxygen can also be seen, which is a signal from

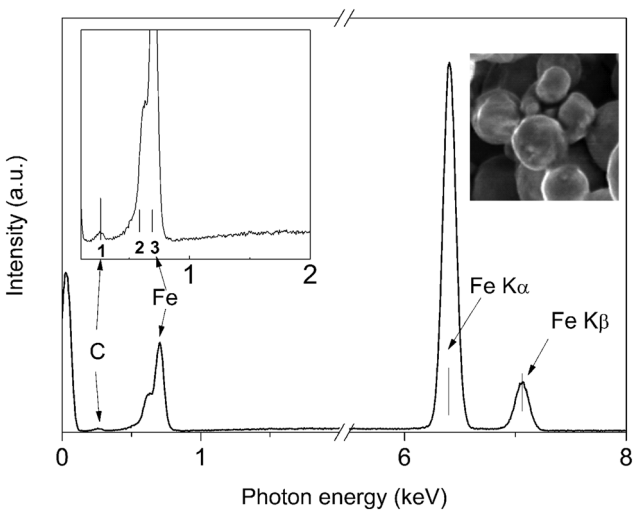

Fig. 2 The EDS spectrum of the surface of the bare CI particles, with magnified details in graph inset: 1-C Kα line, 2 and 3-Fe L lines. The inset image shows the place from where the spectrum was collected.

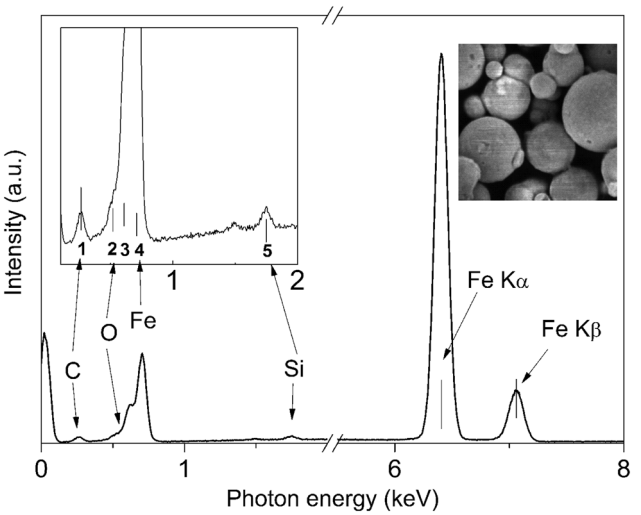

Fig. 3 The EDS spectrum of the surface of the CI–PGMA-1 particles, with magnified details in the graph inset: 1-C Kα line, 2-O Kα line, 3 and 4-Fe L lines, 5-Si Kα line. The inset image shows the place from where the spectrum was collected.

Table 2 Results of EDS elemental analysis

	Atomic%	
Element	Bare CI particles	CI–PGMA-1 particles
Fe	82.1	65.7
C	17.9	27.8
O	0.0	5.7
Si	0.0	0.8
Total	100.0	100.0

the coupling agent as well as from the PGMA polymer chain. However, its Kα emission was overlapped in the low energy shoulder of the broad iron L emission peak (the inset of Fig. 3). The content of observed elements in the samples expressed as atomic percentage is summarized in Table 2. The presence of the nitrogen and bromine elements was not observed, probably due to their low concentration and weak signal.

3.4 Fourier transform infrared spectroscopy

FTIR spectral curves of bare CI particles and PGMA-coated CI particles were compared. Fig. 4 illustrates the differences in wavenumbers of individual spectra. In the spectrum of the CI–PGMA composite particles, the appearance of a characteristic peak at around 1714 cm^{-1} reflects the stretching vibration of the –C═O carbonyl group. Vibrations at 1305 cm^{-1} indicate a C–O–C bond of methacrylate. Sharp peaks at 904 cm^{-1} and 815 cm^{-1} are an oxirane ring contraction vibration and an unsymmetrical expansion.[39,40] Hence, FTIR spectroscopy was another method proving the successful coating of the CI particles.

3.5 Magnetic properties

VSM measurements were performed in order to determine the magnetic properties of bare CI as well as coated CI–PGMA particles. The magnetization curves for bare CI particles and

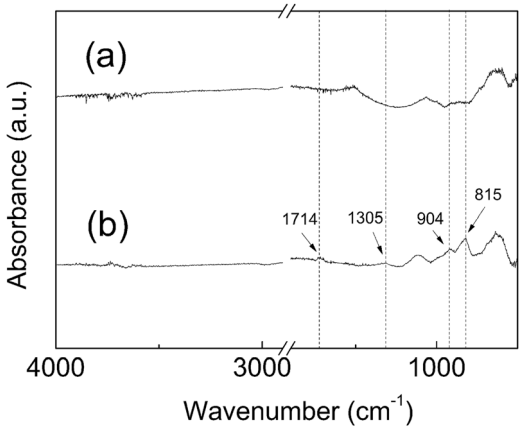

Fig. 4 FTIR spectra of bare CI particles (a), and CI–PGMA-1 particles (b).

both variants of PGMA-coated CI particles exhibit a similar character, as presented in Fig. 5. True saturation magnetization of the particles was not reached due to the insufficient intensity of the external magnetic field. According to de Vicente *et al.*,[41] the saturation magnetization of the CI powder can be reached at a magnetic field strength of 1360 kA m^{-1}. The actual measured magnetization (obtained for a magnetic field strength of 780 kA m^{-1}) of utilized bare CI particles was 178.79 emu g^{-1}. For coated particles, the magnetizations at the same magnetic field strength were 171.77 emu g^{-1} and 169.32 emu g^{-1}, which are only a 3.9% and 5.3% decrease, respectively, compared to bare CI particles. A decrease in observed magnetization was expected due to the non-magnetic polymer shell, but the decrease is negligible. Therefore, the impact on the MR effect should not be severe. In 2014, Kim *et al.*[4] fabricated CI–PGMA particles by cross-linking PGMA with ethylene glycol dimethacrylate, and quite a large magnetization decrease at a comparable magnetic field strength was reported, *i.e.*, from 175 emu g^{-1} to 85 emu g^{-1}, which represents a 51.4% decrease.

The other monitored parameter was coercivity. The lower it is, the better the dynamics of the demagnetization of the particles. VSM measurements show that the polymer coating

Table 3 Results of VSM measurement

Sample code	Magnetization at 780 kA m^{-1} [emu g^{-1}]	Coercivity [kA m^{-1}]
CI	178.79	0.95
CI–PGMA-1	171.77	0.91
CI–PGMA-2	169.32	0.94

hardly affected the coercivity, which is also a positive outcome (Table 3). The measured coercivity of bare CI particles was 0.95 kA m^{-1}, while 0.91 kA m^{-1} for CI–PGMA-1 particles, and 0.94 kA m^{-1} for CI–PGMA-2 particles, respectively. The retained high values of magnetization and unaltered coercivity make the prepared CI–PGMA particles promising candidates for the effective utilization of their MR suspensions in practical applications.

3.6 Thermo-oxidative stability

The weight gain was plotted as a function of temperature as shown in Fig. 6. Clearly, such a weight gain is the result of iron oxide formation. Iron powder takes up to 40 wt% of oxygen and forms oxides as follows: FeO, Fe_3O_4 and finally Fe_2O_3.[42] The figure shows that the reaction requires an exceptionally-wide temperature range to achieve full conversion. The weight of bare CI particles started to increase at lower temperatures compared to core–shell structured CI particles. As expected, the PGMA polymer coating on the surface of CI particles leads to considerable thermo-oxidative resistance enhancement. The first weight changes of bare CI particles were observed at temperatures around 200 °C. Both variants of PGMA-coated CI particles were thermally stable up to 300 °C. A significant increase in the weight of uncoated CI particles occurs at temperatures around 400 °C, while a similar sharp weight gain due to severe oxidation is shifted to temperatures above 500 °C for both coated CI particle variants.

Fig. 6 also demonstrates that the polymer-coated CI particles thermally decompose and the inner iron core is simultaneously oxidized during heating. If the polymer decomposed first, the

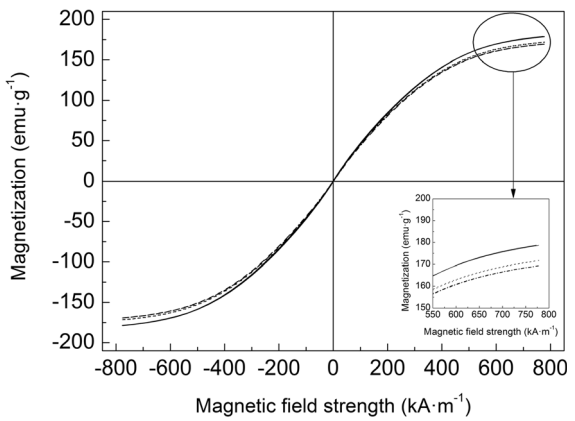

Fig. 5 Magnetization curves of bare CI particles (solid lines), CI–PGMA-1 particles (dotted lines), and CI–PGMA-2 particles (dashed lines).

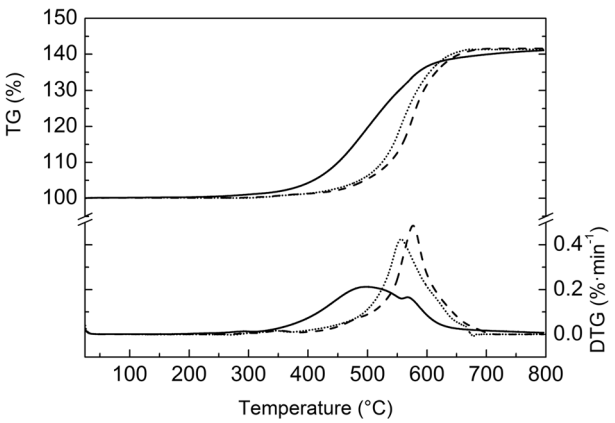

Fig. 6 TG and DTG curves of bare CI particles (solid lines), CI–PGMA-1 particles (dotted lines), and CI–PGMA-2 particles (dashed lines) in the air atmosphere.

weight decrease would be displayed on the thermogram, so the reactions probably took place concurrently. A small weight decrease occurred at around 650 °C in both variants of coated particles. This could be due to some absorbed gases on the particle surface. A grafted polymer coating thus provides a protective over-layer on the CI particles, which shifted the oxidation process to higher temperatures; however, the doubling of its molecular weight further contributes to only a slight improvement in thermo-oxidative resistance.

3.7 Rheological properties in steady shear mode

Fig. 7 illustrates the steady shear behavior of the examined MR suspensions. Almost linear increase of the shear stress and a plateau of viscosity in the off-state suggest nearly Newtonian rheological behavior. On the other hand, when the magnetic field was applied, the shear stress and the shear viscosity of all MR suspensions dramatically increased and the flow became pseudoplastic. These quantities increased with magnetic field strength due to higher toughness of field-induced internal structures. Moreover, the shear stress and consequently viscosity of MR suspensions based on both types of PGMA-coated particles exhibited comparable values with MR suspension of bare CI indicating a similar performance of tested suspensions. However, suspension based on CI–PGMA-2 particles exhibited higher off-state viscosity, due to the improved compatibility and lower on-state viscosity due to more suppressed magnetic properties as a result of thicker polymeric shell. Nevertheless, the results suggest that the MR suspensions based on PGMA-coated particles *via* ATRP are able to develop considerably strong internal structures, which are sufficient for practical applications of such suspensions.

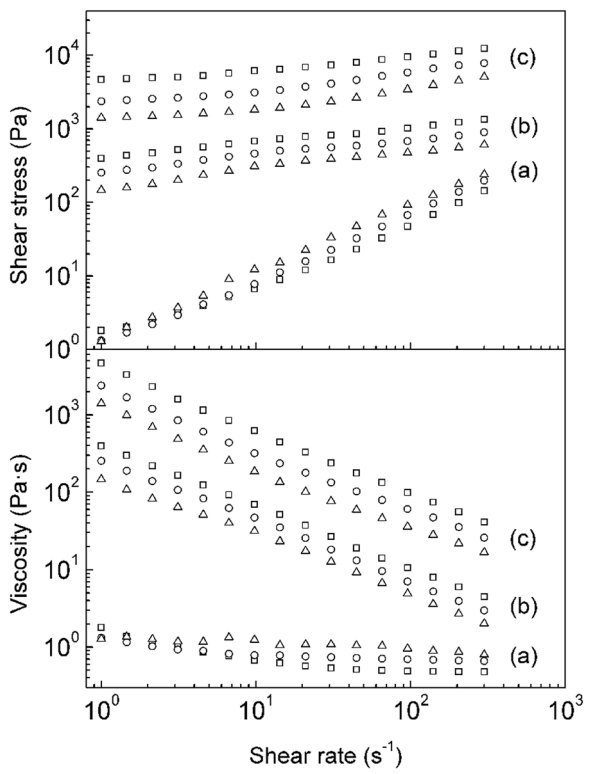

Fig. 7 Rheograms of MR suspensions containing 60 wt% of bare CI particles (open squares), CI–PGMA-1 particles (open circles), and CI–PGMA-2 particles (open triangles) at 0 kA m^{-1} (a), and 87 kA m^{-1} (b), 438 kA m^{-1} (c) magnetic field strengths.

3.8 Rheological properties in oscillatory mode

Oscillatory tests at sufficiently low deformations do not destroy the structure,[43] therefore they were established as a suitable tool to evaluate the behavior of MR suspensions at dynamic strain. The LVR was determined in an amplitude sweep test, which is necessary because the values of G' and loss modulus, G'', have a physical meaning only when the internal structures are not broken.[44] Therefore, the dependence of G' and G'' on γ for oscillatory shear flow was investigated. The position of LVR changes depending on the strength of the applied magnetic field,[6] but the change was negligible in our measurements (Fig. 8). The apparent decrease of G' appeared at a 0.04% amplitude strain for a 60 wt% MR suspension based on bare CI as well as on both variants of CI–PGMA particles. All studied MR suspensions exhibited G'' larger than G' within the whole

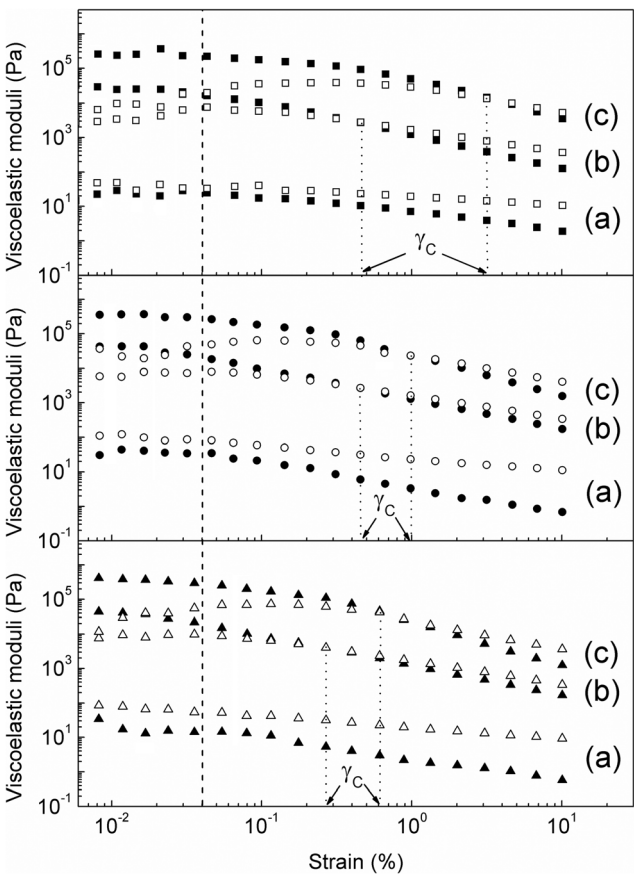

Fig. 8 Storage, G' (solid symbols), and a loss, G'' (open symbols) moduli as a function of strain for MR suspensions containing 60 wt% of bare CI particles (squares), CI–PGMA-1 particles (circles), and CI–PGMA-2 particles (triangles) at 0 kA m^{-1} (a), and 87 kA m^{-1} (b), 438 kA m^{-1} (c) magnetic field strengths. Vertical dashed line refers to the value used for further frequency sweep measurements.

strain range in the absence of a magnetic field, which indicates a liquid-like behavior. After the application of the magnetic field, the MR suspensions exhibited solid-like behavior due to a chain-like structure formation, and G' became higher than G''. However, G'' exhibited non-zero values, which is according to Ramos *et al.*[44] due to the existence of free chains with one or two ends not connected to the surface of the geometry.

As can be seen in Fig. 8, the effect of particle surface modification on the critical strain, γ_C, of MR suspensions was evaluated. Critical strain is defined as the value of the strain where G' and G'' moduli are equal, which represents the transition between the viscoelastic-solid at low strain and the viscoelastic-liquid at high strain values. Moreover, this parameter is responsible for a competition between magnetic forces and hydrodynamic ones.[43] It was observed that a higher magnetic field strength leads to a higher value of γ_C, because a larger magnetic field is able to retain a solid structure to higher strains. MR suspensions containing modified particles exhibited lower values of γ_C at all magnetic field strengths compared to the suspension of bare CI particles. This effect was more obvious in the suspension based on CI–PGMA-2 particles.

The determined strain amplitude of the LVR position was maintained within the range of frequencies (0.1–10 Hz), and the viscoelastic moduli were evaluated. In all measurements, the viscoelastic moduli in the off-state exhibit a slow but gradual increase over a wide range of frequencies. On the other hand, in the on-state, the G' and G'' were almost independent in the measured frequency range. An applied magnetic field strength caused an increase of G' as well as G'' for all prepared suspensions. Comparing suspensions off-state with on-state at 438 kA m^{-1}, G' increased by a factor of 10^5, whereas G'' increased by a factor of 10^4. This phenomenon is similar for all prepared suspensions.

Fig. 9 shows values of G', which is related to chain toughness and G'', which demonstrates heat dissipation in the MR suspensions during dynamic strain, as a function of frequency. The former exhibits similar values for each suspension at the same magnetic field strength with only slight deviations as well as the values of the latter are almost identical. Generally, G' and G'' were negligibly affected by the controlled particle coating.

Frequency sweeps were analyzed at 5 different magnetic field strengths (87 kA m^{-1}, 173 kA m^{-1}, 262 kA m^{-1}, 351 kA m^{-1}, and 438 kA m^{-1}) (data not shown here) in order to determine the dynamic efficiency (e) of MR suspensions, which is defined as: $e(f) = (G_H' - G_0')/G_0'$ where G_H' is the field-on storage modulus, G'_0 is the field-off storage modulus and was evaluated at 1 Hz as a function of applied magnetic field strength (Fig. 10). In all suspensions, dynamic efficiency generally increased with increasing magnetic field strength. At relatively low fields (up to 173 kA m^{-1}), values of the dynamic efficiency exhibited a sharp increase, while at higher magnetic field strengths its values started to plateau. MR suspensions of modified CI particles showed even higher values of dynamic efficiency, which is due to lower off-state storage modulus and comparable on-state modulus. In this case, the molecular weight of grafted PGMA did not have a distinct effect on dynamic efficiency, and only slight deviations between efficiencies of modified suspensions were observed.

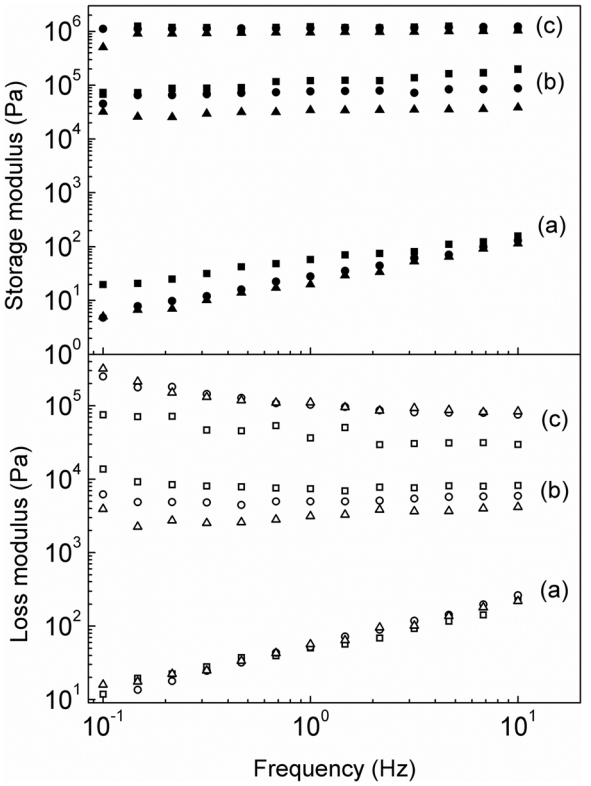

Fig. 9 Storage, G' (solid symbols), and a loss, G'' (open symbols) moduli as a function of frequency for MR suspensions containing 60 wt% of bare CI particles (squares), CI–PGMA-1 particles (circles), and CI–PGMA-2 particles (triangles) at the off-state (a), and 87 kA m^{-1} (b), 438 kA m^{-1} (c) magnetic field strengths.

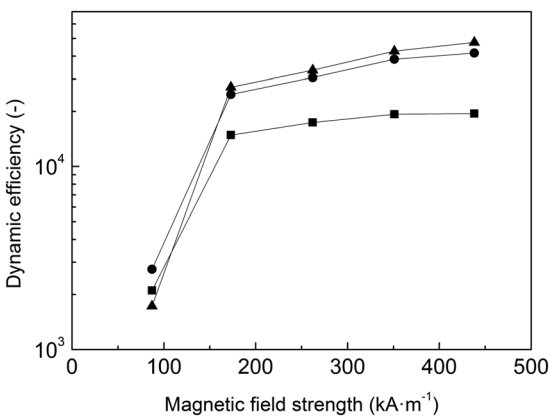

Fig. 10 Dynamic efficiency as a function of magnetic field strength for MR suspensions containing 60 wt% of bare CI particles (squares), CI–PGMA-1 particles (circles), and CI–PGMA-2 particles (triangles).

It can be concluded that the controllably-grafted PGMA layer with quite low molecular weights (6600 and 12 500 g mol^{-1}) almost did not affect magnetic susceptibility. Therefore, the MR suspension containing modified CI particles is able to interact with an external magnetic field comparably to the

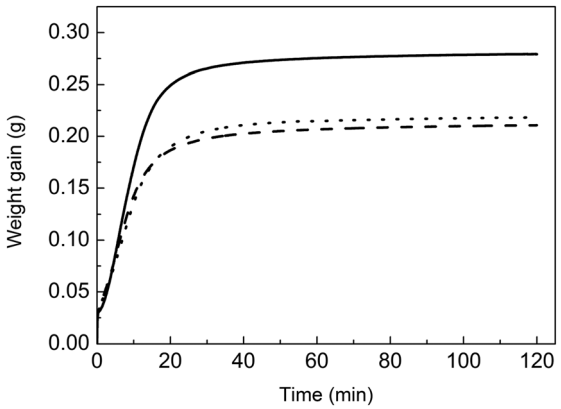

Fig. 11 Time dependence of the weight gain representing settled particles for 10 wt% MR suspensions based on bare CI particles (solid line), CI–PGMA-1 particles (dotted line), and CI–PGMA-2 particles (dashed line) in silicone oil.

suspension of bare CI particles, which was reflected in the almost unaffected values of viscoelastic moduli of prepared MR suspensions. Decreased values of G' in the off-state for modified MR suspensions ultimately led to higher values of dynamic efficiency.

3.9 Sedimentation stability

Fig. 11 shows the weight gain representing settling particles as a function of observation time. Based on the graphical results, it can be confidently asserted that the use of core–shell CI–PGMA particles as a dispersed phase considerably enhanced the sedimentation stability of MR suspensions compared to suspension of the same amount of bare CI particles. Improved sedimentation stability of suspensions containing CI–PGMA particles is due to the presence of PGMA polymer chains which contribute to the reduced bulk density of composite particles[1,2] and provide better compatibility with silicone oil.[38] The suspension based on CI–PGMA-2 particles exhibits only a slight improvement in sedimentation stability compared to the suspension based on CI–PGMA-1, thus the length of polymer chains does not play that important role as expected. The probe entrapping settling particles was placed close to the surface, therefore the phase interface passed through this area after a while; hence the weight gain quickly reached its asymptotic value. Thus, this method provided fast estimation of sedimentation velocity.

4. Conclusion

The surface of CI particles was controllably coated with PGMA in order to enhance thermo-oxidation and sedimentation stability while maintaining their sufficient magnetic properties. These aims were fulfilled with the use of CI–PGMA particles prepared *via* facile SI-ATRP. Two types of core–shell particles were synthesized, in which the polymer shell consisted of PGMA with molecular weights of either 6600 g mol^{-1} or 12 500 g mol^{-1} PDI of 1.32 and 1.29, respectively. The presence of the PGMA shell was proved by EDS and FTIR spectroscopies. A slight decrease in magnetization was detected due to the non-magnetic coating, which was measured at 780 kA m^{-1} as a 3.9% decrease for CI–PGMA-1 particles and a 5.3% decrease for CI–PGMA-2 particles. Surface modification with PGMA further considerably enhanced thermo-oxidation stability and shifted the oxidation of the particles towards higher temperatures about more than 100 °C. However, doubling the molecular weight of PGMA contributed to only a slight improvement.

Moreover, rheological behavior of MR suspensions was investigated at various magnetic field strengths. MR suspensions of 60 wt% particles exhibited promising values of the shear stress and viscosity compared to suspension of bare CI. Also G' and G'' values remained almost on the same level for MR suspensions of PGMA-coated particles due to negligibly-decreased magnetic susceptibility. Furthermore, sedimentation stability was significantly enhanced due to partially reduced bulk density and the presence of the PGMA polymer chains on the particle surface providing better interactions with silicone oil. Therefore, it can be concluded that the SI-ATRP method was favorably utilized as an effective tool for defined modification of particles used in MR suspensions with tunable MR performance and stability properties.

Author contributions

The manuscript was contributed by the listed authors, all of whom have approved of its final form.

Acknowledgements

The authors M. C. and T. P. further thank the internal grant of TBU in Zlin No. IGA/FT/2014/017, funded from specific university research resources. Author M. S. wishes to thank the Grant Agency of the Czech Republic (14-32114P) for financial support. This article was written with support of the Operational Program Research and Development for Innovations co-funded by the European Regional Development Fund (ERDF) and the National Budget of Czech Republic, within the framework of the project Centre of Polymer Systems (CZ.1.05/2.1.00/03.0111). J. M. and M. I. thank the Centre of Excellence FUN-MAT for financial support.

References

1 J. de Vicente, D. J. Klingenberg and R. Hidalgo-Alvarez, Magnetorheological fluids: a review, *Soft Matter*, 2011, 7, 3701–3710.
2 B. J. Park, F. F. Fang and H. J. Choi, Magnetorheology: materials and application, *Soft Matter*, 2010, **6**, 5246–5253.
3 M. Sedlacik, V. Pavlinek, P. Saha, P. Svrcinova and J. Stejskal, Rheological properties of magnetorheological suspensions based on core–shell structured polyaniline-coated carbonyl iron particles, *Smart Materials and Structures*, 2010, **19**, 115008.
4 S. Y. Kim, S. H. Kwon, Y. D. Liu, J. S. Lee, Ch. Y. You and H. J. Choi, Core-shell-structured cross-linked poly(glycidyl

methacrylate)-coated carbonyl iron microspheres and their magnetorheology, *J. Mater. Sci.*, 2014, **49**, 1345–1352.
5 Y. D. Liu and H. J. Choi, Recent progress in smart polymer composite particles in electric and magnetic fields, *Polym. Int.*, 2013, **62**, 147–151.
6 M. Sedlacik, V. Pavlinek, P. Peer and P. Filip, Tailoring the magnetic properties and magnetorheological behavior of spinel nanocrystalline cobalt ferrite by varying annealing temperature, *Dalton Trans.*, 2014, **43**, 6919–6924.
7 M. Yu, X. M. Dong, S. B. Choi and C. R. Liao, Human simulated intelligent control of vehicle suspension system with MR dampers, *Journal of Sound and Vibration*, 2009, **319**, 753–767.
8 E. Atabay and I. Ozkol, Application of a magnetorheological damper modeled using current-dependent Bouc-Wen model for shimmy suppression in a torsional nose landing gear with and without freeplay, *Journal of Vibration and Control*, 2014, **20**, 1622–1644.
9 Q. P. Ha, M. T. Nguyen, J. Li and N. M. Kwok, Smart structures with current-driven MR dampers: modeling and second-order sliding mode control, *IEEE/ASME Transactions on Mechatronics*, 2013, **18**, 1702–1712.
10 Z. Q. Chen, X. Y. Wang, J. M. Ko, Y. Q. Ni, B. F. Spencer, G. Yang and S. Ch. Liu, MR damping system on Donting Lake cable-stayed bridge, *Smart Structures and Materials*, 2003, **5057**, 229–235.
11 K. Karakoc, J. E. Park and A. Suleman, Design considerations for an automotive magnetorheological brake, *Mechatronics*, 2008, **18**, 434–447.
12 D. M. Wang, Y. F. Hou and Z. Tian, A novel high-torque magnetorheological brake with a water cooling method for heat dissipation, *Smart Materials and Structures*, 2013, **22**, 025019.
13 J. Rabinow, The magnetic fluid clutch, *AIEE Trans.*, 1948, **67**, 1308–1315.
14 B. M. Kavlicoglu, F. Gordaninejad and X. Wang, Study of a magnetorheological grease clutch, *Smart Materials and Structures*, 2013, **22**, 125030.
15 H. Herr, A. Wilkenfeld, S. Huseyin, F. Gordaninejad and C. Evrensel, User-adaptive control of a magnetorheological prosthetic knee, *Industrial Robot: An International Journal*, 2003, **30**, 42–55.
16 K. I. Jang, J. Seok, B. K. Min and S. J. Lee, An electrochemo-mechanical polishing process using magnetorheological fluid, *International Journal of Machine Tools and Manufacture*, 2010, **50**, 869–881.
17 A. A. Silva, E. Silva, A. Carrico and E. T. Egito, Magnetic carriers: a promising device for targeting drugs into the human body, *Curr. Pharm. Des.*, 2007, **13**, 1179–1185.
18 G. A. Flores, R. Sheng, J. Liu and S. J. Lee, Medical applications of magnetorheological fluids a possible new cancer therapy, *Journal of Intelligent Material Systems and Structures*, 2001, **10**, 708–713.
19 P. P. Phule and J. M. Ginder, Synthesis and properties of novel magnetorheological fluids having improved stability and redispersibility, *International Journal of Modern Physics*, 1999, **13**, 2019–2027.
20 M. T. Lopez-Lopez, A. Zugaldia, F. Gonzalez-Caballero and J. D. G. Duran, Sedimentation and redispersion phenomena in iron-based magnetorheological fluids, *J. Rheol.*, 2006, **50**, 543–560.
21 S. Alves, M. R. Alcantara, A. M. Figueiredo-Neto and J. D. G. Duran, The effect of hydrophobic and hydrophilic fumed silica on the rheology of magnetorheological suspensions, *J. Rheol.*, 2009, **53**, 651–662.
22 S. T. Lim, H. J. Choi and M. S. Jhon, Magnetorheological characterization of carbonyl iron-organoclay suspensions, *IEEE Trans. Magn.*, 2005, **41**, 3745–3747.
23 H. T. Pu, F. J. Jiang, Z. Yang, B. Yan and X. Liao, Effects of polyvinylpyrrolidone and carbon nanotubes on magneto-rheological properties of iron-based magnetorheological fluids, *J. Appl. Polym. Sci.*, 2006, **102**, 1653–1657.
24 I. Bica, F. J. Jiang, Z. Yang, B. Yan and X. Liao, Magneto-rheological suspension based on mineral oil, iron and graphite micro-particles, *J. Magn. Magn. Mater.*, 2004, **283**, 335–343.
25 B. Hu, A. Fuchs, S. Huseyin, F. Gordaninejad and C. Evrensel, Atom transfer radical polymerized MR fluids, *Polymer*, 2006, **47**, 7653–7663.
26 H. J. Choi, B. J. Park, M. S. Cho and J. L. You, Core–shell structured poly(methyl methacrylate) coated carbonyl iron particles and their magnetorheological characteristics, *J. Magn. Magn. Mater.*, 2007, **310**, 2835–2837.
27 X. Quan, W. Chuah, Y. Seo and H. J. Choi, Core–shell structured polystyrene coated carbonyl iron microspheres and their magnetorheology, *IEEE Trans. Magn.*, 2014, **50**, 1–4.
28 I. B. Jang, H. B. Kim, J. Y. Lee, J. L. You, H. J. Choi and M. S. Jhon, Role of organic coating on carbonyl iron suspended particles in magnetorheological fluids, *J. Appl. Phys.*, 2005, **97**, 10Q912.
29 F. F. Fang, Y. D. Liu and H. J. Choi, Fabrication of carbonyl iron embedded polycarbonate composite particles and magnetorheological characterization, *IEEE Trans. Magn.*, 2009, **45**, 2507–2510.
30 M. Sedlacik, V. Pavlinek, M. Lehocky, A. Mracek, O. Grulich, P. Svrcinova, P. Filip and A. Vesel, Plasma-treated carbonyl iron particles as a dispersed phase in magnetorheological fluids, *Colloids Surf., A*, 2011, **387**, 99–103.
31 M. Mrlik, M. Sedlacik, V. Pavlinek, P. Bazant, P. Saha, P. Peer and P. Filip, Synthesis and magnetorheological characteristics of ribbon-like, polypyrrole-coated carbonyl iron suspensions under oscillatory shear, *J. Appl. Polym. Sci.*, 2013, **128**, 2977–2982.
32 J. S. Wang and K. Matyjaszewski, Controlled living polymerization – atom-transfer radical polymerization in the presence of transition-metal complexes, *J. Am. Chem. Soc.*, 1995, **117**, 5614–5615.
33 K. Matyjaszewski, W. Chuah, Y. Seo and H. J. Choi, Atom Transfer Radical Polymerization (ATRP): Current Status and Future Perspectives, *Macromolecules*, 2012, **45**, 4015–4039.
34 J. Sutrisno, A. Fuchs, H. Sahin and F. Gordaninejad, Surface coated iron particles via atom transfer radical polymerization

for thermal-oxidatively stable high viscosity magnetorheological fluid, *J. Appl. Polym. Sci.*, 2013, **128**, 470–480.

35 J. Mosnacek and M. Ilcikova, Photochemically mediated atom transfer radical polymerization of methyl methacrylate using ppm amounts of catalyst, *Macromolecules*, 2012, **45**, 5859–5865.

36 S. G. Belyavskii, P. G. Mingalyov, F. Giulieri, R. Combarrieau and G. V. Lisichkin, Chemical modification of the surface of a carbonyl iron powder, *Prot. Met.*, 2006, **42**, 244–252.

37 M. Mrlik, M. Ilcikova, V. Pavlinek, J. Mosnacek, P. Peer and P. Filip, Improved thermooxidation and sedimentation stability of covalently-coated carbonyl iron particles with cholesteryl groups and their influence on magnetorheology, *J. Colloid Interface Sci.*, 2013, **396**, 146–151.

38 M. Sedlacik and V. Pavlinek, A tensiometric study of magnetorheological suspensions' stability, *RSC Adv.*, 2014, **4**, 58377–58385.

39 W. C. Wang, Q. Zhang, B. B. Zhang, D. N. Li, X. Q. Dong, L. Zhang and J. Chang, Preparation of monodisperse, superparamagnetic, luminescent, and multifunctional PGMA microspheres with amino-groups, *Chin. Sci. Bull.*, 2008, **53**, 1165–1170.

40 R. Zhao, J. Lu and T. Tan, Preparation of polyglycidylmethacrylate macropore beads and application in Candidaspecies 99-125 lipase immobilization, *Chem. Eng. Technol.*, 2011, **34**, 93–97.

41 J. de Vicente, G. Bossis, S. Lacis and M. Guyot, Permeability measurements in cobalt ferrite and carbonyl iron powders and suspensions, *J. Magn. Magn. Mater.*, 2002, **251**, 100–108.

42 M. A. Abshinova, N. E. Kazantseva, P. Saha, I. Sapurina, J. Kovarova and J. Stejskal, The enhancement of the oxidation resistance of carbonyl iron by polyaniline coating and consequent changes in electromagnetic properties, *Polym. Degrad. Stab.*, 2008, **93**, 1826–1831.

43 J. Claracq, J. Sarrazin and J. P. Montfort, Viscoelastic properties of magnetorheological fluids, *Rheol. Acta*, 2004, **43**, 38–49.

44 J. Ramos, J. de Vicente and R. Hidalgo-Alvarez, Small-amplitude oscillatory shear magnetorheology of inverse ferrofluids, *Langmuir*, 2010, **26**, 9334–9341.

PAPER II

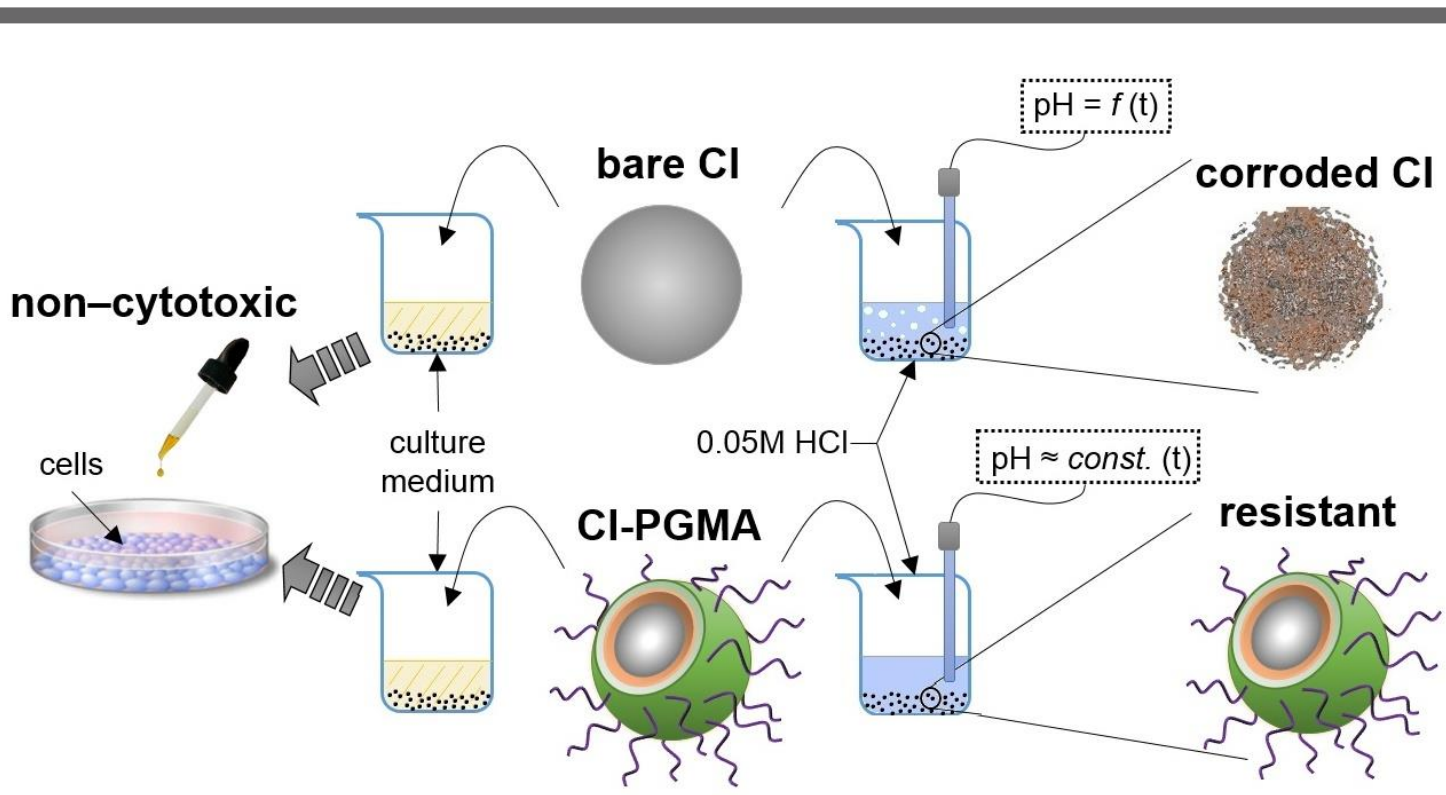

Royal Society of Chemistry

RSC Advances

Accepted: 21st August 2015

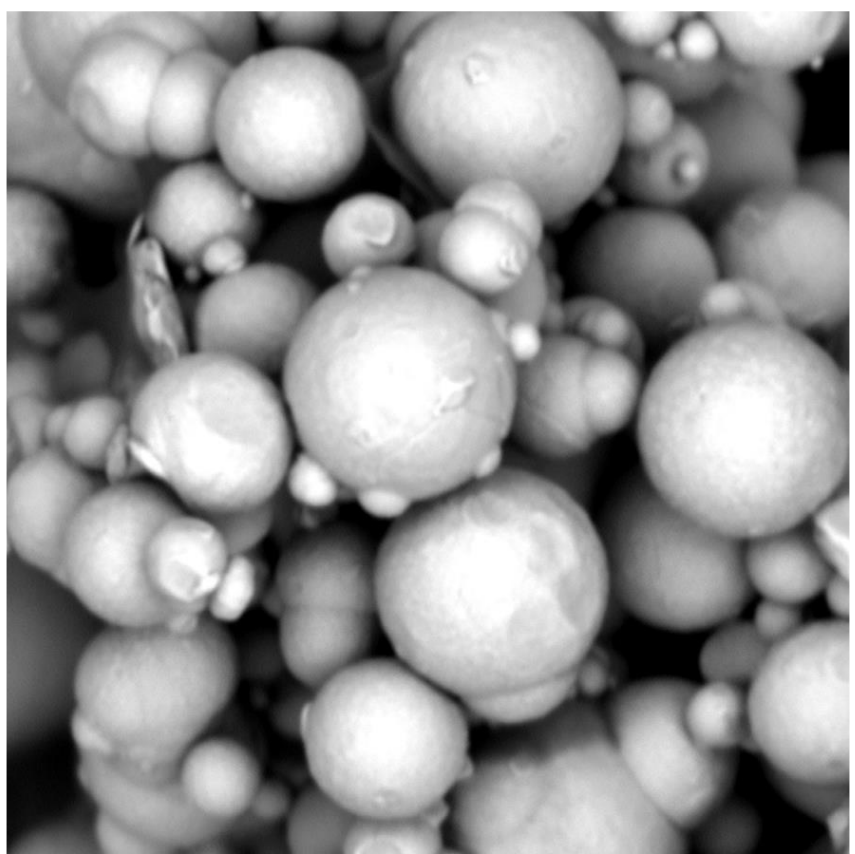

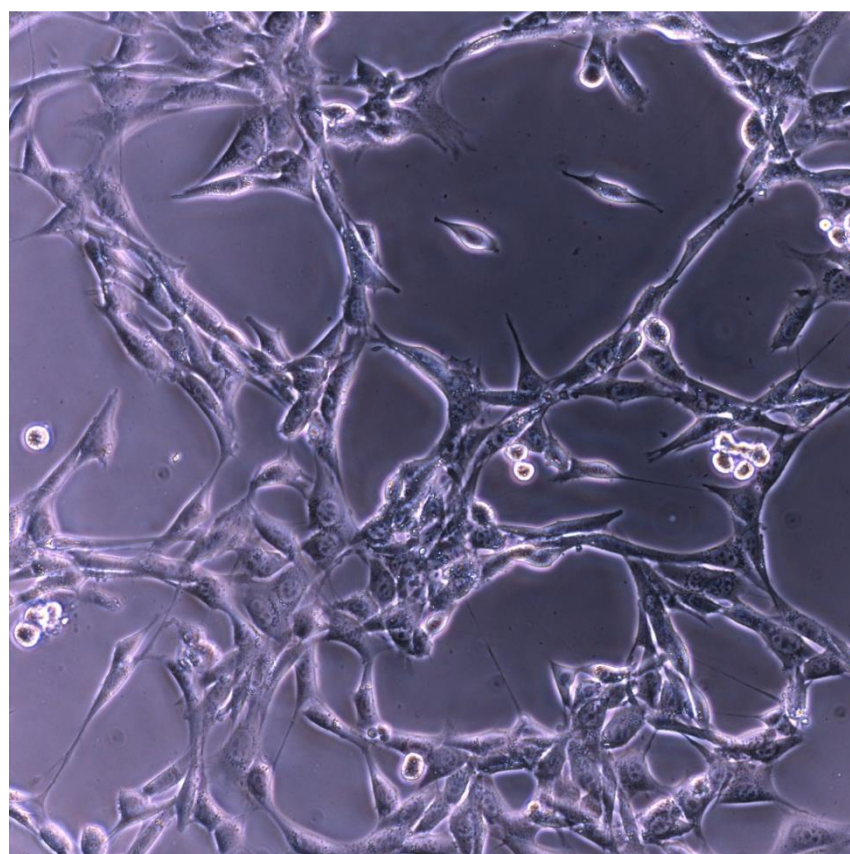

RSC Advances

PAPER

Cite this: *RSC Adv.*, 2015, **5**, 72816

The chemical stability and cytotoxicity of carbonyl iron particles grafted with poly(glycidyl methacrylate) and the magnetorheological activity of their suspensions†

Martin Cvek,[ab] Miroslav Mrlík,*[ac] Markéta Ilčíková,[cd] Jaroslav Mosnáček,[d] Vladimir Babayan,[a] Zdenka Kuceková,[a] Petr Humpolíček[a] and Vladimir Pavlínek[a]

Received 21st June 2015
Accepted 21st August 2015

DOI: 10.1039/c5ra11968e

www.rsc.org/advances

Carbonyl iron (CI) particles were grafted with poly(glycidyl methacrylate) (PGMA) using atom transfer radical polymerization. Compact coating of PGMA largely improved the chemical stability of the particles in an acid environment and thus reduced the common drawback of bare CI particles. Furthermore, due to possible medical applications of CI-polymer systems for magnetic drug targeting, an *in vitro* cytotoxicity test was performed using an NIH/3T3 cell line. The cell viability was evaluated by spectrometric assay (MTT). The results show that the prepared particles are not cytotoxic. Moreover, bare CI particles as well as synthesized core–shell particles were suspended in silicone oil, and the rheological behavior of MR suspensions was investigated in controlled shear rate mode under various magnetic field strengths. Dynamic yield stress as a measure of the rigidity of the created internal structures of the suspensions was determined using the Herschel–Bulkley model, which provided a reasonably good fit for rheological data. MR suspensions of PGMA-coated particles exhibited only slightly decreased yield stresses due to their negligibly-affected magnetic performance.

Introduction

Magneto-responsive magnetorheological (MR) suspensions composed of soft ferromagnetic particles 0.1–10 μm in size dispersed in non-magnetic carrier liquids exhibit remarkable rheological behavior including rapid, reversible and tunable transitions from liquid-like to solid-like states under an applied magnetic field.[1–4] Drastic changes of physical properties, namely viscosity, yield stress or shear modulus occur within a few milliseconds after the application of the magnetic field due to the alignment of dispersed particles into column-like structures, which is a process based on the magnetic field-induced polarization of the particles.[5–7] This phenomenon makes MR suspensions desirable for a significant number of engineering applications incorporating damping systems,[8–10] torque transducers,[11] the finishing of optics,[12] or robotics.[13]

However, poor thermo-oxidation and sedimentation stabilities are crucial problems of classical MR suspensions, which reduce their broader practical utilization.[13,14] Moreover, in many cases an overlooked drawback is also the poor chemical stability of bare CI particles in an acidic environment. Such drawbacks can be efficiently reduced by the modification of the particle surface with polymer chains, allowing for the involvement of core–shell structured particles in the preparation of MR suspensions.[1–3,7,15,16] However, conventional coating methods tend to cause a large decrease in the magnetic permeability of the particles. Using surface-initiated reversible deactivation radical polymerization, such as atom transfer radical polymerization (ATRP), allows the precise control of the molecular weight of grafted polymer chains. This approach also enables control over the polymer layer thickness on an inorganic substrate since the thickness of the layer progressively increases with the molecular weight of the densely-grafted polymer chains.[17] Therefore, such a method enables an adjustment to MR performance *via* the controlled thickness of the polymeric layer on the particles surface.[18]

Generally, MR suspensions are in most cases subjected to shear flow while exhibiting nearly Newtonian behavior in the absence of a magnetic field (off-state), or develop a yield stress and shear rate-dependent apparent viscosity after the application of an external field (on-state).[1,5,10] The behavior of MR suspensions can be characterized by the Bingham plastic

[a]*Centre of Polymer Systems, University Institute, Tomas Bata University in Zlin, Trida T. Bati 5678, 760 01 Zlin, Czech Republic. E-mail: mrlik@cps.utb.cz*

[b]*Polymer Centre, Faculty of Technology, Tomas Bata University in Zlin, nam. T. G. Masaryka 275, 762 72 Zlin, Czech Republic*

[c]*Center for Advanced Materials, Qatar University, P. O. Box 2713, Doha, Qatar*

[d]*Polymer Institute, Slovak Academy of Sciences, Dubravska cesta 9, 845 41 Bratislava 45, Slovakia*

† Electronic supplementary information (ESI) available. See DOI: 10.1039/c5ra11968e

model,[19] which belongs among the most popular models because of its simplicity and sufficient accuracy.[20] Nevertheless, the on-state pseudoplastic behavior of MR suspensions is in contradiction to the Bingham model. Therefore some authors[21–23] have employed the Herschel–Bulkley (HB) model, which replaces constant plastic viscosity in the Bingham model with a shear rate-dependent power-law relation in order to include post-yield stress shear thinning characteristics.

In our preceding paper,[18] we showed that the poly(glycidyl methacrylate) (PGMA) coating of CI particles *via* ATRP resulted in a considerable improvement of thermo-oxidation and sedimentation stabilities, while the response of the modified particles to a magnetic field remained at an acceptable level. However, in real-life applications, the anti-corrosion stability of the particles also plays an important role; for instance in the final polishing of high precision optics, a decrease in pH can improve the MR finishing of certain polycrystalline materials.[24]

The first part of this article deals with the examination of the chemical stability of PGMA-coated CI particles in an acidic environment in order to shift this material closer to potential real-life applications. Moreover, due to possible biomedical applications,[25–28] attention is paid to an indicative *in vitro* cytotoxicity test, which was performed in order to analyze the basic cellular response to the tested substances. PGMA has recently gained interest in drug and biomolecule binding,[29] and for this reason it was chosen as a coating layer for this study. In the second part, the magnetic performance of the bare and modified CI particles was investigated using the Jiles–Atherton (J–A) model, while their suspensions' rheological behavior was studied, and the obtained flow curves were fitted with the HB model in order to predict dynamic yield stresses and thus further evaluate yield stress development as a result of the polymer coating layer applied on the surface of CI particles.

Experimental

Materials

All chemicals were used as received. Carbonyl iron (CI) powder (SL grade) with a purity higher than 99.5% was obtained from BASF (Germany). Glycidyl methacrylate (GMA, 97%), α-bromo isobutyryl bromide (BiBB, 98%), (3-aminopropyl) triethoxysilane (APTES, ≥98%), ethyl α-bromo isobutyrate (EBiB, 98%), triethylamine (Et_3N, ≥99%), *N*,*N*,*N*′,*N*″,*N*″-pentamethyldiethylenetriamine (PMDETA, ≥99%), copper bromide (CuBr, ≥99%), anisole (99%) and aluminum oxide (neural, Brockmann I) were produced by Sigma Aldrich (USA). Other chemicals, namely tetrahydrofuran (THF, p.a.), acetone (p.a.), ethanol (absolute anhydrous, p.a.), toluene (p.a.), and hydrochloric acid (HCl, 35%, p.a.) were purchased from Penta Labs (Czech Republic). MR suspensions were prepared using the silicone oil Lukosiol M200, which is a product of Chemical Works Kolín (Czech Republic; dynamic viscosity of 194 mPa s, density of 0.97 g cm^{-3}, 25 °C).

An NIH/3T3 mouse embryonic fibroblast cell line (ATCC CRL-1658), Dulbecco's Modified Eagle Medium, penicillin/streptomycin (PAA Laboratories GmbH, Austria) and MTT (3-(4,5-dimethylthiazol-2-yl)-2,5-diphenyltetrazolium bromide) (Invitrogen Corporation, USA) were used for cytotoxicity tests.

CI particles grafted with PGMA chains (CI-PGMA) were prepared as described in a previous paper.[18]

Characterization

Monomer conversion during polymerization and the molecular weight of grafted polymer chains were characterized using proton nuclear magnetic resonance (^{1}H NMR) (400 MHz VNMRS Varian NMR spectrometer, Varian, Japan) and gel permeation chromatography (GPC) (PL-GPC220 Agilent, Japan), respectively. The morphology and dimensions of the particles were observed using scanning electron microscopy (SEM) (Tescan Vega II LMU, Czech Republic). Modification of the CI surface with PGMA chains was proved by energy-dispersive spectroscopy (EDS) also performed on Tescan, and Fourier transform infrared spectroscopy (FTIR) (Nicolet 6700, USA) in the attenuated total reflectance (ATR) mode within the wavenumber range of 4000–500 cm^{-1} using a germanium crystal. The magnetic properties of both coated and bare CI particles were evaluated using a vibration sample magnetometry (VSM) (Model 7407, Vibrating Sample Magnetometer, Lakeshore, USA) employing a magnetic field strength of ±870 kA m^{-1}. The non-linear magnetization curve of ferromagnetic particles can be described by the J–A model:[30]

$$M(H) = M_S\left[\coth\left(\frac{H_e}{A}\right) - \left(\frac{A}{H_e}\right)\right] \quad (1)$$

where M denotes magnetization of the material, H the magnetic field strength, and M_S the saturation magnetization; A is the parameter describing magnetization shape without hysteresis, whereas H_e is the effective magnetic field strength given by:

$$H_e = H + \alpha M \quad (2)$$

where α is the coefficient describing coupling between domains. Hence, obtained magnetization curves[18] are further analyzed in this paper. Moreover, the effect of polymer coating on the stability against sedimentation was studied with the help of a Tensiometer Krüss K100 (Krüss GmbH, Hamburg, Germany) at laboratory conditions. The measurements were performed on the MR suspensions based on 10 wt% particle concentration. Such concentration was chosen as an optional for the measurement with respect to the principle of tensiometric method.

Chemical stability

The anti-acid-corrosion stability of bare CI particles and both types of CI-PGMA particles were investigated. The amount of 1 g of appropriate particles was suspended in 20 mL of 0.05 M HCl, and the pH-value was measured as a function of time. The instrument (SensoDirect pH110, Tintometer GmbH, Germany) was previously calibrated using two standard buffers at laboratory temperature. The acidic suspensions were mechanically stirred during the experiment, while prior to each measurement

the probe of the pH-meter was cleaned by rinsing with distilled water and dried.

Cytotoxicity

Determination of cytotoxicity was carried out according to the international standard EN ISO 10993-5 using an NIH/3T3 mouse embryonic fibroblast cell line (ATCC, CRL-1658), which is a commonly used cell line for cytotoxicity testing of materials.[31–34] As a culture medium, Dulbecco's Modified Eagle Medium – high glucose, added 10% calf serum and penicillin/streptomycin, 100 μg mL^{-1} (PAA Laboratories GmbH, Austria) – was used.

Extract preparation. Prior to extraction, the samples were disinfected at 120 °C for 40 minutes (Binder ED 53, Germany). Tested samples – bare CI particles and CI-PGMA-1 particles – were extracted according to ISO 10993-12 in the amount of 0.2 g of powder per 1 mL of culture medium and incubated at (37 ± 1) °C under stirring for (24 ± 1) h. The parent extracts (100%) were diluted in the culture medium in order to obtain extracts of concentrations 75, 50, 25, 10 and 1 vol%. The extracts were used for cytotoxicity testing within 24 h.

Cytotoxicity evaluation. The cells were seeded on microtitration plates (TPP, Switzerland) in a concentration of 1×10^5 per mL and pre-cultivated for 24 h. The culture medium was subsequently replaced with appropriate extracts. The cells were cultivated for 24 h in the presence of individual extracts. The cell viability was evaluated by MTT assay (Invitrogen Corporation, USA). The absorbance was measured at 570 nm with an Infinite M200 Pro NanoQuant absorbance reader (Tecan, Switzerland). All the tests were performed in quadruplicates. Cell viability was expressed as the percentage of cells present in the corresponding extract relative to cells cultivated in a pure growth medium (reference, 100% viability). Values >0.8 were assigned to no cytotoxicity, 0.6–0.8 to mild cytotoxicity, 0.4–0.6 to moderate cytotoxicity, and <0.4 to severe cytotoxicity. The morphology of cells was observed by an inverted Olympus phase contrast microscope (Olympus IX81, Japan).

Sample preparation and rheological properties in steady shear flow

Bare CI particles as well as both types of CI-PGMA were suspended in silicone oil (40 wt% of particles in oil). In order to avoid settling and provide homogeneous samples, the MR suspensions were thoroughly stirred before each measurement. Raw rheological data was measured with a rotational rheometer Physica MCR502 (Anton Paar GmbH, Austria) using parallel plate geometry 20 mm in diameter. The sample suspension was injected between the plates and a magnetic field (0–438 kA m^{-1}) perpendicular to the plates generated with a magnetic cell (Physica MRD 170+H-PTD200) was applied, while the gap between the plates was set to 0.5 mm. The true magnetic field strength was determined with a Teslameter (Magnet-Physik, FH 51, Dr Steingroever GmbH, Germany). Shear rates (10^{-2} to 10^2 s^{-1}) were applied, and a shear stress and viscosity were determined in the absence (off-state) and in the presence (on-state) of a magnetic field. Prior to each on-state measurement, MR suspensions were off-state sheared in order to disrupt possible residual structures. Then, new structures were induced using a given magnetic field strength. The temperature during testing was maintained at 25 °C.

Results and discussion

Synthesis and characterization of PGMA-modified CI particles

The surface modification of CI particles with PGMA chains was performed in several steps[18] as shown in Scheme 1. First, the oxidized CI surface was modified by reaction with an APTES silane agent. With this modifier it is also possible to make the grafted layer desirably stronger due to the horizontal cross-linking between modifier molecules.[35] Subsequently, the introduced amine groups were modified by reaction with BiBB in order to introduce the ATRP initiator on to the CI surface. Finally, a surface-initiated ATRP of GMA was performed. In addition to ATRP initiator bonded on CI particles, a free sacrificial initiator was used in excess to decrease an extent of termination reactions due to a high concentration of active radicals on the CI surface and to allow better control of the molecular weight of PGMA. Two types of CI-PGMA particles varying in shell thickness were obtained by using two monomer/initiator ratios leading to a modification of CI particles with two various molecular weights of PGMA.

The weight- and number-average molecular weights ($\bar{M}_w$, $\bar{M}_n$) were determined by GPC analysis based on free PGMA chains grown from a free sacrificial initiator, under the assumption of the similar growth of the polymer from free and bond initiators.[36] The results are summarized in Table 1. Based on the molecular weights of the grafted polymer chains it was

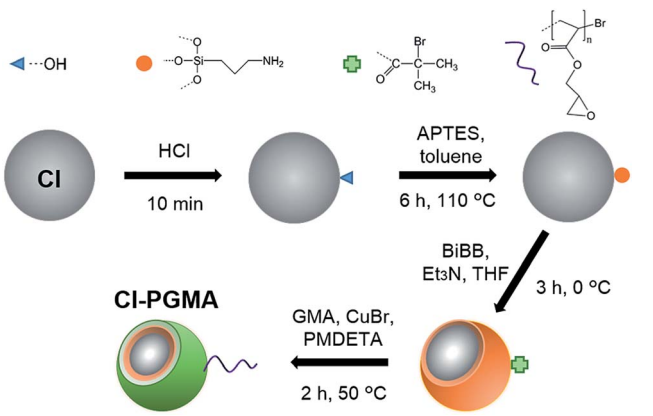

Scheme 1 Schematic picture of the synthesis of CI-PGMA particles.

Table 1 Weight- and number-average molecular weights and the dispersity index $Đ$ of PGMA grafted onto CI particles

Sample code	$\bar{M}_w$ [g mol^{-1}]	$\bar{M}_n$ [g mol^{-1}]	$Đ$ [-]
CI-PGMA-1	6600	5000	1.32
CI-PGMA-2	12 500	9700	1.29

estimated theoretically that maximal lengths of fully stretched PGMA chains, and consequently shell thicknesses, are around 9 nm and 17 nm for the CI-PGMA-1 and CI-PGMA-2, respectively.

Fig. 1 shows SEM images of bare CI (a) and CI-PGMA-1 (b) particles. Particles possess a spherical shape with diameters under 5 microns. As can be seen, particles in both samples have comparable dimensions indicating negligible change in their size due to modification.

The modification of the CI surface was confirmed by EDS and FTIR analyses. In EDS measurements, the electron beams are only able to penetrate a few nanometers deep into the sample surface.[37] This method was preferably employed for confirmation of the presence of characteristic elements in the PGMA layer. Comparing spectra of bare CI and CI-PGMA-1 particles,[18] both of them showed strong Fe L, Kα, and Kβ lines; however, in CI-PGMA-1 particles, a higher content of carbon was determined, implying the presence of a PGMA layer on the surface of the CI particles. Successful CI surface modification was also indicated by substantial characteristic emission peaks, namely a Kα line of oxygen and a Kα line of silicon originated from the modifier.

In FTIR spectra of CI-PGMA-1,[18] carbonyl (C=O) stretching vibrations and the asymmetric stretching of C–O–C from ester groups of PGMA were observed at 1714 cm^{-1} and 1350 cm^{-1}, respectively. In addition, absorption peaks occurring at 904 cm^{-1} and 815 cm^{-1} were distinct indications of the presence of an oxirane ring.

The magnetic properties of the utilized particles were investigated. As shown in Fig. 1, the magnetic behavior of the coated particles was similar to that of the bare ones, but showed slightly lower values of magnetic moments due to a decreased magnetic susceptibility. However, the decreases of magnetizations in the modified particles were negligible in comparison to the bare ones (Fig. 2, inset A), as the thickness of the coatings was controlled *via* ATRP means. Magnetization curves were fitted with the J–A model, which further predicted slightly decreased values of saturation magnetizations. A value of 229 emu g^{-1} was reached for bare CI particles, while PGMA-coated variants exhibited magnetizations of 220 emu g^{-1} and 215 emu g^{-1}, respectively. The values obtained by the application of the J–A equation were higher than those resulting from the experimental measurements, which might have occurred due to incomplete saturation magnetization as a result of the use of an insufficient magnetic field strength.[38] Furthermore,

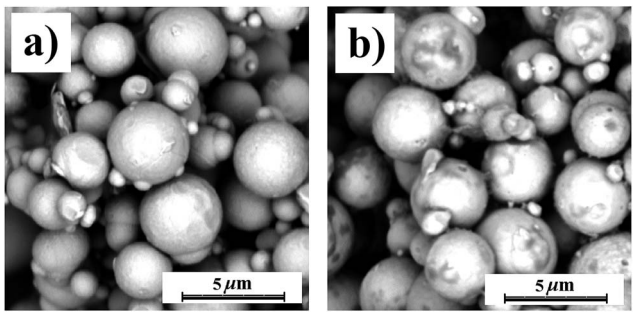

Fig. 1 SEM micrographs of bare CI (a), and CI-PGMA-1 (b) particles.

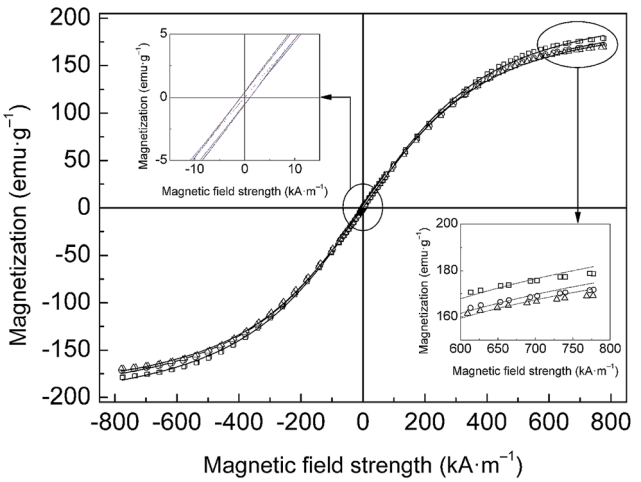

Fig. 2 VSM spectra of bare CI (*open squares*), CI-PGMA-1 (*open circles*), and CI-PGMA-2 particles (*open triangles*). The solid lines represent the Jiles–Atherton model predictions.

the values of α parameter in the J–A model approached zero for all measurements, which indicated almost hysteresis-free curves (Fig. 2, inset B). The A parameter in the J–A equation describing magnetization shape was calculated as 161 kA m^{-1} for bare CI particles, while values of 159 kA m^{-1} and 157 kA m^{-1} were obtained for CI-PGMA-1 particles and CI-PGMA-2 particles, respectively, which stem from a negligible change in the magnetic behavior of the CI particles as a consequence of the controlled surface modification.

Although the magnetic properties of the PGMA-modified particles were only slightly reduced compared to bare CI, their sedimentation stabilities in silicone oil were improved significantly due to enhanced interactions with the dispersion medium. This phenomenon was analyzed in more details in our previous paper.[18]

Chemical stability

Fig. 3 shows the pH value as a function of time for CI particles as well as CI-PGMA particles subjected to an acidic environment. In all measurements, the pH value initially decreases, which might be caused by local sample stabilization in the vicinity of the pH-meter probe. The experiment is based on the reaction of an aqueous HCl solution with Fe. The oxidation of Fe proceeds according to the equation (ESI†).

Shortly after the initiation of the experiment, the pH value of the dispersion containing bare CI particles exhibited a gradual increase accompanied by an intensive H_2 bubble evolution. Approximately after 40 minutes, the leaking amount of H_2 decreased, while an ongoing increase of the pH value was observed.

On the contrary, both types of CI-PGMA particles demonstrated excellent anti-acid corrosion stability. The PGMA shell and its APTES grafting base covered the CI core, and the reaction almost did not proceed. However, minimal production of H_2 was observed, which implied that the APTES base was not fully compact, and thus the chloride ions were still able to react

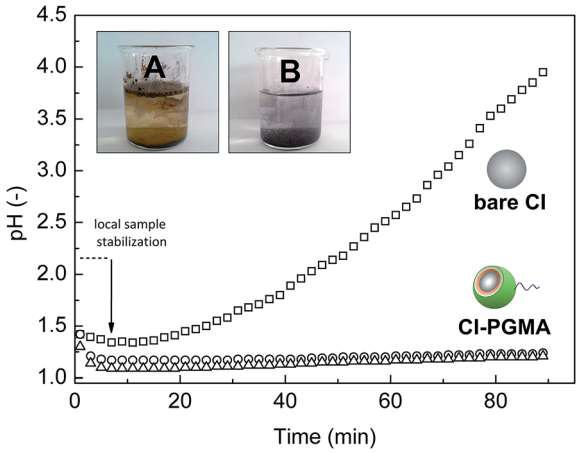

Fig. 3 Resistance of bare CI particles (*open squares*), CI-PGMA-1 particles (*open circles*), and CI-PGMA-2 particles (*open triangles*) against an acidic environment (0.05 M HCl). The inset image shows a tremendous difference in chemical stability between bare CI particles (A) and CI-PGMA-1 particles (B) after a 36 hour exposure.

with the Fe core. Nevertheless, compared to bare CI the improvement in chemical stability was significant. Generally, the pH remained at a similar value throughout the whole experiment. It was also clear that for the purpose of chemical stability enhancement, it was sufficient to modify the CI particles with PGMA chains with a molecular weight of 6600 g mol^{-1}, since no further improvement of chemical stability occurred with the increasing molecular weight of grafted PGMA.

After a 90 minute exposure, a difference of 3 orders on the pH scale was reached, and the measurement was stopped. However, the samples were left in solutions. The inset of Fig. 3 shows that the modified particles were still in a very good condition after a 36 hour exposure. Hence, the results of the stability test showed that CI-PGMA particles are very promising candidates for practical implementation.

Magnetic particles have also found promising applicability in the biomedical field. Cell therapy (cell separation and labeling),[25] cancer therapy,[26] and particularly drug delivery[27] have been examined using such remarkable structures. It was shown that in order to target organs that lie deeply in the body cavity (8–12 cm from the body surface), the use of magnetic microparticles (0.5–5 μm) is necessary. Besides that, PGMA has recently gained a special interest in drug and biomolecule binding where the presence of an epoxy ring represents an ideal site for a coupling reaction with pharmaceuticals.[29,39]

With this knowledge, PGMA was deliberately chosen as a shell material for the ATRP coating of CI particles. Prepared CI-PGMA particles may represent a promising material for drug delivery to organs deep within the body.[28] Thus, in this article the cytotoxicity of prepared particles as an important characteristic was further studied.

Cytotoxicity

The results performed on the NIH/3T3 cell line have shown that tested concentrations of extracts have not distinctly affected the cell viability. The cytotoxicity of bare CI particles belongs to a category with an absence of cytotoxicity within the whole tested concentration range. Nevertheless, the primary interest of this study was to investigate the cytotoxicity of CI-PGMA particles. The maximum loss of cell viability was observed in the 75% extract, where 0.85 cell survival was reached, which is still related to the absence of cytotoxicity. For all other concentrations of extracts, namely 50%, 25%, 10%, and 1%, the absence of cytotoxicity was more obvious, whereas the values of viability in these concentrations were around 1.00 compared to the reference.

Results of the MTT assay were also confirmed by microscopic observations. Fig. 4 shows the effect of extract concentration on changes in cell morphologies. The absence of cytotoxicity of CI-PGMA particles and their gained functionality make them very interesting from a further research point of view, as the appropriate substances can be attached. Considering the observations (Table 2), it can be asserted that CI-PGMA particles have the potential to be successfully used in medicine.

Rheological measurements

The steady shear flow properties of prepared silicone oil MR suspensions were measured in a controlled shear rate mode. The collected data was properly investigated in order to describe the change of rheological behavior upon the application of the external magnetic field. Fig. 5 presents shear stresses of prepared MR suspensions as a function of the shear rates under

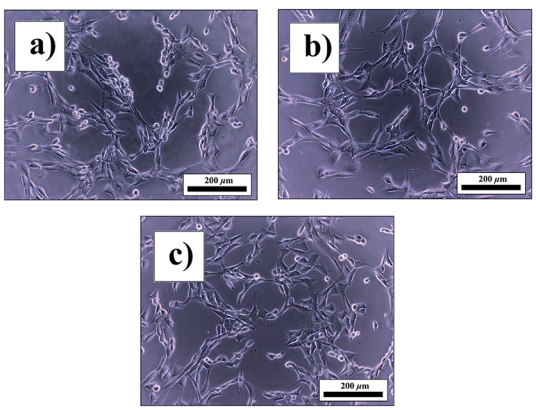

Fig. 4 Micrographs of the NIH/3T3 mouse embryonic fibroblast cell line, ATCC CRL-1658 treated with (a) 50% CI extract, (b) 50% CI-PGMA extract, and (c) reference.

Table 2 The cytotoxicity of CI and CI-PGMA extracts of various concentrations on the NIH/3T3 cell line reported according to the requirements of EN ISO 10993-5 standard

Extract	Control	NIH/3T3, 1.00	Control	NIH/3T3, 1.00
75%	CI	0.97	CI-PGMA	0.85
50%		0.93		0.98
25%		0.99		1.01
10%		0.95		1.02
1%		0.95		0.98

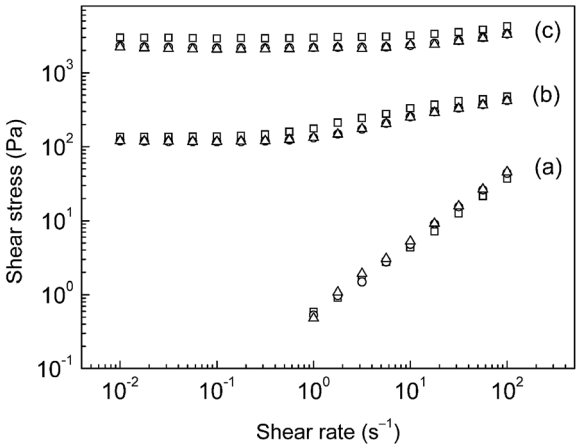

Fig. 5 The dependence of the shear stress on the shear rate for a 40 wt% suspension of CI particles (*open squares*), CI-PGMA-1 particles (*open circles*), and CI-PGMA-2 particles (*open triangles*) in silicone oil under 0 kA m^{-1} (a), 87 kA m^{-1} (b), and 438 kA m^{-1} (c) magnetic field strengths.

various magnetic field strengths. The shear stresses of suspensions based on CI-PGMA particles exhibit similar values when compared to the MR suspension of bare CI, which proves a promising MR performance of the prepared materials. As can be seen, in spite of a relatively low particle loading, the shear stresses increased almost over four orders of magnitude by the application of a 438 kA m^{-1} magnetic field strength in comparison to the off-state behavior at lower shear rates, whereas a shear stress increase by two orders of magnitude was attained at higher shear rates. The on-state behavior can be characterized by the wide shear stress plateau within the shear rate range, which is attributed to the formation of internal chain-like structures resulting in the solid-like character of MR suspensions.[40]

In order to exclude possible data distortion, the off-state flow curves are not shown within the whole shear rate range due to the inappropriateness of measuring MR geometry PP20 for low shear rates as, was also presented by authors.[41]

Flow curves in linear scaling fitted with the HB model (eqn (3)) are depicted in Fig. 6. The displayed rheological data correspond to the MR suspension based on bare CI particles under various magnetic field strengths. Rheograms of MR suspensions containing modified particles are included in ESI (please see Fig. S1†). As can be observed, the off-state behavior of the MR suspension can be denoted as Newtonian, however, in the on-state, the MR suspension exhibits a non-linear increase of shear stress with an increasing shear rate, which can be characterized as non-Newtonian shear thinning behavior. As initially expected, shear stress increased with increasing magnetic field strength due to a more pronounced chain-like formation. A similar behavior was also observed in suspensions of PGMA-coated particles in which, however, shear stresses exhibited slightly lower values. The obtained experimental data was analyzed using the HB model, which is expressed as follows:

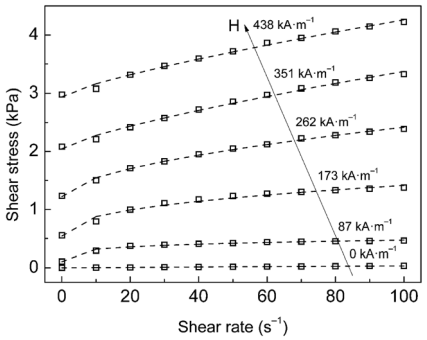

Fig. 6 Rheograms of 40 wt% MR suspension of bare CI particles showing experimental data (*open squares*) fitted with the HB model (*dashed lines*) under various magnetic field strengths.

$$\left.\begin{aligned} \tau = \tau_0\ \mathrm{sgn}(\dot{\gamma}) + K\dot{\gamma}^n, \quad |\tau| > \tau_0 \\ \dot{\gamma} = 0, \quad |\tau| < \tau_0 \end{aligned}\right\} \tag{3}$$

where τ is the shear stress, τ_0 means the dynamic yield stress controlled by the magnetic field strength, sgn denotes the signum function, $\dot{\gamma}$ represents shear rate, K and n are the consistency index and the power-law exponent, respectively. The HB model provided a reasonably good fit with the experimental data, as was further proved by statistical evaluation (Table S1) (ESI†).

The dynamic yield stresses predicted according to the HB model (Fig. 7) are plotted as a function of applied magnetic field strength. Surface modification reduced the magnetic susceptibility of the particles. Therefore, the yield stresses of MR suspensions containing coated particles were lower; however, due to controllable coating the decrease was insignificant. Nevertheless, the increase in the molecular weight of the polymer coating layer caused a further decrease in the yield stress (Table 3).

The displayed dependences exhibit similar patterns, as were described previously by authors.[42,43] According to numerical and mathematical models, the dynamic yield stress varies with $H^{2-1.5}$ depending on a mechanism of the polarization. The behavior of the MR suspensions follows a dipole mechanism at relatively low

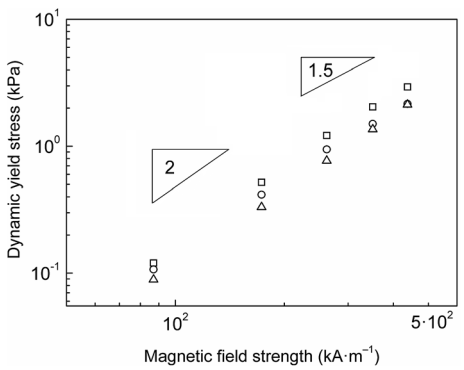

Fig. 7 Predicted dynamic yield stresses of MR suspensions based on bare CI particles (*open squares*), CI-PGMA-1 particles (*open circles*), and CI-PGMA-2 particles (*open triangles*) as a function of magnetic field strength.

Table 3 Summary of yield stress values under various magnetic field strengths

	Dynamic yield stress [kPa] at certain magnetic field strengths				
Dispersed phase	87 kA m^{-1}	173 kA m^{-1}	262 kA m^{-1}	351 kA m^{-1}	438 kA m^{-1}
Bare CI	0.120	0.519	1.215	2.046	2.941
CI-PGMA-1	0.107	0.417	0.944	1.503	2.160
CI-PGMA-2	0.089	0.332	0.768	1.359	2.130

magnetic fields, which is reflected in the quadratic dependence of the yield stress on the magnetic field strength. At higher magnetic fields, local saturation magnetization of the particles arises, and the yield stress further varies only with $H^{1.5}$. Nevertheless, the noticeable change of the slope in Fig. 7 was apparent only in the MR suspension of bare CI particles. This behavior can be associated with exceeding the critical magnetic field strength. MR suspensions of both variants of PGMA-coated particles exhibited an almost linear trend within the whole magnetic field strength range, which can be attributed to the presence of the PGMA shell affecting the contact zones between the particles.

Evaluation of MR efficiency

As for electrorheological suspensions,[44] the performance of MR suspensions can be in some instances described with MR efficiencies rather than absolute values of shear stresses. MR efficiency (e) is defined for any given $\dot{\gamma}$ as:

$$e = \frac{(\eta_E - \eta_0)}{\eta_0} \quad (4)$$

where η_E represents the on-state viscosity of the MR suspension and η_0 denotes the off-state the viscosity at the same $\dot{\gamma}$.

Fig. 8 illustrates e as a function of applied magnetic field strength at $\dot{\gamma} = 1\ s^{-1}$. The highest values of e obviously demonstrate the MR suspension of bare CI particles. MR suspensions of PGMA-coated particles exhibit a similar trend, nevertheless, with lower values of e. The molecular weight of the polymer shell appears to have a negligible effect on e in this case.

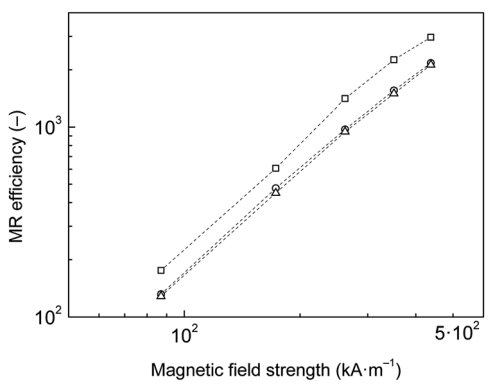

Fig. 8 The dependence of MR efficiency on the applied magnetic field strength for MR suspensions containing 40 wt% of CI particles (*open squares*), CI-PGMA-1 particles (*open circles*), and CI-PGMA-2 particles (*open triangles*) in silicone oil at 1 s^{-1}.

Conclusion

Two types of CI particles grafted with PGMA of different thicknesses were synthesized using a surface-initiated ATRP. It has been found that a PGMA coating layer provides excellent anti-acid corrosion properties. No significant difference in particle chemical stability was observed as the molecular weight of grafted PGMA increased from 6600 to 12 500 g mol^{-1}. Secondly, the *in vitro* cytotoxicity test conducted according to ISO standards shows that CI-PGMA particles are not cytotoxic. The absence of cytotoxicity, the presence of an easily transformable epoxy ring, and a high magnetic response make the prepared CI-PGMA particles a promising material for biomedical applications, especially for drug delivery to organs deep within the body.

The rheological properties of silicon oil-based MR suspensions were evaluated over a magnetic field strength range using the HB model and provided a reasonably good fit with the experimental data, as was supported by statistical evaluation (ESI). MR suspensions of PGMA-coated CI particles generated sufficient dynamic yield stresses compared to the suspension of bare CI particles. However, it was shown that the lower molecular weight of the PGMA was reflected in less suppressed MR activity. In general, yield stresses of the MR suspensions were quadratically dependent on the applied magnetic field strength. Assuming these and previously described findings to be accurate, it can be concluded that CI-PGMA particles obtained using surface-initiated ATRP appear to be a versatile material for miscellaneous applications.

Author contributions

The manuscript was contributed to by all authors, and all authors have approved the final version of the manuscript.

Acknowledgements

This article was written with support of the Operational Program Research and Development for Innovations co-funded by the European Regional Development Fund (ERDF) and the National Budget of the Czech Republic, within the framework of the project Centre of Polymer Systems (CZ.1.05/2.1.00/03.0111). The author M. C. wishes to thank the internal grant of TBU in Zlin No. IGA/CPS/2015/007 funded from specific university research resources. Authors M. I. and J. M. appreciate the financial support of the Centre of Excellence FUN-MAT. Z. K.

and P. H. further thank the Czech Science Foundation (13-08944S) for financial support.

References

1 B. J. Park, F. F. Fang and H. J. Choi, Magnetorheology: materials and application, *Soft Matter*, 2010, **6**, 5246–5253.

2 M. Mrlik, M. Sedlacik, V. Pavlinek, P. Bazant, P. Saha, P. Peer and P. Filip, Synthesis and magnetorheological characteristics of ribbon-like, polypyrrole-coated carbonyl iron suspensions under oscillatory shear: materials and application, *J. Appl. Polym. Sci.*, 2013, **128**, 2977–2982.

3 A. J. F. Bombard, M. Knobel and M. R. Alcantara, Phosphate coating on the surface of carbonyl iron powder and its effect in magnetorheological suspensions, *Int. J. Mod. Phys. B*, 2007, **21**, 4858–4867.

4 F. F. Fang, Y. D. Liu, H. J. Choi and Y. Seo, Core-shell structured carbonyl iron microspheres prepared *via* dual-step functionality coatings and their magnetorheological response, *ACS Appl. Mater. Interfaces*, 2011, **3**, 3487–3495.

5 J. de Vicente, D. J. Klingenberg and R. Hidalgo-Alvarez, Magnetorheological fluids: a review, *Soft Matter*, 2011, **7**, 3701–3710.

6 G. Bossis, S. Lacis, A. Meunier and O. Volkova, Magnetorheological fluids, *J. Magn. Magn. Mater.*, 2002, **252**, 224–228.

7 M. Sedlacik, V. Pavlinek, P. Saha, P. Svrcinova, P. Filip and J. Stejskal, Rheological properties of magnetorheological suspensions based on core-shell structured polyaniline-coated carbonyl iron particles, *Smart Mater. Struct.*, 2010, **19**, 115008.

8 G. Yang, B. F. Spencer, J. D. Carlson and M. K. Sain, Large-scale MR fluid dampers: modeling and dynamic performance considerations, *Eng. Struct.*, 2002, **24**, 309–323.

9 Y. Ding, L. Zhang, H. T. Zhu and Z. X. Li, A new magnetorheological damper for seismic control, *Smart Mater. Struct.*, 2013, **22**, 115003.

10 D. H. Wang and W. H. Liao, Magnetorheological fluid dampers: a review of parametric modelling, *Smart Mater. Struct.*, 2011, **20**, 023001.

11 S. Dai, C. Du and G. Yu, Design, testing and analysis of a novel composite magnetorheological fluid clutch, *J. Intell. Mater. Syst. Struct.*, 2013, **24**, 1675–1682.

12 W. Kordonski and A. Shorey, Magnetorheological (MR) Jet Finishing Technology, *J. Intell. Mater. Syst. Struct.*, 2007, **18**, 1127–1130.

13 T. Kikuchi, K. Oda and J. Furusho, Leg-robot for demonstration of spastic movements of brain-injured patients with compact magnetorheological fluid clutch, *Adv. Robot.*, 2010, **24**, 671–686.

14 M. Sedlacik, V. Pavlinek, M. Lehocky, A. Mracek, O. Grulich, P. Svrcinova, P. Filip and A. Vesel, Plasma-treated carbonyl iron particles as a dispersed phase in magnetorheological fluids, *Colloids Surf., A*, 2011, **387**, 99–103.

15 X. Quan, W. Chuah, Y. Seo and H. J. Choi, Core-shell structured polystyrene coated carbonyl iron microspheres and their magnetorheology, *IEEE Trans. Magn.*, 2014, **50**, 1–4.

16 M. Mrlik, M. Ilcikova, M. Sedlacik, J. Mosnacek, P. Peer and P. Filip, Cholesteryl-coated carbonyl iron particles with improved anti-corrosion stability and their viscoelastic behaviour under magnetic field, *Colloid Polym. Sci.*, 2014, **292**, 2137–2143.

17 K. Matyjaszewski, Atom transfer radical polymerization (ATRP): Current status and future perspectives, *Macromolecules*, 2012, **45**, 4015–4039.

18 M. Cvek, M. Mrlik, M. Ilcikova, T. Plachy, M. Sedlacik, J. Mosnacek and V. Pavlinek, A facile controllable coating of carbonyl iron particles with poly(glycidyl methacrylate): a tool for adjusting MR response and stability properties, *J. Mater. Chem. C*, 2015, **3**, 4646–4656.

19 J. D. Carlson and M. R. Jolly, MR fluid, foam and elastomer devices, *Mechatronics*, 2000, **10**, 555–569.

20 V. C. Kelessidis and R. Maglione, Modeling rheological behavior of bentonite suspensions as Casson and Robertson-Stiff fluids using Newtonian and true shear rates in Couette viscometry, *Powder Technol.*, 2006, **168**, 134–147.

21 M. Yu, S. Wang, J. Fu and Y. Peng, Unsteady analysis for oscillatory flow of magnetorheological fluid dampers based on Bingham plastic and Herschel–Bulkley models, *J. Intell. Mater. Syst. Struct.*, 2013, **24**, 1067–1078.

22 F. Ahmadkhanlou, M. Mahboob, S. Bechtel and G. Washington, An improved model for magnetorheological fluid-based actuators and sensors, *J. Intell. Mater. Syst. Struct.*, 2010, **21**, 3–18.

23 A. Sidpara, M. Das and V. K. Jain, Rheological characterization of magnetorheological finishing fluid, *Mater. Manuf. Processes*, 2009, **24**, 1467–1478.

24 S. D. Jacobs, A. Duparre and R. Geyl, MRF with adjustable pH, *Optical Fabrication, Testing, and Metrology IV*, 2011, **8169**, 816902.

25 J. L. Arias, V. Gallardo, F. Linares-Molinero and A. V. Delgado, Preparation and characterization of carbonyl iron/poly(butylcyanoacrylate) core/shell nanoparticles, *J. Colloid Interface Sci.*, 2006, **299**, 599–607.

26 G. A. Flores and J. Liu, Embolization of blood vessels as a cancer therapy using magnetorheological fluids, *J. Intell. Mater. Syst. Struct.*, 2002, **13**, 641–646.

27 A. K. A. Silva, E. L. Silva, A. S. Carrico and E. S. T. Egito, Magnetic carriers: a promising device for targeting drugs into the human body, *Curr. Pharm. Des.*, 2007, **12**, 1179.

28 F. Akai, M. Maeda, S. Hashimoto, M. Taneda and H. Takagi, A new animal model of cerebral infarction: magnetic embolization with carbonyl iron particles, *Neurosci. Lett.*, 1995, **194**, 139–141.

29 P. F. Canamero, J. L. de la Fuente, E. L. Madruga and M. Fernandez-Garcia, Atom transfer radical polymerization of glycidyl methacrylate: a functional monomer, *Macromol. Chem. Phys.*, 2004, **205**, 2221–2228.

30 F. Liorzou, B. Phelps and D. L. Atherton, Macroscopic models of magnetization, *IEEE Trans. Magn.*, 2000, **36**, 418–428.

31 P. Humpolicek, V. Kasparkova, P. Saha and J. Stejskal, Biocompatibility of polyaniline, *Synth. Met.*, 2012, **162**, 722–727.

32 C. L. Bayer, I. J. Trenchard and N. A. Peppas, Analyzing polyaniline-poly(2-acrylamido-2-methylpropane sulfonic acid) biocompatibility with 3T3 fibroblasts, *J. Biomater. Sci., Polym. Ed.*, 2010, **21**, 623–634.

33 J. Stejskal, M. Hajna, V. Kasparkova, P. Humpolicek, A. Zhigunov and M. Trchova, Purification of a conducting polymer, polyaniline, for biomedical applications, *Synth. Met.*, 2014, **195**, 286–293.

34 M. Bosetti, A. Masse, E. Tobin and M. Cannas, Silver coated materials for external fixation devices: in vitro biocompatibility and genotoxicity, *Biomaterials*, 2002, **23**, 887–892.

35 S. G. Belyavskii, P. G. Mingalyov, F. Giulieri, R. Combarrieau and G. V. Lisichkin, Chemical modification of the surface of a carbonyl iron powder, *Prot. Met.*, 2006, **42**, 244–252.

36 G. Goncalves, P. Marques, A. Barros-Timmons, I. Bdkin, M. K. Singh, N. Emami and J. Gracio, Graphene oxide modified with PMMA via ATRP as a reinforcement filler, *J. Mater. Chem.*, 2010, **20**, 9927–9934.

37 J. Sutrisno, A. Fuchs, H. Sahin and F. Gordaninejad, Surface coated iron particles *via* atom transfer radical polymerization for thermal-oxidatively stable high viscosity magnetorheological fluid, *J. Appl. Polym. Sci.*, 2013, **128**, 470–480.

38 M. Sedlacik, V. Pavlinek, R. Vyroubal, P. Peer and P. Filip, A dimorphic magnetorheological fluid with improved oxidation and chemical stability under oscillatory shear, *Smart Mater. Struct.*, 2013, **22**, 035011.

39 C. Shanthi and K. P. Rao, Chitosan modified poly(glycidyl methacrylate-butyl acrylate) copolymer grafted bovine pericardial tissue–anticalcification properties, *Carbohydr. Polym.*, 2001, **44**, 123–131.

40 S. Y. Kim, S. H. Kwon, Y. D. Liu, J. S. Lee, C. Y. You and H. J. Choi, Core-shell-structured cross-linked poly(glycidyl methacrylate)-coated carbonyl iron microspheres and their magnetorheology, *J. Mater. Sci.*, 2014, **49**, 1345–1352.

41 M. S. Cho, H. J. Choi and M. S. Jhon, Shear stress analysis of a semiconducting polymer based electrorheological fluid system, *Polymer*, 2005, **46**, 11484–11488.

42 F. F. Fang, H. J. Choi and M. S. Jhon, Magnetorheology of soft magnetic carbonyl iron suspension with single-walled carbon nanotube additive and its yield stress scaling function, *Colloids Surf., A*, 2009, **351**, 46–51.

43 J. M. Ginder, L. C. Davis and L. D. Elie, Rheology of magnetorheological fluids: Models and measurements, *Int. J. Mod. Phys. B*, 1996, **10**, 3293–3303.

44 M. Machovsky, M. Mrlik, I. Kuritka, V. Pavlinek and V. Babayan, Novel synthesis of core-shell urchin-like ZnO coated carbonyl iron microparticles and their magnetorheological activity, *RSC Adv.*, 2013, **4**, 996–1003.

PAPER III

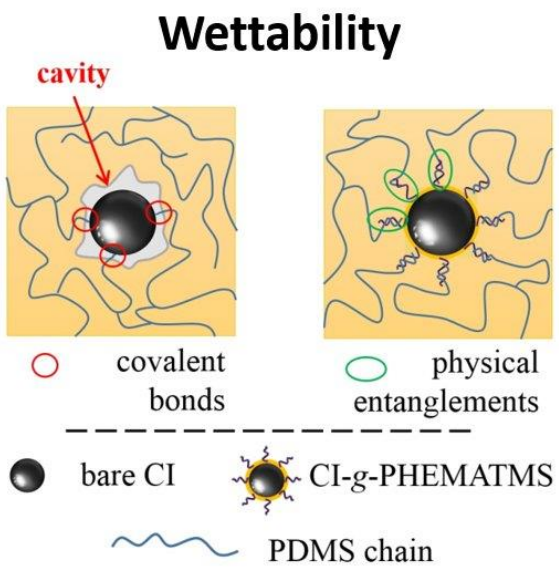

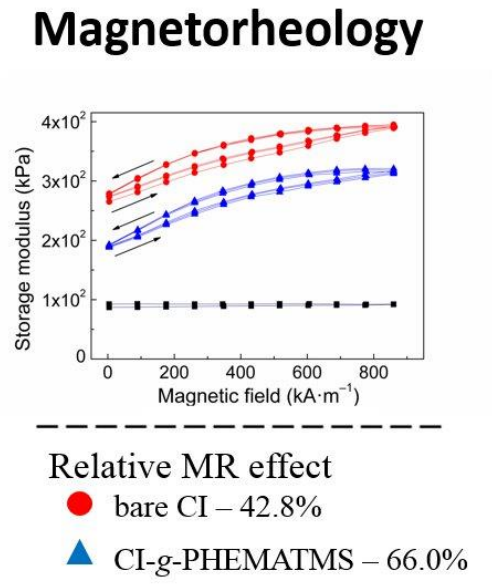

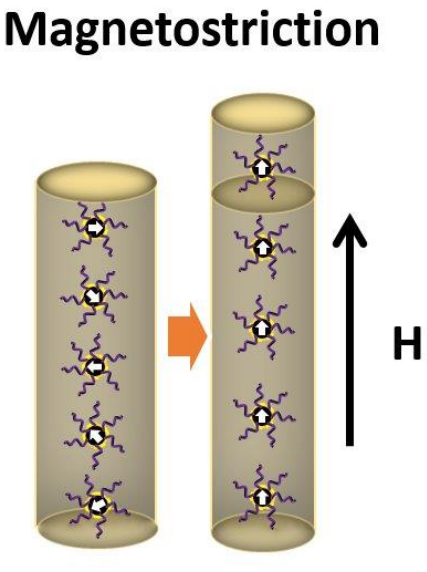

American Chemical Society

Macromolecules

Accepted: 24th February 2017

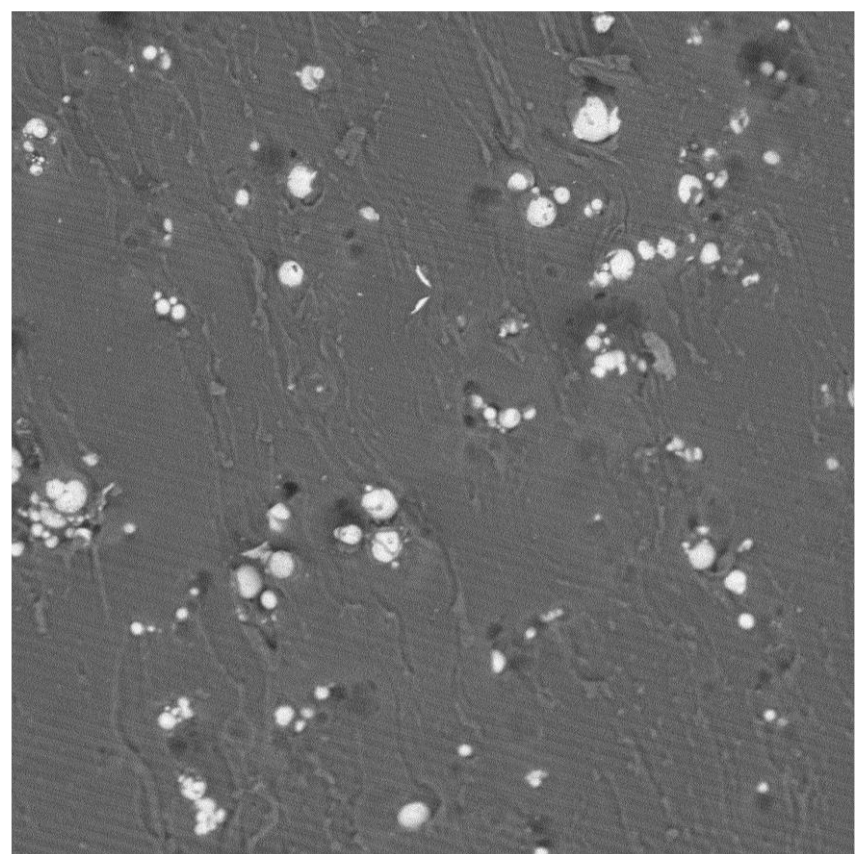

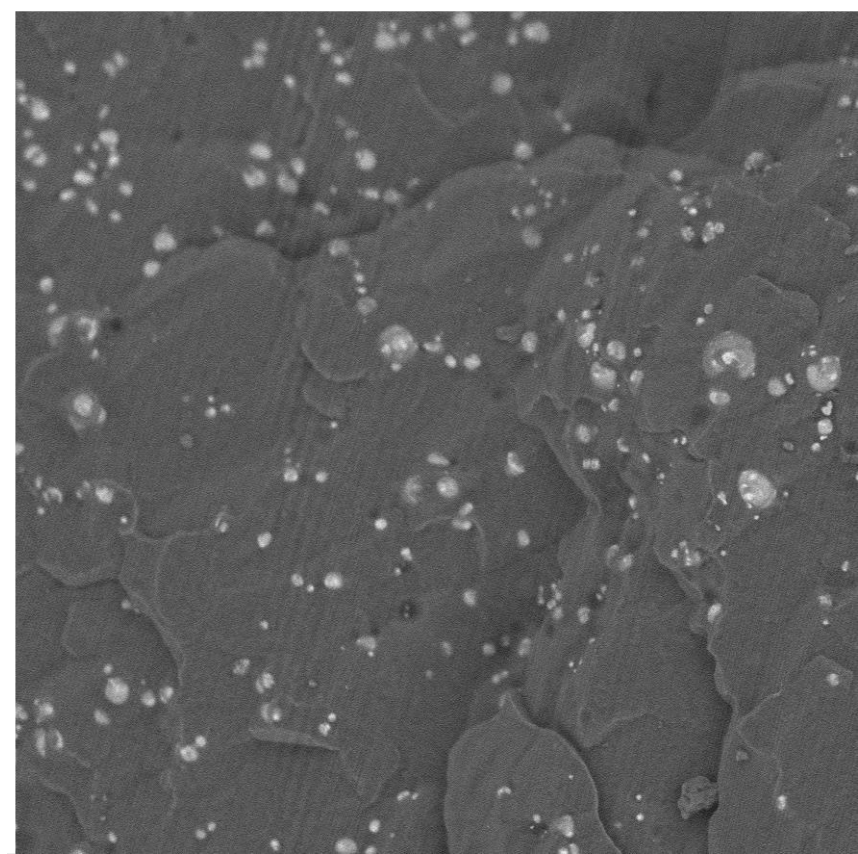

Macromolecules

Article

pubs.acs.org/Macromolecules

Synthesis of Silicone Elastomers Containing Silyl-Based Polymer-Grafted Carbonyl Iron Particles: An Efficient Way To Improve Magnetorheological, Damping, and Sensing Performances

Martin Cvek,[†,‡] Miroslav Mrlík,*[,†] Markéta Ilčíková,[§] Jaroslav Mosnáček,[§] Lukáš Münster,[†] and Vladimír Pavlínek[†]

[†]Centre of Polymer Systems, University Institute, Tomas Bata University in Zlin, Trida T. Bati 5678, 760 01 Zlin, Czech Republic
[‡]Polymer Centre, Faculty of Technology, Tomas Bata University in Zlin, Vavreckova 275, 762 02 Zlin, Czech Republic
[§]Polymer Institute, Slovak Academy of Sciences, Dubravska cesta 9, 845 41 Bratislava 45, Slovakia

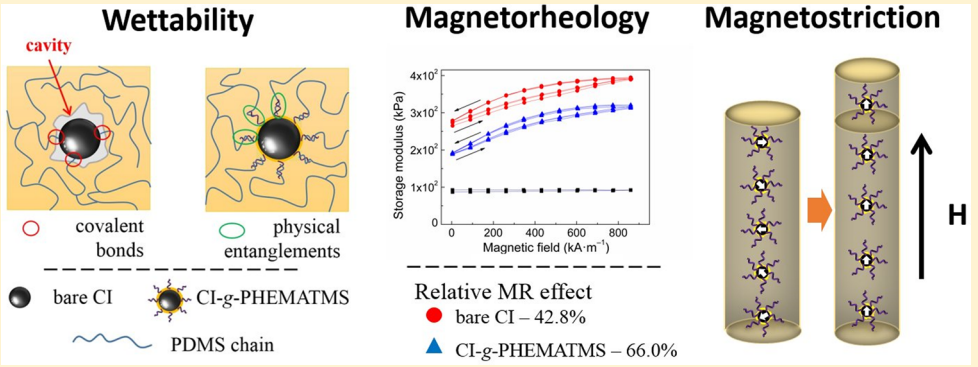

ABSTRACT: The synthesis and characterization of isotropic magnetorheological elastomer (MRE) with significantly enhanced utility properties is presented. Common drawbacks of classical MREs, such as poor particle wettability, dispersibility, low thermo-oxidative stability, low chemical stability, and insufficient durability, were eliminated by grafting the carbonyl iron (CI) particles with poly(trimethylsilyloxyethyl methacrylate) (PHEMATMS) using surface-initiated atom transfer radical polymerization (ATRP). Two sets of the MREs were prepared containing bare CI and CI grafted with PHEMATMS chains (CI-*g*-PHEMATMS). The effects of the coating on magnetorheological behavior in oscillatory shear, as well as the sensing properties of the prepared MREs, were evaluated. The mechanical properties in tensile mode and the particle filler/polydimethylsiloxane (PDMS) matrix interactions were investigated using a dynamic mechanical analysis. The PHEMATMS grafts considerably improved the CI particles' mobility, probably by preventing a partial cross-linking with the PDMS matrix. Besides the plasticizing effect, the MRE containing CI-*g*-PHEMATMS exhibited moderate mechanical performance and a slightly improved relative magnetorheological effect, but significantly enhanced damping factor, improved magnetostriction, and provided good sensing capability, which make such material highly promising for intended practical applications.

INTRODUCTION

Magnetorheological elastomers (MREs) represent a group of smart materials, the rheological or mechanical properties of which can be rapidly and reversibly tuned by an applied external magnetic field. They are also referred to as the solid counterparts of magnetorheological fluids (MRFs), as the oil is replaced by an elastomeric material. Generally, MREs are composed of ferromagnetic particles embedded in a low-permeability elastomeric matrix.[1−4] Such materials are typically fabricated by the addition of magnetic particles to a liquid-state matrix, followed by curing either in the absence (isotropic MRE) or in the presence (anisotropic MREs) of an external magnetic field. It is known that MREs exhibit exceptional properties such as controllable modulus and damping, which make them suitable for utilization in vibration control of cable-stayed bridges, seismic protection of buildings, adaptive damping of automotive or train seats, magnetic-field-induced actuators, or even artificial muscles and electromagnetic shielding materials.[5−8] The main advantage of MREs over MRFs is that the particle sedimentation is eliminated. Also, there is no need of containers or seals to prevent leakage and environmental contamination,[2,9] which make these intelligent systems highly promising for future applications.

However, the utilization of MREs in diverse fields makes challenging demands on their performance. To prepare an effective MRE, several factors need to be considered, including particle aggregation, oxidative and chemical stabilities, and ultimately their durability.[2,10] These requirements are still

Received: September 22, 2016
Revised: February 7, 2017

DOI: 10.1021/acs.macromol.6b02041
Macromolecules XXXX, XXX, XXX−XXX

limiting their ordinary real-life utilization. Generally, as a filler of most MREs, carbonyl iron (CI) is employed due to its excellent magnetic properties, such as high permeability, low remanent magnetization, and high saturation magnetization. The CI surface is under standard conditions, covered with a thin layer of iron oxides, which results in large amounts of oxygen incorporated into the body of the MRE. Iron ions can further enhance the oxidative degradation of rubber matrix materials.[3,11] The interface between particles and the matrix thus plays a key role in the durability of the MRE. The preparation of protective and functional coatings on CI appears to be an effective way to minimize these undesirable phenomena. However, as known from MRF analogues, the thickness of the coatings is crucial, especially when magnetic properties are taken into account. As our research group recently published,[12] the controllable "grafting from" method offers uniform coating layers with tailored molecular weight and without any significant decrease in the magnetization of the magnetic substrate. It was also shown by Fuchs et al.[10] that coating based on poly(fluorostyrene) grafted via atom transfer radical polymerization (ATRP) greatly enhanced the oxidative stability of the particles. A layer of poly(tetrafluoropropyl methacrylate) formed through a combination of reversible addition−fragmentation chain transfer (RAFT) and click chemistry on the iron particles also reduced oxidation but did not significantly change the modulus.[13] However, in these studies the magnetorheological (MR) effect, including hysteresis behavior, was not taken into consideration.

The matrix has a sizable influence on the dynamic properties of MREs.[14] The standard objective of designing MREs is to prepare a material with the highest possible MR effect. A feasible way to enhance this property is a preparation of the MREs based on suitably soft matrices. As an example, Chertovich et al.[15] have developed a MRE with a huge (up to 400 times) increase of the storage shear modulus, G', but on the other hand, its off-state value was only 1 kPa. Such a low off-state G' and reduced mechanical properties can be in many cases undesirable from a practical point of view.

Therefore, sophisticated MRE systems, which eliminate particle drawbacks but at the same time have a suitably designed matrix, need to be developed. This paper comprehensively deals with the effects of a controllable polymer coating on the behavior of MREs. In the first part, we report on the polymerization using surface-initiated ATRP (SI-ATRP) in order to obtain CI particles grafted with poly(trimethylsilyloxyethyl methacrylate) chains (CI-*g*-PHEMATMS). We also studied the effects of the coating on the magnetic performance and thermo-oxidation stability of the CI particles. Further, isotropic MREs containing either bare CI or CI-*g*-PHEMATMS particles were prepared using polydimethylsiloxane (PDMS) as a matrix. PDMS was chosen due to its good elastic properties in highly filled systems, high heat resistance, and chemical inertness.[16] The aim for modification of the CI particle surface was also to enhance particle/matrix compatibility and to prevent the possible formation of covalent bonds of bare CI with the PDMS matrix. This can potentially increase the mobility of the particles and thus adjust the mechanical properties of the MREs. As will be presented in this work, the modification of the CI particles with PHEMATMS chains positively affected a wide range of properties of the MRE material.

EXPERIMENTAL SECTION

Materials. CI particles (SL grade, Fe >99.5%) supplied by BASF Corporation (Germany) were used as a suitable magnetic core for the modification. (3-Aminopropyl)triethoxysilane (ATPES, ≥98%) was used as a linker for the covalent bonding of α-bromoisobutyryl bromide (BiBB, 98%), serving as an initiator, onto the surface of the CI particles. The monomer components 2-hydroxyethyl methacrylate (HEMA, 96%) and chlorotrimethylsilane (TMCS, ≥97%) were purified by passing them through a basic alumina column to remove the inhibitor. Dichloromethane (anhydrous, ≥99.8%) was used as a solvent. Triethyleneamine (TEA, ≥99%) was utilized to trap-form hydrogen chloride in the reaction mixture. Ethyl α-bromoisobutyrate (EBiB, 98%), *N*,*N*,*N*′,*N*″,*N*″-pentamethyldiethylenetriamine (PMDETA, ≥99%), copper bromide (CuBr, ≥99%), and anisole (99%) were used as an initiator, ligand, catalyst, and solvent, respectively. All chemicals were purchased from Sigma-Aldrich (USA). Other reagents, namely tetrahydrofuran (THF, p.a.), acetone (p.a.), ethanol (absolute anhydrous, p.a.), toluene (p.a.), and hydrochloric acid (HCl, 35%, p.a.), were obtained from Penta Laboratories (Czech Republic) and were used as received. A two-component Sylgard 184 kit (silicone elastomer/curing agent, Dow Corning, USA) was employed as an elastomer matrix for the magnetic filler. The components of the elastomer kit were used in a weight ratio of 20:1 in order to obtain a desired cross-linking density and thus to design a suitably soft elastomeric matrix.

Synthesis of Trimethylsilyloxyethyl Methacrylate (HEMATMS). The HEMATMS was prepared using a slightly modified procedure described previously for the synthesis of trimethylsilyloxyethyl acrylate.[17] Argon-purged HEMA (22.64 g, 174 mmol), TEA (26.35 g, 261 mmol), and dry dichloromethane (250 mL) were added to a 500 mL, three-necked, argon-backfilled, round-bottom flask and cooled down to 0−5 °C in an ice bath. Then freshly distilled TMCS (28.45 g, 261 mmol) was added dropwise for 1 h. The mixture was stirred at a temperature of 0−5 °C for an additional hour and then overnight at laboratory temperature. The reaction was stopped by opening the flask. The salt was filtered out, and the solvents were removed using a rotary vacuum evaporator (Heidolph VV 2000, Gemini BV, Germany) (40 °C, 10 mbar). The HEMATMS monomer was stabilized before storage by the addition of ionol (5 mg). The ionol was removed from the monomer by distillation (55 °C, 0.4 mbar) immediately prior to polymerization. The purity of the product was confirmed by ^{1}H NMR analysis. ^{1}H NMR (400 MHz, $CDCl_3$): δ (ppm) 0.12 (s, 9H, Si(CH_3)$_3$), 1.94 (s, 3H, C−CH_3), 3.82 (t, 2H, CH_2−O−Si), 4.21 (t, 2H, COOCH_2), 5.60 (m, 1H, CH_2−C), 6.12 (m, 1H, CH_2−C).

Modification of the CI Particles. The surface of the CI particles was activated by the treatment of the CI powder (100 g) with 0.5 M hydrochloric acid according to the literature.[18] Then, the activated CI particles were functionalized with a silane agent. Briefly, the particles (90 g) were dispersed in toluene and thoroughly agitated at 110 °C. The ATPES (10 mL) was added, and the reaction was stopped after 6 h. The modified material was washed and dried similarly as described elsewhere.[12] Subsequently, the amine groups at the particle surface were used to bond the ATRP initiator. Then, the APTES-treated particles (40 g), dried THF (100 mL), and TEA (16 mL) were mixed in the Schlenk flask under an argon atmosphere. The mixture was placed into an ice bath cooled to 0−5 °C, and BiBB (8 mL) was added dropwise. The initiator-treated CI particles (CI-Br) were then washed with THF (5 times, 100 mL each) and acetone (5 times, 100 mL each) and then dried overnight at 60 °C under 200 mbar.

Surface-Initiated ATRP of HEMATMS. The Schlenk flask containing the CI-Br particles (15 g) was evacuated and then backfilled with argon several times. The argon-purged HEMATMS (10 g, 49.4 mmol), EBiB (0.073 mL, 0.494 mmol), PMDETA (0.103 mL, 0.494 mmol), and anisole (10 mL) were added, and the mixture was degassed by several freeze−pump−thaw cycles in order to eliminate the presence of oxygen. Finally, the flask was filled with argon, the CuBr catalyst (70.9 mg, 0.494 mmol) was quickly added to the frozen mixture under an argon flow, and an additional freeze−pump−thaw

DOI: 10.1021/acs.macromol.6b02041
Macromolecules XXXX, XXX, XXX−XXX

cycle was performed. The reactants were used at a molar ratio of [HEMATMS]:[EBiB]:[CuBr]:[PMDETA] = [100]:[1]:[1]:[1], while anisole served as a solvent in the amount of 50 vol %.

To initiate the polymerization, the flask was immersed into a silicone oil bath preheated to 70 °C. The mixture was mechanically stirred in the compact glovebox (GP [Campus], Jacomex, France) under a nitrogen atmosphere (<10 ppm of O_2). The reaction was stopped by exposure of the mixture to air and cooling down to laboratory temperature. The prepared core−shell structures were purified by washing with THF (5 times, 100 mL each) and acetone (5 times, 100 mL each), using the accelerated decantation method with a magnet at the bottom of the beaker, and then dried overnight at 60 °C under 200 mbar. Scheme 1 illustrates the process of performed SI-ATRP.

Scheme 1. Surface-Initiated ATRP of HEMATMS from the Surface of CI-Br Particles

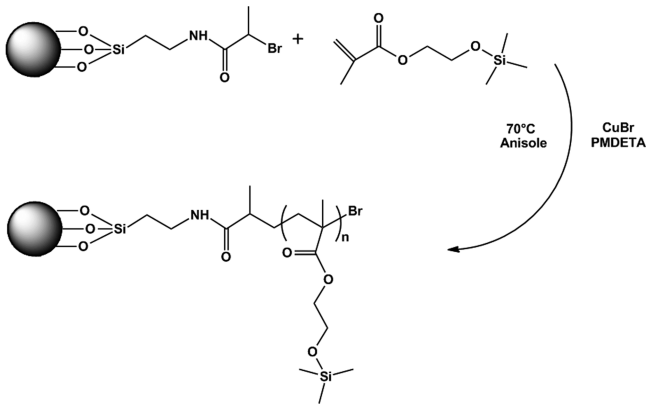

Analysis. The purity of HEMATMS and its conversion during polymerization were determined using nuclear magnetic resonance spectroscopy (NMR, 400 MHz VNMRS Varian, Japan) with deuterated chloroform ($CDCl_3$) as a solvent at a temperature of 25 °C. The molar mass and dispersity ($Đ$) of the PHEMATMS were estimated by the common gel permeation chromatography (GPC) technique using the GPC instrument (PL-GPC220, Agilent, Japan) equipped with GPC columns (Waters 515 pump, two PPS SDV 5 μm columns (diameter of 8 mm, length of 300 mm, 500 Å + 105 Å)) and a Waters 410 differential refractive index detector tempered to 30 °C. The mobile phase was THF of HPLC grade with a flow rate of 1 mL min^{-1}. Anisole was used as an internal standard to correct the fluctuations in the THF flow rate. Prior to the GPC measurement, the sample was diluted with THF and then purified and deprived from the catalyst by passing it through a neutral alumina column.

Characterization of the Particles. A scanning electron microscope (SEM, Tescan Vega II, Czech Republic) equipped with an energy-dispersive spectroscope (EDS) was employed in order to provide information about the elemental composition of the studied samples. To confirm the presence of PHEMATMS brushes on the CI, Fourier transform infrared (FTIR) spectra were measured on a Nicolet 6700 (Nicolet, USA) with the ATR accessory at laboratory conditions using a germanium crystal in the wavenumber range of 3600−600 cm^{-1}. Each spectrum was obtained after 64 scans with a spectral resolution of 4 cm^{-1}. A thickness of grafted layer was observed using a transmission electron microscope (TEM, JEM-2100Plus, Jeol, USA). The samples for TEM analysis were prepared by dispersing the particles in acetone and a dropping onto a copper grid. The densities of bare CI and CI-*g*-PHEMATMS particles were obtained using a gas pycnometer (UltraFoam 1200e, Quantachrome Instruments, Germany). The measurement was performed on dried samples at ambient temperature, while nitrogen was used as a gaseous medium. The magnetic properties of bare CI particles as well as their coated analogues (samples of approximately 150 mg) were investigated in an external magnetic field in the range of ±10 kOe (±780 kA m^{-1}) using a vibrating-sample magnetometer (VSM, Model 7404, Lake Shore, USA) at laboratory conditions. The amplitude of the vibrations was 1.5 mm, and the frequency was set to 82 Hz. The performance of the particles in terms of their thermo-oxidative stability was analyzed using a thermogravimetric analysis (TGA, TA Instruments Q500, USA) in a temperature range of 0−800 °C, operating at a heating rate of 10 K min^{-1} under air atmosphere (flow rate of 50 mL min^{-1}). The resistance of the particles against an acidic environment was examined by an antiacid/corrosion test. In a typical procedure,[8,19] 1 g of the corresponding particles was dispersed in 20 mL of 0.1 M aqueous HCl solution at laboratory temperature. The suspension was mechanically stirred, and the reaction progress was evaluated by observing the pH-value development in time using a pH-meter (SensoDirect pH 110, Tintometer GmbH, Germany), which was calibrated using two standard buffer solutions prior each measurement.

The pellets (diameter of 13 mm, thickness of 0.1 mm) containing bare CI or CI-*g*-PHEMATMS particles were prepared on a laboratory hydraulic press (Trystom Olomouc, H-62, Czech Republic) under a compaction pressure of 7 ± 0.5 MPa, which was applied for a duration of 60 s. Contact angle measurements were performed based on the static sessile drop method using a surface energy evaluation system equipped with a CCD camera (Advex Instruments, Czech Republic). In the experiments, a Sylgard 184 droplet with a volume of 3 μL was carefully dripped on the compressed powder pellet under laboratory conditions (temperature of 22 ± 1 °C, relative humidity of 60 ± 1%). The representative contact angle values are presented as an average value of 10 independent measurements.

Preparation of Magnetorheological Elastomer. The PDMS was prepared by a thorough mixing of the silicone elastomer and curing agent for 10 min. The desired amount of bare CI or CI-*g*-PHEMATMS particles was added to prepare the samples of 60 wt % particle concentration. The homogeneous mixture was degassed (20 min under 10 mbar) using an oil-free membrane vacuum pump in order to remove air trapped in the suspensions and to obtain samples without any defects. Subsequently, the suspension was poured into a PTFE mold (25 × 25 × 1.2 mm); the curing process was accelerated in an oven preheated to 100 °C for 45 min. The postcure treatment included cooling the isotropic MRE samples to laboratory temperature and their storage in a desiccator.

Magnetorheological Characterization. The circular disc specimens of 20 mm in diameter and approximately 1.15 mm in thickness were cut out from the prepared MRE sheets. The dynamic mechanical behavior in the absence as well as under various external magnetic fields was studied with the help of an advanced rotational rheometer (Physica MCR502, Anton Paar GmbH, Austria) equipped with a magneto-device (Physica MRD 180/1T). The employed power supply provided an electric current of 0−3 A, which was correlated to the true magnetic field strength using a teslameter (Magnet Physic, FH 51, Dr. Steingroever GmbH, Germany). The applied magnetic field was perpendicular to the MRE sample, which was placed between a parallel plate (PP20/MRD/TI) geometry and a measuring cell.

The linear viscoelastic region (LVR) was determined under different magnetic field strengths through deformation sweeps using an amplitude of deformation of 10^{-3}−10^{1} % and a fixed frequency of 5 Hz. To ensure that all measurements fall into LVR, the deformation of 0.2% was chosen for the neat matrix as well as both studied MREs. The storage, G', and the loss, G'', moduli, damping factor, tan δ, and normal force, F_N, were then studied within the LVR in the magneto-sweep in the range of 0−860 kA m^{-1} at a frequency of 5 Hz. All measurements were performed at a constant temperature of 25 °C.

Particle/Matrix Interface and Dynamic Mechanical Analysis. A desktop SEM (Phenom Pro, Phenom-World, Netherlands) operating under accelerating voltage of 5 kV was used to thoroughly examine particle/matrix interface in the fabricated MREs. A dynamic mechanical analysis (DMA) in tensile mode was performed on a DMA/SDTA816e (Mettler Toledo, Switzerland). The tested samples were in the form of strips with dimensions of 15 mm in length, 1.8 mm in width, and 1.15 mm in thickness. All measurements were performed in the LVR determined from the strain dependence of tensile storage modulus, E'. Temperature sweeps were examined in a temperature

DOI: 10.1021/acs.macromol.6b02041
Macromolecules XXXX, XXX, XXX−XXX

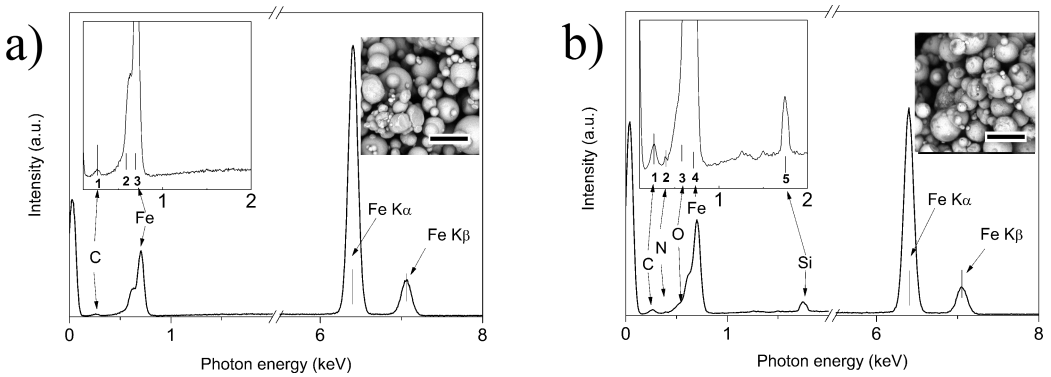

Figure 1. EDS spectra for bare CI particles (a) with corresponding magnified details: 1, C Kα line; 2 and 3, Fe Lα lines; and for CI-*g*-PHEMATMS particles (b) with corresponding magnified details: 1, C Kα line; 2, N Kα line; 3 and 4, Fe Lα lines; 5, Si Kα line. The SEM insets show the sample place from where the spectra were collected; the black bars represent 7 μm.

range from −145 to 50 °C at a heating rate of 3 °C min^{-1} at different frequencies under a nitrogen atmosphere. The conditions were chosen in order to properly investigate the E' evolution, and the glass transition temperature, T_g, as a peak position of tan δ. The samples were measured twice, and average values were used for further evaluation.

In order to compare the interactions and compatibility of the CI particles with the PDMS matrix, the activation energies of PDMS glass transition were calculated eq 1 for neat PDMS, and the MREs containing bare CI as well as CI-*g*-PHEMATMS particles analogously, as was performed by other researchers[20,21] on similar material systems.

$$\ln f = \ln f_0 - \frac{E_a}{RT_g} \quad (1)$$

where f is the tested frequency, f_0 represents the material characteristic constant, T_g denotes the glass transition temperature, and R is the universal gas constant.[20,21]

RESULTS AND DISCUSSION

Modification of the CI Surface with PHEMATMS Chains. The process of modification of the CI surface is schematically outlined in Scheme 1. First, the CI surface was modified with an ATRP initiator by the reaction of the activated CI with APTES and the subsequent amidation of amine groups with BiBB. Then, the SI-ATRP of HEMATMS from the CI-Br particles was performed. The polymer shell thickness onto the CI surface can be partially controlled by tailoring the molar mass of the polymer chains attached to the CI surface. The molar mass can be controlled by the monomer: initiator ratio and monomer conversion. Since the exact amount of the initiator attached to the CI-Br surface is difficult to determine, in order to achieve good control of the molar mass, a sacrificial initiator, such as EBiB, was used in excess with respect to the expected amount of ATRP initiator covalently attached to the CI-Br surface. In addition, the use of the sacrificial initiator enabled the easy determination of molar mass by GPC and monomer conversion by NMR spectroscopy. The feed ratio of monomer:initiator was kept at 100:1 to tailor the shell of maximal theoretical thickness in a range of 10−20 nm. The polymerization was stopped after 2 h at 90% conversion. The molar mass of HEMATMS was determined to be of 9200 g mol^{-1} with a $Đ$ of 1.28. The determination was based on the assumption of the similar growth of the polymer from the sacrificial and bond initiators.[22] A relatively low $Đ$ implies a high polymerization control via ATRP, indicating a good uniformity of the grafted polymer layer.

To prove the presence of the PHEMATMS chains on the CI surface, an elemental analysis was performed. Figure 1a illustrates the EDS spectrum of bare CI particles. A set of strong peaks (0.78 and 6.40 keV) represented a predominant occurrence of iron. The small amount of carbon (0.28 keV) can be considered as an impurity. On the contrary, Figure 1b shows the spectrum obtained for the CI-*g*-PHEMATMS particles. The signals corresponding to silicone (1.74 keV) and oxygen (0.53 keV) come from residues of APTES, BiBB, and predominantly from PHEMATMS chains. The peak from oxygen was to a certain degree overlapped with a low-energy shoulder of the broad iron Lα peak. Also, nitrogen (0.39 keV) originated from the coupling agent was observable in the spectrum. The bromine was not occurring in the spectrum, probably due to its negligible concentration in the sample and its possible peak interference with the background noise. However, the EDS results indicated that the PHEMATMS shell was present on the surface of the CI.

In order to further confirm the result of the EDS analysis, the FTIR spectra of bare CI, CI-Br, and CI-*g*-PHEMATMS particles are shown in Figure 2. The absorption band visible

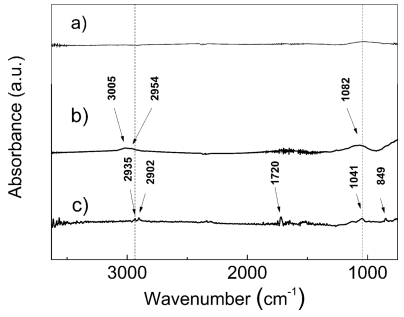

Figure 2. FTIR spectra of bare CI (a), CI-Br (b), and CI-*g*-PHEMATMS (c) particles with denoted characteristic wavenumbers.

at around 3000 cm^{-1} corresponds to the CH stretching vibrations from the $-CH_3$ and $-CH_2-$ groups. The peak at 1720 cm^{-1} occurring for CI-*g*-PHEMATMS particles can be attributed to C=O stretching vibrations. Raised absorption peaks at 1082 and 1041 cm^{-1} were assigned to Si−O−Si stretching, which is typical for organosilicon compounds. Finally, the peak at 849 cm^{-1} can be assigned to Si−CH_3 rocking present in the pendant groups of the PHEMATMS. These peaks confirmed that the expected functional groups

DOI: 10.1021/acs.macromol.6b02041
Macromolecules XXXX, XXX, XXX−XXX

were present in the sample and the modification of the CI surface was successful.

Thickness of PHEMATMS Layer. Figure 3 shows TEM images of bare CI and CI-*g*-PHEMATMS particles. The former

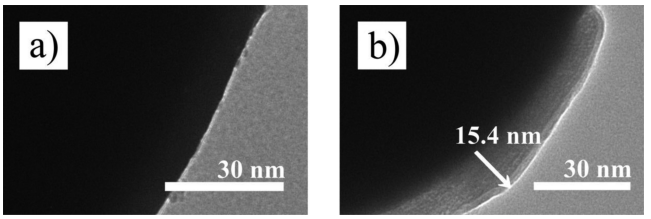

Figure 3. Detailed TEM images of bare CI (a) and the CI-*g*-PHEMATMS (b) showing a part of the corresponding single particle.

particles exhibited smooth surface without any impurities, whereas the latter particles had rougher surface due to the presence of PHEMATMS grafts. The grafted layer was quite uniform with a thickness of around 15 nm, which correlates very well with the theoretical estimation.

Density and Magnetic Properties of CI-*g*-PHEMATMS. The obtained densities for bare CI and CI-*g*-PHEMATMS particles were 7.79 and 7.35 g cm^{-3}, respectively, which is a similar result as was found by Fang et al.[23] on polystyrene nanobead-coated CI particles. Further, the effect of polymer coating on the magnetic properties was investigated. As presented in Figure 4, the magnetizations of the CI-*g*-

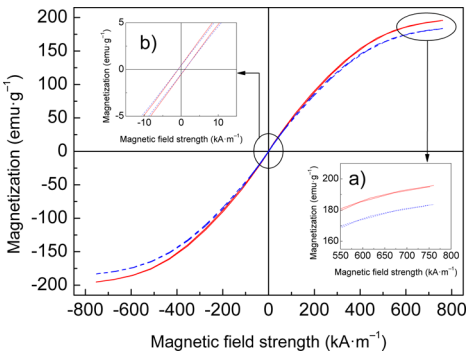

Figure 4. Magnetic hysteresis loops of bare CI (solid lines) and the CI-*g*-PHEMATMS (dashed lines) particles. Inset a highlights the particle magnetizations at magnetic fields above 550 kA m^{-1}, while inset b points out their hysteresis.

PHEMATMS particles decreased due to presence of non-magnetic coatings, which was also observed on similar material systems.[19,24] Nevertheless, the decrease in magnetization was insignificant, as can be seen in more detail (Figure 4, inset a). The level of decrease was given by the shell thickness, which was controlled to be in nanometer scale using the SI-ATRP technique. At the maximum employed field (780 kA m^{-1}), the PHEMATMS coating decreased magnetization by only 6.2% when compared to the magnetization of bare CI. The small decrease in magnetization is in agreement with the obtained densities. Moreover, at the examined temperature the particles exhibited almost hysteresis-free loops, small coercivities, and remanent magnetizations (Figure 4, inset b), suggesting fast demagnetization processes important for the implementation in MRE applications.

Thermo-Oxidative Stability of CI-*g*-PHEMATMS. Recently, MRFs have been used in oil and gas exploration applications, where operational temperatures can be high due to geothermal gradients and viscous heating.[25] Because of the similar application fields of the MREs and considering their oncoming practical applications, the thermal stability of the MREs is equally important. Therefore, the TGA was used to estimate the thermo-oxidative stability of studied particles in air. The stability was specified as a temperature, at which the sample gained 5% of its original weight due to an oxidation process. As can be seen in Figure 5, bare CI particles were

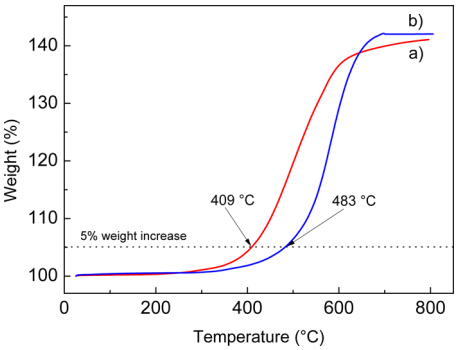

Figure 5. TGA curves of bare CI (a) and CI-*g*-PHEMATMS (b) particles in air atmosphere.

relatively stable up to 409 °C when their oxidation proceeded, which was accompanied by a pronounced weight gain due to the formation of oxides, i.e., FeO, Fe_3O_4, and Fe_2O_3.[12] A similar feature was observable in CI-*g*-PHEMATMS particles; however, in this case the rapid oxidation process started at 483 °C. This analysis revealed that the thin PHEMATMS shell served as a protective coating for the CI cores, resulting in a substantial enhancement (74 °C) of their thermo-oxidation stability.

Chemical Stability. In the practical applications of the MREs, the chemical stability of the incorporated particles is very important factor affecting their long-term stability and durability. The acidic reactive species, e.g. acid rains, sea humidity, or operating fluid leakage, can initiate the oxidation of the untreated iron particles followed by a decrease of their magnetic properties.[8] In the MREs, the magnetic particles are embedded in a matrix; nevertheless, their corrosion is still possible after the reactive species diffusion through the polymeric matrix. Therefore, the chemical stability of studied materials was compared using a facile corrosion test.[19] As can be seen in Figure 6, bare CI particles were relatively unstable

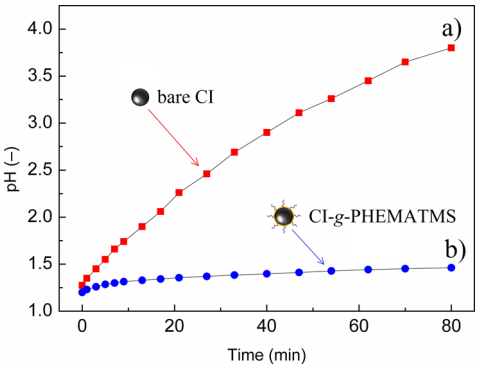

Figure 6. Resistance to acidic conditions of bare CI (a) and CI-*g*-PHEMATMS (b) particles.

DOI: 10.1021/acs.macromol.6b02041
Macromolecules XXXX, XXX, XXX−XXX

and the reaction immediately proceeded. A degradation of bare CI particles was accompanied by the presence of hydrogen bubbles leaking from the tested suspension. On the contrary, CI-*g*-PHEMATMS particles were extremely stable under these acidic conditions, which proves that the grafted layer was uniform without any defects as was indicated from the TEM (Figure 3). Thus, the performed modification significantly enhanced particle resistance against acidic environment, which improved their durability and widened the scope of their practical employment.

Surface Wettability Analysis. In order to evaluate the wettability between bare CI or CI-*g*-PHEMATMS particles and the Sylgard 184 matrix, the contact angles were investigated using the static sessile drop method (Figure 7). Bare CI particles exhibited a contact angle of 83.2 ± 7.4°, while after SI-ATRP it decreased to only 42.1 ± 6.2°, indicating the significantly enhanced wettability of CI-*g*-PHEMATMS particles with the Sylgard 184 matrix. The results further indicate improved particle dispersibility in the silicone matrix and the enhanced compatibility of the MRE containing CI-*g*-PHEMATMS.

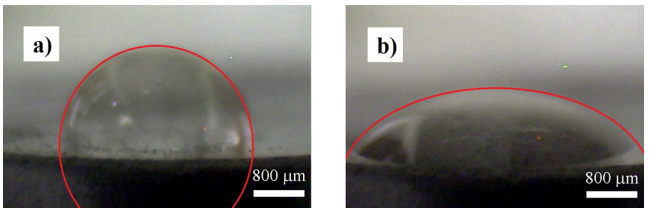

Figure 7. Images from a CCD camera of Sylgard 184 droplets on the surface of a compressed powder pellet containing bare CI (a) and CI-*g*-PHEMATMS (b) particles. The red lines define the interface of the droplets.

Magnetorheological Properties of MREs. An external magnetic field has a substantial effect on the spatial arrangement of the particles in the MRE matrix. In the magnetic field, the particles tend to align themselves and to develop chainlike structures in a manner similar to MRFs,[26] resulting in a field-responsive modulus. Moreover, the rearrangement of the particles within the elastomer leads to a change of specimen dimensions (shrinkage/elongation), which is called magnetostriction.[27] Recently, it was shown that besides these phenomena, MREs also exhibit hysteresis behavior when they are exposed to ascending/descending magnetic fields. These findings were considered, and the effects of particle modification on the aforementioned phenomena were investigated. The samples were characterized at a constant strain amplitude of 0.2%, which ensured that all the data fell into the LVR. The oscillation frequency was set as 5 Hz, as this frequency belongs to the region of interest (further analyzed in frequency sweeps). Further, the experiment was performed similarly as was reported by Sorokin et al.[27] The moduli were measured in an increasing magnetic field when the electric current was linearly increased from 0 to 3 A in 0.3 A steps. The maximum electric current was chosen due to the possible inhomogeneity of magnetic fields in the measuring cell above this value.[28] Then, the current was analogously decreased to its zero value. True magnetic field strengths (H) were measured using a Hall probe, which revealed their values in the range up to 860 kA m^{-1}, which corresponded to the current of 3 A. The shear viscoelastic moduli, i.e., the storage, G', and the loss, G'', damping factor, tan δ, and the normal force, F_N, were recorded as a function of H. The ascending/descending character of H is denoted by the arrows. The results for the MREs containing bare CI, as well as CI-*g*-PHEMATMS analogues, are shown in Figure 8.

First, the effect of the addition of magnetic particles on viscoelastic properties was compared to those of the neat PDMS matrix. As a reference point, the characteristics of the neat matrix were analyzed. It is known that the MR effect is more pronounced when the matrix is suitably soft.[15] Therefore, the desired plasticity of the matrix was obtained by using a modified silicone elastomer/curing agent ratio (as specified in the Materials section). At the studied conditions, the G' of the neat matrix was around 90 kPa, and it was independent of the applied H due to the absence of magnetic particles. The G' of both MREs was distinctly increased by the addition of the CI fillers, since rigid inorganic particles have a much higher stiffness than the polymer matrix.[29] The presence of both the bare CI and CI-*g*-PHEMATMS particles also increased G'', which can be associated with energy dissipating as heat due to friction between the particles and the matrix.

The effect of the magnetic field on G' as well as G'' of the MREs was also noticeable, as they increased with an increasing H. This phenomenon stems from MRE nature, and it was thoroughly studied in several publications.[1−10,13−15,26,27,30−32] An increase of G' in magnetic fields can be explained by enhanced particle magnetization and magnetic interactions resulting in particle network formation, which reinforces the composite structure. The G'' also exhibited a substantial increase with H, which was observed by Sorokin et al.[27] They speculated that this phenomenon is not only due to friction between the particles but also due to the possible rupture of polymer segments, which contributes to large energy dissipation.

Further, the effect of polymer coating on viscoelastic properties was evaluated. The G' of the MRE containing CI-

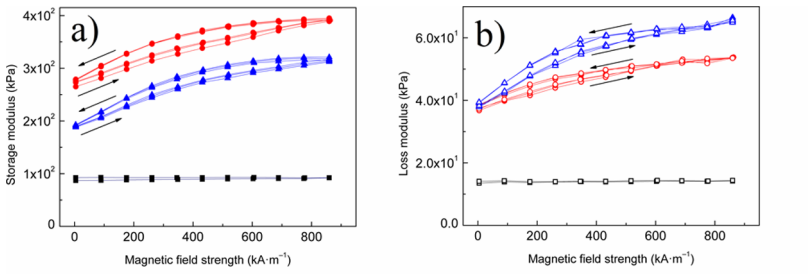

Figure 8. Storage, G' (a) (solid symbols), and the loss, G'' (b) (open symbols), moduli of the neat matrix (squares) and the isotropic MREs containing bare CI (circles) and CI-*g*-PHEMATMS (triangles) particles as a function of the applied magnetic field strength, H.

DOI: 10.1021/acs.macromol.6b02041
Macromolecules XXXX, XXX, XXX−XXX

g-PHEMATMS particles was moderately lower when compared to the G' of the MRE containing bare CI. Regarding the effect of particles modification on G', several researchers[33,34] have reported that the modification of the particles surface will increase storage modulus of the MREs, while others formulated just opposite conclusions.[32] We believe that this discrepancy is based on the reactivity of the MRE components. In more details, Li et al.[34] used the CI coated with poly(methyl methacrylate) and ethyl vinyl silicone rubber vulcanized by double methyl double benzoyl hexane as a matrix. Khimi et al.[33] employed the iron sand coated with bis(3-triethoxysilylpropyl) tetrasulfate and natural rubber, zinc oxide, stearic acid, *n*-cyclohexyl-2-benzothiazole sulfonamide, tetramethylthiuram disulfide, paraffin oil, and naphthenic oil as a vulcanizing system. There is no evidence in the literature that using these systems covalent bonding between the bare particles and the matrix can be formed. In our case, covalent bonding between bare CI and the matrix may take place probably due to the reaction of the hydroxyl groups on the metal surface with the silane groups of the curing agent.[4] In order to clarify this phenomenon, a broad DMA investigation has been performed (more details are presented further in text).

On the contrary, the G'' of the MRE containing CI-*g*-PHEMATMS was higher compared to the G'' of the MRE containing bare CI particles. The latter particles can covalently bond to the PDMS elastomeric matrix as indicated in the previous paragraph. Therefore, the mobility of bare CI within the matrix can be suppressed. On the other hand, the PHEMATMS chains grafted onto the CI surface increased the mobility of the embedded particles, as the covalent bonds were replaced by physical entanglements between the PHEMATMS and PDMS chains. The increased G'' represented a dissipative heat loss due to better particle mobility and hence a greater friction. The results correlate with the damping properties of studied materials (Figure 9). Generally, damping

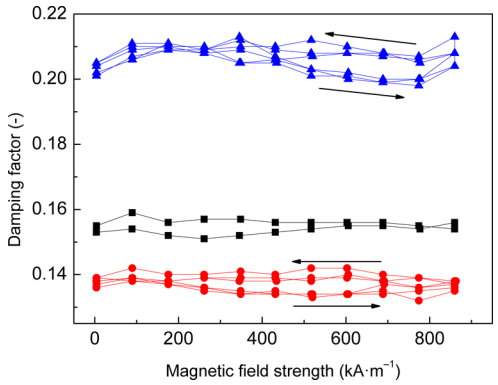

Figure 9. Damping factor, tan δ, of the neat matrix (squares), the isotropic MREs containing bare CI (circles), and the CI-*g*-PHEMATMS (triangles) particles as a function of the applied magnetic field strength, H.

in composites involves several energy dissipation mechanisms. However, in the MREs, there are two main damping sources. One represents damping of the elastomeric matrix, and the other can be assigned to the friction between particles and the matrix.[30,35] The damping of the particles can be neglected compared with that of the matrix.[14] As demonstrated in Figure 9, the bare CI particles exhibit reinforcing properties, which lead to a lower damping factor compared to the neat matrix. The incorporation of CI-*g*-PHEMATMS particles increased particle mobility and energy dissipation (associated with interfacial slipping between particles and the matrix), and a dramatic enhancement of damping properties occurred. Thus, the damping was enhanced by the chemical grafting on the CI particles. A similar phenomenon was recently observed by Wang et al.[36] dealing with the *in situ* physical core−shell structuring of complex microparticles in the MRE based on the rubber matrix.

To compare the magnetorheological activity of both materials, the relative MR effect (e) (eq 2), defined as

$$e = \frac{G'_H - G'_0}{G'_0} \tag{2}$$

where G'_H is the maximum field-on modulus and G'_0 is the field-off modulus, was evaluated from magneto-sweep measurements. Table 1 summarizes the field-off and maximum field-on

Table 1. Field-Off/On G' of Prepared Isotropic MREs and Their Relative MR Effects

filler for the MRE	G'_0 (kPa)	G'_H (kPa)	e (%)
bare CI	274 ± 5	392 ± 2	42.8 ± 3.5
CI-*g*-PHEMATMS	191 ± 2	316 ± 3	66.0 ± 1.6

(860 kA m^{-1}) G' moduli and the relative MR effects of the studied composites. Interestingly, the G'_0 was lower in the MRE containing CI-*g*-PHEMATMS particles. This behavior can be attributed to the increased plasticity of the matrix on the CI-*g*-PHEMATMS/PDMS interface. Hence, the PHEMATMS chains probably tend to loosen the cross-linking density. A similar feature was observed in the MREs containing surfactant-modified particles embedded in the elastomeric PDMS matrix.[4] Thus, PHEMATMS grafts appear to not only possess a plasticizing effect but also enhance thermo-oxidation stability of the particles while improving their wettability with the matrix at the same time. Nevertheless, the common plasticizers are generally low molecular weight chemicals and have a tendency to migrate through the polymer matrix.[37] This drawback can be eliminated using the system with covalently bonded PHEMATMS grafts, which is an undisputable advantage of this newly designed MRE.

The results further suggest that even though the G'_0 and G'_H moduli of MRE containing CI-*g*-PHEMATMS are lower, the relative MR effect of this material is ultimately more than 23% higher, while the magneto-induced modulus[38] ($\Delta G' = G'_H - G'_0$) was preserved, implying the versatility and better applicability of the MRE based on modified particles. The current literature describes the MREs with even larger relative MR effects. However, these effects are achieved due to very low G'_0 (1 kPa),[15] which is in most cases undesirable from a practical point of view or due to introducing higher amounts of magnetic particles[34,39] or the application of a higher H (>850 kA m^{-1}),[27,39] where the homogeneity of the magnetic field strength and thus performance of such MRE are rather speculative.[28] Further, we discuss the changes of $\Delta G'$, that as was shown recently can be enhanced by the incorporation of higher amounts of the particles[27] and/or by the fabrication of the MREs with different inner structure (iso- and anisotropic).[14] In the presented research, the particle fraction was maintained at the same level (60 wt %), and both variants of the fabricated MREs were in isotropic state. Therefore, we believe that any significant changes of the $\Delta G'$ cannot be

DOI: 10.1021/acs.macromol.6b02041
Macromolecules XXXX, XXX, XXX−XXX

expected; nevertheless they were preserved after the particle modification. To conclude, the presented MRE containing CI-*g*-PHEMATMS provides a high *e* at a relatively low *H*, while the G_0' value is still well-suited from the practical applications point of view.

More detailed investigation also showed that extraordinary changes of the normal force, F_N, occurred under the magnetic field. The sample was clamped between the plates of a PP20 geometry using the initial 0.85 ± 0.05 N normal force to exclude the possible slipping of the sample. Then, the measurement was immediately started to limit the relaxation behavior of the sample. As clearly obvious in Figure 10, the F_N of both studied materials increased with the applied *H*. This behavior was explained as a consequence of magnetostriction,[2,27] as the MREs were about to elongate in the direction of the applied *H* (parallel to plates), but their height was limited with geometry. The increase of F_N was considerably larger (Figure 10) in the MRE containing modified particles, which can be also attributed to significantly enhanced plasticity due to the presence of PHEMATMS grafts. Therefore, enhanced elastomer plasticity leads to a greater relative MR effect and also a greater magnetostriction effect, expressed as an F_N increase.

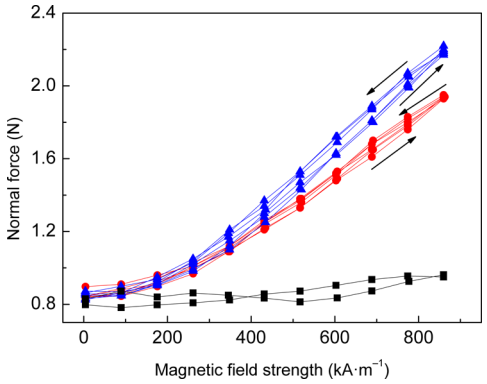

Figure 10. Normal force, F_N, of the neat matrix (squares), the isotropic MREs containing bare CI (circles), and the CI-*g*-PHEMATMS (triangles) particles as a function of the applied magnetic field strength, *H*.

As apparent from Figures 8−10, both studied MREs exhibited hysteresis behavior of their mechanical properties when exposed to increasing/decreasing magnetic fields. This phenomenon can be explained as a consequence of the high strength of the magnetic filler network, which cannot be easily destroyed by restoring elastic forces.[27] Thus, the restoration of properties can be achieved when the magnetic field drops below some critical value when magnetic and elastic forces equal each other. Regarding the hysteresis phenomenon, Gundermann et al.[40] studied the reversibility of particle motion by X-ray microcomputed tomography. They have found that after switching off the magnetic field, the positions of the particles slightly varied. This means that the process of particle motion in their system was not fully reversible, which they attributed to the inhomogeneity of the matrix as a consequence of reduced polymerization in the vicinity of the particles. The modification of the CI particles with PHEMAMTS chains appears to have a negligible effect on hysteresis behavior, as the experiments yielded a similar character of the hysteresis loops.

Additionally, MREs can be used in the development of systems exhibiting sensing capabilities.[41] Therefore, the next part of our work was focused on studying the sensing properties of prepared MREs. In the previous measurements, the gap between the measuring cell and the measuring plate was set to a constant value. As a result, changes in F_N were observed under an applied magnetic field (Figure 10). First by studying the MRFs, researchers have found that magnetically induced F_N can push the plate apart even in the absence of shearing.[42] Here, we have acceded to a different approach, using the static normal force measurements in magnetic fields in order to investigate the magnetically induced strain, δ, of the MREs in a vertical direction, which represents the intended sensing property. The samples were clamped between the plates using the constant F_N of 0.5 or 1 N, respectively. Because of an increasing *H*, the samples elongated, which pushed the upper plate in order to preserve the given contact force. The δ was calculated eq 3 according to

$$\delta = \frac{d_H - d_0}{d_0} \times 100\% \tag{3}$$

where d_H and d_0 represented the field-on and field-off gaps, respectively, and thus the vertical dimension of the sample. As can be seen in Figure 11, δ significantly changed when the magnetic field was imposed. Under both clamping forces, the δ was larger in the MRE containing CI-*g*-PHEMATMS particles due to better particle mobility within the matrix. The results correlate with the enhanced relative MR effect of the prepared novel MRE. As also illustrated in Figure 11, a noticeable change of δ was obtained only after exceeding some critical value of *H*, which allowed the overcoming of the applied clamping force. The investigation has shown the enhanced elongation ability and thus better sensitivity of the MRE sensor containing CI-*g*-PHEMATMS particles, which was able to achieve a δ of approximately 0.5% at the maximum applied *H*.

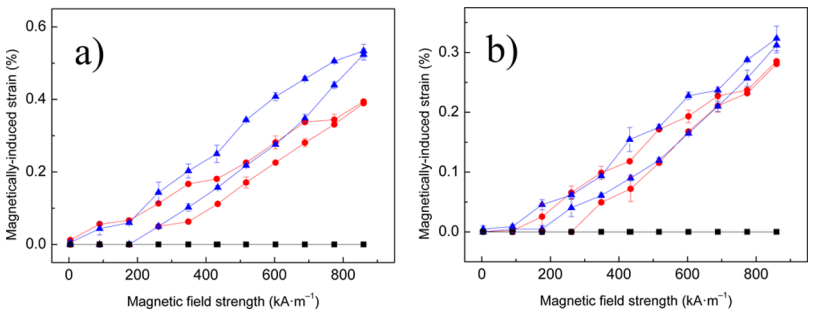

Figure 11. Magnetically induced vertical strain, δ, of the neat matrix (squares) and the isotropic MREs containing bare CI (circles) and CI-*g*-PHEMATMS (triangles) particles under 0.5 N (a) and 1 N (b) clamping forces as a function of the applied magnetic field strength, *H*.

DOI: 10.1021/acs.macromol.6b02041
Macromolecules XXXX, XXX, XXX−XXX

Particle/Matrix Interface and Dynamic Mechanical Analysis. The actuators and sensors based on the MREs operate under dynamic loading (magnetic field repeatedly switching on/off), which changes the sample dimensions. Therefore, not only magnetically induced strain but also the interactions and compatibility between the CI particles and PDMS matrix are crucial parameters. These phenomena were studied using SEM and DMA at various temperatures and different frequencies.

Figure 12 shows the SEM images of the investigated freeze-fractured MREs. As apparent from the micrographs, bare CI

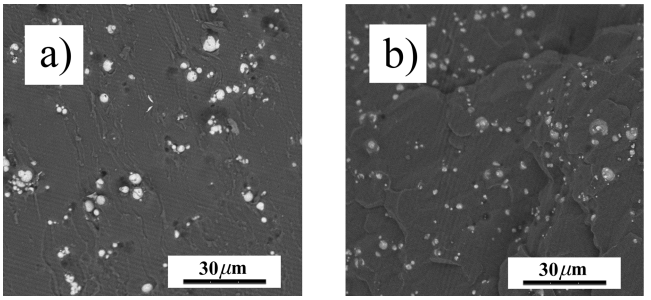

Figure 12. SEM images of the isotropic MREs containing bare CI (a) and CI-*g*-PHEMATMS (b) particles.

particles exhibited tendency to aggregate and the wettability with the PDMS matrix is lower compared with their CI-*g*-PHEMATMS analogues. The results of SEM analysis are in a good agreement with those obtained by the contact angle measurements (Figure 7) and the activation energy investigations (Figure 14a). Moreover, the detailed figure showing the particle/matrix interface will be presented further in text.

Regarding the mentioned applications operating under dynamic loading, the DMA investigation was considered as a more suitable evaluating tool compared to the static mechanical testing.[31] As can be seen in Figure 13, the investigated samples exhibited temperature-dependent behavior typical for elastomers.[21] At low temperatures, below T_g, the highest E' was obtained for the MRE containing CI-*g*-PHEMATMS particles (Figure 13a), which were well-dispersed in the PDMS matrix due to modification with a polymer shell. On the other hand, the MRE containing bare CI particles possessed the lowest E', indicating the presence of agglomerates and thus the significant disintegration of this sample, which was pronounced at lower temperatures. Above T_g, however, the situation was completely different. Around −40 °C the melting of PDMS crystalline phase occurred (Figure 13); then at higher temperatures bare CI particles in the form of agglomerates possessed a strong reinforcing effect due to their possible covalent bonding with the PDMS matrix, which significantly enhanced the mechanical properties of the composite.[4] On the contrary, the MRE containing CI-*g*-PHEMATMS particles exhibited, above melting region, higher E' values than the neat PDMS, but lower ones when compared to that of the MRE containing bare CI. The results suggest that the mechanical properties of studied materials are strongly related to the crystalline phase of the matrix. Thus, the neat PDMS without any reinforcing agents (bare CI or CI-*g*-PHEMATMS) exhibited the lowest mechanical performance when the whole crystalline phase was melted. This is a crucial phenomenon first addressed in this article taking into account that a potential applicability is strictly lying above the melting region.

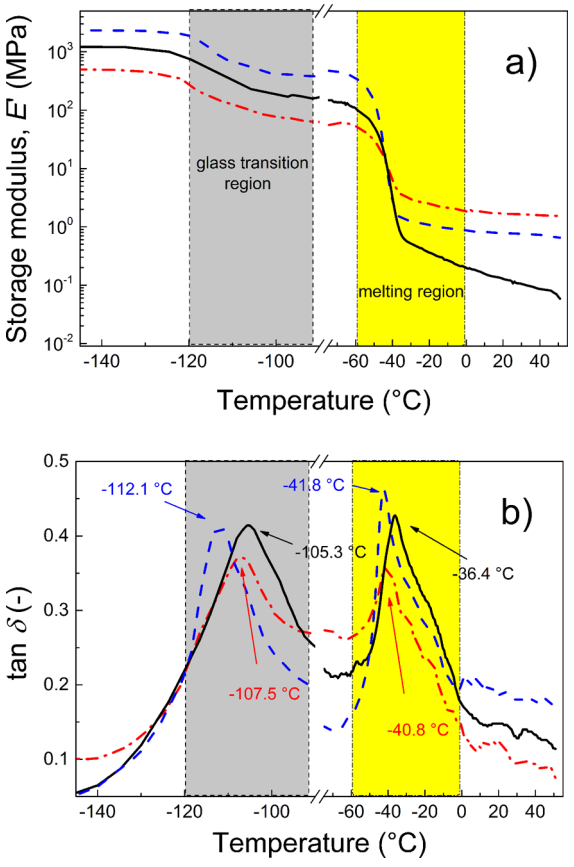

Figure 13. Evolution of the tensile storage modulus, E' (a), and damping factor, tan δ (b), with temperature for the neat PDMS matrix (black solid lines), the isotropic MREs containing bare CI (red dash/dotted lines), and CI-*g*-PHEMATMS (blue dashed lines) particles.

The softening behavior was further clarified by the dependence of the tan δ on the temperature. As shown in Figure 13b, both MREs exhibited lower values of T_g, namely −107.5 and −112.1 °C, for those containing bare CI and CI-*g*-PHEMATMS particles, respectively, when compared with the T_g value of the neat matrix (−105.3 °C) at a frequency of 1 Hz. Above the melting temperature, the E' trends of the composites were in good correlation with the G' trends observed in the results from a rotational rheometer (Figure 8). Thus, the E' of the MRE containing CI-*g*-PHEMATMS was moderately lower and the tan δ was noticeably higher when compared to those of the MRE containing bare CI. It was confirmed that the introduction of PHEMATMS grafts onto the CI particle surface moderately reduced E' as well as G', due to its plasticizing effect, but largely enhanced the damping performance of the as-prepared, PDMS-based MREs.

Finally, in order to investigate the interactions of the CI fillers with the PDMS matrix, a DMA at various frequencies was performed. As depicted in Figure 14, all samples exhibited Arrhenius-type behavior, indicating the relaxation of the backbone polymer chains. Therefore, the calculations of the E_a of PDMS glass transition were used to provide information on how PHEMATMS chains grafted onto the CI surface affected the interactions between the CI and PDMS matrix. As summarized in Table 2, the highest E_a was calculated to be 224 kJ mol^{-1} for the MRE containing CI-*g*-PHEMATMS particles, which indicated the best particle/matrix interactions. This enhancement can be explained as a consequence of the physical

DOI: 10.1021/acs.macromol.6b02041
Macromolecules XXXX, XXX, XXX−XXX

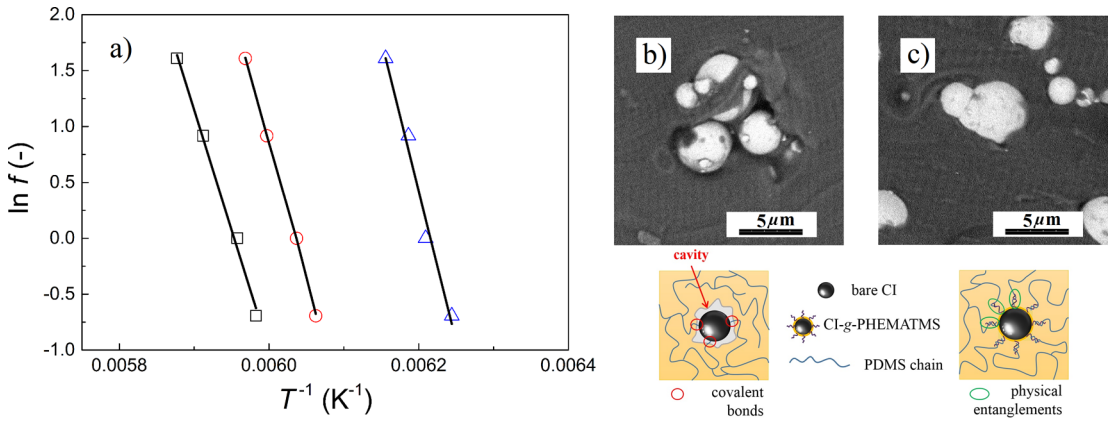

Figure 14. Arrhenius plots (a) for the neat matrix (open squares), the isotropic MREs containing bare CI (open circles), and CI-*g*-PHEMATMS (open triangles) particles. The SEM figures displaying the particle/matrix interface in the MRE containing bare CI particles (b) with possible covalent bonds with the matrix, but surrounded by cavities as a consequence of poor particle/matrix adhesion, and the MRE containing CI-*g*-PHEMATMS particles (c) with better wettability and the presence of physical entanglements of PHEMATMS grafts with the PDMS chains together with their schematic representation.

Table 2. Summarized Values of T_g and E_a for the Neat PDMS and Both Isotropic MRE Composite Samples

	T_g (°C)				
sample based on	0.5 Hz	1 Hz	2.5 Hz	5 Hz	E_a (kJ mol^{-1})
neat PDMS	−106.0	−105.3	−104.1	−102.9	178
bare CI	−108.2	−107.5	−106.4	−105.6	202
CI-*g*-PHEMATMS	−112.9	−112.1	−111.5	−110.7	224

interactions among the PHEATMS grafts on CI particles and the PDMS matrix due to their similar chemical structure, which is an analogous phenomenon, as was recently demonstrated on thermoplastic elastomers filled with modified carbon nanotubes.[43,44] On the contrary, the introduction of bare CI particles into the system potentially provided covalent bonds with the matrix;[4] however, the bonding was limited due to their low adhesion to the PDMS matrix, which explains its lower E_a.

CONCLUSIONS

Trimethylsilyloxyethyl methacrylate was used as a monomer for the SI-ATRP to form a polymer shell onto the CI particles. The successful grafting process was confirmed using the EDS and FTIR techniques as well as the TEM investigations. The CI-*g*-PHEMATMS particles exhibited reduced magnetization by only 6.2°% (at 780 kA m^{-1}) due to negligible coating thickness (10−20 nm) when compared to the magnetization of bare CI particles. However, the polymer coating remarkably enhanced the thermo-oxidation stability of the CI (by 74 °C) and antiacid/corrosion properties. The isotropic MREs based on the PDMS elastomer matrix containing 60 wt % of bare CI particles or their PHEMATMS-grafted analogues were fabricated. Despite the poor wettability of the bare CI particles with the PDMS matrix, they possessed a strong reinforcing effect in the MRE due to possible covalent bonding with silicone components. On the other hand, covalent bonding was restricted by the CI modification with PHEMTMS grafts, leading to the presence of physical entanglements on the particle shell/matrix interface and the enhanced mobility of the particles within the matrix causing the considerable plasticizing effect. As a result, the MRE containing CI-*g*-PHEMATMS particles exhibited a moderately lower G', a higher G'', and thus significantly higher damping factor. Moreover, increased particle mobility substantially enhanced the relative MR effect by more than 23%, indicating the better practical applicability of the material containing CI-*g*-PHEMATMS particles. The polymer coating did not significantly affect the hysteresis behavior of the MRE. On the other hand, the MRE containing CI-*g*-PHEMATMS particles exhibited enhanced magnetostriction, implying its better sensing capability. A dynamic mechanical analysis revealed better particle/matrix interactions together with the in-depth SEM investigations in the MRE containing modified particles. Based on this work, fabricated MRE containing CI-*g*-PHEMATMS having dual functionality (protecting shell and plasticizer) can find applications both in damping systems, in which demanding operating conditions including high thermo-oxidation stability and antiacid/corrosion properties are required, and also provide sufficient magnetostriction capabilities for sensor development.

AUTHOR INFORMATION

Corresponding Author

*E-mail: mrlik@cps.utb.cz (M.M.).

ORCID

Miroslav Mrlík: 0000-0001-6203-6795

Notes

The authors declare no competing financial interest.

ACKNOWLEDGMENTS

M.C. thanks the Internal Grant Agency of Tomas Bata University in Zlin (project no. IGA/CPS/2016/008) for financial support. This work was also supported by the Ministry of Education, Youth and Sports of the Czech Republic - Program NPU I (LO1504). M.I. and J.M. gratefully acknowledge the Slovak grant agencies for financial support through the projects VEGA-2/0142/14 and APVV-14-0891.

REFERENCES

(1) Fan, Y. C.; Gong, X. L.; Xuan, S. H.; Zhang, W.; Zheng, J. A.; Jiang, W. Q. Interfacial Friction Damping Properties in Magneto-rheological Elastomers. *Smart Mater. Struct.* **2011**, *20*, 035007.

(2) Li, Y. C.; Li, J. C.; Li, W. H.; Du, H. P. A State-of-the-Art Review on Magnetorheological Elastomer Devices. *Smart Mater. Struct.* **2014**, *23*, 123001.

DOI: 10.1021/acs.macromol.6b02041
Macromolecules XXXX, XXX, XXX−XXX

(3) Lokander, M.; Reitberger, T.; Stenberg, B. Oxidation of Natural Rubber-Based Magnetorheological Elastomers. *Polym. Degrad. Stab.* **2004**, *86*, 467−471.
(4) Rabindranath, R.; Bose, H. On the Mobility of Iron Particles Embedded in Elastomeric Silicone Matrix. In *13th Int. Conf. Electrorheol. Fluids Magnetorheol. Suspensions*; Unal, H. I., Ed.; Iop Publishing Ltd.: Bristol, 2013; Vol. *412*.
(5) Bose, H.; Rabindranath, R.; Ehrlich, J. Soft Magnetorheological Elastomers as New Actuators for Valves. *J. Intell. Mater. Syst. Struct.* **2012**, *23*, 989−994.
(6) Lam, K. H.; Chen, Z. H.; Ni, Y. Q.; Chan, H. L. W. A Magnetorheological Damper Capable of Force and Displacement Sensing. *Sens. Actuators, A* **2010**, *158*, 51−59.
(7) Li, Y. C.; Li, J. C.; Li, W. H.; Samali, B. Development and Characterization of a Magnetorheological Elastomer Based Adaptive Seismic Isolator. *Smart Mater. Struct.* **2013**, *22*, 035005.
(8) Sedlacik, M.; Mrlik, M.; Babayan, V.; Pavlinek, V. Magnetorheological Elastomers with Efficient Electromagnetic Shielding. *Compos. Struct.* **2016**, *135*, 199−204.
(9) Shuib, R. K.; Pickering, K. L.; Mace, B. R. Dynamic Properties of Magnetorheological Elastomers Based on Iron Sand and Natural Rubber. *J. Appl. Polym. Sci.* **2015**, *132*, 41506.
(10) Fuchs, A.; Sutrisno, J.; Gordaninejad, F.; Caglar, M. B.; Yanming, L. Surface Polymerization of Iron Particles for Magnetorheological Elastomers. *J. Appl. Polym. Sci.* **2010**, *117*, 934−942.
(11) Malecki, P.; Kolman, K.; Piglowski, J.; Kaleta, J.; Krzak, J. Sol-Gel Method as a Way of Carbonyl Iron Powder Surface Modification for Interaction Improvement. *J. Solid State Chem.* **2015**, *226*, 224−230.
(12) Cvek, M.; Mrlik, M.; Ilcikova, M.; Plachy, T.; Sedlacik, M.; Mosnacek, J.; Pavlinek, V. A Facile Controllable Coating of Carbonyl Iron Particles with Poly(glycidyl methacrylate): A Tool for Adjusting MR Response and Stability Properties. *J. Mater. Chem. C* **2015**, *3*, 4646−4656.
(13) Behrooz, M.; Sutrisno, J.; Zhang, L. Y.; Fuchs, A.; Gordaninejad, F. Behavior of Magnetorheological Elastomers with Coated Particles. *Smart Mater. Struct.* **2015**, *24*, 035026.
(14) Xu, Y. G.; Gong, X. L.; Xuan, S. H.; Zhang, W.; Fan, Y. C. A High-Performance Magnetorheological Material: Preparation, Characterization and Magnetic-Mechanic Coupling Properties. *Soft Matter* **2011**, *7*, 5246−5254.
(15) Chertovich, A. V.; Stepanov, G. V.; Kramarenko, E. Y.; Khokhlov, A. R. New Composite Elastomers with Giant Magnetic Response. *Macromol. Mater. Eng.* **2010**, *295*, 336−341.
(16) Abshinova, M. A.; Kuritka, L.; Kazantseva, N. E.; Vilcakova, J.; Saha, P. Thermomagnetic Stability and Heat-Resistance Properties of Carbonyl Iron Filled Siloxanes. *Mater. Chem. Phys.* **2009**, *114*, 78−89.
(17) Nese, A.; Mosnacek, J.; Juhari, A.; Yoon, J. A.; Koynov, K.; Kowalewski, T.; Matyjaszewski, K. Synthesis, Characterization, and Properties of Starlike Poly(n-butyl acrylate)-b-poly(methyl methacrylate) Block Copolymers. *Macromolecules* **2010**, *43*, 1227−1235.
(18) Belyavskii, S. G.; Mingalyov, P. G.; Giulieri, F.; Combarrieau, R.; Lisichkin, G. V. Chemical Modification of the Surface of a Carbonyl Iron Powder. *Prot. Met.* **2006**, *42*, 244−252.
(19) Cvek, M.; Mrlik, M.; Ilcikova, M.; Mosnacek, J.; Babayan, V.; Kucekova, Z.; Humpolicek, P.; Pavlinek, V. The Chemical Stability and Cytotoxicity of Carbonyl Iron Particles Grafted with Poly(glycidyl methacrylate) and the Magnetorheological Activity of Their Suspensions. *RSC Adv.* **2015**, *5*, 72816−72824.
(20) Bao, S. P.; Tjong, S. C. Mechanical Behaviors of Polypropylene/Carbon Nanotube Nanocomposites: The Effects of Loading Rate and Temperature. *Mater. Sci. Eng., A* **2008**, *485*, 508−516.
(21) Geethamma, V. G.; Kalaprasad, G.; Groeninckx, G.; Thomas, S. Dynamic Mechanical Behavior of Short Coir Fiber Reinforced Natural Rubber Composites. *Composites, Part A* **2005**, *36*, 1499−1506.
(22) Goncalves, G.; Marques, P.; Barros-Timmons, A.; Bdkin, I.; Singh, M. K.; Emami, N.; Gracio, J. Graphene Oxide Modified with PMMA via ATRP as a Reinforcement Filler. *J. Mater. Chem.* **2010**, *20*, 9927−9934.
(23) Fang, F. F.; Choi, H. J.; Seo, Y. Sequential Coating of Magnetic Carbonyliron Particles with Polystyrene and Multiwalled Carbon Nanotubes and Its Effect on Their Magnetorheology. *ACS Appl. Mater. Interfaces* **2010**, *2*, 54−60.
(24) Mrlik, M.; Ilcikova, M.; Pavlinek, V.; Mosnacek, J.; Peer, P.; Filip, P. Improved Thermooxidation and Sedimentation Stability of Covalently-Coated Carbonyl Iron Particles with Cholesteryl Groups and Their Influence on Magnetorheology. *J. Colloid Interface Sci.* **2013**, *396*, 146−151.
(25) Ocalan, M.; McKinley, G. H. High-Flux Magnetorheology at Elevated Temperatures. *Rheol. Acta* **2013**, *52*, 623−641.
(26) Boczkowska, A.; Awietjan, S. F.; Wroblewski, R. Microstructure-Property Relationships of Urethane Magnetorheological Elastomers. *Smart Mater. Struct.* **2007**, *16*, 1924−1930.
(27) Sorokin, V. V.; Stepanov, G. V.; Shamonin, M.; Monkman, G. J.; Khokhlov, A. R.; Kramarenko, E. Y. Hysteresis of the Viscoelastic Properties and the Normal Force in Magnetically and Mechanically Soft Magnetoactive Elastomers: Effects of Filler Composition, Strain Amplitude and Magnetic Field. *Polymer* **2015**, *76*, 191−202.
(28) Laun, H. M.; Gabriel, C. Measurement Modes of the Response Time of a Magneto-Rheological Fluid (MRF) for Changing Magnetic Flux Density. *Rheol. Acta* **2007**, *46*, 665−676.
(29) Fu, S. Y.; Feng, X. Q.; Lauke, B.; Mai, Y. W. Effects of Particle Size, Particle/Matrix Interface Adhesion and Particle Loading on Mechanical Properties of Particulate-Polymer Composites. *Composites, Part B* **2008**, *39*, 933−961.
(30) Ju, B. X.; Tang, R.; Zhang, D. Y.; Yang, B. L.; Yu, M.; Liao, C. R. Temperature-Dependent Dynamic Mechanical Properties of Magnetorheological Elastomers under Magnetic Field. *J. Magn. Magn. Mater.* **2016**, *398*, 305−305.
(31) Khimi, S. R.; Pickering, K. L. Comparison of Dynamic Properties of Magnetorheological Elastomers with Existing Antivibration Rubbers. *Composites, Part B* **2015**, *83*, 175−183.
(32) Malecki, P.; Krolewicz, M.; Krzak, J.; Kaleta, J.; Piglowski, J. Dynamic Mechanical Analysis of Magnetorheological Composites Containing Silica-Coated Carbonyl Iron Powder. *J. Intell. Mater. Syst. Struct.* **2015**, *26*, 1899−1905.
(33) Khimi, S. R.; Pickering, K. L. The Effect of Silane Coupling Agent on the Dynamic Mechanical Properties of Iron Sand/ Natural Rubber Magnetorheological Elastomers. *Composites, Part B* **2016**, *90*, 115−125.
(34) Li, J. F.; Gong, X. L.; Zhu, H.; Jiang, W. Q. Influence of Particle Coating on Dynamic Mechanical Behaviors of Magnetorheological Elastomers. *Polym. Test.* **2009**, *28*, 331−337.
(35) Ciprari, D.; Jacob, K.; Tannenbaum, R. Characterization of Polymer Nanocomposite Interphase and Its Impact on Mechanical Properties. *Macromolecules* **2006**, *39*, 6565−6573.
(36) Wang, Y.; Zhang, X.; Chung, K.; Liu, C.; Choi, S. B.; Choi, H. J. Formation of Core−Shell Structured Complex Microparticles During Fabrication of Magnetorheological Elastomers and Their Magnetorheological Behavior. *Smart Mater. Struct.* **2016**, *25*, 115028.
(37) Yang, D. L.; Pacheco, R.; Henderson, K.; Hubbard, K.; Devlin, D. Diffusion and Sorption of Nitroplasticizers in Vinyl Copolymer Elastomer and Its Composites. *J. Appl. Polym. Sci.* **2014**, *131*, 40729.
(38) Ju, B. X.; Tang, R.; Zhang, D. Y.; Yang, B. L.; Yu, M.; Liao, C. R.; Yuan, X. L.; Zhang, L. W.; Liu, J. H. Dynamic Mechanical Properties of Magnetorheological Elastomers Based on Polyurethane Matrix. *Polym. Compos.* **2016**, *37*, 1587−1595.
(39) Liao, G. J.; Xu, Y. G.; Wang, F. J.; Wei, F. Y.; Wan, Q. Influence of γ Radiation on the Shear Modulus of Magnetorheological Elastomer. *Mater. Lett.* **2016**, *174*, 79−81.
(40) Gundermann, T.; Odenbach, S. Investigation of the Motion of Particles in Magnetorheological Elastomers by X-μCT. *Smart Mater. Struct.* **2014**, *23*, 105013.
(41) Keshoju, K.; Sun, L. Mechanical Characterization of Magnetic Nanowire-Polydimethylsiloxane Composites. *J. Appl. Phys.* **2009**, *105*, 023515.
(42) Yao, X. Y.; Yu, M.; Fu, J. Magnetic-Enhanced Normal Force of Magnetorheological Fluids. *Smart Mater. Struct.* **2015**, *24*, 035001.

DOI: 10.1021/acs.macromol.6b02041
Macromolecules XXXX, XXX, XXX−XXX

(43) Ilcikova, M.; Mrlik, M.; Sedlacek, T.; Doroshenko, M.; Koynov, K.; Danko, M.; Mosnacek, J. Tailoring of Viscoelastic Properties and Light-Induced Actuation Performance of Triblock Copolymer Composites Through Surface Modification of Carbon Nanotubes. *Polymer* **2015**, *72*, 368−377.
(44) Ilcikova, M.; Mrlik, M.; Sedlacek, T.; Slouf, M.; Zhigunov, A.; Koynov, K.; Mosnacek, J. Synthesis of Photoactuating Acrylic Thermoplastic Elastomers Containing Diblock Copolymer-Grafted Carbon Nanotubes. *ACS Macro Lett.* **2014**, *3*, 999−1003.

DOI: 10.1021/acs.macromol.6b02041
Macromolecules XXXX, XXX, XXX−XXX

PAPER IV

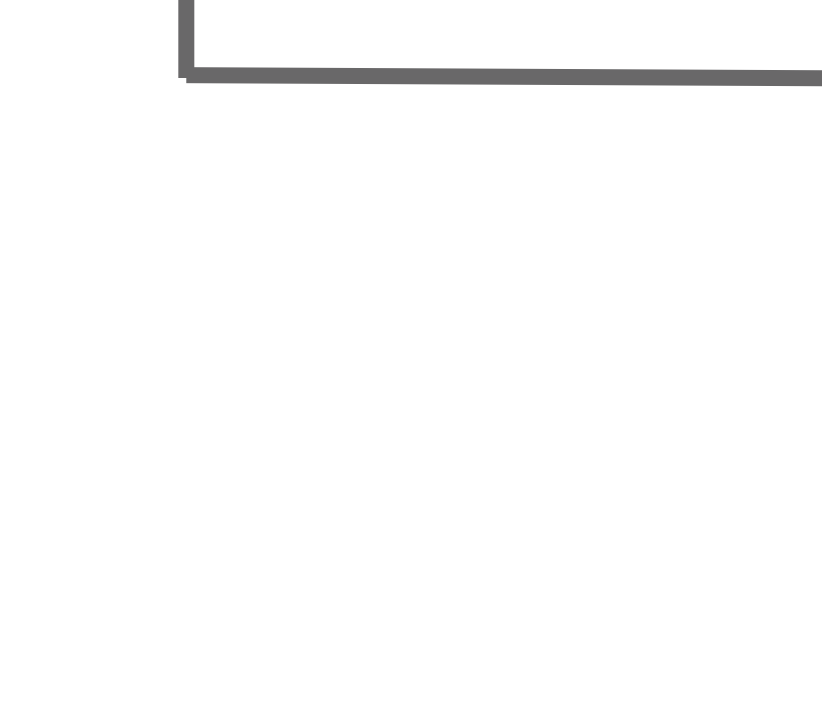

Submitted manuscript

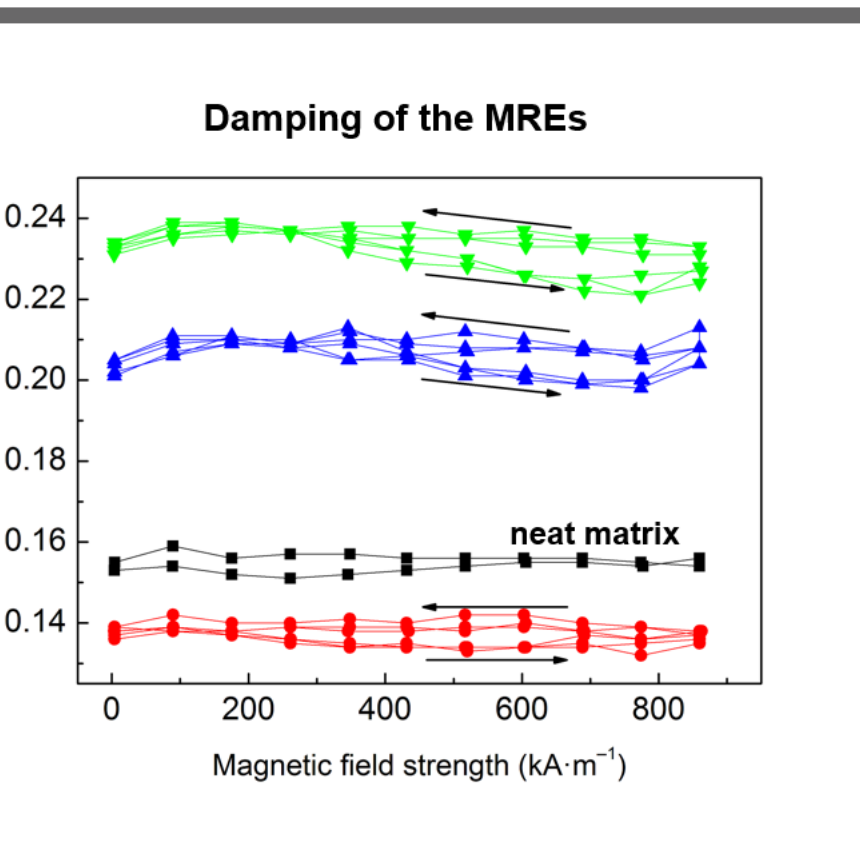

Tailoring performance, damping and stability properties of magnetorheological elastomers via particle-grafting technology

Martin Cvek,[a,b*] *Miroslav Mrlik,*[a] *Marketa Ilcikova,*[c] *Michal Sedlacik,*[a] *Jaroslav Mosnacek,*[c]

[a] Centre of Polymer Systems, University Institute, Tomas Bata University in Zlín, Trida T. Bati 5678, 760 01 Zlín, Czech Republic

[b] Polymer Centre, Faculty of Technology, Tomas Bata University in Zlín, Vavreckova 275, 760 01 Zlín, Czech Republic

[c] Polymer Institute, Slovak Academy of Sciences, Dubravska cesta 9, 845 41 Bratislava 45, Slovakia

*corresponding author: cvek@utb.cz

Abstract. Damping control of the magnetorheological elastomers (MREs) can be executed by a reduction of matrix cross-link density or by the incorporation of components that can transform from a semicrystalline solid to a liquidated soft material once the temperature is increased above a certain point. However, these approaches fail when the MREs are exposed to demanding operating conditions such as extreme temperatures or chemically contaminated environment, which can induce particle degradation. This study presents a new concept, which allows tailoring performance, damping, and stability properties of the MREs all at the same time via advanced particle-grafting technology.

Keywords: magnetorheology; silicone elastomer; atom transfer radical polymerization; grafting; damping; polymer coating

Introduction.

In the last years, magnetorheological elastomers (MREs) have attracted much attention in scientific as well as industrial fields due to their rapidly-tunable viscoelastic properties once they are exposed to an external magnetic field. The MREs represent composite systems comprising the ferromagnetic particles embedded in an elastomeric matrix, thus they can be perceived as solid analogues to the magnetorheological fluids (MRFs) [1]. The indisputable advantage of the MRFs over the MREs is the ability to increase their rheological properties (yield stress, viscosity, viscoelastic moduli) by several orders of magnitude [2, 3]. In the MREs, the magneto-induced effects are generally less pronounced, however, their application can eliminate a serious sedimentation stability problem of the MRFs [3-6]. Moreover, other common drawbacks of the MRFs such as sealing issues, possible leakage or environmental contamination can be successfully suppressed [5]. High stability and tunable viscoelastic moduli changes make the MREs suitable materials for the applications such as vibration absorbers, adaptive dampers or stiffness tunable mounts [7-10]. Undoubtedly, pioneer applications such as artificial muscles [11], micro-fluid transport systems [12], radio-absorbers [13], sensors [14], or active elements of electric circuits [15] based on the MREs' concept have been reported.

Magnetic, rheological, and mechanical properties of the MREs can be affected by many variables during their fabrication process; among the most important aspects belong the particle concentration, their size, magnetic properties, spatial distribution within the matrix, *etc*. These phenomena were recently studied by Khimi et al. [16] who due to complexity of the issue designed the Taguchi method (a statistical method identifying the performance trends among multiple factors and determining their combination that yields the optimum results) to investigate the effects of a number of factors (particle concentration, size and distribution, applied magnetic field during curing). They found that the particle concentration had the

greatest influence of studied quantity, namely, the loss tangent, followed by the effect of particle size and intensity of applied magnetic field.

Besides the particle-related factors, the selection of matrix also plays a key role in designing the effective MREs. Generally, the matrix should be highly elastic to retain its shape [17], while allowing the rearrangement of the particles to enhance the damping properties at the same time [18]. In some applications, the weight and flexibility of the matrix are desired, thus the MREs based on porous matrices can be preferred [19]. Recently, Fan et al. [20] showed that the notable increase in the MREs damping properties can be evoked by a reduction of the binding force of the matrix exerted on the particles. In their study, such reduction was a consequence of reduced cross-link density of the *cis*-polybutadiene rubber (BR) matrix. Other approach in controlling the MREs damping properties involves the addition of polycaprolactone (PCL) as a temperature-controlling component also into the BR matrix. The PCL can transform from a semicrystalline solid to a liquidated soft material once the surrounding temperature is increased above the PCL melting point [21]. The damping properties of such MREs can be controlled by varying the PCL content and a temperature. Rabindranath et al. [22] found that final MREs' properties and stress transfer between the particles and the matrix can be efficiently modulated by an incorporation of the particles treated with various surfactants such as fatty acids or calcium and aluminum soaps. Their MRE was however based on the polydimethylsiloxane (PDMS). It has to be mentioned that bare carbonyl iron (CI) particles were less mobile in such matrix due to the possible covalent bonding between the hydroxyl groups on their surface and the silane groups of the cross-link agent. Unfortunately, introducing the surfactants into the MREs can initiate several issues related to the durability of these systems. The surfactants are not covalently bonded onto the magnetic substrate, thus their diffusion through the polymer matrix can arise. Also, the addition of common plasticizers can cause durability problems as these low-molecular weight substances have a tendency to migrate through the polymer

matrix [23]. Although the reviewed approaches are effective in tuning the MREs properties, they rather omit a protection of the incorporated particles against high temperatures or acidic environment, which is essential in some practical applications [24]. Thus, there is a need to address the demands related to both performance and stability properties of the MREs, ideally in a single-step way.

In our previous study [25], we have shown that the CI particles covalently grafted with poly(trimethylsilyloxyethyl methacrylate) (PHEMATMS) chains (CI-*g*-PHEMATMS) via surface-initiated atom transfer radical polymerization (SI-ATRP) exhibited high thermo-oxidation stability, excellent chemical stability, enhanced dispersibility and significant wettability with PDMS matrix. Moreover, the presence of the PHEMATMS grafts restricted the covalent bonding between the CI particles and the PDMS, which resulted in increased relative MR effect and damping factor.

Herein, we present a novel method to tailor the MR performance, damping properties, and stability of the MREs. The core of this method stems from the incorporation of the particles grafted with PHEMATMS of different molecular weights, which are expected to affect the PDMS cross-link density to a various degree, which ultimately can lead to different particle rearrangements and MREs performance. The SI-ATRP was chosen as a suitable technique as the thickness of grafted polymer layer is a crucial parameter to preserve sufficient magnetization of the particles [26] and it can be easily controlled using this polymerization technique. The goal of this study was to investigate the effect of different polymer graft lengths on the above-described characteristics, and thus to be able to tune the behavior of the MREs through controllable coating of the magnetic particles, which is to the best of our knowledge a concept that has never been published elsewhere before.

Experimental section.

Materials. The CI particles (SL grade) supplied by BASF Corporation (Germany) represented a suitable magnetic substrate. The 2-hydroxyethyl methacrylate (HEMA, 96%) and chlorotrimethyl silane (TMCS, ≥97%) were used as the components to prepare trimethylsilyloxyethyl methacrylate (HEMATMS) monomer in dichloromethane (anhydrous, ≥99.8%) solution, while triethylamine (TEA, ≥99%) served as a proton scavenger. The (3-aminopropyl)triethoxysilane (ATPES, ≥98%) was utilized as a linker to further bond the α-bromoisobutyryl bromide (B*i*BB, 98%) initiator attached to the particle surface. The ethyl α-bromoisobutyrate (EB*i*B, 98%) was used as a sacrificial initiator, while the *N,N,N′,N′′,N′′*-pentamethyldiethylenetriamine (PMDETA, ≥99%) served as a ligand increasing the solubility of copper bromide (CuBr, ≥99%) initiator. The ATRP was performed in the anisole (99%). Aluminum oxide (neutral) is a depriving agent employed to remove the catalyst before the chromatography measurements. All chemicals were purchased from Sigma Aldrich (USA). Solvents and purification agents, namely tetrahydrofurane (THF, p.a.), acetone (p.a.), ethanol (absolute anhydrous, p.a.), toluene (p.a.), and hydrochloric acid (HCl, 35%, p.a.) were obtained from Penta (Czech Republic) and used as received. The MREs were prepared using Sylgard 184/catalyst kit (Dow Corning, USA).

Monomer synthesis and preparation of CI-*g*-PHEMATMS particles. The HEMATMS was synthesized via esterification reaction of argon-purged HEMA and freshly-distilled TMCS, while the CI-*g*-PHEMATMS particles were prepared following the procedures reported previously [25]. The preparation scheme of grafting the particles via SI-ATRP is outlined in Figure 1. To obtain the particles varying in shell thickness, different monomer-to-initiator ratios and reaction times were employed (Table 1, sample code 1 and 2). The prepared particles were thoroughly washed in THF, ethanol and acetone following the procedures [26] and were further used for the fabrication of the MREs.

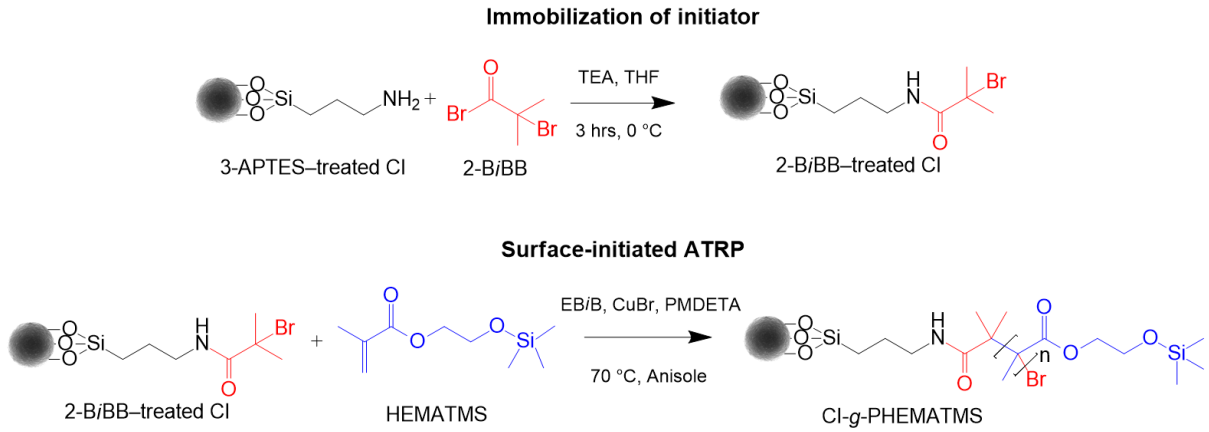

Figure 1. The preparation scheme of the CI-*g*-PHEMATMS via SI-ATRP.

Table 1. Reaction stoichiometry and experimental conditions for SI-ATRP of PHEMATMS grafts.

sample code	M	I	CuBr	L	anisole (vol. %)	time (h)
CI-*g*-PHEMATMS-1	100	1	1	1	50	2
CI-*g*-PHEMATMS-2	300	1	1	1	50	4

M, I, and L denote monomer (HEMATMS), macroinitiator (EB*i*B), and ligand (PMDETA), respectively.

Fabrication of MREs.

The isotropic MREs containing bare CI particles or two variants of their PHEMATMS–grafted analogues were fabricated. The particle fractions in the MREs were maintained at 60 wt.%. Firstly, the silicone elastomer and its curing agent (weight ratio of 20:1) were thoroughly mixed for 10 minutes; subsequently the specified amount of magnetic particles was added followed by mechanical mixing using a pestle for additional 10 minutes at laboratory temperature to obtain well-dispersed systems. The resulting mixtures were degassed for 20 minutes under 10 mbar, and finally poured into PTFE molds (25 × 25 × 1.2 mm). The curing was performed

in an oven pre-heated to 100 °C for 45 minutes. The corresponding products were a thin MRE sheets, from which the specimens were cut out.

Characterizations.

Characterization of PHEMATMS coatings.

Purity of monomer and polymerization progresses during SI-ATRP were investigated using nuclear magnetic resonance spectroscopy (^{1}H NMR, 400 MHz VNMRS Varian, Japan) equipped with 5 mm ^{1}H-19F/15N-31P PFG AutoX DB NB probe at 25 °C using deuterated chloroform as a solvent. Apparent molecular weights (weight, $\bar{M}_{\mathrm{W}}$, and number, $\bar{M}_n$, averages) and dispersity indexes ($Đ$) were determined using gel permeation chromatography (GPC, PL–GPC220, Agilent, Japan) consisted of a Waters 515 pump, two PPS SDV 5 μm columns (d = 8 mm, l = 300 mm; 500 Å + 105 Å) and a Waters 410 differential refractive index detector with THF as an eluent at flow rate of 1.0 mL·min^{-1}. The instrument was calibrated using polystyrene standards, while anisole served as an internal standard to correct possible fluctuations in THF flow rate.

Characterization of core-shell particles.

Fourier-transform infrared spectroscopy (FTIR) was utilized in attenuated total reflectance mode to prove the presence of PHEMATMS layer grafted onto the CI surface. The FTIR examination was conducted on Nicolet 6700 (Thermo Scientific, USA) under laboratory conditions employing the Ge crystal in a typical wavenumber region of 3600–600 cm^{-1}. To observe the thicknesses of grafted layers, the transmission electron microscopy (TEM) images were acquired using JEM-2100Plus (Jeol, Japan). TEM samples were prepared by ultrasonic dispersion (Sonopuls HD 2070, Bandelin electronic, Germany) of the particles in acetone and dropping them onto a carbon coated copper grid (Agar Scientific, 300 mesh). In order to limit

the particle drifts during the image acquiring, the second copper grid was used as a protection cover. The effects of grafted PHEMATMS layers on particle density and magnetic properties were analyzed using a gas pycnometry (UltraFoam 1200e, Quantachrome Instruments, Germany) with nitrogen as a gaseous medium, and a vibrating-sample magnetometry (VSM, Model 7404, Lake Shore, USA) in a range of ±10 kOe (±780 $kA \cdot m^{-1}$), respectively. Both analyzes were performed at ambient temperature. The presented density data are the average values of the measurements from five samples with five measurements for each sample, which is a similar procedure as published elsewhere [27]. The thermo-oxidation stability of synthesized particles was evaluated via thermogravimetric analysis (TGA, TA Instruments Q500, USA) and is presented as the first derivative of the TGA curve (DTG). For each test, the sample mass of approx. 5 mg was exposed to temperature range of 25–800 °C. The air was used as a purge gas with a flow rate of 50 $mL \cdot min^{-1}$ and the heating rate was set to 10 $°C \cdot min^{-1}$. The chemical stability of the particles was examined by a facile corrosion test [28-30], in which 1 g of particles was dispersed in 20 mL of 0.1M aqueous HCl acid solution at laboratory temperature and the pH-value was recorded as a function of time with the help of calibrated pH meter (SensoDirect pH110, Tintometer, Germany). The conditions (0.1M HCl) for this test were specifically chosen to suitably accelerate the corrosion process of tested materials.

Characterization of MREs.

The microstructure of the samples was observed by using the scanning electron microscopy (SEM, Phenom Pro, Phenom-World, Netherlands). The presented micrographs were taken on the freeze-fractured MRE surfaces at an accelerating voltage of 5 kV. Magnetorheological performance of the MREs was studied using a rotational rheometer Physica MCR502 (Anton Paar, Austria) equipped with a magneto-device (Physica MRD 180/1T) and the parallel-plate geometry (PP20/MRD/TI) with a diameter of 20 mm. The circular MRE specimens of thickness

approximately 1.15 mm were subjected to external magnetic field (0–860 $kA \cdot m^{-1}$ corresponding to coil current of 0–3 A), which was generated by a power source (PS-MRD/5A) and their proper contact with the geometry was ensured by applying an initial normal force of 0.85 N. All the viscoelastic measurements were carried out at a constant temperature of 25 °C, which was maintained by a temperature control unit (Julabo FS18, Germany). The amplitude–sweeps were performed employing a range of deformation amplitude from 10^{-3} to 10^{1} % and a constant frequency of 5 Hz. Subsequently, the storage, *G'*, and the loss, *G''*, moduli as well as the damping factor, tan δ, of the MREs were collected in the magneto–sweep measurements, which were performed in ascending/descending magnetic fields at a frequency of 5 Hz and a constant amplitude strain of 0.2 % (ensuring linear viscoelastic region). As known, after several magneto-shear-loading cycles the viscoelastic moduli saturates and the stable values can be obtained [31]. After such pre-conditioning, the frequency–sweeps were performed in a frequency range from 10^{-1} to 4×10^{1} Hz.

Results and discussion

Synthesis.

The synthesis of CI-*g*-PHEMATMS particles using SI-ATRP involves the end-linking of HEMATMS monomer units onto B*i*BB-treated particles, having homolytically cleavable alkyl-bromide bond, via radical coupling reaction. Generally, in ATRP the polymer chain lengths can be controlled by monomer-to-initiator ratio in combination with monomer conversion [32], which can be affected by temperature, reaction time, type of transition metal and ligand used, solvent etc. Herein, the reactions were conducted under various stoichiometry when the monomer-to-initiator molar ratio was altered (Table 1, sample code 1 and 2). In order to obtain better control over the molar ratio and enable determination of molecular characteristics of the

polymer, a sacrificial initiator was used in excess when compared to initiator bonded on the CI surface. As a result, well-defined CI-*g*-PHEMATMS particles of two different molecular weights with narrow $Đ$ and thus different shell thicknesses were obtained. The monomer conversions determined from ^{1}H NMR spectra and molecular characteristics from GPC are listed in Table 2.

The successful modification of the CI particles by PHEMATMS polymer grafts was proved via FTIR where peaks indicating the characteristic groups were revealed [25]. In the FTIR spectra of CI-*g*-PHEMATMS, the –CH stretching from $–CH_3$ and $–CH_2–$ groups was observed at around 3000 $cm^{–1}$. Further, the peak at 1720 $cm^{–1}$ was attributed to C=O stretching, while raised absorption levels at 1082 and 1041 $cm^{–1}$ were a distinct indications of Si–O–Si stretching. In addition, the peak occurring at 849 $cm^{–1}$ was assigned to be $–Si–CH_3$ rocking.

Table 2. Results of CI-*g*-PHEMATMS particle syntheses.

sample code	conversion[a] (%)	$\bar{M}_W$ (g·mol$^{–1}$)	$\bar{M}_n$[a] (g·mol$^{–1}$)	$Đ$ (–)
CI-*g*-PHEMATMS-1	90	11 800	9 200	1.28
CI-*g*-PHEMATMS-2	75	23 500	17 900	1.31

[a]based on ^{1}H NMR spectra.

Thicknesses of grafted layers.

The TEM images (Figure 2) clearly show the presence of a lower-contrast shell grafted onto the darker CI core, thus the desired core-shell structure has been successfully revealed. As seen, the grafted layers were generally uniform in both cases of modified particles as a result of effective SI-ATRP. Due to PHEMATMS modification the density of the particles decreased from ~7.79 to ~7.35 and ~7.12 g·cm$^{–3}$, respectively, which is in accordance with the observed thicknesses of layers being ~15 nm and ~35 nm for CI-*g*-PHEMATMS-1 and CI-*g*-

PHEMATMS-2, respectively. The determined thickness values are slightly higher than those calculated for fully-stretched polymer chains based on molecular weights of PHEMATMS (11 and 22 nm, respectively), most probably due to different hydrodynamic volume of PHEMATMS in comparison with polystyrene, which was used as a standard in the GPC system. Nevertheless, the results are in a good agreement with the expectation that the polymer layer thickness increases with the increasing molecular weight of the grafted polymer.

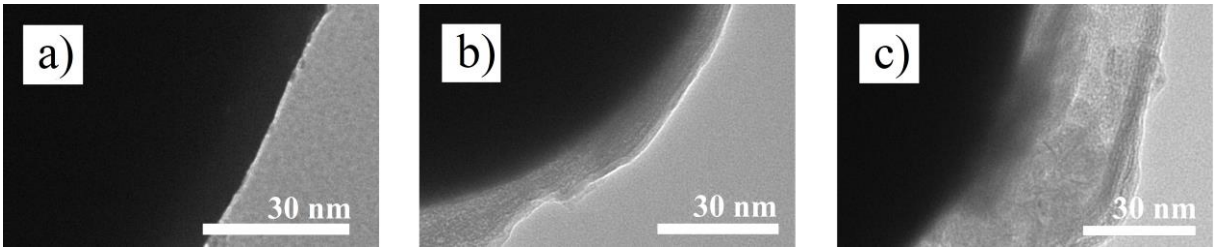

Figure 2. TEM images of bare CI (*a*), CI-*g*-PHEMATMS-1 (*b*), and CI-*g*-PHEMATMS-2 (*c*) showing a part of the corresponding single particle.

Magnetic properties.

As known, particle magnetization is a crucial factor to obtain high MR effect [3]. Figure 3 represents the magnetization curves of bare CI particles and both of their grafted analogues. Having grafted non-magnetic material, the mass magnetization of resulting core-shell structures decreases. However, the decrease in magnetization was relatively small for CI-*g*-PHEMATMS-1 and slightly more pronounced for CI-*g*-PHEMATMS-2 particles as the thickness of polymer layer was in nanometric scale (Figure 2). These results are in agreement with the recent data obtained on poly(glycidyl methacrylate)-modified CI particles, which were successfully used to prepare stable MR suspensions [28]. The results suggest that SI-ATRP is a well suitable tool for controllable modification of magnetic substrate.

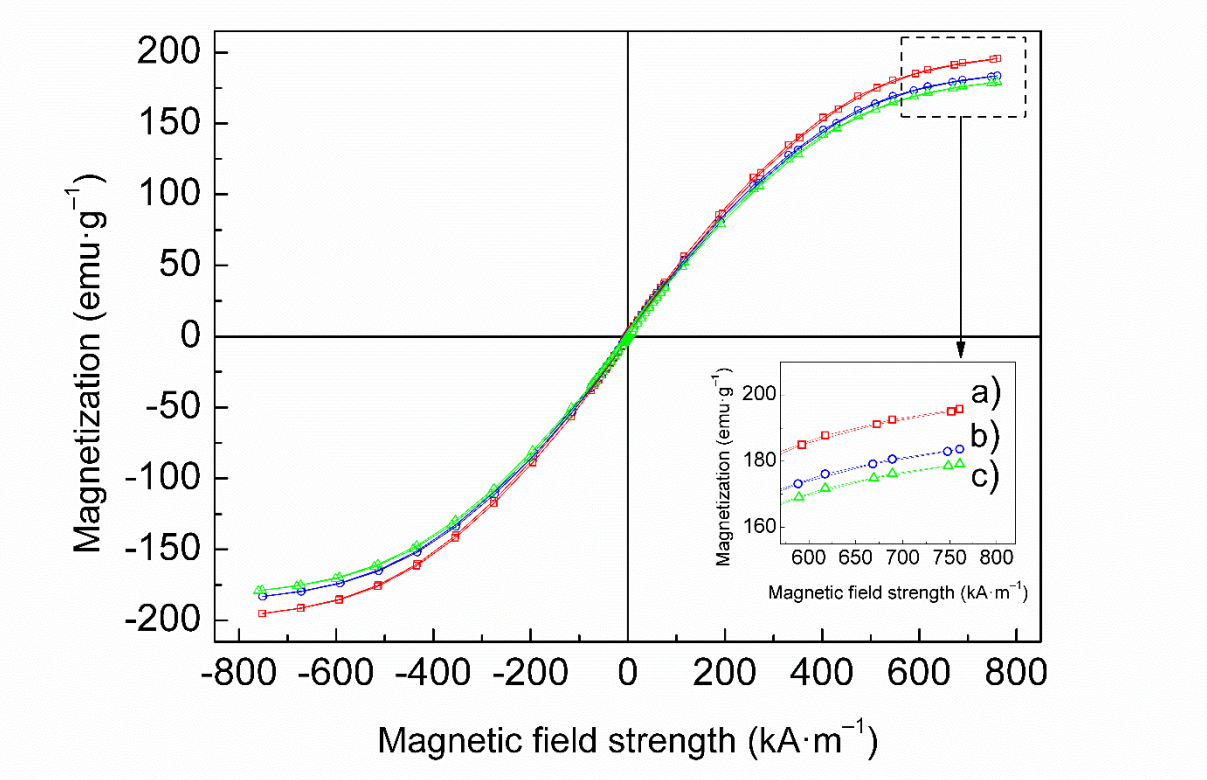

Figure 3. Magnetization curves of bare CI (*a*), CI-*g*-PHEMATMS-1 (*b*), and CI-*g*-PHEMATMS-2 (*c*) particles obtained via VSM. The inset figure shows the data differences near the saturation magnetization, M_S.

Stability properties of CI-g-PHEMATMS.

The MREs can be exposed to demanding operating conditions such as high temperatures or acidic reactive species (e.g. acid rains, sea humidity, operating fluid leakage), which are factors affecting their long-term stability and durability properties [4]. Therefore, the effects of PHEMATMS shell thickness on thermo-oxidation stability and chemical stability of the particles were thoroughly investigated. Figure 4 demonstrates the DTG curves of studied particles showing a significant difference between the curve for bare CI particles and those representing both of their PHEMATMS-grafted analogues. As the testing was performed under air atmosphere, bare CI particles formed oxides such as FeO, Fe_3O_4 and Fe_2O_3 at relatively low temperatures [33]. The presence of compact PHEMATMS layers prevented the oxidation of the

CI core, and shifted the thermo-oxidation process to higher temperatures followed by the thermal decomposition of the shell. The stability of the particles can be evaluated comparing the peaks in DTG diagram. As seen, bare CI exhibited peak at a temperature of ~497 °C, while the grafted particles CI-*g*-PHEMATMS-1 and CI-*g*-PHEMATMS-2 peaked at ~583 and ~592 °C, respectively. Figure 4 also shows the results from an anti-acid/corrosion test. Bare CI particles were relatively unstable and reacted with the acid leading to the formation of less magnetic products [29]. On the contrary, both variants of CI-*g*-PHEMATMS particles were extremely stable under these acidic conditions, regardless the thickness of the layer, which imply that the PHEMATMS layers were uniform without any defects and the iron cores were efficiently protected. A significant difference (more than 3 times higher value) on the pH scale in the case of bare CI particles was considered to be a conclusive result to stop the testing after 80 minutes.

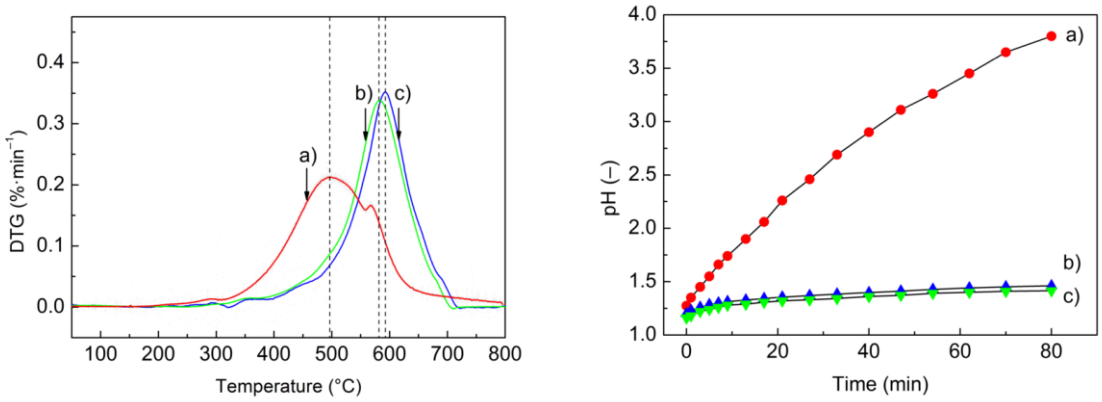

Figure 4. DTG curves (*left-hand side*), and resistance to acidic conditions (*right-hand side*) of bare CI (*a*), CI-*g*-PHEMATMS-1 (*b*), and CI-*g*-PHEMATMS-2 (*c*). Vertical dashed lines represent the DTG peak temperatures.

Magnetorheological performance.

To understand the effect of PHEMATMS molecular weight on the MR behavior, the MREs were subjected to oscillatory shearing under an external magnetic field with

ascending/descending character due to their hysteresis behavior [31]. Figure 5 displays the storage modulus, *G'*, dependence on applied magnetic field strength, *H*. Obviously, the lowest *G'* exhibited neat PDMS matrix, while in the final MREs the *G'* was readily increased by adding the micro-particles since the rigid inorganic matter have a much higher stiffness than the polymer matrix [34]. The highest *G'* possessed the MRE containing bare CI particles due to already mentioned particle/matrix covalent bonding between the hydroxyl groups on the metal surface and the silane groups of PDMS curing agent [22]. Nevertheless, the bonding was limited due to particle/matrix incompatibility as shown via microstructure analysis (Figure 6). Bare CI particles embedded in PDMS were surrounded by cavities, which is also a negative precondition related to the MRE durability. For more details, the reader is referred to authors' previous study [25]. Any remarkable difference between the MREs containing both variants of the grafted particles was indistinguishable from the SEM micrographs (Figure 6b, c). The evidence of cavities presented in the MRE containing bare CI will be further discussed in a connection to damping capabilities.

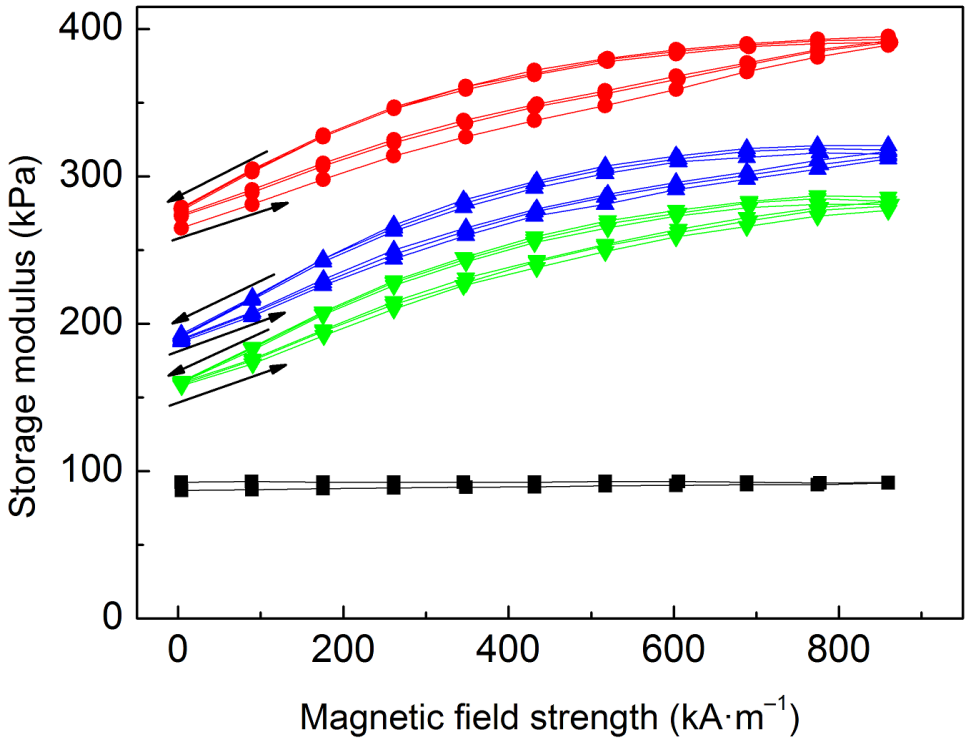

Figure 5. The storage modulus, *G'*, of neat PDMS matrix (*squares*), and the MREs containing bare CI (*red circles*), CI-*g*-PHEMATMS-1 (*blue up–triangles*), and CI-*g*-PHEMATMS-2 (*green down–triangles*) particles as a function of applied magnetic field strength, *H*.

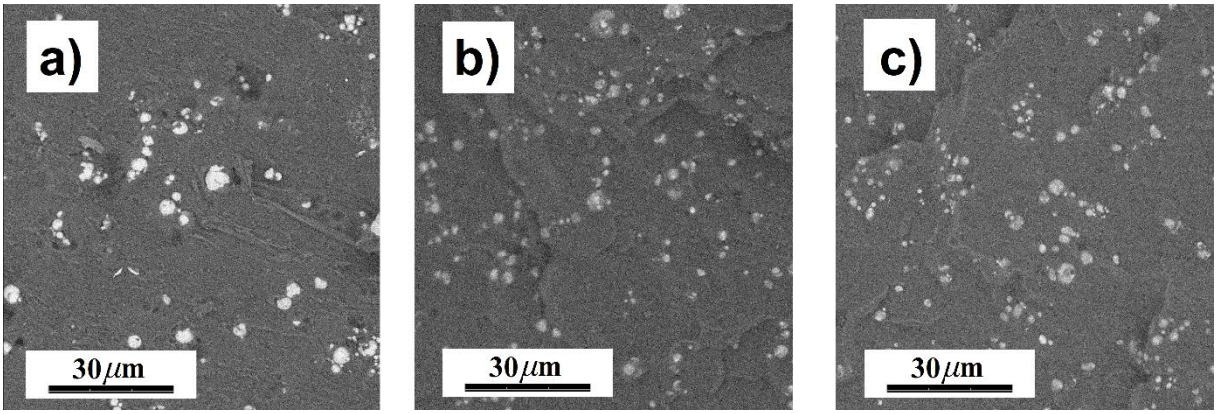

Figure 6. SEM images of the MREs containing bare CI (*a*), CI-*g*-PHEMATMS-1 (*b*), and CI-*g*-PHEMATMS-2 (*c*) particles.

In the MREs containing CI-*g*-PHEMATMS particles the covalent bonding was restricted, thus the particle/matrix interactions were executed by the physical entanglements between the PHEMATMS grafts and PDMS chains. As known, the interactions provided via polymer chain entanglements are weaker than those provided via covalent bonds, which resulted in lowering the *G'* of the MREs containing the PHEMATMS–grafted magnetic particles (Figure 5). When the molecular weight of PHEMATMS was increased, the *G'* of modified MRE further decreased. This trend can be attributed to the different level of polymer chain entanglement in the vicinity of modified particles. It appears that the presence of ATRP–grafted PHEMATMS can increase the mobility of CI particles, and this effect is dependent on the PHEMATMS molecular weight. Similar results were drawn by Fan et al. [18] who observed an analogous phenomenon by adding a different amounts of naphthenic oil as a plasticizer into the BR matrix. The results not only suggest a plasticizing effect of the PHEMATMS grafts, but also describe the influence of their molecular weight.

The plasticizing effect of the PHEMATMS grafts was further evaluated using a relative MR effect, *e*, formalism. This quantity can be calculated according to the equation (Eq. 1):

$$e = \frac{(G'_H - G'_0)}{G'_0} \times 100 = \frac{\Delta G'}{G'_0} \times 100 \quad (1)$$

where G'_{H} is the field-on storage modulus (at a certain magnetic field) and G'_0 is the field-off storage modulus. As seen in Figure 7, the *e* of studied MREs showed the increasing trends with increasing *H* almost reaching the saturation plateau at high *H*. The employed magneto-cell is capable of reaching even higher magnetic fields, however those were not used due to possible inhomogeneity of magnetic field profile as demonstrated by Laun et al. [35]. Based on the results observed in Figure 7, it is obvious, that the MRE containing bare CI particles exhibited the lowest relative MR effect, while its analogues containing PHEMATMS–grafted particles exhibited higher ones. This phenomenon was the most significant in the MRE containing the

CI-*g*-PHEMATMS-2 particles probably due to loosen cross-link density caused by higher molecular weight grafts, which facilitated the particle rearrangement. So even though the modified particles exhibited slightly lower magnetization (Figure 3), their MREs were able to develop higher relative MR effect.

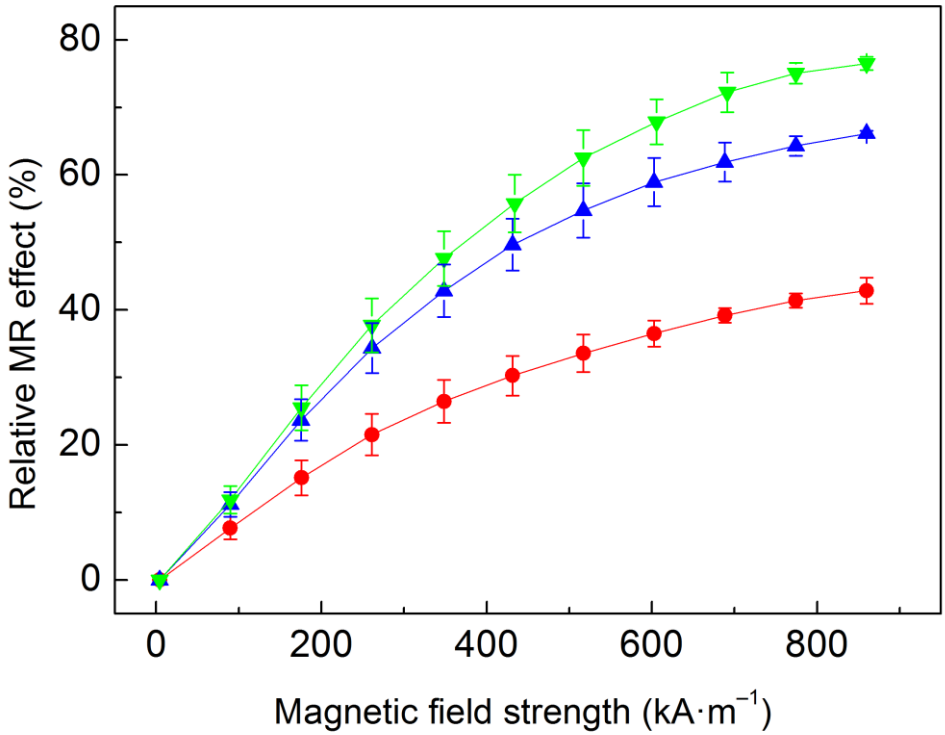

Figure 7. Relative MR effect, *e*, of the MREs containing bare CI (*red circles*), CI-*g*-PHEMATMS-1 (*blue up–triangles*), and CI-*g*-PHEMATMS-2 (*green down–triangles*) particles as a function of applied magnetic field strength, *H*.

The effect of frequency on the *G'* of the MREs containing bare CI or their PHEMAMTS–grafted analogues was studied. The off-state (Figure 8a) as well as the on-state (Figure 8b) data in terms of the *G'* values were in accordance with those obtained from the magneto–sweep experiments (Figure 5). As seen, the *G'* of all the samples was sensitive to the excitation frequency, which is a typical behavior for a viscoelastic material [36]. At higher frequencies (a

shorter timescale), the elastic portion of their complex behavior is usually resulting in higher *G'*; this tendency was obvious in all our studied samples (Figure 8). The frequency dependency was also clearly apparent for neat matrix as the relaxation characteristics of PDMS molecular chains were not disturbed [36]. The inclusion of bare CI particles obstructed the motion of PDMS molecules due to already mentioned particle/matrix covalent bonding leading to a reduction of frequency dependence phenomenon. On the contrary, the presence of both variants of PHEMATMS–grafted CI particles reduced the cross-link density supporting the movement of the matrix molecular chains, which resulted in a steeper *G'* increase with frequency especially above 10 Hz.

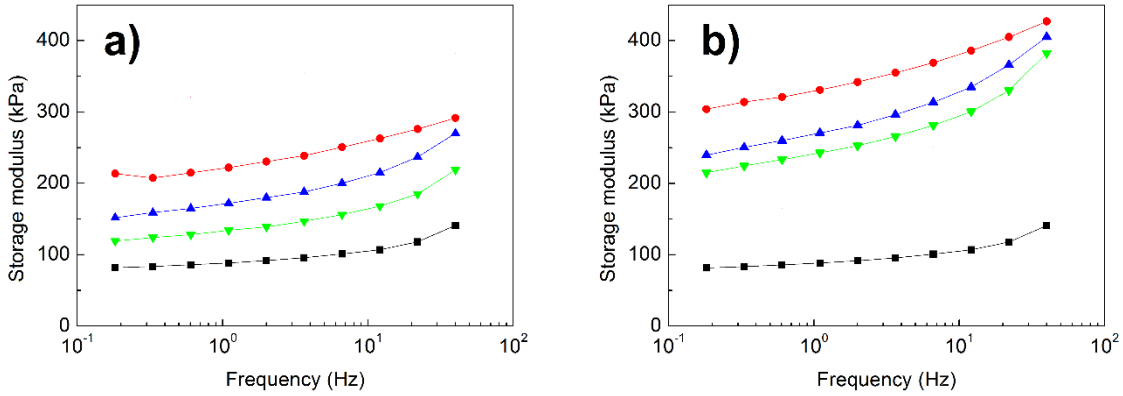

Figure 8. The off-state (*a*) and the on-state (860 kA·m^{-1}) (*b*) storage modulus, *G'*, of neat matrix (*black squares*), and the MREs containing bare CI (*red circles*), CI-*g*-PHEMATMS-1 (*blue up–triangles*), and CI-*g*-PHEMATMS-2 (*green down–triangles*) particles as a function of frequency, *f*.

Further, the effect of the PHEMATMS molecular weight on the damping capacity of the MREs was investigated (Figure 9). Based on the literature, the topic of the damping of the MREs can still evoke a controversy – while in some papers it is stated that magnetic field does not have any remarkable effect on damping [37], other scientists claim that damping of the MREs changes due to the applied magnetic field [5]. Recently, Shuib et al. [38] in their comprehensive

study proposed a mathematical damping model, which matched well with the experimental trends showing that the damping capacity of the MREs is dependent on magnetic field up to magnetic saturation. Herein, the employed magnetic fields were still below the particle magnetic saturation [28], thus the total damping is further discussed as the average value of tan δ obtained through the whole *H* range. The total damping capacity of the MREs includes several mechanisms, namely damping by the viscous flow of the rubber matrix, interfacial damping, and magnetism-induced damping [38].

The first-mentioned mechanism is provided by the viscoelastic polymer matrix, which is typically characterized following the Kelvin–Voight model [38]. In the interfacial damping, two classes are distinguished. According to the Schoeck's theory [39], the damping in the systems with strongly bonded interfaces (matrix molecules are bonded to the surface of the filler particles) can be attributed to the energy required to bring about viscous flow of constrained materials in the vicinity of the particle interfaces [38]. The damping in the systems with weakly bonded interfaces is caused mainly due to internal friction between the particles and matrix and can be estimated based on Lavernia's analysis [40]. Finally, magnetism-induced damping is represented by the energy absorbed to overcome magnetic interactions between the particles [38] and can be modelled as presented by Jolly et al. [41].

As can be seen in Figure 9, the viscous flow mechanism appears to be the main contribution to damping as the average tan δ of neat PDMS matrix was ~0.155. The inclusion of the particles enabled additional damping mechanisms, however, the tan δ of the MRE containing bare CI was only ~0.138 due to limited bonding of the CI particles that rather represented micro-cavities in the body of the matrix (Figure 5) therefore the damping mechanism for strongly bonded interfaces is not relevant. On the other hand, the interfacial damping (for weakly bonded particles) and magnetism-induced damping were manifested in the MRE containing CI-*g*-PHEMATMS-1 particles very well, which resulted in total damping factor of ~0.208. Further

enhancement in damping factor was achieved by the incorporation of CI-*g*-PHEMATMS-2 particles and the MRE containing these particles exhibited the average damping factor of ~0.234. Assuming the same magnetism-induced damping in both modified systems, it can be concluded that the enhancement in the latter system (CI-*g*-PHEMATMS-2) was mainly caused by additional interfacial friction and thus higher energy dissipation as a result of higher-molecular weight PHEMATMS grafts occurrence.

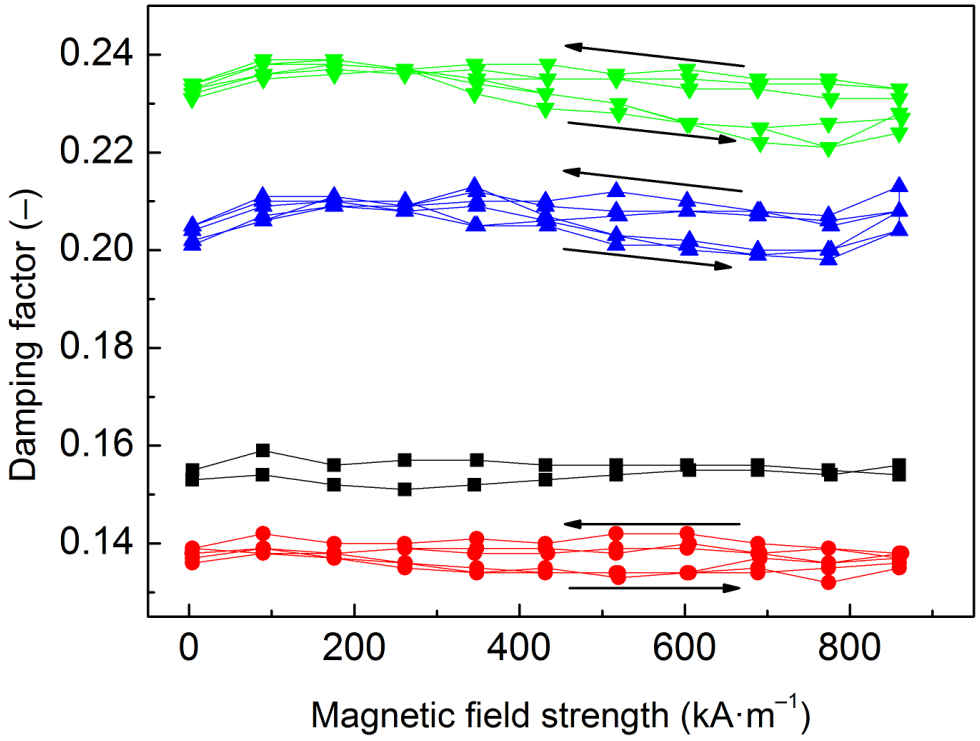

Figure 9. The damping factor, tan δ, of neat PDMS matrix (*black squares*), and the MREs containing bare CI (*red circles*), CI-*g*-PHEMATMS-1 (*blue up–triangles*), and CI-*g*-PHEMATMS-2 (*green down–triangles*) particles as a function of applied magnetic field strength, *H*.

Conclusions

In this paper, two types of CI-*g*-PHEMATMS particles varying in molecular weight of their grafts were synthesized via SI-ATRP, and the multiple function of PHEMATMS grafts on the stability and performance of their PDMS-based isotropic MREs was investigated. The compact PHEMATMS layers protected the CI particles against thermo-oxidation and prevented their degradation in acidic environment. The presence of PHEMATMS further enhanced the properties of the MREs by modifying the particles/matrix interface. Despite lowering the *G'*, the presence of CI-*g*-PHEMATMS particles probably loosened the PDMS cross-link density which facilitated the particle rearrangement in magnetic fields. Although the modified particles exhibited slightly lower magnetization, their MREs were able to develop higher relative MR effects when compared to bare CI particles, and their MREs, respectively. The modified particle/matrix interface was also more effective in damping due to higher energy dissipation as a result of PHEMATMS grafts occurrence. This phenomenon was the most significant in the MRE containing the particles grafted with PHEMATMS of higher molecular weight. Grafting technology enabled tuning the MR performance and damping capacity of the MREs, while significantly enhancing the thermo-oxidation and chemical stability of the magnetic particles.

Acknowledgements

The authors wish to thank the Czech Science Foundation (17-24730S) for financial support. Author M. C. thanks the Internal Grant Agency of Tomas Bata University in Zlín (project no. IGA/CPS/2017/004) for financial support. This work was also supported by the Ministry of Education, Youth and Sports of the Czech Republic – Program NPU I (LO1504). Authors M. I. and J. M. gratefully acknowledge the SRDA agency through project APVV-15-0545 for financial support.

References

[1] A. Boczkowska, S.F. Awietjan, R. Wroblewski, Smart Mater. Struct. 16 (2007) 1924-30.

[2] M. Cvek, M. Mrlik, V. Pavlinek, J. Rheol. 60 (2016) 687-94.

[3] J. de Vicente, D.J. Klingenberg, R. Hidalgo-Alvarez, Soft Matter 7 (2011) 3701-10.

[4] M. Cvek, R. Moucka, M. Sedlacik, V. Pavlinek, Smart Mater. Struct. 26 (2017) 105003.

[5] Y.C. Li, J.C. Li, W.H. Li, H.P. Du, Smart Mater. Struct. 23 (2014) 123001.

[6] B.J. Park, F.F. Fang, H.J. Choi, Soft Matter 6 (2010) 5246-53.

[7] H. Bose, R. Rabindranath, J. Ehrlich, J. Intell. Mater. Syst. Struct. 23 (2012) 989-94.

[8] B. Dyniewicz, J.M. Bajkowski, C.I. Bajer, Mech. Syst. Signal Pr. 60-61 (2015) 695-705.

[9] S.B. Choi, W.H. Li, M. Yu, H.P. Du, J. Fu, P.X. Do, Smart Mater. Struct. 25 (2016) 043001.

[10] S.R. Khimi, K.L. Pickering, Composites, Part B 83 (2015) 175-183.

[11] M. Zrinyi, D. Szabo, International Journal of Modern Physics B, 15 (2001) 557-563.

[12] M. Behrooz, F. Gordaninejad, Smart Mater. Struct. 25 (2016) 025011.

[13] M. Cvek, R. Moucka, M. Sedlacik, V. Babayan, V. Pavlinek, Smart Mater. Struct. 26 (2017) 095005.

[14] K. Keshoju, L. Sun, J. Appl. Phys. 105 (2009) 023515.

[15] I. Bica, E.M. Anitas, M. Bunoiu, B. Vatzulik, I. Juganaru, J. Ind. Eng. Chem. 20 (2014) 3994-99.

[16] S.R. Khimi, K.L. Pickering, B.R. Mace, J. Appl. Polym. Sci. 132 (2015) 41506.

[17] A.V. Chertovich, G.V. Stepanov, E.Y. Kramarenko, A.R. Khokhlov, Macromol. Mater. Eng. 295 (2010) 336-41.

[18] Y.C. Fan, X.L. Gong, S.H. Xuan, L.J. Qin, X.F. Li, Ind. Eng. Chem. Res. 52 (2013) 771-8.

[19] T. Plachy, O. Kratina, M. Sedlacik, Compos. Struct. 192 (2018) 126-30.

[20] Y.C. Fan, X.L. Gong, W.Q. Jiang, W. Zhang, B. Wei, W.H. Li, Smart Mater. Struct. 19 (2010) 055015.

[21] X.L. Gong, Y.C. Fan, S.H. Xuan, Y.G. Xu, C. Peng, Ind. Eng. Chem. Res. 51 (2012) 6395-403.

[22] R. Rabindranath, H. Bose, in On the mobility of iron particles embedded in elastomeric silicone matrix, In 13th Int. Conf. Electrorheol. Fluids Magnetorheol. Suspensions, H.I. Unal Ed., Iop Publishing Ltd, Bristol 412 (2013).

[23] D.L. Yang, R. Pacheco, K. Henderson, K. Hubbard, D. Devlin, J. Appl. Polym. Sci. 131 (2014) 40729.

[24] M. Ocalan, G.H. McKinley, Rheol. Acta, 52 (2013) 623-41.

[25] M. Cvek, M. Mrlik, M. Ilcikova, J. Mosnacek, L. Munster, V. Pavlinek, Macromolecules 50 (2017) 2189-200.

[26] M. Cvek, M. Mrlik, M. Ilcikova, T. Plachy, M. Sedlacik, J. Mosnacek, V. Pavlinek, J. Mater. Chem. C, 3 (2015) 4646-56.

[27] R.X. Tan, Z.Q. Fan, Z.Y. Xie, M.Y. Zhang, K.J. He, Q.H. Huang, Carbon 101 (2016) 439-48.

[28] M. Cvek, M. Mrlik, M. Ilcikova, J. Mosnacek, V. Babayan, Z. Kucekova, P. Humpolicek, V. Pavlinek, RSC Adv. 5 (2015) 72816-24.

[29] M. Sedlacik, M. Mrlik, V. Babayan, V. Pavlinek, Compos. Struct. 135 (2016) 199-204.

[30] M. Sedlacik, V. Pavlinek, RSC Adv. 4 (2014) 58377-85.

[31] V.V. Sorokin, G.V. Stepanov, M. Shamonin, G.J. Monkman, A.R. Khokhlov, E.Y. Kramarenko, Polymer 76 (2015) 191-202.

[32] K. Matyjaszewski, Macromolecules 45 (2012) 4015-39.

[33] M.A. Abshinova, L. Kuritka, N.E. Kazantseva, J. Vilcakova, P. Saha, Mater. Chem. Phys. 114 (2009) 78-89.

[34] S.Y. Fu, X.Q. Feng, B. Lauke, Y.W. Mai, Composites, Part B 39 (2008) 933-961.

[35] H.M. Laun, C. Gabriel, G. Schmidt, J. Non-Newtonian Fluid Mech. 148 (2008) 47-56.

[36] U.R. Poojary, S. Hegde, K.V. Gangadharan, J. Mater. Sci. 53 (2018) 4229-41.

[37] G.Y. Zhou, Smart Mater. Struct. 12 (2003) 139-46.

[38] R.K. Shuib, K.L. Pickering, J. Appl. Polym. Sci. 133 (2016) 43247.

[39] G. Schoeck, Phys. Status Solidi 32 (1969) 651-8.

[40] E.J. Lavernia, R.J. Perez, J. Zhang, Metall. Mater. Trans. A 26 (1995) 2803-18.

[41] M.R. Jolly, J.D. Carlson, B.C. Munoz, Smart Mater. Struct. 5 (1996) 607-14.

PAPER V

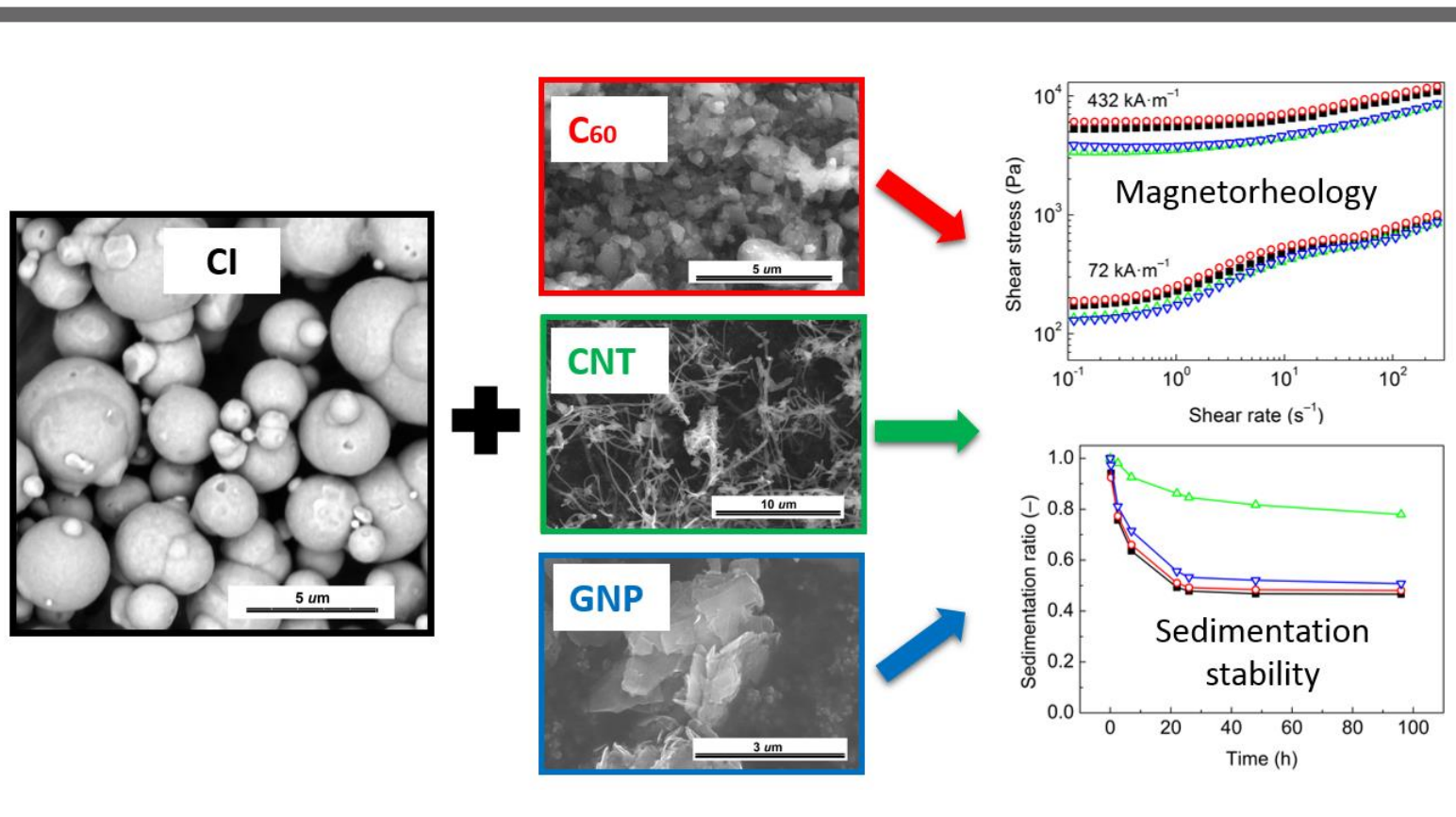

ELSEVIER

Colloids and Surfaces A

Accepted: 25th January 2018

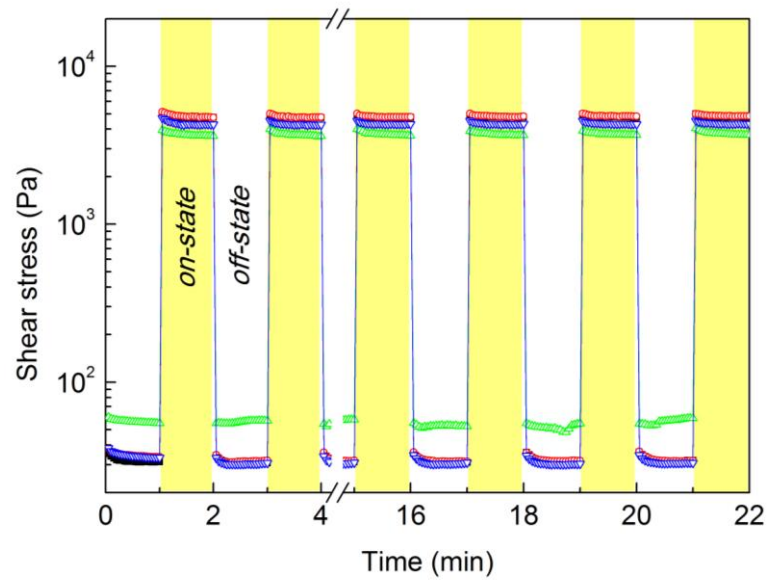

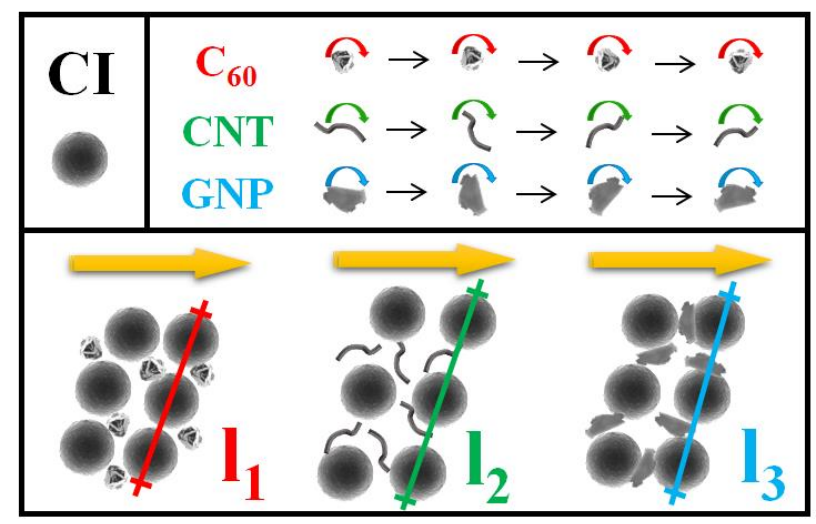

Colloids and Surfaces A 543 (2018) 83–92

Contents lists available at ScienceDirect

Colloids and Surfaces A

journal homepage: www.elsevier.com/locate/colsurfa

A systematical study of the overall influence of carbon allotrope additives on performance, stability and redispersibility of magnetorheological fluids

Martin Cvek[a,b,*], Miroslav Mrlik[a], Robert Moucka[a], Michal Sedlacik[a]

[a] Centre of Polymer Systems, University Institute, Tomas Bata University in Zlin, Trida T. Bati 5678, 760 01, Zlin, Czech Republic
[b] Polymer Centre, Faculty of Technology, Tomas Bata University in Zlin, Vavreckova 275, 760 01, Zlin, Czech Republic

GRAPHICAL ABSTRACT

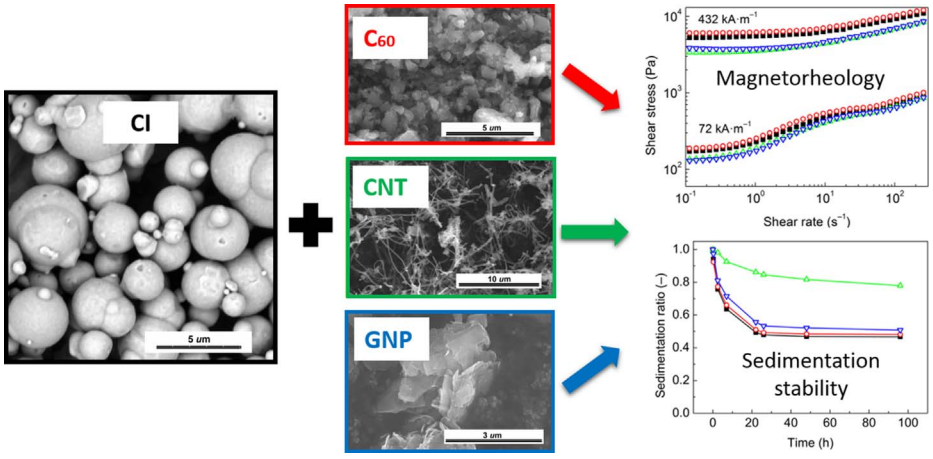

ARTICLE INFO

Keywords:
Magnetorheology
Additive
Graphene
Suspension stabilization
Redispersibility
Modeling

ABSTRACT

To this date many different additives have been used in order to stabilize the magnetorheological fluids or to enhance their performance, but their ranking in terms of the efficiency is still lacking. To design the efficient magnetorheological fluid it is necessary to analyse the overall effects of the additives on its complex behavior. In this study, carbon allotropes – fullerene powder, carbon nanotubes, graphene nanoplatelets – were added into the carbonyl iron-based magnetorheological fluids to examine their effect on stability and utility properties. The magnetorheological behavior of designed mixtures was investigated and obtained experimental data were numerically evaluated using the Robertson–Stiff model. While the fine fullerene powder acted as a gap-filler reinforcing field-induced structures, the other additives employed rather disrupted the microstructure during the shear. The role of the additives during the formation of field-induced structures was pointed out. The sedimentation stability was examined using Turbiscan analyzer as well as by direct observation method. Both approaches revealed that the carbon nanotubes possessed the highest stabilization effect. They also most effectively prevented packing the iron microparticles into a stiff sediment as was confirmed via redispersibility measurements.

* Corresponding author at: Centre of Polymer Systems, University Institute, Tomas Bata University in Zlin, Trida T. Bati 5678, 760 01, Zlin, Czech Republic.
E-mail addresses: cvek@utb.cz, cvek@cps.utb.cz (M. Cvek).

https://doi.org/10.1016/j.colsurfa.2018.01.046
Received 25 October 2017; Received in revised form 16 January 2018; Accepted 25 January 2018
Available online 02 February 2018

1. Introduction

Magnetorheological fluids (MRFs) are a type of field-responsive system composed of micron-sized magnetic particles dispersed in a non-magnetic medium. Such systems exhibit Newtonian-like behavior in the absence of magnetic field, but in a fraction of a millisecond they solidify when an external magnetic field is applied. The field-induced transformation of their rheological properties known as magnetorheological (MR) effect is tunable and reversible. This phenomenon is based on the polarization of the particles that consequently attract each other resulting in rigid chain/column-like particle structures which span the flow domain [1–3]. These unique features make the MRFs suitable for applications in vibration dampers [4] and shock absorbers [5], clutches [6], brakes [7] or polishing devices [8].

As a dispersed phase, the carbonyl iron (CI) particles are considered to be suitable candidates for MRF preparation due to their appropriate size, high saturation magnetization, and low hysteresis. However, high density of the CI compared to disperse medium causes serious sedimentation issues [3,9].

To overcome this drawback, various strategies have been proposed involving the modification of the CI surface with various polymers (even electrically-conductive polymers) [9,10], inorganics [11] or self-assembled monolayers [12]. The modification layer can be fabricated via a number of methods. The simple dispersion polymerization [13] or emulsion polymerizations [14] belong to the early methods used. More advanced techniques such as atom transfer radical polymerization [9,15] or reversible addition fragmentation chain transfer and click chemistry [16] allowing the control of grafting layer at molecular level were used to precisely control the final properties of the particles and consequently the behavior of the MRFs. In the recent work, Choi et al. [17] utilized a supercritical carbon dioxide as a physical foaming agent to tune the properties of grafted layer onto the magnetic particles. Generally, all the mentioned approaches enhanced utility properties and practical applicability of the MRFs to a certain degree. However, the application of the modifying layers can be time consuming, involves problematic large-scale production and often requires the use of environmentally harmful chemicals.

Use of additives in the MRFs is a well-known approach to enhancement of performance and stability properties of the MRFs. This approach is straightforward, hence effective and no special or toxic chemicals are needed, thus it appears to be beneficial also from the environmental point of view. The incorporated additives are mostly submicron-sized gap-fillers that occupy the interspaces between the magnetic particles reducing their sedimentation rate while increasing the dispersion stability [3,18]. The diverse additives including fumed silica [19], organoclays [20], γ-Fe_2O_3 nanoparticles [21], graphene oxide [3] *etc*. were utilized in the MRFs for mentioned enhancing effects. Recent study [22] further investigates the effect of non-magnetic rod-like ferrous oxalate dihydrate particles and their magnetic iron oxide rod-like analogues on the MR effect and stability properties.

Obviously, the materials of different elemental compositions, and different shapes [3,9,23,24] (spherical, rod-like/fibrous, plate-like) were used as additives for the MRFs. Based on the literature survey, it is also important to mention that the MRFs containing the additives were tested under different conditions (particle/additive ratio, dispersion medium, applied magnetic field) thus the genuine effect of the individual additives is not easy to compare, since the studies were carried out and evaluated differently. In other words, the comparison of the overall efficiency of the employed additives is still unclear.

The aim of this study was to investigate the influence of different additives on the performance of the MRFs under the representative conditions. The chosen additives were based on different carbon allotropes of various morphologies, which were represented by fullerene (C_{60}) powder, carbon nanotubes (CNTs), and graphene nanoplatelets (GNPs). The MR performance of as-designed MRFs was assessed by the evaluation of their rheological data using the Robertson–Stiff (R–S) model, which appears to be a better alternative and more reliable tool to describe rheological data of the MRFs in the steady shear regime, when compared to the conventional Herschel–Bulkley model [25]. The effect of additives on the toughness of the induced particle structures was examined using magneto-oscillatory measurements. Finally, the sedimentation stability and redispersibility of the MRFs as the important factors influencing their practical effectivity [19,26] were investigated and compared.

2. Materials and methods

2.1. Materials

The carbonyl iron (CI) particles (SL grade; BASF, Germany) and silicone oil (SO) (Lukosiol M200, Chemical Works Kolín, Czech Republic; dynamic viscosity of 197 mPa s, density of 0.97 g cm^{-3} at 25 °C) were used as a dispersed phase and a suspending medium, respectively, for a preparation of MRFs. The additives were represented by fine fullerene powder (C_{60}; 99.5%, density of 1.65 g cm^{-3}), multi-walled carbon nanotubes (CNTs; > 90% carbon basis, diameter of 110–170 nm; length of 5–9 μm, density of 1.70 g cm^{-3}), and graphene nanoplatelets powder (GNPs; density of 1.90 g cm^{-3}) – all obtained from Sigma (Sigma–Aldrich, USA). All materials were used as received, fullerenes were gently ground into fine powder using a pestle and mortar.

2.2. Microscopy characterization of the particles

The morphology observations of the CI particles and the employed additives were performed on a field-emission scanning electron microscope (SEM) (FEI, Nova NanoSEM 450, Japan). While the dimensions and morphology of the CI particles were studied at 10 kV accelerating voltage in high vacuum mode, the SEM micrographs of the carbonaceous additives were taken in low vacuum mode using the Helix detector.

2.3. Preparation of MRFs

To prepare the MRFs, the CI particle content was fixed to 60 wt.% (~15.7 vol.%), while the amounts of 1 or 3 wt.% additives were introduced into the mixtures. The CI particles, SO, and the corresponding additive as the components of the MRFs were thoroughly mixed using a dispersing instrument Ultra Turrax T 10 standard (IKA® Werke, Germany) for 5 min and then sonicated for additional 2 min with the help of an ultrasonic device (K-12LE, Kraintek, Slovakia) to obtain well-dispersed systems. The temped bath was used to maintain the temperature of the samples at desired 25 °C during the sonication process. After the preparation, the MRFs were immediately characterized. The names of the samples are coded using a following key: MRF-*additive-amount of additive*.

2.4. Magnetorheological measurements

A rotational rheometer Physica (MCR502, Anton Paar GmbH, Austria) equipped with a magneto–device (Physica MRD 170/1T) was used to investigate the rheological properties of prepared MRFs. The gap size between the non-magnetic titanium plate (PP20/MRD/TI) geometry and the static steel plate was 0.5 mm, while 0.2 mL of MRF sample was injected between them. The steady shear experiments were performed in a control shear rate mode within the shear rate range of 0.01–250 s^{-1}. The electric current (0–1.5 A) generated using a power station (PS/MRD/5A) was correlated with true magnetic field (0–432 kA m^{-1}) perpendicular to the samples with a Teslameter (Magnet Physic, FH 51, Dr. Steingroever GmbH, Germany). The detailed measuring protocol of the steady shear investigations can be found in our previous study [25]. The rheological data were collected

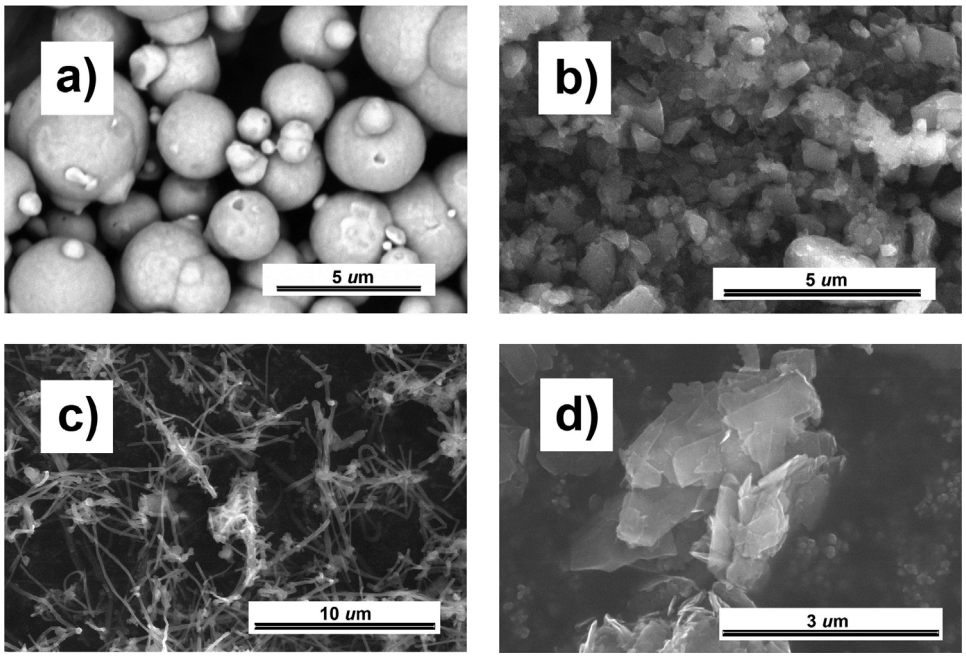

Fig. 1. SEM images of the CI particles (*a*) and the carbonaceous additives, namely, fine C_{60} powder (*b*), CNTs (*c*), and GNPs (*d*).

three times with freshly prepared samples in order to ensure repeatability and accuracy of the measurements. The average values of corresponding rheological quantities were calculated, used for the numerical evaluation and presented in rheograms. In addition, the response time of the MRFs to magnetic field and reproducibility of the internal structure formation were investigated using the on/off tests. The condition in this characterization included a constant shear rate of 50 s^{-1}, while the field of 0 kA m^{-1} the 288 kA m^{-1} was periodically applied in 60 s intervals.

Dynamic rheological tests based on amplitude sweeps under various magnetic fields were conducted. These experiments were performed in order to clarify the role of additives on the MRF behavior within the linear viscoelasticity region and beyond. In the amplitude sweep, a sinusoidal stress at a constant frequency of 10 Hz with a strain amplitude in the range of 10^{-3}–10^{1} % was applied to the investigated sample and thus the storage modulus, *G'*, and the loss modulus, *G"*, dependences were obtained.

To impose the same initial conditioning before each test run, the MRF was pre-sheared at a shear rate of 50 s^{-1} for 60 s. Moreover, the corresponding magnetic field was applied for 30 s before each on–state measurement in order to fully develop the field-induced structures in the system. All MR measurements were performed at a constant temperature of 25 °C maintained by a thermostatic unit (Julabo FS18, Germany).

2.5. Sedimentation stability

The stability of the MRFs can be determined using several approaches. Besides instrumented optical method [27], or direct observation [22,28], also alternatives such as tensiometric [29] or inductance [30,31] measurements can be successfully employed. In this study, Turbiscan® Lab (Formulaction, France) analyzer was used to investigate the sedimentation stability of testes samples. The instrument is equipped with two synchronous optical sensors that measure the transmitted and the backscattered (BS) near-infrared monochromatic light (λ = 880 nm), i.e. light which goes through the sample and light scattered backwards by the sample, respectively. In practice, the MRFs are placed in flat-bottomed cylindrical glass tubes (volume of 4 mL), while the detection head periodically scans a sample by moving vertically along the analysis cell and acquiring data every 40 μm. Due to sample instability, the differences in transmitted, and BS signals versus time are recorded. The measurements were performed on freshly-dispersed samples at a constant temperature of 25 °C. Detailed description of Turbiscan® apparatus principle can be found elsewhere [32].

The long-term MRF stability was obtained performing the naked-eye observation method. The well-dispersed MRFs were transferred into cylindrical tubes (inner diameter of 13 mm, height of 48 mm) and the position of macroscopic phase boundary between the concentrated fraction and relatively clear oil-rich phase was recorded as a function of time [18]. The sedimentation ratio was expressed as a height of the particle-rich phase relative to the total MRF height. The advantages as well as drawbacks of both methods related to sedimentation stability were finally discussed.

2.6. Redispersibility

The redispersibility tests were performed on the basis of the ASTM-D5-05a standard, which was originally designed to determine the penetration of bituminous materials. Nevertheless, as shown elsewhere [11,26] this concept can be also applied for MRFs testing. This testing method can be further modified for the MRFs' testing in repeated penetration/extraction steps as shown recently by Portillo et al. [33]. Herein, the M350-5 CT (Testometric Company, Lancashire, UK) device was used to execute the controlled motion of the standard needle at a desired velocity of 10 mm min^{-1}. The needle penetrated the MRF and the stiffness of the sediment, expressed as a force needed to overcome the needle buoyancy and to penetrate the sample, was recorded by an analytical balance (KERN KB 360-3N, Germany) with an accuracy of 1 mg (9.8×10^{-3} mN). The data were automatically read/collected by a computer. The representative MRFs were prepared by ultrasonic dispersing (Sonopuls HD 2070, Bandelin electronic, Germany) prior to their testing. All the experiments were carried out at laboratory conditions after 168-hour inactivity.

3. Results and discussion

3.1. Microstructure analysis

The size and morphology of the MRF components can remarkably affect the overall behavior of the MRFs, therefore the SEM was chosen

as a suitable analytical tool to explore these characteristics. Fig. 1 depicts the SEM micrographs of the employed MRFs particulate components. As seen, the CI particles were almost perfectly spherical with quite smooth surface and diameter in a range of 1–5 μm. The ground C_{60} powder exhibited irregular shapes with sharp edges and the grain size in sub-micron range similarly as in work by Zhao et al. [34]. The CNTs with a high aspect ratio developed self-entangled clusters, while the GNPs formed micron-size several layer-thick sheets. The obtained information about particle morphology is further discussed with the connection to tested MRF characteristics.

3.2. Magnetorheological activity under steady shear

The performance of the MRFs in magnetic field is a crucial requirement for many engineering applications, therefore the steady shear measurements on formulated MRFs were performed and evaluated. In a shearing mode, the MR activity can be evaluated via different viscoplastic models among which, the most popular are the Bingham plastic, and the Herschel–Bulkley models. In our preceding study, we have shown that predictive/fitting capabilities of the R–S model are superior and thus this model can provide more accurate fits with the experimental data, which was also proven via statistical analysis [25]. The R–S model employing the parameters applicable for the MRFs has following form:

$$\tau = \left[K^{\frac{1}{n}} |\dot{\gamma}|^{\frac{n-1}{n}} + \left(\frac{\tau_0}{|\dot{\gamma}|} \right)^{\frac{1}{n}} \right]^n \dot{\gamma} \quad (1)$$

where τ is the shear stress, the τ_0 is the yield stress controlled by the magnetic field strength (H), $\dot{\gamma}$ denotes the shear rate, while K and n are the consistency index and power–law exponent, respectively [25,35].

3.2.1. Off-state evaluation

We compared the MR flow behavior of the MRFs with and without additives to examine their effect as shown in Fig. 2. As seen, the presence of the additives at the amount as low as 1 wt.% influenced the MR characteristics.

Firstly, the attention was paid to the evaluation of the MRFs off-

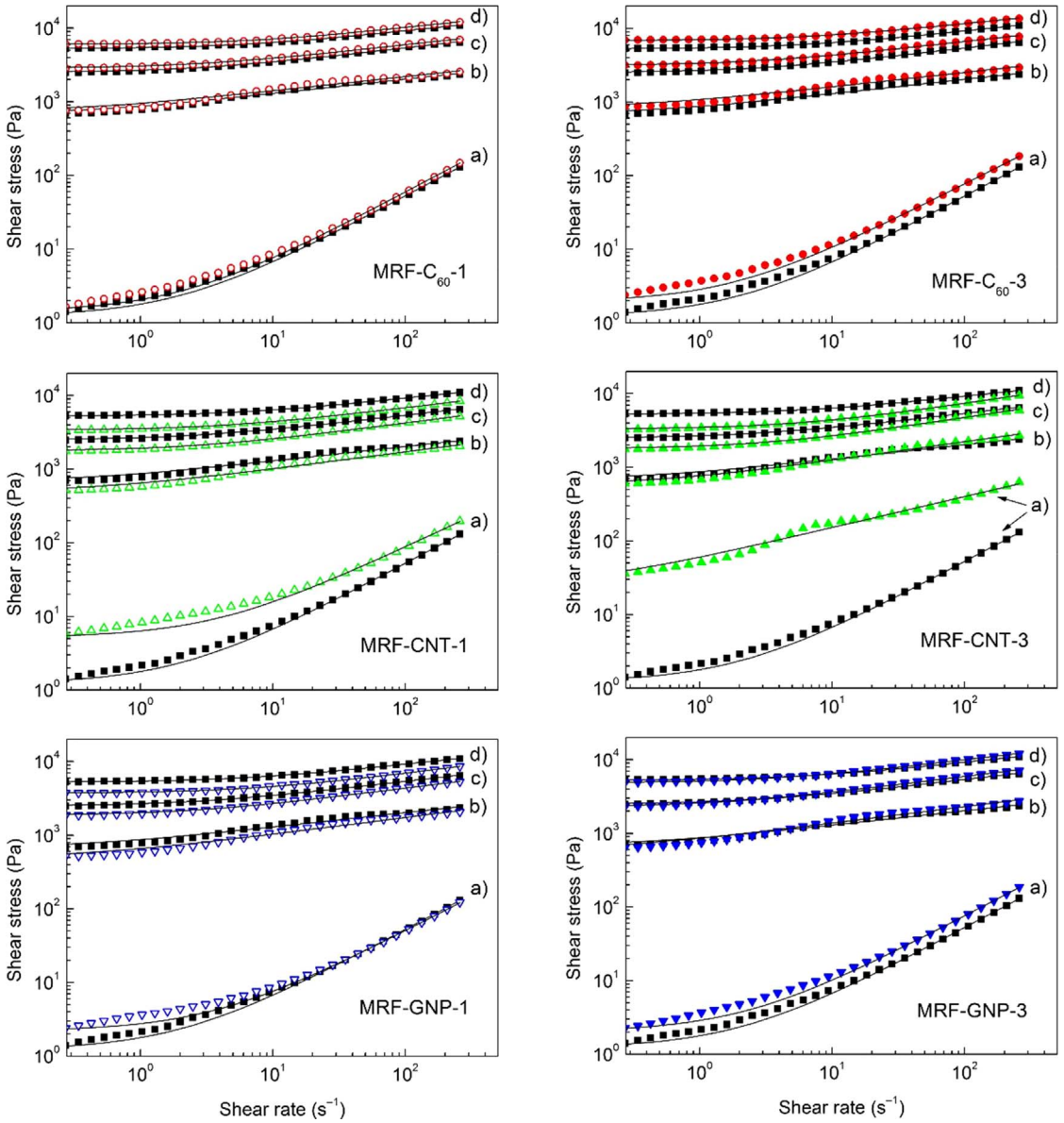

Fig. 2. The shear stress vs. shear rate dependences for the reference sample (*solid squares*), and the MRFs containing 1 wt.% (*open symbols*) or 3 wt.% (*solid symbols*) of fine C_{60} powder (*circles*), the CNTs (*up-triangles*), or the GNPs (*down-triangles*) at the off-state (*a*), and at 144 (*b*), 288 (*c*), 432 kA m^{-1} (*d*) magnetic field strengths. The solid lines refer to the R–S model predictions.

Table 1
Calculated R–S model parameters for the CI-based MRFs containing different amounts of the carbon additives under various magnetic field strengths.

Magnetic field	0 kA m^{-1}	72 kA m^{-1}	144 kA m^{-1}	216 kA m^{-1}	288 kA m^{-1}	360 kA m^{-1}	432 kA m^{-1}
MRF (reference sample)							
τ_0	1.211	153.6	680.4	1489	2518	3787	5270
K	0.6102	250.6	818.3	1391	2034	2792	3735
n	0.9639	0.2362	0.1968	0.2077	0.2108	0.2059	0.1938
MRF-C_{60}-1							
τ_0	1.399	170.5	744.0	1667	2878	4363	6011
K	0.6880	288.9	898.5	1597	2350	3181	4107
n	0.9644	0.2245	0.1940	0.1977	0.2008	0.1994	0.1954
MRF-CNT-1							
τ_0	5.173	123.7	501.6	1088	1780	2560	3394
K	1.684	209.3	587.8	1016	1435	1951	2496
n	0.8534	0.2532	0.2327	0.2318	0.2340	0.2259	0.2171
MRF-GNP-1							
τ_0	2.193	117.2	506.2	1123	1874	2720	3751
K	0.6553	209.1	604.3	1040	1524	2010	2430
n	0.9371	0.2541	0.2296	0.2315	0.2273	0.2247	0.2265
MRF-C_{60}-3							
τ_0	1.895	204.6	846.5	1865	3147	4773	6839
K	1.101	336.3	1008	1775	2589	3566	4806
n	0.9195	0.2146	0.1987	0.2006	0.2028	0.1994	0.1885
MRF-CNT-3							
τ_0	24.59	149.2	587.7	1138	1800	2553	3327
K	57.10	362.2	688.3	1013	1324	1691	2090
n	0.4227	0.2359	0.2548	0.2626	0.2760	0.2766	0.2715
MRF-GNP-3							
τ_0	2.018	137.3	598.4	1322	2308	3463	4895
K	0.9475	277.3	820.5	1412	2107	2846	3725
n	0.9478	0.2475	0.2243	0.2263	0.2245	0.2213	0.2123

state flow behavior. The off-state τ generally increased due to the presence of the carbon additives, which was also observed elsewhere on nano-silica filler [36]. The off-state τ of the MRF-C_{60}-1 and MRF-GNP-1 was comparable with the τ of reference sample. On the other hand, the MRF-CNT-1 exhibited the highest increment of this quantity probably due to high-volume-to-surface ratio of the CNTs. Such trends were also confirmed and quantified via n parameter of the R–S model, which compares the flow behavior of the MRF with a Newtonian fluid. When n approaches 1, the typical Newtonian behavior is obtained, while n value in the range of $0 < n < 1$ corresponds to shear thinning flow behavior. The n as a fitting parameter of the R–S model was close to 1 for the reference sample as well as MRF-C_{60}-1 and MRF-GNP-1, which is in accordance with the character of the obtained flow curves. The MRF-CNT-1 exhibited n equal to ~0.78 referring to more pronounced pseudoplasticity.

Fig. 2 also shows the flow curves of the tested MRFs containing 3 wt. % of the additives. The presence of the higher amount of all additives further increased the off-state τ values when compared with the situation for the MRFs containing only 1 wt.% of the additives. Similar effect was observed by Zhang et al. [3] on various CI/graphene oxide mixtures with different ratios of the components. Again, this phenomenon was the most significant in the MRF-CNT-3, while remaining two systems almost preserved the original values of the reference system. These results were consistent with the numerical results (Table 1), as the MRF-C_{60}-3 and the MRF-GNP-3 exhibited n values around ~0.90, while in the MRF-CNT-3 the n was calculated to be only ~0.41 reflecting the severe pseudoplasticity of the system. All numerical results and fitting parameters are included in Table 1.

3.2.2. On-state evaluation

At the on-state, the significant increase of the τ values can be observed (Fig. 2) due to the formation of chain-like structures spanning the geometry. Thus, the MRFs possessed a solid-like behavior accompanied by breaking and reforming of the particle chains during the shear flow [24]. Interestingly, the MRF containing fine C_{60} powder exhibited slightly higher on-state τ values at corresponding magnetic fields when compared with the reference sample. This phenomenon was observed on different additives [3,20,37] and can be explained as a consequence of the gap-filling the interspaces among the CI particles with the nano-sized additives. Therefore, the fine C_{60} powder at such small amounts can enhance the contact of the CI particles resulting in more robust field-induced structures.

However, the effect of other carbonaceous additives on the performance of the MRF followed the opposite trends. The presence of CNTs and GNPs decreased the on-state τ values, while the former demonstrated also already mentioned notably increased off-state leading to lower efficiency of the system in terms of its relative MR performance. These additives reduced the contact between the CI particles due to their morphological structure (Fig. 1) and caused decreased toughness of the internal particle chains, which fits well with the literature dealing with non-magnetic nano-additives [20,37]. Admittedly, the CNTs were recently reported [38] as an additive enhancing the MR properties. However, the previous research was performed using the single-walled CNTs (purity of ~50%), which possessed certain magnetic properties even after purification process due to the presence of residual iron catalyst introduced during the synthesis [38]. In, this case the CNTs and GNPs underwent collisions with the CI chain-like structures and instead of the gap-filling effect they possess the weakening effect on the formation of induced structures due to their 2-dimensional structure. As seen in Table 1, this assertion is supported by numerical description obtained from empirical modeling. The K parameter of the R–S model physically reflects the rigidity of the particle internal structures as shown in our previous paper [25]. Thus, the trends in K parameter value confirm the hardening/weakening effects of the employed additives.

3.2.3. Yield stress evaluation

Despite an ongoing debate whether true τ_0 exists or not, the concept

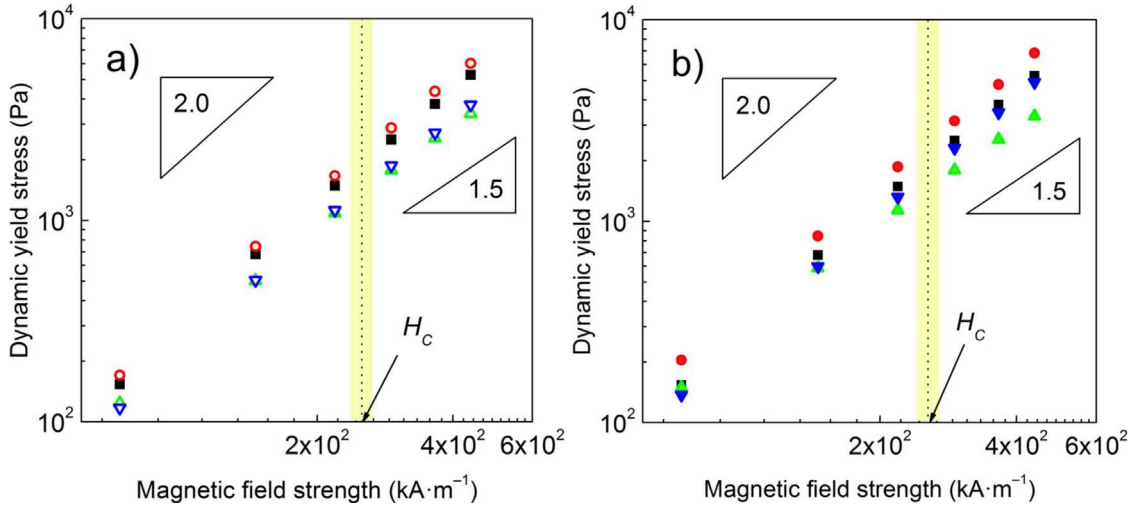

Fig. 3. The dynamic yield stress vs. magnetic field strength dependences for the reference sample (*solid squares*), and the MRFs containing 1 wt.% (*a; open symbols*) or 3 wt.% (*b; solid symbols*) of fine C_{60} powder (*circles*), the CNTs (*up-triangles*), or the GNPs (*down-triangles*).

of τ_0 is very useful and desirable in many practical application, once it is properly defined and delineated [39]. This quantity is commonly determined using appropriate rheological models [40,41]. Based on the numerical results, one can notice that studied MRFs exhibited small τ_0 even at the off-state. Similar phenomenon was observed elsewhere and was explained as a consequence of the particle aggregation [42]. Nevertheless, this can be expected as some force is required to initiate deformation or flow of the MRFs even at the off-state. As we demonstrated, such small $\tau_0$can be determined when appropriate models are used.

The dependence of the dynamic τ_0 predicted according to the R–S model on the applied magnetic field strength is plotted in Fig. 3. As seen, the data followed well-known magnetic-polarization model that predicts a relation between the field-dependent τ_0 and the strength of applied field [27]. The τ_0 increases with the exponent 2.0, when a weak magnetic field is imposed. At a certain magnetic field strength, known as critical magnetic field, H_C, the local particle saturation becomes apparent and the slope of the dependence decreases to 1.5 [43]. This transition behavior was apparent in all MRFs, while the H_C was found to be ~250 kA m^{-1} as the nano-additives in such small amounts had a negligible effect on this quantity.

Generally, the fine C_{60} powder acted as the gap-filler among the CI micro-particles making the induced structures more rigid, while the other two additives involved disrupted the particle structures during the steady shearing in external magnetic field. The similar trend was observed when 3 wt.% of the nano-additives were employed, nevertheless the MRF-GNP-3 exhibited similar τ_0 as the reference, whereas the MRF-CNT-3 possessed slightly lower τ_0 especially at high magnetic field strengths when compared with the reference. Comparing the data (Table 1), it can be noticed that the τ_0 values were interestingly higher when larger amounts of corresponding additives were incorporated. This phenomenon can be explained as follows: higher amount of additive results in lower relative portion of SO, which has a thickening effect on the MRF behavior and gives rise to the on-state values including the τ_0.

3.3. Magnetorheological activity under dynamic magnetic field

The important characteristics of the MR phenomenon such as very fast process rate and the reversibility were considered. The presence of non-magnetic additives might negatively affect the rate of the CI structure formation and possible destruction of certain brittle additives during repeatable shearing can induce problems with reproducibility of the process. As expected, the τ values followed similar trends as obtained in steady shear magnetorheology (Fig. 2) and from obvious above-indicated reasons the presence of fine C_{60} powder slightly increased its value, while the MRFs containing other additives exhibited rather lower τ values. To address the repeatability, in all investigated MRFs the repeatable on-state increase of τ values was followed by their decrease to original off-state values as seen in Fig. 4. The process was generally characterized by an abrupt increase/decrease of the τ as a reaction to switching magnetic field through several operating cycles. The additives can be perceived as physical barriers acting against the CI particles' locomotion. Their presence however did not significantly affect the rate of the structure formation as this process is driven by strong magnetic forces and the additives were incorporated in relatively low amounts. Generally, the key characteristics of the MR effect were sufficiently retained showing the potential of designed MRFs in the MR devices.

3.4. Dynamic magnetorheological properties

In order to explore the strength of the field-induced particle chains the oscillatory tests comprising amplitude sweeps under various

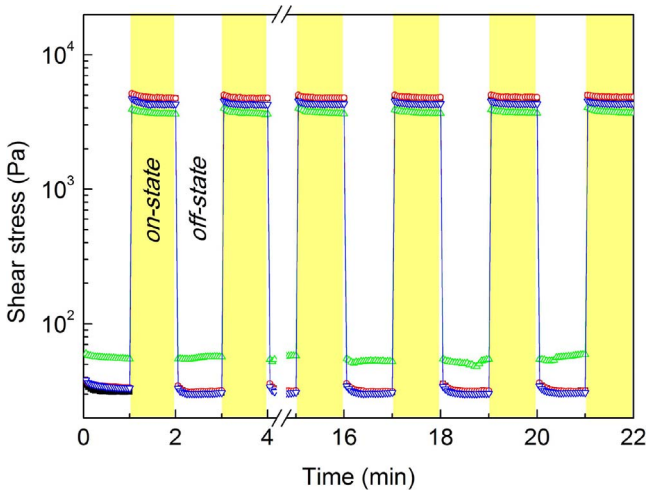

Fig. 4. The shear stress vs. time dependences during periodically switching off/on magnetic field (~288 kA m^{-1}) at a shear rate of 50 s^{-1} for the reference sample (*black squares*), and the MRFs containing 1 wt.% of fine C_{60} powder (*red circles*), the CNTs (*green up-triangles*), or the GNPs (*blue down-triangles*). The white/yellow regions refer to off/on states. (For interpretation of the references to colour in this figure legend, the reader is referred to the web version of this article).

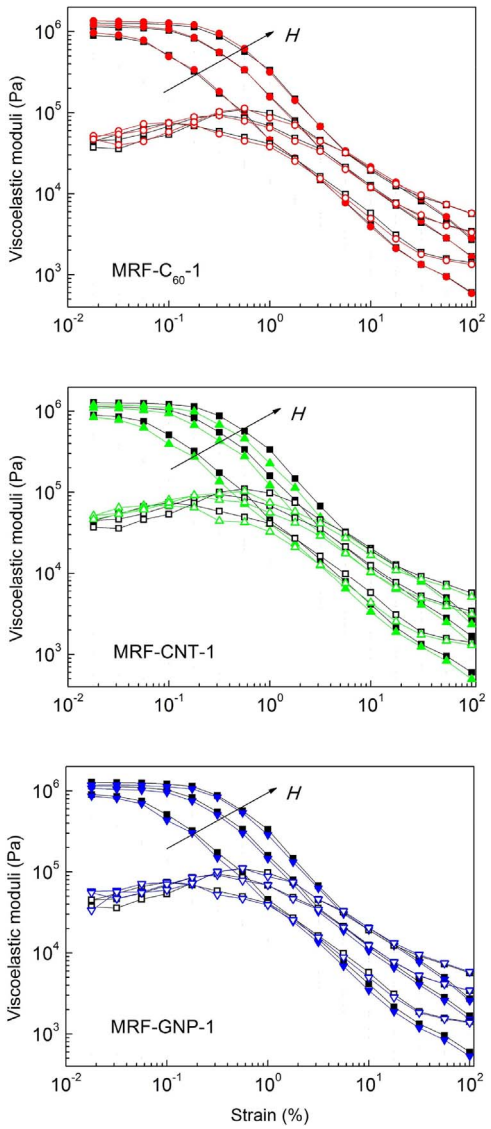

Fig. 5. The storage (*solid symbols*) and the loss (*open symbols*) moduli vs. strain dependences for the reference sample (*black squares*), and the MRFs containing 1 wt.% of fine C_{60} powder (*red circles*), the CNTs (*green up-triangles*), or the GNPs (*blue down-triangles*) under increasing magnetic field strength (144, 288, and 432 kA m^{-1}) denoted by the arrow. (For interpretation of the references to colour in this figure legend, the reader is referred to the web version of this article).

magnetic field strengths were acquired. Analogously to magneto-steady shear, the presence of applied magnetic field yielded the formation of chain-like structures resulting in an increase of both the *G'* and *G''*. As seen, all curves exhibited similar character and the onset of nonlinearity was manifested at relatively low strain amplitudes, similarly as obtained by other researchers [38]. Interestingly, the effects of additives during magneto-oscillatory-shear were manifested in lower degree when compared to the situation under the magneto-steady shear, thus the differences in *G'* values were generally less pronounced when compared to the reference (Fig. 5). To address this phenomenon, the mechanisms of the additives' action on the formation of the CI structures were proposed.

3.5. Theoretical mechanisms of carbonaceous additive's action on the formation of the CI structures

As seen above (Fig. 2), all tested additives increased the off-state τ of the MRFs as their presence increased frictional forces and the hydrodynamic volume [44]. However, the trend in the on-state

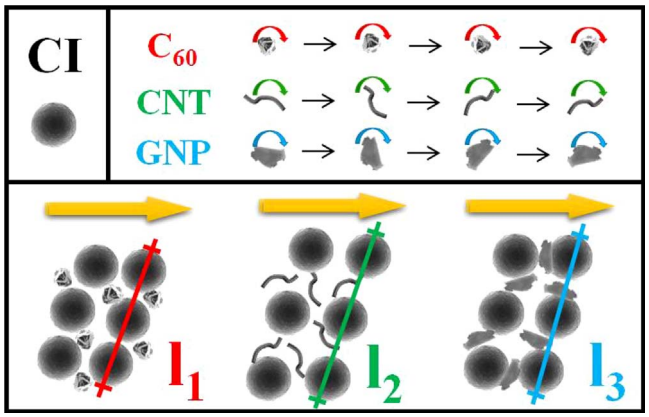

Fig. 6. Schematic representation of fine C_{60} powder, CNTs and GNPs added into the CI-based MRF. The lines represent the average distance between three neighboring CI particles ($l_1 < l_3 < l_2$), which is related to the intensity of induced magnetic moments.

rheological behavior varied based on the additive employed. As a submicron-sized material, fine C_{60} powder possessed a gap-filling effect based on the bridging the gaps among the adjacent CI particles and thereby enhancing the rigidity of the internal structures and MR properties (shear stress, yield stress) [27]. On the contrary, the presence of the CNTs and GNPs interrupted chain formation of the CI particles causing them less resistant against applied force. The situation was more pronounced under steady shear conditions when compared to small amplitude oscillatory shear. In the former case, the particles including the additives can rotate due to Couette flow velocity profile (Fig. 6). The rotations can increase the hydrodynamic volume of the additives, which leads to higher distances between the CI particles lowering the magnetic dipole–dipole interactions and consequently the MR performance [13]. This feature was more pronounced for non-spherical additives such as CNTs and GNPs. Similar phenomena were observed in the literature dealing with the non-magnetic additives [3,44] or even non-magnetic coatings [13,28] applied on the CI particles' surface. The results suggest, that under the oscillatory shear the additives integrated the CI particle structures to higher degree leading to only slight decrease of on-state *G'* values when compared to the reference. In this study, the most obvious effect was attributed to the presence of the CNTs, which from a wider perspective showed their indisputable advantages for sedimentation stabilization purposes, as will be shown further in text.

3.6. Sedimentation stability

The short-term sedimentation properties of the MRFs were investigated using an optical analyzer. In the principle, the instrument measures the BS signals, which vary with the cell height (Y-axis) over time [27]. Fig. 7 displays Turbiscan profiles, in which the bottom of the sample is represented on the left-hand side of the graph, while the top of the sample corresponds to its right-hand side. The scanning is repeated over time, which is denoted by the color of the lines. Presented results are displayed in delta, Δ, mode, i.e. the first scan is subtracted from all other scans, which allows easier visualization of the variations.

As known, the occurrence of significant BS variation at the top of the spectra indicates the clarification phenomenon. The ΔBS decreases as the particles in the suspension sediment, and as a result the BS signal is lower. On the contrary, the changes at the bottom of the spectra denote developing sedimentation cake, and the BS signal increases due to locally increased concentration of the particles. The stability of the MRFs containing 1 wt.% of the carbon additives was evaluated. As seen in Fig. 7, the reference sample and the MRF-C_{60}-1 displayed similar Turbiscan spectra regarding the position of the peaks and their intensity. However, in fact a broader clarification peak in the latter

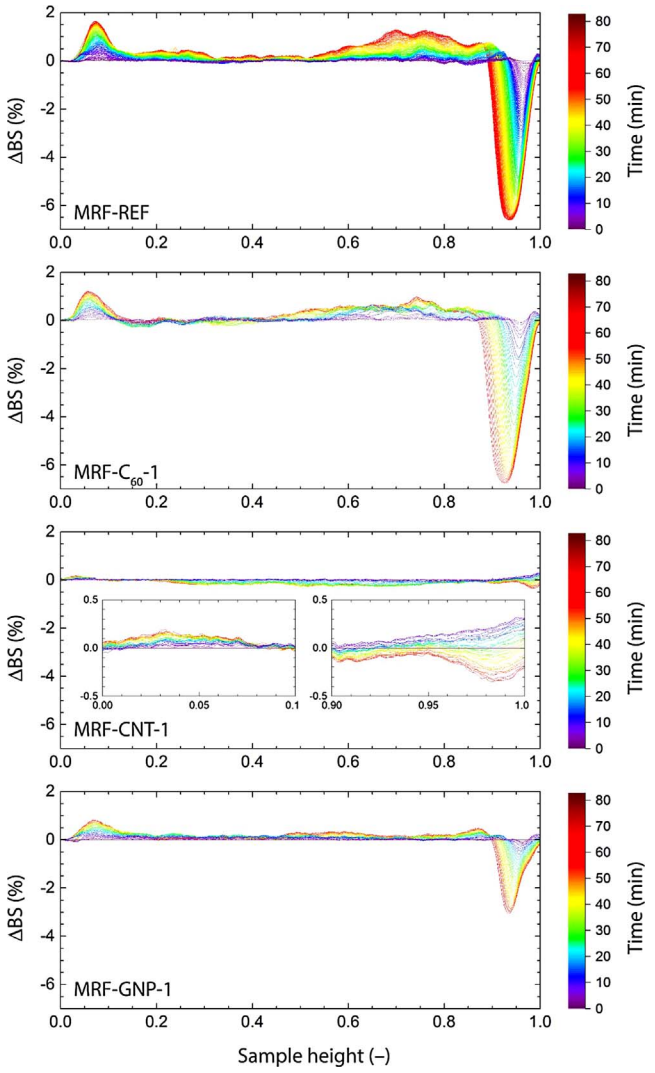

Fig. 7. Turbiscan spectra of tested MRFs containing 60 wt.% of the CI particles and 1 wt. % of individual carbon additives. Insets in the MRF-CNT-1 spectrum show a sedimentation peak (*left*) and a clarification peak (*right*), respectively. (For interpretation of the references to colour in the text, the reader is referred to the web version of this article).

suspension indicated that a small amount of fine C_{60} powder slightly reduced stability of the suspension. The lowest BS variation exhibited MRF-CNT-1, which corresponded to the most stable MR system. The remarkable stability enhancement due to the presence of CNTs can be attributed to increased friction force as a result of their high specific surface area, which affects the MRF viscosity [45]. Finally, the presence of GNPs increased suspension stability to a certain degree, but not as significantly as the CNTs at the same amount. The Turbiscan spectra of the MRFs containing 3 wt.% of the carbon additives are included in electronic supplementary information (ESI) (please see Figure S1).

The Turbiscan® technology enables fast detection (typically less than hour) of all the destabilization phenomena (including clarification, sedimentation, agglomeration etc.) occurring in the samples during their aging [46]. Thus, one hour experiment was considered to be long enough to reliably assess and compare the sedimentation stability of the designed MRFs. In practice, the inactivity timespan can however reach several days (e.g. storage) [33] therefore the long-term experiment based on simple observation method was included. As can be seen in Fig. 8, the MRF-C_{60}-1 exhibited similar stability when compared to the reference. The presence of small amount of fine C_{60} powder did not significantly affected the sedimentation process of the CI particles. Similar result was observed by Jang et al. [21] after adding the γ-Fe_2O_3

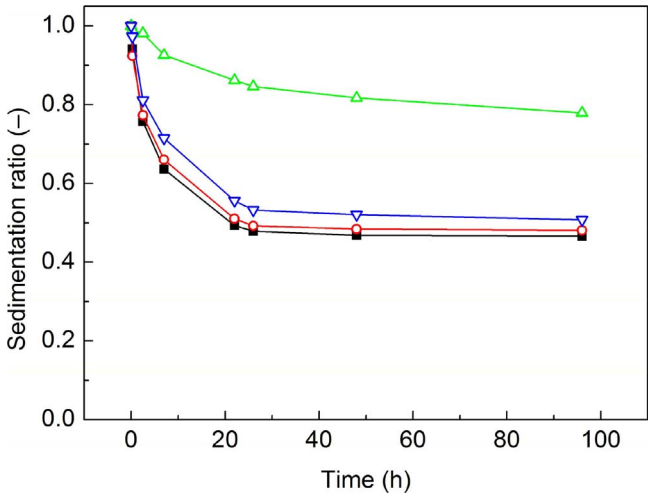

Fig. 8. The sedimentation ratio vs. time for the reference sample (*solid squares*), and the MRFs containing 1 wt.% of fine C_{60} powder (*open circles*), the CNTs (*open up-triangles*), or the GNPs (*open down-triangles*).

nanoparticles into the CI-based MRF. On the contrary, the presence of the GNPs slightly enhanced the suspension stability which was attributed to the plate-like morphology of the GNPs (Fig. 1d). Considering the additive architecture, the GNPs most probably represented the spatial barriers decreasing the sedimentation velocity of the CI particles. Finally, the CNTs manifested as the most effective additive for the MRF stabilization. Their stabilization effect was caused by the buoyancy of the low-density additive particles [30] and is further closely-connected to relatively high off-state viscosity (Fig. 2) of their suspensions. This type of behavior was recently observed on the electrorheological fluids containing the graphene oxide-wrapped titanium dioxide nanoparticles. Such additives act as a parachute that effectively prevents the dispersed particles from settling [47]. Finally, it should be mentioned that the naked eye observation can be interpreted as a subjective method from two main reasons. The first reason is connected to the opacity of the MRFs [30], while the second one appears because the macroscopic phase boundary between particle-rich phase and oil-rich one is not always sharply defined. This phenomenon occurs as the particles do not sediment with the same velocity which stems from their size distribution. These drawbacks can be eliminated using the inductance-based methods, which are at a stage of prototype development [30,48]. However, direct observation is a sufficient method to establish the sample stability in a longer period of time and as demonstrated, the results were consistent with those obtained via Turbiscan method.

3.7. Redispersibility

Once the sedimentation occurs, the inter-particle aggregation is favored causing severe redispersibility problems [2]. However, despite its practical importance the redispersibility of the MRFs is rarely investigated [11,26,49]. This property can be enhanced by the use of the additives, which can eliminate direct contact of the CI particles leading to the effective prevention of rigid sedimentation cake occurrence during the long-term storage of the MRFs [37]. As shown in Fig. 9, the CI particles exhibited good packing thus the height of the sedimentation cake was the lowest and the penetration force started to increase at the highest depth. The addition of fine C_{60} powder and GNPs slightly disturbed the packing properties of the CI, which was reflected in higher sediment, thus the penetration force increase at lower depth when compared with the reference. Finally, the CNTs cannot be easily structured, thus their presence prevented the packing of neighboring CI particles into stiff sedimentation cake. Therefore, the systems stabilized with the CNTs can be readily used after longer on-state inactivity when compared with the reference sample.

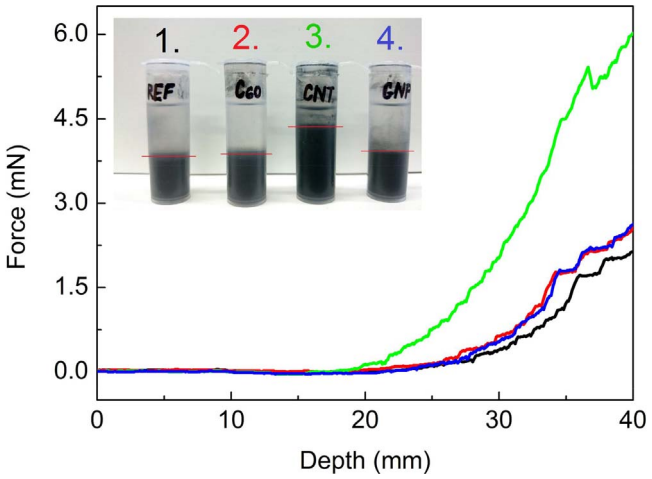

Fig. 9. Penetration force as a function of depth for the reference sample (*black lines*), and the MRFs containing 1 wt.% of fine C_{60} powder (*red line*), the CNTs (*green line*), or the GNPs (*blue line*) measured on after 168-hour sedimentation. The inset shows the height of the sedimentation cake in the reference sample: 1; and the MRFs containing C_{60}, CNTs, and GNPs: 2, 3, and 4, respectively. (For interpretation of the references to colour in this figure legend, the reader is referred to the web version of this article).

4. Conclusions

The effects of carbon additives on performance, stability and redispersibility of the magnetorheological fluids were investigated. It was found that fine fullerene powder added at low concentrations occupied the micro-cavities in the carbonyl iron field-induced structures possessing the noticeable reinforcing effect during magneto-steady shear. The presence of the carbon nanotubes and graphene nanoplatelets rather disrupted the chain-like structures, which was reflected in lower τ_0 and lower K parameter values after numerical quantification using the Robertson–Stiff model. The effect of the employed additives on toughness of the internal structures was less prevailing under oscillatory measurements. Although the addition of carbon nanotubes generally decreased the magnetorheological performance, the Turbiscan characterization as well as long-term direct observation showed that they remarkably enhanced sedimentation stability, which was attributed to increased friction force as a result of their high specific surface area. The presence of fine fullerene powder as well as the graphene nanoplatelets had rather minimal effect on sedimentation stability and redispersibility. Based on the results, it appears that the optimization of the magnetorheological fluids could be based on combining the additives varying in mechanism of their action (gap-filling and sedimentation enhancing effect) to ensure the both, rigidity of the internal structures as well as the sufficient sedimentation stability.

Acknowledgements

Author M. C. wishes to thank the Internal Grant Agency of Tomas Bata University in Zlin [project no. IGA/CPS/2017/004] for the financial support. This work was also supported by the Ministry of Education, Youth and Sports of the Czech Republic – Program NPU I [LO1504].

Appendix A. Supplementary data

Supplementary material related to this article can be found, in the online version, at doi:https://doi.org/10.1016/j.colsurfa.2018.01.046.

References

[1] M. Ashtiani, S.H. Hashemabadi, A. Ghaffari, A review on the magnetorheological fluid preparation and stabilization, J. Magn. Magn. Mater. 374 (2015) 716–730.
[2] J. de Vicente, D.J. Klingenberg, R. Hidalgo-Alvarez, Magnetorheological fluids: a review, Soft Matter 7 (2011) 3701–3710.
[3] W.L. Zhang, S.D. Kim, H.J. Choi, Effect of graphene oxide on carbonyl-iron-based magnetorheological fluid, IEEE Trans. Magn. 50 (2014) 4.
[4] Z. Strecker, I. Mazurek, J. Roupec, M. Klapka, Influence of MR damper response time on semiactive suspension control efficiency, Meccanica 50 (2015) 1949–1959.
[5] J.D.G. Duran, G.R. Iglesias, A.V. Delgado, L.F. Ruiz-Moron, J. Insa, F. Gonzalez-Caballero, Stability and flow behavior of a magnetorheological lubricant in a magnetic shock absorber, Tribol. Trans. 51 (2008) 271–277.
[6] S.Q. Dai, C.B. Du, G.J. Yu, Design, testing and analysis of a novel composite magnetorheological fluid clutch, J. Intell. Mater. Syst. Struct. 24 (2013) 1675–1682.
[7] D.M. Wang, Y.F. Hou, Z.Z. Tian, A novel high-torque magnetorheological brake with a water cooling method for heat dissipation, Smart Mater. Struct. 22 (2013) 025019.
[8] W. Kordonski, A. Shorey, Magnetorheological (MR) jet finishing technology, J. Intell. Mater. Syst. Struct. 18 (2007) 1127–1130.
[9] M. Cvek, M. Mrlik, M. Ilcikova, T. Plachy, M. Sedlacik, J. Mosnacek, V. Pavlinek, A facile controllable coating of carbonyl iron particles with poly(glycidyl methacrylate): a tool for adjusting MR response and stability properties, J. Mater. Chem. C 3 (2015) 4646–4656.
[10] M. Sedlacik, V. Pavlinek, P. Saha, P. Svrcinova, P. Filip, J. Stejskal, Rheological properties of magnetorheological suspensions based on core-shell structured polyaniline-coated carbonyl iron particles, Smart Mater. Struct. 19 (2010) 115008.
[11] M. Machovsky, M. Mrlik, T. Plachy, I. Kuritka, V. Pavlinek, Z. Kozakova, T. Kitano, The enhanced magnetorheological performance of carbonyl iron suspensions using magnetic Fe3O4/ZHS hybrid composite sheets, RSC Adv. 5 (2015) 19213–19219.
[12] M. Mrlik, M. Ilcikova, M. Cvek, V. Pavlinek, A. Zahoranova, Z. Kronekova, P. Kasak, Carbonyl iron coated with a sulfobetaine moiety as a biocompatible system and the magnetorheological performance of its silicone oil suspensions, RSC Adv. 6 (2016) 32823–32830.
[13] I.J. Moon, M.W. Kim, H.J. Choi, N. Kim, C.Y. You, Fabrication of dopamine grafted polyaniline/carbonyl iron core-shell typed microspheres and their magnetorheology, Colloids Surf. A 500 (2016) 137–145.
[14] W.Q. Jiang, H. Zhu, C.Y. Guo, J.F. Li, Q. Xue, J.H. Feng, X.L. Gong, Poly(methyl methacrylate)-coated carbonyl iron particles and their magnetorheological characteristics, Polym. Int. 59 (2010) 879–883.
[15] J. Sutrisno, A. Fuchs, H. Sahin, F. Gordaninejad, Surface coated iron particles via atom transfer radical polymerization for thermal-oxidatively stable high viscosity magnetorheological fluid, J. Appl. Polym. Sci. 128 (2013) 470–480.
[16] M. Behrooz, J. Sutrisno, L.Y. Zhang, A. Fuchs, F. Gordaninejad, Behavior of magnetorheological elastomers with coated particles, Smart Mater. Struct. 24 (2015) 035026.
[17] W.H. Chuah, W.L. Zhang, H.J. Choi, Y. Seo, Magnetorheology of core-shell structured carbonyl iron/polystyrene foam microparticles suspension with enhanced stability, Macromolecules 48 (2015) 7311–7319.
[18] M. Sedlacik, V. Pavlinek, R. Vyroubal, P. Peer, P. Filip, A dimorphic magnetorheological fluid with improved oxidation and chemical stability under oscillatory shear, Smart Mater. Struct. 22 (2013) 8.
[19] S.T. Lim, M.S. Cho, I.B. Jang, H.J. Choi, Magnetorheological characterization of carbonyl iron based suspension stabilized by fumed silica, J. Magn. Magn. Mater. 282 (2004) 170–173.
[20] M.J. Hato, H.J. Choi, H.H. Sim, B.O. Park, S.S. Ray, Magnetic carbonyl iron suspension with organoclay additive and its magnetorheological properties, Colloids Surf. A 377 (2011) 103–109.
[21] D.S. Jang, Y.D. Liu, J.H. Kim, H.J. Choi, Enhanced magnetorheology of soft magnetic carbonyl iron suspension with hard magnetic gamma-Fe2O3 nanoparticle additive, Colloid Polym. Sci. 293 (2015) 641–647.
[22] T. Plachy, M. Cvek, Z. Kozakova, M. Sedlacik, R. Moucka, The enhanced MR performance of dimorphic MR suspensions containing either magnetic rods or their non-magnetic analogs, Smart Mater. Struct. 26 (2017) 025026.
[23] N. Jahan, S. Pathak, K. Jain, R.P. Pant, Enchancment in viscoelastic properties of flake-shaped iron based magnetorheological fluid using ferrofluid, Colloids Surf. A 529 (2017) 88–94.
[24] S.H. Piao, M. Bhaumik, A. Maity, H.J. Choi, Polyaniline/Fe composite nanofiber added softmagnetic carbonyl iron microsphere suspension and its magnetorheology, J. Mater. Chem. C 3 (2015) 1861–1868.
[25] M. Cvek, M. Mrlik, V. Pavlinek, A rheological evaluation of steady shear magnetorheological flow behavior using three-parameter viscoplastic models, J. Rheol. 60 (2016) 687–694.
[26] G.R. Iglesias, M.T. Lopez-Lopez, J.D.G. Duran, F. Gonzalez-Caballero, A.V. Delgado, Dynamic characterization of extremely bidisperse magnetorheological fluids, J. Colloid Interface Sci. 377 (2012) 153–159.
[27] F.F. Fang, Y.D. Liu, H.J. Choi, Y. Seo, Core-shell structured carbonyl iron microspheres prepared via dual-step functionality coatings and their magnetorheological response, ACS Appl. Mater. Interfaces 3 (2011) 3487–3495.
[28] M. Mrlik, M. Ilcikova, M. Sedlacik, J. Mosnacek, P. Peer, P. Filip, Cholesteryl-coated carbonyl iron particles with improved anti-corrosion stability and their viscoelastic behaviour under magnetic field, Colloid Polym. Sci. 292 (2014) 2137–2143.
[29] M. Sedlacik, V. Pavlinek, A tensiometric study of magnetorheological suspensions' stability, RSC Adv. 4 (2014) 58377–58385.
[30] G.R. Iglesias, A. Roldan, L. Reyes, L. Rodriguez-Arco, J.D.G. Duran, Stability behavior of composite magnetorheological fluids by an induction method, J. Intell. Mater. Syst. Struct. 26 (2015) 1836–1843.
[31] G.R. Iglesias, L.F. Ruiz-Moron, J.I. Monesma, J.D.G. Duran, A.V. Delgado, An experimental method for the measurement of the stability of concentrated magnetic fluids, J. Colloid Interface Sci. 311 (2007) 475–480.

[32] X.G. Cao, H. Ren, H.Y. Zhang, Preparation and microwave shielding property of silver-coated carbonyl iron powder, J. Alloys Compd. 631 (2015) 133–137.
[33] M.A. Portillo, G.R. Iglesias, Magnetic nanoparticles as a redispersing additive in magnetorheological fluid, J. Nanomater. (2017) 8.
[34] D.G. Zhao, J.A. Ning, S.Y. Li, M. Zuo, Synthesis and thermoelectric properties of C-60/Cu2GeSe3 composites, J. Nanomater. (2016) 7.
[35] P. Filip, J. David, Axial Couette-Poiseuille flow of power-law viscoplastic fluids in concentric annuli, J. Pet. Sci. Eng. 40 (2003) 111–119.
[36] M. Ashtiani, S.H. Hashemabadi, The effect of nano-silica and nano-magnetite on the magnetorheological fluid stabilization and magnetorheological effect, J. Intell. Mater. Syst. Struct. 26 (2015) 1887–1892.
[37] S.H. Piao, W.L. Zhang, H.J. Choi, Magnetic carbonyl iron suspension with sepiolite additive and its magnetorheological property, IEEE Trans. Magn. 50 (2014) 4.
[38] F.F. Fang, H.J. Choi, M.S. Jhon, Magnetorheology of soft magnetic carbonyl iron suspension with single-walled carbon nanotube additive and its yield stress scaling function, Colloids Surf. A 351 (2009) 46–51.
[39] H.A. Barnes, The yield stress - a review or' pi alpha nu tau alpha rho epsilon iota' - everything flows? J. Non-Newtonian Fluid Mech. 81 (1999) 133–178.
[40] M.T. Balhoff, L.W. Lake, P.M. Bommer, R.E. Lewis, M.J. Weber, J.M. Calderin, Rheological and yield stress measurements of non-newtonian fluids using a marsh funnel, J. Pet. Sci. Eng. 77 (2011) 393–402.
[41] K.W. Song, Y.S. Kim, G.S. Chang, Rheology of concentrated xanthan gum solutions: steady shear flow behavior, Fibers Polym. 7 (2006) 129–138.
[42] C. Galindo-Gonzalez, M.T. Lopez-Lopez, J.D.G. Duran, Magnetorheological behavior of magnetite covered clay particles in aqueous suspensions, J. Appl. Phys. 112 (2012) 11.
[43] J.M. Ginder, L.C. Davis, Shear stresses in magnetorheological fluids - role of magnetic saturation, Appl. Phys. Lett. 65 (1994) 3410–3412.
[44] D.H. Bae, H.J. Choi, K. Choi, J. Nam, M.S. Islam, N. Kao, Microcrystalline cellulose added carbonyl iron suspension and its magnetorheology, Colloids Surf. A 514 (2017) 161–167.
[45] A. Peigney, C. Laurent, E. Flahaut, R.R. Bacsa, A. Rousset, Specific surface area of carbon nanotubes and bundles of carbon nanotubes, Carbon 39 (2001) 507–514.
[46] H. Buron, O. Mengual, G. Meunier, I. Cayre, P. Snabre, Optical characterization of concentrated dispersions: applications to laboratory analyses and on-line process monitoring and control, Polym. Int. 53 (2004) 1205–1209.
[47] X.F. Dong, S. Huo, M. Qi, Comparison of electrorheological performance between urea-coated and graphene oxide-wrapped core-shell structured amorphous TiO2 nanoparticles, Smart Mater. Struct. 25 (2016) 10.
[48] C. Galindo-Gonzalez, G.R. Iglesias, F. Gonzalez-Caballero, J.D.G. Duran, Stability of concentrated aqueous clay-magnetite suspensions, Colloids Surf. A 306 (2007) 150–157.
[49] J.R. Morillas, A.J.F. Bombard, J. de Vicente, Preparation and characterization of magnetorheological fluids by dispersion of carbonyl iron microparticles in PAO/1-octanol, Smart Mater. Struct. 25 (2016) 015023.